universität wien

Dissertation

Titel der Dissertation

Temperatursensitivität phänologischer und nivaler Grössen

Verfasser

MMag. Christian Maurer

angestrebter akademischer Grad

Doktor der Naturwissenschaften (Dr. rer. nat.)

Wien, im Oktober 2012

Studienkennzahl lt. Studienblatt:	A 091 415
Dissertationsgebiet lt. Studienblatt:	Meteorologie
Betreuer:	emer. O. Univ.-Prof. Dr. Michael Hantel

Inhaltsverzeichnis

Zusammenfassung

Der Einfluss von *Saisonmitteltemperaturen* auf *phänologische* (besonders Weinlesedatum) und *nivale* (Schneebedeckung und Hochgebirgsvegetation) Größen ist Gegenstand der vorliegenden Dissertation. Diese eint, dass die Temperatur, unter allen Einflüssen, der bedeutendste ist.
Aus historischen Quellen wird in einer ersten Arbeit eine nahezu vollständige Zeitreihe von *Weinlesedaten 1523-2007* für den Großraum Wien gewonnen, aus der aufgrund einer beachtlichen *Korrelation zur Mai-Juni-Juli-Mitteltemperatur Dekadenmitteltemperaturen* bis ins 16. Jahrhundert zurück abgeschätzt werden können. Ausgehend von einem Temperaturniveau, das jenem der 1990er Jahren entspricht, sinkt die rekonstruierte Temperatur bis zu einem Minimum Ende des 18. Jahrhunderts ab. Anzeichen für einen Temperaturanstieg im Ausmaß der letzten 40 Jahre fehlen in der 470-jährigen Untersuchungsperiode.
In einer zweiten Arbeit liegt der Focus auf *Extremereignissen*, welche auf Basis einer *Synopsis von phänologischen Daten*, rekonstruierten und gemessenen *Mitteltemperaturen* sowie *dokumentarischen Quellen* gesucht werden. Für den Bereich Österreich, Schweiz und Nordostfrankreich werden mithilfe einer 105-jährigen Referenzperiode und zweifacher Standardabweichung als Grenzwert 36 extreme Jahre definiert, wobei in einem gegebenen Jahr mindestens zwei von den Parametern Weinlesedatum, rekonstruierte oder gemessene Mitteltemperatur den Grenzwert überschreiten müssen und die dokumentarische Quellen als Zusatzinformation dienen.
Hinsichtlich der nivalen Parameter sollen eine *formalisierte und quantitative Darstellung der mittleren Schneebedeckungsverhältnisse* in den Alpen sowie der *Vegetationsverhältnisse* an einem ausgewählten Alpengipfel in Abhängigkeit von der Temperatur gezeigt werden. Dabei wird besonderes Augenmerk auf die *Temperaturempfindlichkeit* der betrachteten Zustandsgröße sowie auf jene *Höhe*, in der diese erreicht wird, gelegt.
Unter Weiterentwicklung einer bereits vorhandenen Theorie kann in einem ersten Schritt das Konzept der *Medianschneelinie im Winter* (Dezember-Jänner-Februar) präsentiert werden. Das ist jene Höhenlinie, die alle Punkte mit einer 50%-Wahrscheinlichkeit für Schnee verbindet und auf klimatische Veränderungen besonders sensibel reagiert. Entscheidend dabei ist, dass man ein Konzept verwendet, durch das *Lokaltemperaturen in Klimaeffekt und Effekt der Koordinaten* (Länge, Breite, Höhe) *zerlegt* werden können.
In einem zweiten Schritt wird die Lage der *Medianschneelinie im Sommer* mit der Lage des *alpin-nivalen Ökotons* auf einem ausgewählten Alpengipfel verglichen. Letzteres ist jene Grenzlinie im Hochgebirge, die durch eine 50%-Wahrscheinlichkeit für nivale und eine ebenso hohe Wahrscheinlichkeit für alpine Vegetation ausgezeichnet ist. Obwohl man es mit zwei sehr verschiedenen Eingangsdaten, nämlich mit einem Zeitdauerverhältnis auf der einen und mit einem Flächenverhältnis auf der anderen Seite zu tun hat, welche auch auf Temperaturänderungen unterschiedlich schnell reagieren, liegen beide Medianhöhen im gleichen Niveau. Dies untermauert quantitativ die ökologische These, dass das alpin-nivale Ökoton von der Sommerschneebedeckung gesteuert wird.
Nach dieser zunächst nur auf die Medianlinien angewendeten Entwicklung, wird das vorhandene Werkzeug genutzt, um beliebige Schneelinien (5-95%) zu generieren. Damit soll das *Schneelinienklima der Alpen* beschrieben werden. Durch die nunmehrige Anwendung des Konzeptes der *Generalisierten Linearen Modelle* kann eine wahrscheinlichkeitstheoretisch fundierte Anpassung erreicht werden. Gleichzeitig wird im Zuge dieser Arbeit die lokale Gültigkeit der Schneelinientheorie diskutiert und die *Dominanz des Prädiktors Temperatur* hervorgehoben.

Summary

The impact of *seasonal mean temperatures* on *phenological* (especially grape harvest dates) and *nival* (snow cover and vegetation in high mountain areas) quantities is the issue of the present thesis. These are unified by the fact, that temperature, among all other influences, is the most relevant.

The first paper collects a nearly continuous series of *grape harvest dates 1523-2007* for Greater Vienna from historical sources. Based upon this data *decadal mean temperatures* back to the 16th century can be estimated due to a remarkable *correlation to the mean temperature* for the months of *May-June-July*. Starting from a temperature level, which is comparable to that of the 1990s, the reconstructed temperature drops until reaching a minimum value at the end of the 18th century. Signs for a raise in temperature to the extent of the past 40 years are lacking in the 470 years of investigation.

The second paper focuses on *extreme events*, which are researched on the basis of a *synopsis of phenological data*, reconstructed and measured *mean temperatures* as well as *documentary sources*. For the region of Austria, Switzerland and north-eastern France 36 extreme years are defined with the help of a reference period lasting 105 years and double standard deviation as a threshold. At least two of the parameters grape harvest date, reconstructed or measured mean temperature in a given year must exceed that threshold; the documentary sources serve as additional information.

With regard to the nival parameters a *formalized and quantitative presentation of both the mean snow cover conditions* in the Alps and the *vegetation conditions* on a selected Alpine peak as a function of temperature shall be given. A special focus shall be placed on the *temperature sensitivity* of the state quantity considered as well as on the *altitude* at which the corresponding sensitivity is adopted.

Further developing an already existing theory leads to the concept of the *median snowline in winter* (December-January-February). This line equals the altitude line which connects all points with a 50% probability for snow cover and which is most sensitive to climate change. Using a concept through which *local temperatures are separated into the climate effect and the effect of coordinates* (longitude, latitude, altitude) is essential.

In a second step the position of the *median snowline in summer* is contrasted to the position of the *alpine-nival ecotone* at a selected Alpine peak. The latter depicts the boundary in high mountains which is characterized by a 50% probability for nival as well as for alpine vegetation. Despite two completely different input data sets - namely a time duration ratio on the one hand and an area ratio on the other hand - which above all react differently quickly to temperature changes, both median lines can be found at the same altitude. This fact confirms the ecological thesis quantitatively that the alpine-nival ecotone is driven by the summer snow cover.

By extending this basic theoretic development, at first only applied to the median lines, the available tool is used to generate arbitrary snowlines (5-95%). Thereby the *snowline climate of the Alps* shall be described. Applying henceforth the method of *Generalized Linear Models* yields a theoretically sound fitting procedure. At the same time the local validity of the snowline theory at some individual climate stations is discussed in the course of the paper, just as stating the *predominance of the predictor temperature*.

Danksagung

Mein Dank gilt in erster Linie meinem Betreuer emer. o. Univ. Prof. Dr. Michael Hantel, dessen unermüdliches Engagement, Begeisterung für wissenschaftliches Arbeiten und Ausdauer wesentlich zum erfolgreichen Gelingen dieser Dissertation beigetragen haben. Er konnte so meine Motivation trotz teils widriger Umstände - sei es im Hinblick auf Rückschläge beim Publizieren oder aber im Hinblick auf fehlende Geldmittel- aufrecht erhalten. Nicht minder bedeutsam ist sein in langjähriger Tätigkeit gesammeltes Fachwissen, von dem ich profitieren durfte.

Weiters möchte ich mich bei a. o. Univ. Prof. Dr. Leopold Haimberger bedanken, der stets ein offenes Ohr hatte, wenn ich mich bei technischen Problemen oder scheinbar nicht erklärbaren Programmabstürzen an ihn wandte. Für die gute (interdisziplinäre) Zusammenarbeit und nützliche Anregungen danke ich Dr. Elisabeth Koch, Dr. Christa Hammerl, Priv. Doz. Dr. Michael Gottfried, Dr. Harald Pauli, Mag. Ruth Töchterle und emer. o. Univ. Prof. Dr. Georg Grabherr. Nicht vergessen möchte ich an dieser Stelle auch Dr. Lucia-Maria Hirtl-Wielke, die mir am Anfang meiner Arbeit die notwendige Starthilfe gab sowie all jene Kolleginnen und Kollegen, die mir bei diversen Problemen mit Rat und Tat zur Seite standen.

Ebenso danken möchte ich meinen Eltern, die mir das Meteorologie- und Geophysikstudium finanziell ermöglichten, was die Grundlage meines heutigen Erfolges bildet.

Die Dissertation wurde im Rahmen der interfakultativen Forschungsplattform "Sensitive Mountain Limits of Snow and Vegetation" der Universität Wien sowie der interdisziplinären, internen Projekte BACCHUS I-III ("Klosterneuburg, Retz and Gumpoldskirchen Wine and Climate Change in Lower Austria") der Zentralanstalt für Meteorologie und Geodynamik (ZAMG) durchgeführt.

Kapitel 1

Einleitung

1.1 Motivation

Die winterliche Schneebedeckung als auch der Weinbau sind in Österreich prägende Landschaftselemente und stellen zudem relevante Wirtschaftsfaktoren dar. Ihre Witterungsabhängigkeit bedingt, dass sie für den Klimatologen von besonderem Interesse sein sollten - erst recht in einer Zeit von offensichtlichem Klimawandel. Wenn auch aus unterschiedlichen Gründen: Während historische Aufzeichnungen über *(para-)phänologische Stadien* im Weinbau und *önologische Merkmale Rückschlüsse über die Temperaturverhältnisse* in der vorinstrumentellen Zeit ermöglichen, ist bei der winterlichen *Schneebedeckung* der vergangenen Jahrzehnte bzw. der Gegenwart deren *Reaktion* auf zurückliegende oder zu erwartende *Temperaturschwankungen* Gegenstand des Interesses.

Der Weinbau hat seit der Römerzeit in Österreich eine lange Tradition und der Wohlstand bzw. wirtschaftliche Niedergang von Städten oder ganzen Gegenden war in der Vergangenheit eng mit seiner Entwicklung verknüpft (siehe z.B. LANDSTEINER (1999)) Dies bringt mit sich, dass es sowohl für Historiker als auch Klimatologen lohnende detailreiche Aufzeichnungen hinsichtlich des Weinbaus in diversen Stadt- und Stiftsarchiven (z.B. Stift Klosterneuburg) gibt, die sich für klimatologische Zwecke nützen lassen. Forschungen auf diesem Gebiet ermöglichen somit auch eine spannende interdisziplinäre Zusammenarbeit zwischen einem Bereich der Geistes- und der Naturwissenschaften.

Da das betrachtete Untersuchungsgebiet, nämlich Niederösterreich, *temperaturmäßig als nordöstlichstes Grenzgebiet für den Weinbau* gilt, dürfen *beträchtliche Korrelationen* zu ausgewählten, der Ernte vorangehenden, *Saisonmitteltemperaturen während der Vegetationsperiode* und im Grunde recht *gute Rekonstruktionen* derselben erwartet werden. Neben einer Rekonstruktion bietet der Vergleich von "historischen" und "modernen" (letzte Jahrzehnte) Weinlesereihen einen Einblick in die *geänderten Praktiken und Prioritäten* bei der Weinproduktion. Entsprechend dem IPCC-Report von 2007 (SOLOMON et al., 2007) sind Temperaturrekonstruktionen aus Proxy-Daten verschiedener Art einerseits dazu geeignet die *Signifikanz von Temperaturschwankungen*, wie sie in Klimamodellen simuliert werden oder gegenwärtig auftreten, zu beurteilen und andererseits *anthropogene Klimaeffekte* zu detektieren und zu quantifizieren. In diesem Zusammenhang ist auch eine Information über Jahre hilfreich, in welchen (para-)phänologische und önologische Kenngrößen *extreme Werte* annahmen. Rein *deskriptive Beschreibungen* außergewöhnlicher Witterungsverhältnisse in der vorinstrumentellen Periode bergen oft einen *Mangel an Objektivität* in sich, was unter anderem zu einer Glättung im niederfrequenten Teil des Frequenzspektrums führt, sodass es sich lohnt, auf den *umfangreichen Pool an nicht deskriptiven*

Proxy-Daten, also biologische Daten, zurückzugreifen.

Eine der ersten Arbeiten auf dem Gebiet der Temperaturrekonstruktion aus (para-) phänologischen Daten, konkret Weinlesedaten, stammt vom Österreicher Friedrich Lauscher (LAUSCHER, 1978, 1983), dessen Publikationen in deutscher Sprache leider zu wenig Widerhall fanden, sodass dieses Themengebiet erst im letzten Jahrzehnt - offenbar ausgelöst durch den extremen Sommer 2003 in Europa - reges Interesse hervorrief.

Was das Klimaelement Schnee anlangt, so hat kaum ein anderes Klimaelement für die Menschen, die im alpinen Raum leben, so große Bedeutung. Zum einen verändert der Schnee in sehr kurzen Zeiträumen das Landschaftsbild erheblich und bringt für jeden Fotographen eine Fülle von lohnenden Motiven mit sich, schützt aber auch die Vegetation vor strengen Frösten. Zum anderen gehen von diesem Klimaelement seit jeher Gefahren (wie z.B. Lawinen) und Probleme (wie. z.B. Verkehrsbehinderungen) aus, sodass die "Beziehung" der meisten Menschen zum Schnee wohl recht ambivalent ist. Nicht vergessen werden darf in diesem Zusammenhang, dass das Vorhandensein einer (ausreichenden) Schneedecke mit dem Einzug des Wintertourismus in den Alpen im 20. Jahrhundert zu einem wirtschaftlich relevanten Faktor geworden ist. Ein Fehlen des Schnees in den Wintersportorten der Alpen sorgt spätestens Ende November des betreffenden Jahres für Gesprächsstoff und findet in allen Medien Widerhall. Dies umso mehr, als dass das allfällige Ausbleiben der winterlichen Schneedecke sofort als Zeichen eines gerade statt findenden globalen Klimawandels interpretiert wird.

Wissenschaftlich bzw. klimatologisch besonders interessant ist es bei der Betrachtung der Schneebedeckung jene mittlere Grenze (Linie) zu kennen, die den Bereich, in dem über den gesamten Winter (Dezember-Jänner-Februar) hindurch Schnee liegt, von jenem Gebiet trennt, das sich schneefrei präsentiert. An dieser ausgezeichneten Linie, der *Medianschneelinie*, beträgt die Wahrscheinlichkeit Schnee anzutreffen bzw. keinen Schnee vorzufinden jeweils genau 50%. Der große Klimatologe und Direktor der Zentralanstalt für Meteorologie und Geodynamik in Wien Julius von Hann beschäftigte sich bereits Ende des 19./Anfang des 20. Jahrhunderts mit dieser Materie (HANN (1883) und HANN (1908)). Während Hann all seine Schneebeobachtungen händisch auswerten musste und daher auch keine aufwendigen Modellvorstellungen einfließen lassen konnte, stehen dem heutigen Klimatologen umfangreiche und sehr leistungsfähige Werkzeuge zur Verfügung um eine enorme Anzahl von Daten zu einer prägnanten Aussage zu kondensieren.

Im vergangenen Jahrzehnt haben sich die Autoren HANTEL et al. (2000), WIELKE et al. (2004), HANTEL and HIRTL-WIELKE (2007) und HIRTL-WIELKE (2007) daran gemacht, die Schneebedeckungsverhältnisse in den Alpen statistisch zu quantifizieren. Dabei legten sie besonderes Augenmerk auf die *Empfindlichkeit der Schneebedeckungsdauer* gegenüber Veränderung in der großräumigen, von der geographischen Lage unabhängigen Temperatur, der *Klimatemperatur*. Auch wenn zahlreiche weitere Faktoren (Niederschlag, Exposition ect.) das Vorhandensein/Nichtvorhandensein einer Schneedecke beeinflussen, bleibt doch die Temperatur der entscheidende Antrieb. In diesem Zusammenhang erinnere man sich an den kalten Winter 2005/2006 (JUNG et al., 2010), der in Wien eine lang andauernde Schneebedeckung mit sich brachte, den gleich darauffolgenden extrem warmen, sturmreichen Winter 2006/2007 (YIOU et al., 2007) aber auch an den Sommer 2003 (SCHÄR and JENDRITZKY, 2004), in dem sich die Gletscher der Alpen aper präsentierten.

Im Rahmen der dritten, vierten und fünften in der Dissertation aufgelisteten Publikationen wurde das aus den früheren Arbeiten ableitbare Konzept der *Schneelinien* und als Spezialfall jenes der *Medianschneelinie* entwickelt. Letztere zeichnet sich dadurch aus, dass sie mit dem Ni-

veau der maximalen Klimaempfindlichkeit der Schneebedeckung zusammenfällt. Ziel war es, mit Hilfe einer Modellvorstellung ein Feld von Schneelinien mit verschiedenen Schneewahrscheinlichkeiten (5-95%) aus den Beobachtungsdaten von über 200 Klimastationen der Alpen (Stationen in Deutschland, der Schweiz, Frankreich, Italien, Österreich und Slowenien) zu generieren. Durch die Kooperation im Rahmen der interfakultativen Forschungsplattform "Sensitive Mountain Limits of Snow and Vegetation" der Universität Wien mit Landschaftökologen wurde die praktische Bedeutung der Medianschneelinie jenseits der Klimatologie erkannt, da jene mittlere Linie im Sommer (Juni-Juli-August) die Lage des *alpin-nivalen Ökotons* (Grenze zwischen alpiner und nivaler Vegetation, siehe GOTTFRIED et al. (1998) oder PAULI et al. (1999)) steuert bzw. mit ihm auf ungefähr gleichem Niveau liegt, was durch die Auswertung von zwei verschieden Datensätzen (Vegetations-und Schneedaten) quantifiziert werden konnte.

1.2 Publikationen

Die hier vorliegende Dissertation enthält fünf Publikationen zu dem Themengebiet, an denen der Autor maßgeblich mitgewirkt hat:

- **C. Maurer**, E. Koch, C. Hammerl, T. Hammerl and E. Pokorny, 2009: BACCHUS temperature reconstruction for the period 16th to 18th centuries from Viennese and Klosterneuburg grape harvest dates, *J. Geophys. Res.*, **114**, D22106
- **C. Maurer**, C. Hammerl, E. Koch, T. Hammerl and E. Pokorny, 2011: Extreme grape harvest data of Austria, Switzerland and France from A.D. 1523 to 2007 compared to corresponding instrumental/reconstructed temperature data and various documentary sources, *Theor. Appl. Climatol.*, **106**, 55-68
- M. Hantel and **C. Maurer**, 2011: The median winter snowline in the Alps, *Meteorol.Z.*, **20**(3), 267-276
- M. Gottfried, M. Hantel, **C. Maurer**, R. Toechterle, H. Pauli and G. Grabherr, 2011: Coincidence of the alpine–nival ecotone with the summer snowline, *Environ.Res.Let.*, **6**, 12pp
- M. Hantel, **C. Maurer** and D. Mayer, 2012: The snowline climate of the Alps 1961-2010, *Theor. Appl. Climatol.*, DOI 10.1007/s00704-012-0688-9 (published online)

Der konkrete Beitrag des Autors der Dissertation zu den beiden zuerst genannten Publikationen bestand in der Durchführung aller Datenauswertungen und in der Erstellung nahezu des gesamten Manuskripts bzw. nahezu aller Abbildungen. Lediglich das Kapitel "Data" wurde in beiden Publikationen fast zur Gänze von der an dem Projekt beteiligten Historikerin verfasst. Die Wahl der statistischen Methoden geschah im Zuge von Diskussionen mit der Projektleitung.

Was die drei anderen Publikationen anlangt, so trug der Autor der Dissertation durch alle erforderlichen Programmierungen bzw. Auswertungen (mit Ausnahme der Berechnung des sogenannten Nivalitätsindex in GOTTFRIED et al. (2011)), die für die Ergebnisse der Publikationen notwendig waren, durch die Erstellung eines Großteils der Abbildungen sowie durch die kritischen Prüfung der Manuskripte bei. Darüber hinaus kam es infolge der Anregung seitens des Autors zu einer deutlichen Änderung in der Wahl der Auswertemethode (Verwendung des "Nonlinear" Fits statt des zuvor immer verwendeten "Extended" Fits), was erstmals in der

Publikation HANTEL and MAURER (2011) berücksichtigt wurde (siehe auch erstes Kapitel im Appendix). In diesem Zusammenhang konnte durch Monte Carlo Rechnungen, die in der nun vorliegenden Form durch den Autor der Dissertation konzipiert wurden, das Verständnis im Hinblick auf das Verhalten der Auswertemethode unter verschiedenen Randbedingungen vertieft werden. Dabei kam erstmals eine realistische Datensimulation in der Art zur Anwendung, dass der keinesfalls perfekten Korrelation zwischen Temperatur und Schneebedeckung Rechnung getragen wurde (siehe ebenfalls Appendix). In der Publikation HANTEL et al. (2012) lag der Beitrag des Autors der Dissertation vor allem in der lokalen Evaluation der Modellergebnisse, wozu Abbildungen der Art von Fig. 16 kreiert wurden. Die Abhängigkeit der lokalen (z.B. Fig. 16) und globalen Modellperformance (Figs. 9 und 11 mit der Verteilung der Residuen der Gebirgstemperatur) von der Korrelation zwischen Temperatur und Schneebedeckung sowie die räumliche Verteilung der Korrelationen und die sich daraus ergebenden Konsequenzen sind ebenfalls vom Autor der Dissertation maßgeblich beleuchtet worden.

1.3 Überblick über die Publikationen

1.3.1 Temperatursensitivität phänologischer Größen

Um *Saisonmitteltemperaturen* bis ins 16. Jahrhundert zurück rekonstruieren zu können (MAURER et al., 2009), musste zunächst eine ausreichend lange *paraphänologische Zeitreihe* etabliert sowie *verlässliche Temperaturaufzeichnungen* in einer entsprechenden *Überlappungsperiode* akquiriert werden. Um Transkriptionsfehlern möglichst vorzubeugen, wurden nur primäre (Manuskripte) und eine gute sekundäre Quelle (PRIBRAM et al., 1938) mit Informationen zum Weinbau in Wien (Wiener Bürgerspital) und Niederösterreich (Stift Klosterneuburg) herangezogen bzw. die entsprechenden Daten extrahiert. Das Ergebnis sind nahezu kontinuierliche jährliche Zeitreihen von *Weinlesedaten* (aber auch von Blühdaten, Beerenweichedaten, Weinqualität und Weinquantität) für unterschiedliche Perioden. Für *Wien* liegen Weinlesetermine von *1523-1749* und von *1960-1999* vor, für *Klosterneuburg* von *1730-1879* und von *1970-2007*. *Homogenisierte Monatsmitteltemperaturen* der Station *Wien Hohe Warte* wurden aus der "Historical Instrumental Climatological Surface Time Series of the Greater Alpine Region (HISTALP)" Datensammlung von AUER and et al. (2007) in der Bias-korrigierten Version von BOEHM et al. (2010) übernommen.

Ein erster wichtiger Schritt war es zu prüfen (t-Test), ob die beiden historischen Weinlesereihen des Bürgerspitals und von Klosterneuburg im Überlappungszeitraum 1730-1749 einen signifikanten Unterschied im Mittelwert aufweisen (Varianzen sind identisch). Nachdem dies ausgeschlossen worden war, wurden sowohl *lineare Gesamtkorrelationen* als auch *"Running Correlations"* (also gleitende Korrelationen) für die Überlappungsperiode 1775-1879 zwischen dem Lesedatum und verschiedenen, jenem Datum vorangehenden, Saisonmittel- und Monatsmitteltemperaturen berechnet. Dabei zeigt sich, dass die *höchste Gesamtkorrelation von -0.79* (p=0.01) für die *Saison Mai-Juni-Juli* erreicht wird (dicht gefolgt von jener für April-Mai-Juni-Juli), wobei die Werte der "Running Correlations" zwischen 1775 und 1850, der Kalibrierungsperiode, sogar zwischen -1.0 und -0.7 (p=0.05) zu finden sind. Korrelationen mit einzelnen Monatsmitteltemperaturen erweisen sich hingegen als unbrauchbar. Nach Aufstellen einer *einfachen Regressionsgleichung* beträgt das Fehlermaß "Reduction of Error" in der Verifikationsperiode 1851-1879 0.32 (1.0 wäre perfekte Rekonstruktion), was angesichts der niedrigen gleitenden Korrelationen in diesem Zeitabschnitt wohl als unteres Limit anzusehen ist. Die zu *Dekadenmitteltemperaturen*

gemittelten Saisonmitteltemperaturen zeigen ein warmes beginnendes 16. Jahrhundert, danach dann einen allmählichen Abfall im Temperaturniveau. Das sogenannte "Maunder Minimum" Ende des 18. Jahrhunderts ist gut ausgeprägt. Nichtsdestotrotz gibt es erhebliche Diskrepanzen zu anderen Rekonstruktionen, die im letzten Jahrzehnt publiziert wurden und von denen zwei zum Vergleich herangezogen worden sind (CASTY et al. (2005); DOBROVOLNÝ and et al. (2010)), besonders vor 1660.

In diesem Zusammenhang ist nicht zu vernachlässigen (siehe z.B. GARNIER et al. (2011)), dass Weinlesedaten vom Menschen beeinflusst werden, weshalb auch die Bezeichnung "paraphänologisch" dafür verwendet wird. Anhand von zwei 30-jährigen Subperioden lässt sich zeigen, dass sich die *Weinbaupraktiken* (z.B. Sorten und/oder Geschmack) zumindest zwischen Mitte des 19. und Ende des 20./Anfang des 21. Jahrhunderts *deutlich verändert* haben (mittleres Lesedatum als auch Saisonmitteltemperatur nehmen zu), mit einer Tendenz zu späteren Leseterminen, offenbar um die Qualität des Weines zu erhöhen.

Die für das eben beschriebene Ziel einer Temperaturrekonstruktion gesammelten Daten wurden in einem weiteren Vorhaben zur Detektierung von *hinsichtlich der Temperaturverhältnisse extremen Jahren* verwendet (MAURER et al., 2011), wobei zusätzliche historische Quellen (Rechnungen des Bürgerspitals) aus dem Stadtarchiv *Retz*, aber auch Sekundärliteratur (LÖSCHNIG and STEFL (1935); PUNTSCHERT (1894); APELDAUER (1933)) als Ergänzung herangezogen wurden.

Ein Jahr wird dieser Auswertung entsprechend als extrem bezeichnet, wenn *mindestens zwei* in diesem Jahr *verfügbare Parameter* die *doppelte Standardabweichnung* bezüglich einer 105-jährigen Referenzperiode erreichen bzw. überschreiten. Bei eben diesen verfügbaren Parametern handelt es sich einerseits um die schon bekannten *Weinlesedaten* aus *Wien* und aus *Klosterneuburg*, um Daten aus der *Schweiz* (Schweizer Plateau, siehe CHUINE et al. (2004)) und aus *Nordostfrankreich* (Burgund, siehe MEIER et al. (2007)). Andererseits dienen gemessene, homogenisierte und gemittelte *April-Mai-Juni-Juli-Saisonmitteltemperaturen* aus der HISTALP-Datenbank von *Wien Hohe Warte*, *Basel-Binningen*, *Geneva-Cointrin* und *Strasbourg-Entzheim* sowie *rekonstruierte April-Mai-Juni-Juli-Temperaturmittel* (Central European temperature reconstruction CEuT) in der vorinstrumentellen Periode von DOBROVOLNÝ and et al. (2010) als Input-Daten. *Deskriptive Berichte* aus *Wien*, *Klosterneuburg* und *Retz* bezüglich Weinqualität, Weinquantität sowie allgemein die Witterung betreffend sollten die gefundenen Jahre in ihrer Außergewöhnlichkeit bestätigen bzw. Widersprüche zu der paraphänologischen Information sowie zwischen den deskriptiven Beschreibungen selbst aufzeigen. Letztendlich wurden auch die Extremjahrevaluationen von CASTY et al. (2005) und ETIEN et al. (2008) bzw. historische Berichte von BRÁZDIL and KOTYZA (2000) und BRÁZDIL et al. (2008) den Ergebnissen gegenübergestellt.

Für Österreich, die Schweiz und Nordostfrankreich zusammen genommen stechen die Jahre *1542, 1718, 1811, 1822, 2003, 2006* und *2007* hervor, wobei *bis auf 1542* alle inter-regional auftretenden Extremjahre durch *außergewöhnlich späte Weinlese* gekennzeichnet sind. Die Temperaturextrema beziehen sich aber natürlich nur auf die *Verhältnisse im Spätfrühling und Frühsommer*, da dies jene Jahreszeit ist, die für die Weinlese die größte Bedeutung hat. Es ist auch anzumerken, dass in sehr schlechten Jahren für den Weinbau (z.B. 1740) wahrscheinlich oft kein Lesedatum vermerkt wurde, weil die Ernte so desaströs ausfiel. Bezogen auf die Referenzperiode 1775-1879 weist die CEuT-Zeitreihe von 1523 bis 1774 kein einziges negatives April-Mai-Juni-Juli Extremum, jene von Wien Hohe Warte überhaupt kein Extremum zwischen 1874 und

1983 auf. Die Übereinstimmung von extremen April-Mai-Juni-Juli-CEuT-Mitteltemperaturen mit den Lesedaten von Wien (Bürgerspital), vom Schweizer Plateau und von Burgund in der vorinstrumentellen Periode ist in 19, 38 und 33% der Fälle gegeben, für die Lesedaten von Klosterneuburg, dem Schweizer Plateau und Burgund ist eine Übereinstimmung mit April-Mai-Juni-Juli-Stationsmitteltemperaturen von Wien Hohe Warte, Basel&Genf und Strasbourg in 31, 43 und 33 % der Fälle gegeben, was die *nicht perfekte Korrelation* zwischen Weinlese und vorangehenden Mitteltemperaturen demonstriert, wobei die Festsetzung eines bestimmten Zahlenwertes zur Extremwertdefinition (im vorliegenden Fall 2σ) wohl zur mangelnden Kohärenz beiträgt.

Aufgrund *fehlender Daten* für Wien und Klosterneuburg zwischen 1879 und 1960, muss damit gerechnet werden, dass einige Extremjahre nicht als solche definiert werden können. Auch bei der Suche nach Extremjahren ist wie bei der Temperaturrekonstruktion darauf hinzuweisen, dass *allmähliche Änderungen in den Weinbaupraktiken* (z.B. Sortenwechsel, veränderter Geschmack, Verbesserungen in der Infrastruktur), aber auch *einmalige Ereignisse* (wie Feste, Kriege oder kommerzielle Entscheidungen) die *Amplituden* von Extrema nur *beschränkt vergleichbar*, wenn sie nicht sogar überhaupt das *Auffinden* der Extrema *unmöglich* machen. Somit ist die Ende des 20. Jahrhunderts auftretenden *besonders stark positive Lesedatenabweichung* (1980 in Wien) sicher eine *Überschätzung* der tatsächlichen Verhältnisse, die im Vergleich zum Schweizer Plateau und zu Burgund *markant geringeren negativen Abweichungen* (2003 und 2007) sicher eine *Unterschätzung* der Realität.

1.3.2 Temperatursensitivität nivaler Größen

In einem ersten Schritt sollte ein Formalismus entwickelt werden, um die so genannte *Medianschneelinie* zu erhalten (HANTEL and MAURER, 2011). Dieser leitet sich aus dem Konzept der *Mountain Temperature* bzw.*Gebirgstemperatur* ab (siehe auch HANTEL and HIRTL-WIELKE (2007)), die nichts anderes als eine *lineare Entwicklung der großräumigen Mitteltemperatur nach den Stationskoordinaten* darstellt und den großskaligen *Klimaeinfluss* vom *Einfluss der geographischen Position* (Höhe, Länge, Breite) auf die Schneebedeckung *separiert*. Dies impliziert, dass die Medianschneelinie durch die großskalige Klimatemperatur, im konkreten Fall der Alpen die "Europatemperatur", gesteuert wird. Eine Schneelinie wird durch die Schnittlinie einer Fläche konstanter Gebirgstemperatur mit der Orographie erzeugt. Ersetzt man die Stationsmitteltemperaturen durch eben diesen Ansatz der Gebirgstemperatur und passt eine analytische, nichtlineare Modellfunktion, die *Zustandsfunktion der Schneedauer*, an relative Schneebedeckungswerte (zw. 0 und 1) bei vorgegebener Schneehöhe an, kann man aus den so ermittelten Parametern und einer frei festlegbaren Mitteltemperatur die Lage der Medianschneelinie (50% Schneewahrscheinlichkeit) quer über die Alpen bestimmen. Die Medianschneelinie der Alpen 1961-2000 im Winter bei einer Schneehöhe von mindestens 5cm befindet sich am Referenzpunkt (Nordtirol) der linearen Klimatemperaturentwicklung bei rund 641m.

Die (extreme) *Temperaturempfindlichkeit der Schneebedeckung* in diesem Niveau beträgt -0.17°C^{-1}. Das heißt, dass sich bei einer Temperaturzunahme um 1°C die Schneebedeckungsdauer im Niveau der Medianschneelinie ausgehend von 45 Tagen im Winter um rund 15 Tage reduzieren würde. In *sehr geringen* und *sehr großen Höhen* ist die *Empfindlichkeit* hingegen *nahe Null* anzusetzen. Im Vergleich zu der mit der Höhe unterschiedlichen Empfindlichkeit der Schneebedeckung, ist die *Temperaturempfindlichkeit aller Schneelinien* über das gesamte Untersuchungsgebiet *konstant* und liegt bei rund 123m/°C. Je nach Temperatur des jeweiligen Winters

bewegt sich die Schneelinie so auf- und abwärts, wie es die Intuition erwarten lässt. Für die Neigung der Medianschneelinie in West-Ost und Süd-Nordrichtung ergeben sich der signifikante Wert von -56m/°Länge und der insignifikante Wert von 52m/°Breite. Diese Neigungen sind ebenso wie die Temperaturempfindlichkeit für sämtliche Schneelinien als konstant anzunehmen.

Mit diesem Werkzeug war nun die Voraussetzung geschaffen in einer interfakultativen Zusammenarbeit Hochgebirgsvegetation bzw. deren Zusammensetzung und Sommerschnee (JJA) in Beziehung zu setzen. Dass zwischen den beiden Größen ein enger Zusammenhang besteht ist bereits lange bekannt (KÖRNER, 2003), doch galt es in einer Arbeit (GOTTFRIED et al., 2011) zu zeigen, dass eine *statistische Auswertung* von Vegetations-und Schneebedeckungsdaten für das *alpin-nivale Ökoton* und die *Medianschneelinie im Sommer* in etwa das *gleiche Niveau* liefert. Als alpin-nivales Ökoton bezeichnet man den *Übergangsbereich* zwischen dem niedriger gelegenen *alpinen Grasland* bzw. der *Tundrazone* und der höher gelegenen *spärlich bewachsenen nivalen (=schneetoleranten) Vegetationszone* im Gebirge.

Es wurden zwei grundsätzlich verschiedene Datensätze mit dem gleichen Auswerteverfahren analysiert: Die *relative Schneebedeckungsdauer* als *Zeitdauerverhältnis* zwischen der Anzahl an Tagen mit einer definierten Schneebedeckung und der Länge der gesamten Saison einerseits und der *Nivalitätsindex* als *Flächenverhältnis* zwischen von nivalen Pflanzen bewachsenen Bereichen eines Messquadrats und der gesamten von Pflanzen bewachsenen Fläche in eben diesem Messquadrat andererseits. Zwar lassen sich diese beiden Datensätze formal gleich behandeln, doch ist zu beachten, dass im Gegensatz zur Sommerschneedecke, die von der mittleren saisonalen Temperatur des betreffenden Sommers gesteuert wird, die Vegetation ein "Gedächtnis" von mehreren Jahren, ja sogar Jahrzehnten, besitzt. Diesem Umstand wurde mit dem *Prior-Konzept* Rechnung getragen, in dem Vegetationsbeobachtungen vom Schrankogel (3497m) in den Stubaier Alpen (Tirol) aus 1994 mit der großräumigen Klimamitteltemperatur von 1975-1994 und jene aus 2004 mit jener von 1985-2004 in Beziehung gesetzt wurden. Dies erklärt auch, dass die Untersuchungsperiode für die Sommerschneedauer mit 1975-2004 gewählt wurde.

Als Ergebnis für die *Lage des Ökotons* am Schrankogel erhält man rund 2967m, was sich *kaum von der Lage der Medianschneelinie* der Alpen bei einer Schneebedeckung von mindestens 2cm im Sommer, rund 2897m, *unterscheidet*. Das sind gerade jene Höhen mit der maximalen Temperaturempfindlichkeit. *Beide wandern* unter dem Einfluss einer schwachen Erwärmung zwischen den Subperioden 1975-1994 und 1985-2004 *aufwärts*, wobei das Ökoton der Medianschneelinie folgt. Dabei sitzt das gesamte Höhenintervall, in dem der Übergang von der alpinen hin zur nivalen Vegetation stattfindet, unmittelbar im Zentrum des (gaussischen) Profils der Schneesensitivität, was das Ergebnis robust macht. Die Temperaturempfindlichkeit der beiden ausgezeichneten Linien liegt bei rund 47m/°C im Fall der Vegetation und bei rund 346m/°C im Fall des Schnees. Der aus der Temperatursensitivität und der Erwärmung zwischen den Subperioden ableitbare Trend in der Wanderung des Ökotons entspricht mit rund 20 Metern den Beobachtungen vor Ort. Da der Lebensraum der nivalen Pflanzen nach oben hin durch die maximalen Gipfelhöhen beschränkt ist, dürfte das Ergebnis - auch wenn es vorläufig nur durch eine Fallstudie abgesichert ist- beträchtliche *Konsequenzen für die Biodiversität im Gebirge* haben (GOTTFRIED et al., 1999).

In einer abschließenden Arbeit (HANTEL et al., 2012) wurden die zuvor gefundenen Ergebnisse (HANTEL and MAURER, 2011) vertieft und abgesichert. Nicht nur die Medianschneelinie, sondern das gesamte *Feld der Schneelinien* war Gegenstand der Untersuchung. Daneben sollte die praktische, *über eine klimatologische Aussage* für die gesamten Alpen *hinausgehen-*

de, *Verwertbarkeit der Theorie* diskutiert werden. Die Modellanordnung bedingt, dass nur an denjenigen Stationen die errechnete mittlere Höhe beliebiger Schneelinien mit der Wirklichkeit gut übereinstimmen kann, an denen eine *ausreichende Korrelation zwischen Schneebededeckung und Temperatur* besteht. Das heißt, dass die Schneebedeckung nicht hauptsächlich durch andere Faktoren, wie z.B. die Niederschlagsmenge, bestimmt wird. Nur dann ist die der Auswertung zugrunde liegenden Modellvorstellung erfüllt. Besonders *hohe, inneralpine Stationen erfüllen* diese *Voraussetzung im Winter schlecht*, was sich durch Berechnung des Korrelationskoeffizienten zwischen Klimatemperatur und Schneebedeckung an den einzelnen Stationen quantifizieren lässt. An eben solchen Stationen führt eine höhere Durchschnittstemperatur zu einer Zunahme der Schneedauer aufgrund mehr verfügbarer Feuchte bzw. häufigerem und/oder stärkerem Schneefall. *Im Sommer stört* hingegen *nicht geschmolzener Schnee* des vorangegangenen Winters die eben erwähnte Korrelation.

Ein zentraler Punkt der Arbeit ist auch die *Verbesserung in der Modellanpassung*. In allen vorangegangenen Berechnungen wurde stets die *Abweichung* zwischen der beobachteten *relativen Schneebedeckungsdauer* und der durch das Gauß' sche Fehlerintegral *modellierten Schneebedeckungsdauer* minimiert, was aber aufgrund der vorliegenden *Binomialverteilung* des Prädiktanden eine *nicht normalverteilte Residuenverteilung* ergibt (siehe HIRTL-WIELKE (2007)). Diesem Umstand wird durch das Konzept der *Generalisierten Linearen Modelle*, wie etwa in FAHRMEIR and TUTZ (2001) beschrieben, begegnet. Der Mehrwert dieser Methode liegt darin, dass der *Prädiktand durch die inverse Modellfunktion auf Normalverteilung transformiert* wird und man so das *Fitverfahren auf eine multilineare Regression vereinfachen* kann. Die *Residuen* weisen in weitere Folge eine *Normalverteilung* auf; der *Zusammenhang* zwischen *erklärter, nicht erklärter und Gesamtvarianz* ist gegeben, womit sich ein korrektes, allgemein verständliches, Qualitätsmaß für die Anpassung angeben lässt.

Die Untersuchungsperiode umfasst nun 1961-2010, das *Untersuchungsgebiet* ist aus Gründen der Datenverfügbarkeit auf *Österreich und die Schweiz beschränkt*. Ein *Vergleich* der Parameter mit der Auswertung für die *gesamten Alpen* zeigt aber, dass die *Zahlen in beiden Fällen nahezu ident* sind. Bei einer Schneebedeckung von mindestens 5cm im Winter liegt die Medianschneelinie am Referenzpunkt der Gebirgstemperatur bei rund 793m, was sehr gut zu den zuvor gefundenen 641m passt, vor allem wenn man bedenkt, dass der Berechnung der Höhe nun die Mitteltemperatur von 1961-2010 (mit dem sehr warmen Winter 2006/2007) zugrunde liegt. Im Sommer findet man die Medianschneelinie bei einer Schneebedeckung von mindestens 2cm bei rund 3083m, was ebenfalls sehr gut zu dem Wert von 2897m passt, der von GOTTFRIED et al. (2011) gefunden wurde, wobei auch hier unterschiedliche Mitteltemperaturen (1961-2010 gegenüber 1975-2004) eingehen. Da im Sommer nur ein Zehntel des Datenumfangs im Winter vorliegt, ist die Höhe der Medianschneelinie im Sommer mit einer wesentlich größeren Unsicherheit behaftet als im Winter. Insbesondere liegen die Schneebeobachtungen im Sommer praktisch alle oberhalb der Medianschneelinie, wohingegen diese im Winter gut durch Beobachtungen abgesichert ist. Die ebenfalls ermittelte Höhenlage der 90%-Schneelinie liegt um rund 500m über jener der Medianschneelinie. Während im *Winter* auch bei dieser Arbeit ein *signifikanter Abfall des Feldes* aller Schneelinien *nach Osten* (rund -35m/°Länge) sichbar wurde, kehren sich *im Sommer* die Verhältnisse komplett um. Man erhält hier einen *Anstieg des Schneelinienfeldes nach Osten* und eine *deutlichen Abfall nach Norden*. Dieses Ergebnis ist zwar aufgrund des geringen Datenumfangs nicht signifikant, aber dennoch sehr plausibel.

Betrachtet man den jährlichen Verlauf jener Fläche der Alpen, die im Mittel (1961-2010)

oberhalb der Medianschneelinie zu finden ist, so erkennt man, dass der Zeitreihe nebst starkem Rauschen ein schwach negativer Trend (rund -7%/10yr) überlagert ist. Vor allem aber stechen einzelne Jahre heraus: 1963 zeichnet sich durch eine Verdopplung der Fläche oberhalb der Medianschneelinie aus, 2007 betrug die Fläche nur 55% des langjährigen Mittels.

Überprüft man die Qualität der Ergebnisse an einer *einzelnen Klimastation* wie z.B. Innsbruck Flugplatz auf 579m Seehöhe, zeigt sich zum einen, dass die *Modellwerte* der jährlichen Schneelinie, die der beobachteten Schneebedeckungsdauer entsprechen, *in Einzeljahren deutlich von der tatsächlichen Schneelinie abweichen.* Zum anderen wird in Innsbruck eine positive *systematische Abweichung* von rund 130m sichtbar. Diese, im Grunde leicht korrigierbare Verschiebung bedeutet, dass das Modell die Schneebedeckungsverhältnisse in Innsbruck so darstellt, als wäre die Station 130m höher gelegen als dies tatsächlich der Fall ist. An anderen Stationen gibt es aber auch negative systematische Abweichungen. Insgesamt sind die *systematische Abweichungen zufriedenstellend klein.*

Als letzter Punkt in der Arbeit wurden die *zeitlichen Trends* der Schneebedeckung und der Schneelinien diskutiert. Mit dem *positiven, aber deutlich insignifikanten Trend in der großräumigen Klimatemperatur* (1961-2010, Winter: 0.30±0.17°C) lassen sich mit den zugehörigen Sensitivitäten die Trends von Schneebedeckung und Schneelinienfeld berechnen. *Ersterer* ist gemäß der Erwartung *leicht negativ*, *Zweiterer* hingegen *leicht positiv.* Vergleicht man den direkt, ohne Modellvorstellung, aus den relativen Schneebedeckungswerten in einem Höhenintervall um die Medianschneelinie ermittelten (maximalen) Trend von rund -0.033/10a mit dem errechneten Trend von rund -0.054/10a so sieht man, dass das *Modell, über das gesamte Untersuchungsgebiet und über die gesamte Untersuchungsepoche betrachtet, die Wirklichkeit gut wiedergibt.* Hat man nun einen verlässlichen Trend der Klimatemperatur, so lassen sich die zukünftigen Schneebedeckungsverhältnisse im Mittel abschätzen.

1.4 Schlussfolgerungen und Ausblick

Mit den ersten beiden Arbeiten wurde gezeigt, wie *historische Quellen* genutzt werden können, um *klimatologische Aussagen* zu gewinnen. Die Mitarbeit eines sachkundigen Historikers ist dabei unerlässlich, da wohl kaum ein Naturwissenschaftler in der Lage wäre, die vorhandene Information (Manuskripte) richtig zu interpretieren. Das Ergebnis der mühsamen Kleinarbeit (Fotografieren der Manuskripte, Transkription, Anordnung der Information in für die Weiterverarbeitung geeignete Listen) brachte durchaus beachtliche Resultate hervor: Nahezu kontinuierliche *Weinlesedaten* für *1523-1879* und *1960-2007* (Wien und Klosterneuburg), *Weinblütedaten* für *1732-1879*, *Beerenweichedaten* für *1731-1879* und Aussagen über *Weinqualität* und *Weinquantität* für *1540-1879.*

Mit der simplen Technik der *linearen Regression* wurden aus den *Weinlesedaten Mai-Juni-Juli-Saisonmitteltemperaturen bzw. Dekadenmitteltemperaturen* gewonnen. Mit einem "Reduction of Error" von 0.7 und einer erklärten Varianz von 70 % in der Kalibrierungsperiode 1775-1850 scheint diese einfache Herangehensweise gerechtfertigt. Dass der "Reduction of Error" in der Verifikationsperiode 1851-1879 nur bei 0.32 liegt, wird durch einen Blick auf die "Running Correlations" verständlich und dieser Wert könnte für die Rekonstruktion durchaus als unteres Limit angesehen werden. An dieser Stelle wirft sich allerdings die Frage auf, welche Ursache den *Schwankungen der Korrelation* zugrunde liegt. Diese Frage lässt sich jedoch bis dato ebenso wenig beantworten wie die Frage, ob es in früherer Zeit (Bürgerspitalreihe) einen *schleichenden,*

praktisch nicht feststellbaren Wandel in den Weinbaupraktiken gab, der die *Korrelation systematisch nachteilig* beeinflusst. Die Tatsache, dass es sich bei Weinlesedaten um *paraphänologische* Information handelt, ist wahrscheinlich deren *größte Schwäche*, wobei sich die Folgen nicht quantifizieren lassen. Selbst wenn man mehrere *Metadaten* (z.B. Sortenwechsel, Kriegseinflüsse, Feste) zur Verfügung hat, bleiben noch immer die nachteiligen Effekte von ganz langsam, nahezu unbemerkt ablaufenden Prozessen, wie ein geänderter Geschmack der Konsumenten oder Verbesserungen in der Infrastruktur (Motorisierung, Straßenbau) bestehen.

Das eben Gesagte trifft auch auf die Parameter *Weinqualität* und in begrenztem Maße auch auf die *Weinquantität* (Änderung der Anbaufläche) zu, wenngleich Letztere aufgrund ihrer *Sensibilität gegenüber Einmalereignissen* (z.B. Frost und Hagel) für Klimaaussagen nicht wirklich herangezogen werden kann. Der *optimale Fall* wären *Blüh(beginn)daten*, die eindeutig einer *Sorte zugeordnet* werden können und aus einem *einzigen Weingarten* stammen. In diesem Fall würde es sich um *direkte phänologische Daten* handeln. Eine derartige Reihe in einem Archiv zu finden ist aber recht unwahrscheinlich, zumal die Lese für die Winzer größere Bedeutung als die Blüte hat und daher Letztere viel eher notiert wurde. *Beerenweichedaten* sind wiederum sehr *subjektiv* geprägt und der Begriff "Beerenweiche" ist kaum eindeutig definierbar und hat sich im Laufe der Zeit auch geändert. Somit kann die *publizierte Temperaturreihe* nur als *eine unter vielen Abschätzungen* des Temperaturverlaufes zwischen dem 16. Jahrhundert und dem Beginn von Temperaturmessungen angesehen werden.

Die gleichen Einschränkungen gelten auch bei der Abschätzung von Extremwerten der Mitteltemperaturen im Spätfrühling bzw. im Frühsommer der Vergangenheit mithilfe von Weinlesedaten. Wählt man etwa für die österreichischen Lesedaten eine Referenzperiode vor dem 20. Jahrhundert und wendet diese auf Lesedaten der letzten Jahrzehnte an, so wird aufgrund *vieler stark positiver Abweichungen* und nur *schwacher negativer Abweichungen* bei *gleichzeitig gestiegener Temperatur* unmittelbar klar, dass der *menschliche Einfluss* auf die Weinlese das *Bild verzerrt*. Andererseits scheinen andere Weinbauregionen in Europa nicht/wesentlich schwächer von einer derartigen Veränderung in den Weinbaupraktiken- zumindest in der vorliegenden Untersuchungsperiode- betroffen zu sein. Jedenfalls stellen die *Lesedaten* aber eine wertvolle *Ergänzung zu den rein deskriptiven, ebenfalls subjektive beeinflussten, Quellen* dar. Somit ist es wichtig, diese in den Archiven der einzelnen Länder auch weiterhin aufzuspüren und einer internationalen Community zugänglich zu machen, um eine möglichst realitätsnahe Beschreibung der Klimavergangenheit aus all diesen "Bausteinen" zu erhalten.

In den anderen drei Arbeiten wurde das *Konzept der Schneelinien* entwickelt, vertieft und in einer interfakultativen Zusammenarbeit auf eine Vegetationsgrenze, das *alpin-nivale Ökoton*, angewendet. Essentiell dabei ist das *Ersetzen der Stationsmitteltemperaturen* in der Anpassung der nichtlinearen *Zustandsfunktion der Schneedauer* durch die *Gebirgstemperatur*. Diese *lineare Entwicklung der Klimatemperatur nach den Stationskoordinaten separiert den großskaligen Klimaeinfluss vom Einfluss der geographischen Position* auf die Schneebedeckung und macht so das Schneelinienfeld überhaupt erst verfügbar. Durch die Anpassung wird eine *Vielzahl von Messwerten* in wenigen, leicht verständlichen Parametern (inklusive den Schneelinienhöhen) *zusammengefasst* und der klimatologische Charakter in Bezug auf die Schneebedeckung oder die Vegetation einer Region (hier der Alpen) oder eines Berggipfels (hier der Schrankogel) greifbar gemacht. Die *Medianschneelinie* ist dabei ausgezeichnet, da sie das *Niveau maximaler Temperaturempfindlichkeit* markiert und zudem *im Sommer (JJA) mit der Höhenlage des alpin-nivalen Ökotons zusammenfällt*.

Wählt man kleine Schneebedeckungshöhen (5cm im Winter und 2cm im Sommer) erhält man für die Medianschneeline Höhen (je nach Datenbasis und Fitmethode 641m bzw. 793m im Winter und 2897m bzw. 3083m im Sommer), die sehr gut zu jenen Höhen für die beiden Medianlinien passen, die Hann (HANN, 1908) vor über 100 Jahren (bei einem kühleren Klima) ermittel hat (667m im Winter und 2575m im Sommer im Inntal). Darüber hinaus liefert die *erklärte Varianz mit Werten gleich oder größer als 50%* einen eindeutigen Beleg dafür, dass das in den Publikationen präsentierte *Verfahren vor allem für Schneehöhen bis ca. 10cm geeignet* ist.

Die Einschränkungen der Methode ergeben sich in zweierlei Hinsicht: Zum einen ist der *Datenumfang im Sommer* oder aber *im Winter bei Schneehöhen deutlich jenseits der 10cm* selbst bei Betrachtung der gesamten Alpen sowohl *quantitativ als auch qualitativ stark reduziert*. Dies liegt im Sommer weniger an einem Mangel an Klimastationen, sondern einfach daran, dass selbst die höchsten Alpengipfel schlicht und einfach zu niedrig sind, um ausreichend Schnee beobachten zu können. Das Problem mangelnder Datenverfügbarkeit trat in Form von *enormen Unsicherheiten der Parameter* bei den Vegetationsdaten, wo für die gezeigten Auswertungen nur zwei Beobachtungsjahre an einer einzelnen Bergflanke zur Verfügung standen, verstärkt hervor. *Satellitenmessungen* (wie z.B. jene von MODIS) sind, was die Schneebedeckung betrifft, bei entsprechender Länge der Zeitreihen sowohl im Sommer als auch im Winter wichtige Datenquellen, die *in zunehmendem Maß an Bedeutung gewinnen*. Einer allfällige Kritik, dass die zwischen Ökoton und Medianschneelinie des Sommers gefundene Übereinstimmung bloß ein Zufallsergebnis für einen Berggipfel wäre, kann letztendlich nur durch weitere Forschung auf diesem Gebiet entgegnet werden. Nichtdestotrotz wurde durch die statistische Analyse auf Basis einer Modellfunktion ein *Werkzeug geschaffen*, um den *Zusammenhang von Sommerschnee und nivaler Vegetation dynamisch zu analysieren*.

Die andere Einschränkung der Methode resultiert aus der grundsätzlichen Annahme, dass die *Schneebedeckung nur von der Temperatur gesteuert* wird. Selbst wenn sich *andere Einflüsse* über die *gesamten Alpen* betrachtet, aber auch teilweise im *langjährigen Mittel an Einzelstationen*, als *Rauschen* präsentieren, wie das in der Arbeit HANTEL et al. (2012) anhand der Verteilung der Residuen der Gebirgstemperatur gezeigt wird, sind an *einzelnen Stationen* (und da vor allem in Einzeljahren) *Niederschlag und Exposition* sicher *nicht zu vernachlässigende Einflüsse*, die mit *steigender Höhe und Komplexität der Orographie zunehmen*. Im Hinblick auf eine praktische Nutzung des Schneelinienkonzeptes, könnte eine *Parametrisierung der Exposition*, ähnlich wie das im Appendix für eine Flanke des Schrankogels gezeigt wird, erfolgreich sein. Den Niederschlag neben der Temperatur als zweiten zeitabhängigen Prädiktor miteinzubeziehen, dürfte hingegen wenig erfolgversprechend sein, da saisonale Prognosen des Niederschlags nicht seriös sind. Hier stößt man bereits bei der Temperatur sehr rasch an die Grenzen des Machbaren, sodass *bei der gegebenen Qualität der langfristigen Temperaturprognosen* eine *prognostische Anwendung des Modells* für einzelne Saisonen *unabhängig von seinen inherenten Unzulänglichkeiten* momentan noch *keinen großen Mehrwert* hat.

BACCHUS temperature reconstruction for the period 16th to 18th centuries from Viennese and Klosterneuburg grape harvest dates

C. Maurer, E. Koch, C. Hammerl, T. Hammerl and E. Pokorny

J. Geophys. Res., 2009, **114**, D22106

JOURNAL OF GEOPHYSICAL RESEARCH, VOL. 114, D22106, doi:10.1029/2009JD011730, 2009

BACCHUS temperature reconstruction for the period 16th to 18th centuries from Viennese and Klosterneuburg grape harvest dates

C. Maurer,[1] E. Koch,[1] C. Hammerl,[1] T. Hammerl,[1] and E. Pokorny[1]

Received 8 January 2009; revised 23 July 2009; accepted 13 August 2009; published 24 November 2009.

[1] In the scientific project "Klosterneuburg Wine and Climate Change in Lower Austria" (BACCHUS), we focused on developing a grape harvest date (GHD) time series for the period 1523–2007 in the area of and around Vienna, one of the northeasternmost regions in Europe where vines are grown professionally. Since grape harvest dates are strongly influenced by spring to (early) summer temperatures, especially in a vine-growing region at a climatic border, we found highly significant correlation coefficients between homogenized multiple monthly mean temperatures at Vienna, Hohe Warte, and GHD. For example, correlation values reach -0.76 ($p = 0.01$) between GHD and April to July mean temperature or -0.79 ($p = 0.01$) between GHD and May to July mean temperature. This made it possible to reconstruct May to July mean temperatures, starting in 1523. The years from 1775 to 1850 were used as calibration period for determining the temperature sensitivity of GHD, as the running correlation coefficients (10 year moving window) were most pronounced in this period, varying between almost -1 and -0.7 ($p = 0.05$). We found warm decades in the 16th century, at the beginning of our series, which were as warm as the 1990s. Afterwards the mean May to July temperatures started to drop; the coldest decade of the record was from 1771 to 1780. A constant temperature increase for more than 30 years, as from the 1970s to the present, seems to be unprecedented during the last 470 years.

Citation: Maurer, C., E. Koch, C. Hammerl, T. Hammerl, and E. Pokorny (2009), BACCHUS temperature reconstruction for the period 16th to 18th centuries from Viennese and Klosterneuburg grape harvest dates, *J. Geophys. Res.*, *114*, D22106, doi:10.1029/2009JD011730.

1. Introduction

[2] A reliable reconstruction of the climate prevalent in preinstrumental times is of great importance in an age of apparently rapid climatic change. Many attempts have already been made to gain information about temperature conditions in Europe during past centuries [e.g., *Pfister et al.*, 2001; *Briffa et al.*, 2002; *Shabalova and van Engelen*, 2003; *Chuine et al.*, 2004; *Luterbacher et al.*, 2004, 2007; *Xoplaki et al.*, 2005; *Guiot et al.*, 2005; *Brázdil et al.*, 2005; *Büntgen et al.*, 2006; *Meier et al.*, 2007; *Casty et al.*, 2005a, 2005b; *Moberg et al.*, 2005; *Etien et al.*, 2008; *Böhm et al.*, 2009]. Their main targets are to check the significance of variability simulated by climate models and to detect and quantify anthropogenic effects [*Intergovernmental Panel on Climate Change* (*IPCC*), 2007].

[3] There are two main sources for climate proxies: human and natural archives. Natural archives are for instance coral reefs or tree rings. Human archives are historical documents as annals, weather diaries or legal acts. Here we concentrated on paraphenological, phenological and enological data which we found in libraries and historical archives in and around Vienna, Austria. Thus we could use both types of sources combining their advantages: absolute numerical values of natural proxies and the distinct time stamp from the chronicles.

[4] Reconstructions based on natural proxies do not suffer from the overflattening of the low frequency signal as reconstructions based on documentary evidence do. In the latter case the author can only refer to his own memory within a relatively short lifespan. The description "warmer/colder than usual" is relative, subjective and based on an experience covering only some decades. Reconstructions based on natural proxies are more consistent in time and the proxies offer absolute values (e.g. tree ring density, date of flowering or harvest) on an interannual time scale. But when using harvest dates, as we did, a short period of bad weather can cause a later harvest date than optimum physiological ripeness would let us expect it. And during several centuries there might have been some changes in the varieties of vines leading to a different temperature response.

[5] Paraphenological, phenological and enological data can be useful in establishing meaningful climate reconstructions, only if the data continuously span a long-term period including the instrumental era [*Pfister*, 1985]. Long parallel time series of instrumental and proxy records are necessary to set up stable correlations between both records enabling a calibration of the noninstrumental data.

[1] Zentralanstalt für Meteorologie und Geodynamik, Vienna, Austria.

0148-0227/09/2009JD011730$09.00

[6] We built up a grape harvest date (GHD) time series for the area of (and around) Vienna (mean date at Klosterneuburg and Vienna between 5 and 14 October, depending on the time span considered) for the period 1523–2007. Information pertaining to subperiods within this overall time span is presented in this paper, which deals not only with the climate of the past, but also with aspects of changing vine growing practices and their consequences for the reliability of proxy data. We drew on primary and secondary sources rather than using materials already published, in order to start reconstructions from the basic data and to avoid mistakes arising from later transcriptions and editions (secondary literature). This entails the possibility of collecting additional proxy data, which are analyzed in the present study and may be used in future, for example flowering (mean date at Klosterneuburg of 8 June) or the ''mellowness'' (mean date at Klosterneuburg of 14 August) of grapes referred to in one Klosterneuburg chronicle. Harvest, flowering and mellowness dates are specified as number of days from 1 January onwards.

[7] As harvest dates and mellowness dates can be used for reconstructing (early) mean summer temperatures, flowering dates allow for the reconstruction of spring mean temperatures. We focused on temperature because it has the most significant impact on vegetation in temperate and cold climates [*Rutishauser et al.*, 2007], especially if the considered genus, such as grape vine, grows at the border of its distribution area [*Landsteiner*, 1999]. Late spring and early summer temperatures are decisive seasons for plant development, agriculture and thus for climate impact studies based on phenological observations [*Menzel et al.*, 2006; *Defila*, 2003; *Chmielewski and Rötzer*, 2001]. Furthermore temperature is recognized as one of the most important parameters for climate analysis. The date of the harvest depends to a great deal on the temperature of the preceding months. The correlation of GHD with (a combination of) mean temperatures of the foregoing months was successfully used already, for instance, by *Chuine et al.* [2004] and *Meier et al.* [2007], who studied the GHD series of France and the Swiss Plateau respectively. Since vines do not start growing until a temperature level of about 12 to 15°C [*Pfister*, 1985] is reached, the temperature influence slowly increases at the end of March and gradually declines at the end of September. Nevertheless, September temperatures and duration of sunshine [*Bauer*, 2008] play an important role in augmenting the sugar content of the grapes. August temperatures evidently have little influence on GHD, because three to six weeks after pollination the vines stop growing [*Pfister*, 1985]; thus GHD are assumed to be predominantly influenced by spring to (early) summer temperatures [*Lauscher*, 1983; *Pfister*, 1985; *Meier*, 2007]. Therefore this work aims at quantifying correlations between these temperatures and GHD as well as parameters that are correlated to the latter (like flowering and mellowness).

[8] Dates of vine flowering and mellowness of grapes would generally be preferable for temperature reconstructions, because they are less influenced by the activities of the vine grower and by weather conditions at harvest time. In years when the harvest is late, it can be impaired by snow or frost [*Pfister*, 1985], and flowering dates are more consistent among different varieties [*Meier*, 2007]. Records of these dates, however, are much more fragmentary than those about harvests and thus could not be used for the temperature reconstruction in our present study. The anthropogenic influence gives rise to an uncertainty, which is extremely difficult to quantify [*Etien et al.*, 2008]. This is discussed later when comparing ''modern'' series with ''historical'' ones.

2. Data

[9] Different sources were investigated to create ''wine'' time series for Vienna and the neighboring Klosterneuburg (Lower Austria). The terms ''historical'' and ''modern'' refer to data collected for the periods from 1523 to 1879 and 1960 to 2007, respectively. We worked exclusively with original primary or secondary sources in order to start reconstructions from the basic data and to avoid mistakes, which may arise using secondary literature only.

2.1. Data for Klosterneuburg

[10] Klosterneuburg (48°18′N, 16°20′E) is a city in Lower Austria, with a current population of 24,442. It is located at the Danube, in the close vicinity of Vienna. Klosterneuburg has always been a center for vine growing. In the middle of the 19th century it was a small vinegrower's town with about 5,000 inhabitants. Klosterneuburg belongs to the Pannonian climate zone. Predominant soils are residual soils from sandrocks of the Tertiary, partially layered by loess. One can find also some pure loess soils, or loess soils partially more sandy or limey.

[11] Relevant manuscript (MS) sources were studied in the archives of the Klosterneuburg monastery; the information used for reconstructing temperature came from Manuscript 121: ''Gedenkbuch und Weinchronik,'' a wine chronicle written by Josef Bittmann, Klosterneuburg, in 1880. Bittmann used his own records and older records of different writers to compile his ''wine chronicle''. It contains highly detailed information about vine growing from 1540 to 1879; in our study this period is defined as ''historical.'' The wine chronicle was passed on from one family member to another. Josef Bittmann, born in 1812, copied and continued the chronicle of his father Matthias for the period 1836–1880. Matthias copied and continued the chronicle of his brother-in-law Leopold Köttner for the period 1800–1836. Leopold Köttner wrote his chronicle for 1777–1800 and partially gained information from his grandfather Kasper Köttner, who wrote the chronicle for 1730–1777.

[12] Further, we read through Manuscript 102, a chronicle covering the time span from 1577 to 1742 written in 1775, copying information from so called ''Schreibkalender''; Manuscript 122/1, a contemporary chronicle from 1781 to 1813, reporting national and international events; Manuscript 122/2, a continuation of 122/1 from 1813 to 1833; Manuscript D 73, a contemporary chronicle from 1796 to 1803 of the monastery St. Dorothea in Vienna; and Box 221, Wetter und Zufällechronik, compiled by Willibald Leyrer in 1789. Leyrer was archivist at the monastery of Klosterneuburg, which means that he used original sources stored in the archives for his compilation. We got information for the time span 1322 to 1691.

[13] We also had a look into chronicles or compilations of older sources concerning Klosterneuburg, for instance, records concerning legal acts or administration, as well as statements of account of the 18th century, but they contained only little relevant information. No germane information is available for the period from 1880 to 1969.

[14] Only GHD for the so-called "modern" period from 1970 to 2007 are available. They were compiled at Lehr- und Forschungszentrum für Wein- und Obstbau Klosterneuburg [*Sommer*, 2008] from the original material (B. Schmuckenschlager, Lesedaten Agneshof Klosterneuburg (manuscript)).

[15] Apart from general information about weather and climate, specific information was collected about vintage, vine flowering, "mellowness" of grapes, wine quality and wine quantity, but no remarks could be found concerning vine varieties in the "historical" period, in contrast to the Burgundy series, where Pinot noir has been grown since the 14th century [*Robinson et al.*, 1999].

2.2. Data for Vienna

[16] Vienna, the capital of Austria, located in northeastern Austria, at the easternmost extension of the Alps into the Vienna Basin, has a long history in vine growing. Grape seed findings prove that already the Celts and the Illyrians produced wine 500 years B.C. in the Vienna area. The Romans introduced cultivated vine growing to the city. Until the late Middle Ages, vines were grown inside the ramparts of Vienna. Today's vineyards are situated mainly on the outskirts of Vienna. Vine growing with about 700 ha in Vienna, plays an important economic role. In the mid 18th century the population of Vienna was about 175,000. It increased to more than 2 million inhabitants in the course of the 19th century as long as Vienna was the capital of the Austro-Hungarian monarchy. Today Vienna has about 1.7 million inhabitants. Vienna is in the same climate zone as Klosterneuburg. Annual temperature, sunshine duration and precipitation (1961–1990) average 9.7°C, 1919 h and 607 mm. Shale, gravel, clay and loess are predominant soils.

[17] For the Vienna series a comprehensive reliable secondary source, a standard work, [*Pribram et al.*, 1938] was used for the "historical" period 1523–1785 (Vienna/Buergerspital). Pribram evaluated primary sources, which can be inspected at the municipal and state archives of Vienna. For the period of 1786 to 1959 no relevant information is available.

[18] Data of the "modern" period 1960–1999 again stem from the Lehr- und Forschungszentrum für Wein- und Obstbau Klosterneuburg [*Sommer*, 2008] and were extracted from the original material (Mitteilungen Klosterneuburg 1962–2000).

[19] Data from the sources *Pribram et al.* [1938] and *Sommer* [2008] about vintage for the periods 1523–1749 (σ = 8.9 days) and 1960–1999 (σ = 9.9 days), about wine quality for the period 1540–1785 and about wine quantity for the period 1540–1785 were obtained for Vienna/Buergerspital and used for our investigations. Data for Klosterneuburg (MS 102, MS 121, MS 122/1, 122/2, D73, Box 221) are about vintage in the periods 1668–1879 (σ = 8.3 days) and 1970–2007 (σ = 9.9 days), about vine flowering in the period 1732–1878 (σ = 9.0 days), about "mellowness" of grapes in the period 1732–1879 (σ = 12.3 days), about wine quality in the period 1668–1879 and about wine quantity in the period 1668–1879, but were used for our present study only from MS 121 and *Sommer* [2008]. See Figures 1a and 1b for the "historical" period.

2.3. Temperature Data

[20] Instrumental monthly temperature station data for Hohe Warte, Vienna (starting in 1775), are derived from the Historical Instrumental Climatological Surface Time Series of the Greater Alpine Region (HISTALP) data collection [*Auer et al.*, 2007] in the bias-corrected version 2008 [*Böhm et al.*, 2009].

3. Methods

3.1. Different Grape Harvest Time Series

[21] The data series concerning the Vienna/Buergerspital GHD (1523–1749 and 1960–1999) and the Klosterneuburg GHD (1730–1879 and 1970–2007), as well as vine flowering (1732–1878) and grape mellowness (1732–1879) were evaluated first to get an overview of the continuousness and the decadal variations of these (para-) phenological data. The "modern" Klosterneuburg data consist of median values calculated from the harvest dates of four different vine varieties. Figure 2 shows Gaussian 10 years low pass filtered GHD from Vienna and Klosterneuburg as well as from Burgundy [*Chuine et al.*, 2004] and from the Swiss Plateau Region [*Meier et al.*, 2007]; gaps result from missing data.

3.2. Indices of Quality and Quantity

[22] Subsequently indices of quality and quantity were assigned to the descriptive information concerning these two parameters. Quality was defined by numbers 1 to 4: 1 was used for a "bad", 2 for a "mediocre", 3 for a "good" and 4 for a "very good" quality of wine. Quantity was also labeled by numbers 1 to 4 for Klosterneuburg: 1 stands for a harvest of "low", 2 for one of "mediocre", 3 for one of "good" and 4 for one of "rich" quantity. For Vienna/Buergerspital the numbers 1 to 3 were used: 1 stands for a harvest of "low", 2 for one of "mediocre" and 3 for one of "high" quantity. These parameters are available at present only for the "historical" periods.

3.3. Linear Correlations

[23] Linear correlation coefficients (R) between several parameters were calculated together with their levels of significance. When ordinally scaled index data were involved, the correlation coefficients were calculated according to Spearman instead of Pearson. Running correlations between GHD and different mean temperatures were evaluated for the period 1785 to 1879 (3 curves are discussed in the paper).

3.4. Combination of Adjacent Overlapping Grape Harvest Series

[24] For the overlapping periods of Buergerspital and of Klosterneuburg, GHD were submitted to a two sample t test, in order to clarify if the two sets of data belong to the same population. The latter condition must be met when using the two different time series, as if it was one continuous data

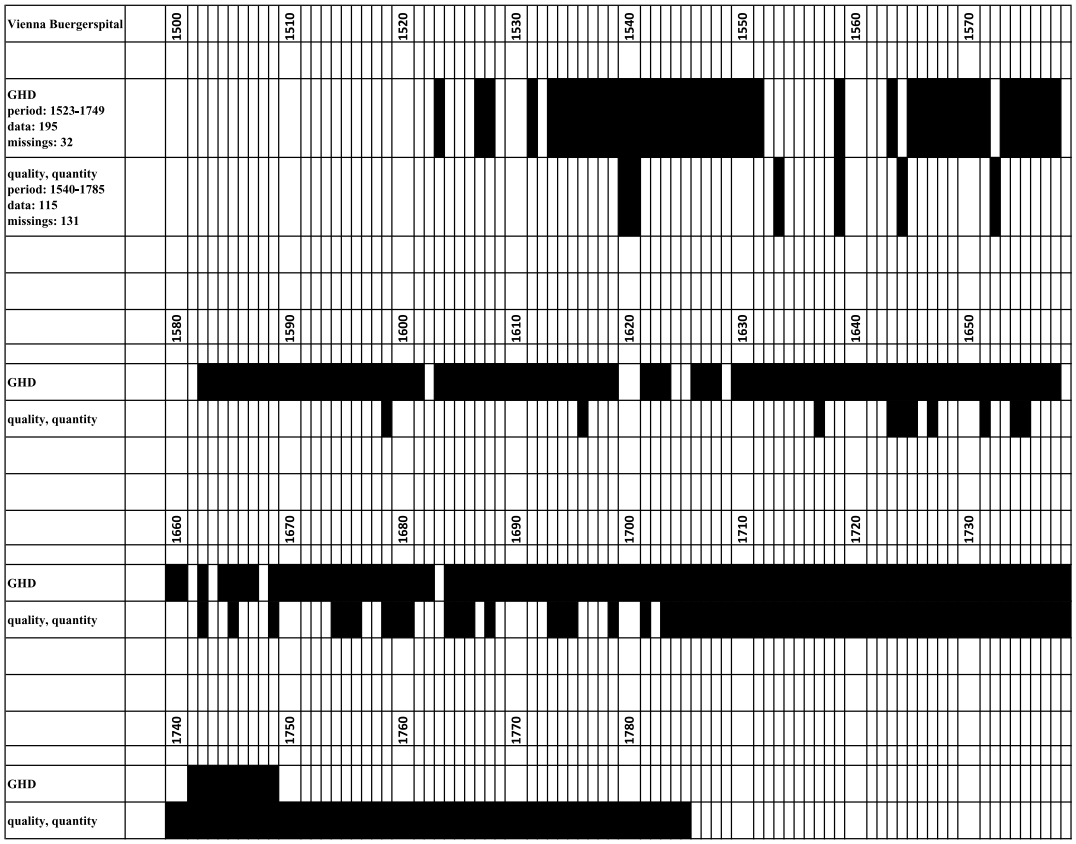

Figure 1a. "Historical" period where information was available (black) and gaps (white) of information in the Vienna/Buergerspital data.

set. The same kind of test was also employed to verify if mean GHD and, if available, mean May to July temperatures on both sites experienced a significant shift when turning from a "historical" 30 year period to a "modern" one.

3.5. Temperature Reconstruction

[25] We tried to reconstruct the mean decadal May to July temperatures back to 1523 at Hohe Warte, Vienna, with the help of the Buergerspital and Klosterneuburg GHD. These two different harvest series can be considered as a single row, as is shown in section 4.3. The GHD and the temperature measurements overlap between 1775 and 1879. 1775–1850 was used as calibration period and 1851–1879 as verification period. This enabled us to reconstruct the mean decadal May to July temperatures for more than 250 years back in history. The reduction of error *RE* [*Meier*, 2007], defined as

$$RE = 1.0 - \frac{\sum_{i=1}^{n} (x_i - x_{ri})^2}{\sum_{i=1}^{n} (x_i - \bar{x}_c)^2} \quad (1)$$

with x_i being the observed value, x_{ri} being the reconstructed value and $\bar{x}_c$ being the mean of the observed data during the calibration period was determined in order to check the reconstruction skill.

3.6. Spectral Analysis

[26] Furthermore, we performed a discrete Fourier transformation for comparing the spectral content (normalized power spectrum) of the observed and the reconstructed temperatures in the period 1775 to 1879. Given a sampling frequency of one year, the Nyquist frequency $f_{Ny} = 1/2\Delta t$, where Δt is the sampling interval [*Yilmaz and Doherty*, 1994], adds up to 0.5 yr^{-1}, conforming to a period of two years.

3.7. Comparison to Other Recent Reconstructions

[27] Finally, we compared our reconstructed May to July mean temperature values from the decade 1661–1670 to the decade 1871–1880 (May to July mean temperatures can be calculated with the help of monthly values) with the data from *Casty et al.* [2005a, 2005b]. These authors used a combination of long instrumental station data and documentary proxy evidence, applying principal component regression analysis to reconstruct seasonal (before 1661)

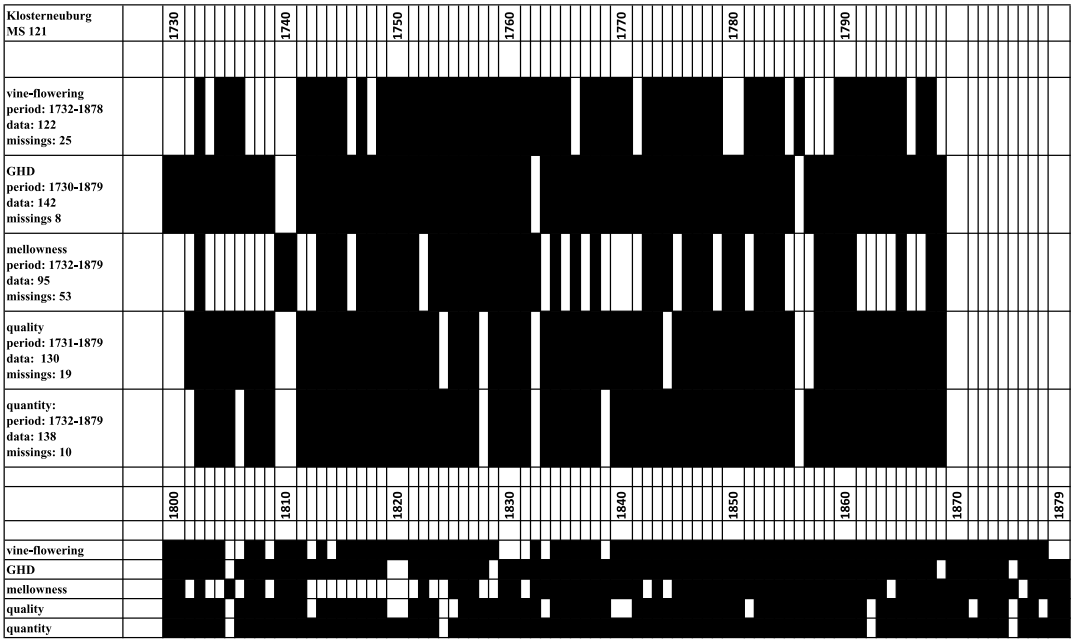

Figure 1b. "Historical" period where information was available (black) and gaps (white) of information in the MS 121 Klosterneuburg data.

and monthly (until 1900) mean values of temperature and precipitation back to 1500. From 1901 up to 2000 *Casty et al.*'s [2005a, 2005b] data is equivalent to the Climatic Research Unit Time Series version 2 (CRU TS 2.0) data set.

[28] In addition we contrasted our temperature reconstruction to a most recent one for Central Europe done by *Dobrovolný et al.* [2009]. They developed a mean monthly temperature reconstruction between 1500 and 1759 (afterwards instrumental records until 2007) from documentary index series from Germany, Switzerland and the Czech Republic.

4. Results

4.1. Linear Correlations

[29] Tables 1a, 1b, and 1c show some important linear correlation coefficients together with their levels of significance for the "historical" (1523–1879) and the "modern" (1960–2007) periods. Correlations are investigated between

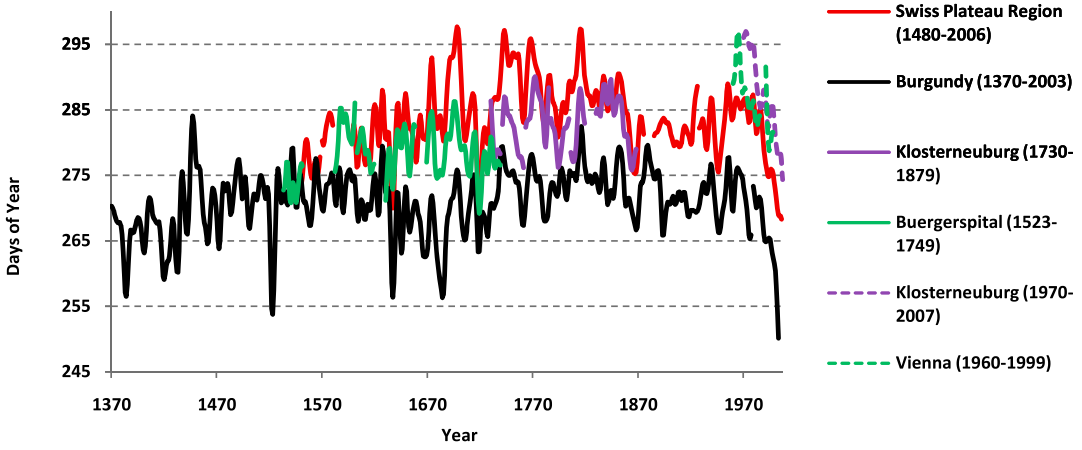

Figure 2. Comparison of Gauss-filtered grape harvest dates (days of year) per year for the Swiss Plateau Region, Burgundy, Klosterneuburg, and Buergerspital/Vienna.

Table 1a. Enological Parameters and (Para-) Phenological Phases to be Correlated, Value of Correlation Together With its Level of Significance, and R^2 [a]

Correlation	R (Level of Significance)	R^2
Quality Index−Harvest Date	−0.46 (99%)	0.21
Quality Index−Flowering Date	−0.37 (99%)	0.14
Quality Index−Mellowness Date	−0.51 (99%)	0.26
Quality Index−Harvest Date/Buergerspital	−0.51 (99%)	0.26
Quantity Index−Harvest Date	−0.23 (99%)	0.05
Quantity Index−Flowering Date	−0.23 (95%)	0.05
Quantity Index−Mellowness Date	−0.24 (95%)	0.06
Quantity Index−Harvest Date/Buergerspital	−0.30 (95%)	0.09
Price−Mellowness Date (1834−1879)	−0.49 (99%)	0.24
Number of Rain/Shower Events (sum from 1.4. until 31.10.)−Harvest Date	0.29 (99%)	0.09
Number of Rain/Shower Events (sum from 1.4. until 31.10.)−Flowering Date	0.34 (99%)	0.12

[a]If no location is mentioned, the values refer to Klosterneuburg.

enological parameters and (para-) phenological phases (Table 1a), between several mean temperatures and (para-) phenological phases or enological parameters (Table 1b) and between the (para-) phenological phases themselves (Table 1c). From Table 1a it becomes clear that the quality index and the quantity index are always negatively correlated with harvest, flowering and mellowness dates, reaching a maximum negative value of −0.46 in the case of quality and harvest date correlation at Klosterneuburg.

[30] Furthermore, mean monthly and mean seasonal surface temperatures constantly exhibit negative correlations to all (para-) phenological data (harvest, flowering and mellowness) and positive correlations to enological data (see Table 1b); a fact well known in the literature. In case of the "historical" period the two strongest correlations occur for mean May to July temperature and harvest date with a value of −0.79 and for mean April to July temperature and harvest date with a value of −0.76. In case of the "modern" period we find the two strongest correlations between mean April to July temperature and harvest date with a value of −0.89 and between May to July mean temperature and harvest date with a value of −0.87. Concerning the "100 day rule" assumed by e.g. *Chuine et al.* [2004] we get the result of 124 days mean difference (σ = 8.1 days) between flowering and harvest date. Looking at the correlation between these two phases, we find only a moderate value of 0.55. Harvest and flowering dates are even negatively correlated to mean annual temperatures (*Lauscher*, 1983); yielding a correlation coefficient in the "historical" period of −0.63 and −0.56 respectively.

[31] Since an advance of the (para-) phenological stages is accompanied by a high quality index and, although to a lesser extent, by a high quantity index on the one hand and by positive spring to early summer temperature anomalies on the other, a positive correlation coefficient between quality/quantity and spring to early summer temperatures can be expected. This was verified by two examples concerning the correlation between mean seasonal temperature from June to July (following the information given by *Pfister* [1985]) and the quality (R = 0.65) and quantity (R = 0.36) indices (see Table 1b).

4.2. Change in Vinification

[32] Since in 2003, when spring and early summer temperatures proved to be anomalously hot, the grape

Table 1b. Several Mean Temperatures and (Para-) Phenological Phases or Enological Parameters to be Correlated, Value of Correlation Together With its Level of Significance, and R^2 [a]

	Historic Data		Modern Data	
Correlation	R (Level of Significance)	R^2	R (Level of Significance)	R^2
Annual Mean Temperature−Harvest Date	**−0.63 (99%)**	**0.39**	**−0.69 (99%)** −0.39 (95%), Vienna	**0.48** 0.15, Vienna
Mean Temperature of April−Harvest Date	−0.25 (95%)	0.06	**−0.65 (99%)** not significant at 95%, Vienna	**0.42** not significant at 95%, Vienna
Mean Temperature of May−Harvest Date	−0.50 (99%)	0.25	**−0.72 (99%)** −0.57 (99%), Vienna	**0.51** 0.32, Vienna
Mean Temperature of June−Harvest Date	−0.55 (99%)	0.30	−0.59 (99%) −0.36 (95%), Vienna	0.35 0.13, Vienna
Mean Temperature of July−Harvest Date	**−0.63 (99%)**	**0.40**	−0.58 (99%) not significant at 95%, Vienna	0.34 not significant at 95%, Vienna
Mean Temperature of April to July−Harvest Date	**−0.76 (99%)**	**0.58**	**−0.89 (99%)** −0.58 (99%), Vienna	**0.79** 0.33, Vienna
Mean Temperature of May to June−Harvest Date	**−0.70 (99%)**	**0.48**	**−0.76 (99%)** **−0.61 (99%), Vienna**	**0.59** **0.38, Vienna**
Mean Temperature of May to July−Harvest Date	**−0.79 (99%)**	**0.63**	**−0.87 (99%)** −0.59 (99%), Vienna	**0.75** 0.35, Vienna
Annual Mean Temperature−Flowering Date	−0.56 (99%)	0.31		
Mean Temperature of May−Flowering Date	**−0.66 (99%)**	**0.44**		
Mean Temperature of March to May−Flowering Date	**−0.69 (99%)**	**0.47**		
Mean Temperature of June−Mellowness Date	−0.46 (99%)	0.22		
Mean Temperature of July−Mellowness Date	−0.47 (99%)	0.22		
Mean Temperature of June to July−Mellowness Date	−0.59 (99%)	0.35		
Mean Temperature of June to July−Quality Index	**0.65 (99%)**	**0.42**		
Mean Temperature of June to July−Quantity Index	0.36 (99%)	0.13		

[a]Correlations above an absolute value of 0.60 and their corresponding R^2 values are bold. If no location is mentioned, the values refer to Klosterneuburg.

Table 1c. Paraphenological and Phenological Phases to be Correlated, Value of Correlation Together With its Level of Significance, and R^2 [a]

Correlation	R (Level of Significance)	R^2
Flowering Date−Harvest Date	0.55 (99%)	0.31
Flowering Date−Mellowness Date	**0.75 (99%)**	**0.65**
Mellowness Date−Harvest Date	**0.67 (99%)**	**0.45**
Harvest Dates Klosterneuburg−Burgundy	0.52 (99%)	0.27
Harvest Dates Klosterneuburg−Swiss Plateau Region	0.54 (99%)	0.29
Harvest Dates Buergerspital−Burgundy	0.46 (99%)	0.39
Harvest Dates Buergerspital−Swiss Plateau Region	**0.65 (99%)**	**0.42**
Harvest Dates Burgundy−Swiss Plateau Region	**0.79 (99%)**	**0.62**

[a]Correlations above an absolute value of 0.60 and their corresponding R^2 values are bold. If no location is mentioned, the values refer to Klosterneuburg.

harvest at Klosterneuburg was advanced only by 19 days with regard to a reference period of 1775–1879 and thereby was surpassed by several other years (e.g. 1822) all showing advances of 20 or more days, we wanted to investigate if this fact indicated changing practices in viniculture in the region of Vienna. We have therefore considered means of 30 years, each with the "historical" and the "modern" period. As for the Buergerspital/Vienna, the mean harvest date of 1686–1715 (279.9) proves to be significantly different from the 1969–1999 mean (285.8, 1987 is missing) on the 99% level. Similarly, the mean harvest date of 1831–1860 at Klosterneuburg (285.8) differs on a 92% significance level from the one of 1970–1999 (289.6). Temperature means of the two periods at Klosterneuburg are actually different on the 99.5% level. The respective relative frequency distributions for Klosterneuburg are shown in Figures 3a and 3b.

[33] The trend of GHD during the "modern" period amounts to about 6 days advance per 10 years in Klosterneuburg and to about 3 days advance per 10 years in Vienna as can be seen in Figure 4, similar to the findings of *Menzel et al.* [2006]. According to Figure 5 the temperature sensitivity in the two subperiods 1831 to 1860 and 1970 to 1999 of the GHD to the mean May to July temperature changed from about 5.2 days earlier harvest per one degree Celsius increase to 7.9 days in the "modern" period. This points also to a change of viticulture/vinification from "historical" to "modern" times.

4.3. Combination of Adjacent Overlapping Grape Harvest Series

[34] Before combining the "historical" GHD from Vienna Buergerspital and Klosterneuburg to one single series for a temperature reconstruction back to the 16th century, we tested if a significant difference in the population mean could be found. With regard to the difference in the arithmetic mean of about 2 days in the overlapping period, a two-sample t test revealed that the null hypotheses of equal population means cannot be rejected. So there seems to be no systematic difference between the two different time series in the overlapping time span.

4.4. Temperature Reconstruction and Running Correlations

[35] The last part of this section is devoted to the reconstruction of the mean decadal May to July surface temperature at Hohe Warte, Vienna, with the help of the Buergerspital and Klosterneuburg GHD. In order to test the stability of the correlation between GHD and May to July mean temperature, we performed a running correlation calculation with moving correlation windows of 10 years. The result, shown in Figure 6, is rather astonishing: The correlation coefficients between grape harvest and May to July mean temperature (thick black curve) vary between nearly −1 around 1815 and about −0.4 between 1860 and

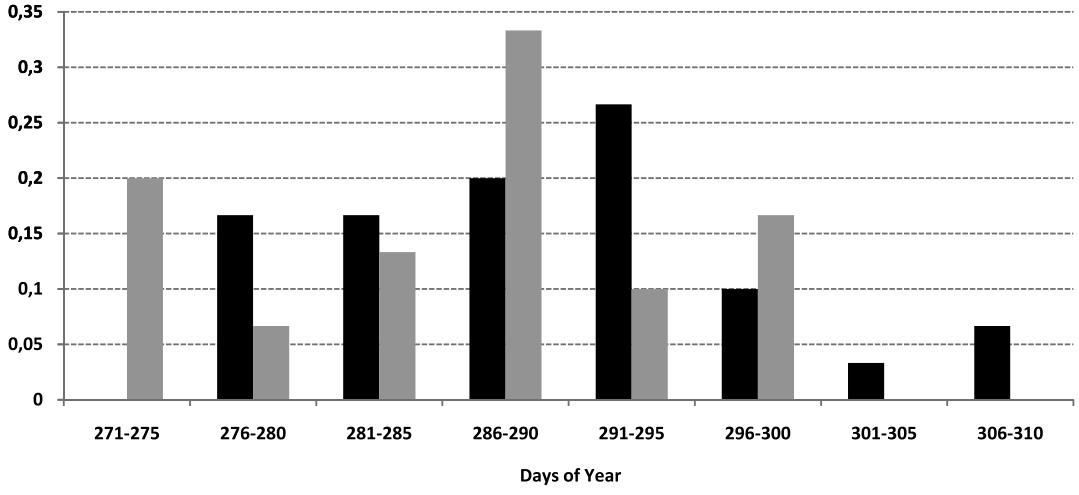

Figure 3a. Relative frequencies of grape harvest dates at Klosterneuburg during 1831–1860 (grey) and 1970–1999 (black).

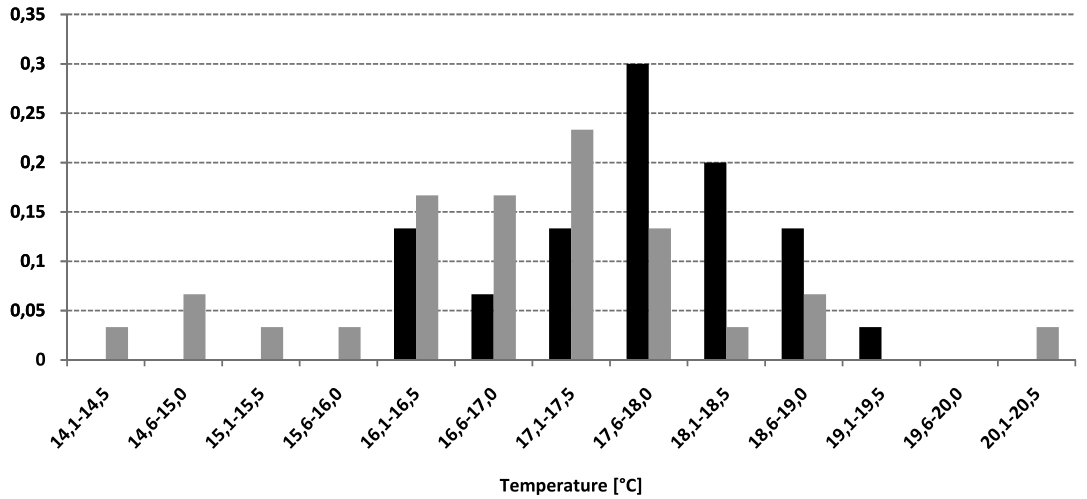

Figure 3b. Relative frequencies of May to July mean temperatures at Hohe Warte, Vienna, during 1831–1860 (grey) and 1970–1999 (black).

1870, thereby dropping below the 95% and even the 90% significance level. Looking at the sum of squared errors we can actually find a maximum in the corresponding decade (1861–1870) of the temperature reconstruction. The correlation between April to July mean temperatures and grape harvest (grey dashed curve) shows a very similar run, although with slightly more outliers. Correlation coefficients between the mean monthly temperature of June and harvest dates (thin black curve) vary extremely, ranging from about −0.9 around 1815 to 1830 to +0.5 around 1865.

[36] The details of the temperature reconstruction have already been described in section 3. The course of decadal temperatures can be seen in Figure 7. The calculation of the reduction of error *RE* gives values of 0.7 in the calibration period (1775–1850) and of 0.32 in the verification period (1851–1879), thereby surpassing the quality of the estimation given by the simple climatologic mean. A perfect reconstruction would be obtained when *RE* reaches a value of 1.0; a reconstruction only as good as the climatologic mean would yield a *RE* of 0.0.

4.5. Spectral Analysis

[37] Apart from judging our temperature reconstruction in terms of deviations of (tenth parts) degrees Celsius, we compared the normalized power spectra of reconstructed and observed temperatures. In general the same frequencies are emphasized in both spectra in Figure 8, but some peaks towards the long-period end (around 15 and 7 years) in the

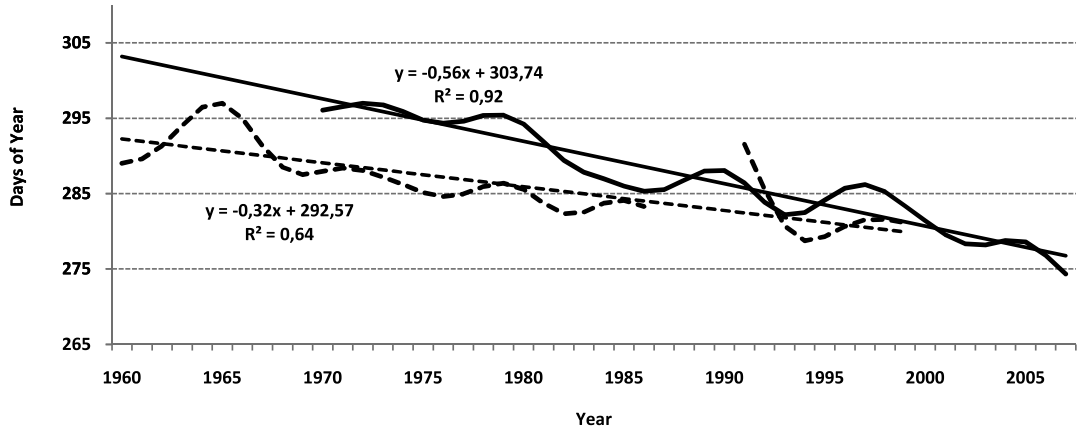

Figure 4. Gauss-filtered median grape harvest dates of four different varieties at Klosterneuburg (solid line, 1970–2007), and Gauss-filtered grape harvest dates at Vienna (dashed line, 1960–1999) together with their linear trends.

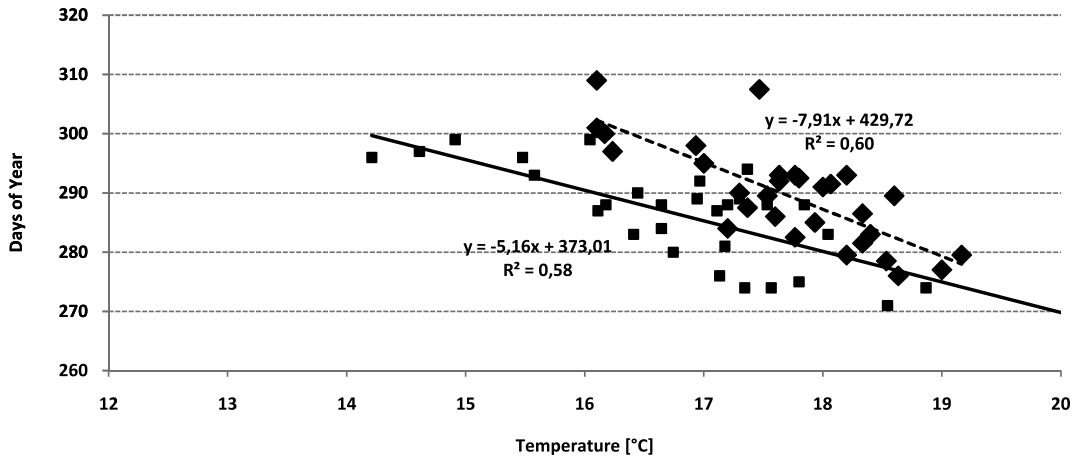

Figure 5. Grape harvest dates of Klosterneuburg plotted against mean May to July temperature for the "historical" 1831–1860 period (small squares) and the "modern" 1970–1999 period (big rhomboids) together with linear regression.

spectrum, belonging to the reconstructed temperatures, must be regarded as artificial. Both spectra exhibit their absolute, normalized maximum (1.0) at a period of 3.4 years.

5. Discussion

5.1. Data

[38] Klosterneuburg GHD before 1730 (starting in 1668) had to be neglected, since they are highly fragmentary and, moreover, stem from a different chronicle. A drawback of our times series is that there are no flowering or mellowness dates in the "historical" Buergerspital period, which would not be as much disturbed by human interaction as GHD are.

5.2. Linear Correlations

[39] The earlier the phenological phases and the harvest occur, the more and better grapes will be harvested. This relation is also highlighted, for example, by *Harflinger et al.* [2002]. The lower correlation with quantity results from the sensitivity of this parameter to local influences (e.g. frost during flowering or maturation, hail, strong winds, fungal decay, variety, age of the vines, fertilization) and from a known relationship to the midsummer temperatures of the previous year [*Pfister*, 1985, 1999]. Difficulties concerning the quality index stem from changed demands (which particularly complicates the indexing of "normal" or "medium" qualities [*Bauer*, 2008] in the course of decades

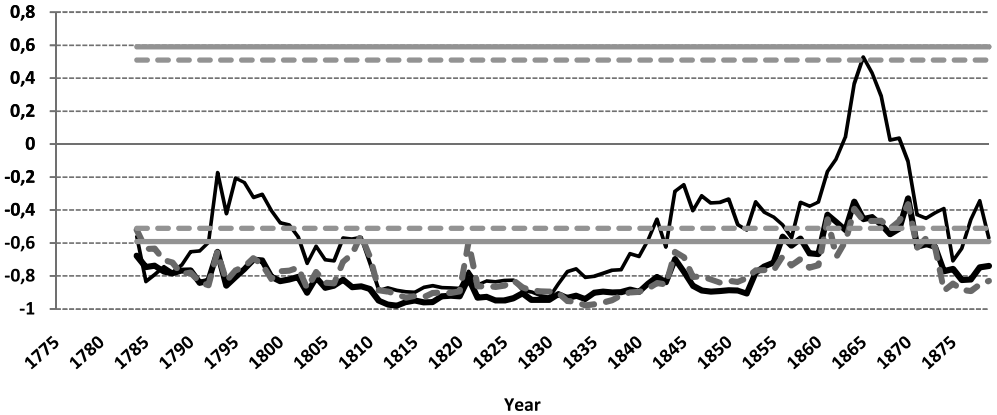

Figure 6. Running correlation between different mean temperatures and harvest dates for the period 1785–1879 using a moving 10 year window; black thick line is running correlation with May to July mean temperature, black thin line is running correlation with mean June temperature, grey thick dashed line is running correlation with April to July mean temperature, and horizontal grey solid and horizontal grey dashed lines are 95% and 90% significance level.

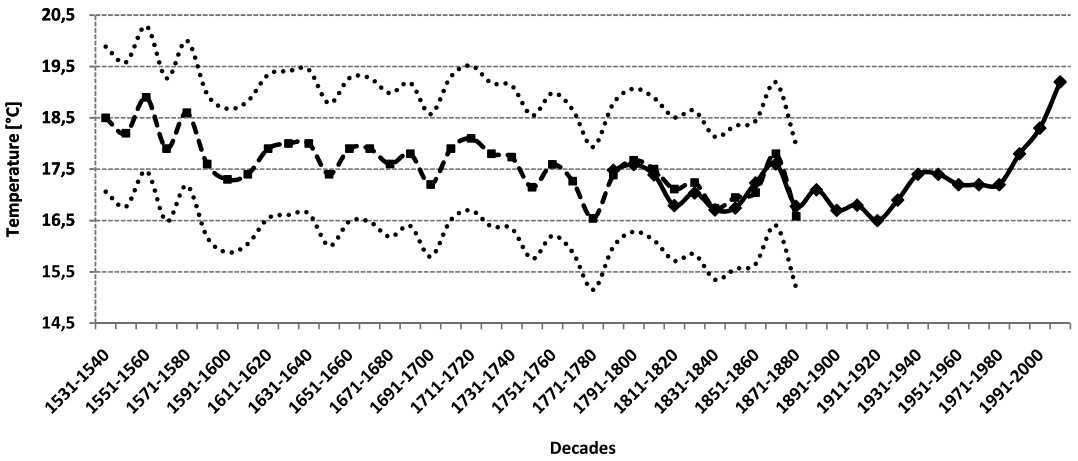

Figure 7. Observed (solid line, 1781–2007) and reconstructed (dashed line, 1531–1879) mean decadal May to July temperature at Hohe Warte, Vienna, together with uncertainty (dotted lines, 1531–1879) given a 95% confidence level.

and from modifications in viticulture (e.g. premature harvest or the cultivation of sour, but profit-yielding varieties in earlier times [*Pfister*, 1985]).

[40] Concerning the correlation of (para-) phenological phases to single or multi monthly mean temperatures, different information can be found with regard to the month(s) having the greatest impact on the respective parameter. In general, combining two or three months yields the best results. The "modern" Klosterneuburg period is characterized by the fact that seven out of eight correlation coefficients show a higher absolute value than the ones in the "historical" period, whereas with the "modern" Vienna data circumstances are the other way round (see Table 1b). We attributed this mainly to the nonmixed/mixed data concerning the different vine varieties. Mixing harvest dates from early and late varieties in the course of time evidently disturbs the correlation with temperature conditions. But the change, over centuries, of vine varieties in a certain vine-growing area must be seen as a fact. The climate signal, which can be extracted out of GHD, namely the correlation between this kind of proxy data and single to multimonthly mean temperatures, suffers a deterioration, independently from the accuracy of the individual observers in the course of time.

5.3. Change in Vinification

[41] The means of temperature and grape harvest dates develop in the same directions, when comparing the "historical" and the "modern" periods at Klosterneuburg. So we have to assume that practices in viniculture have altered. Looking at the "modern" period of Vienna, we

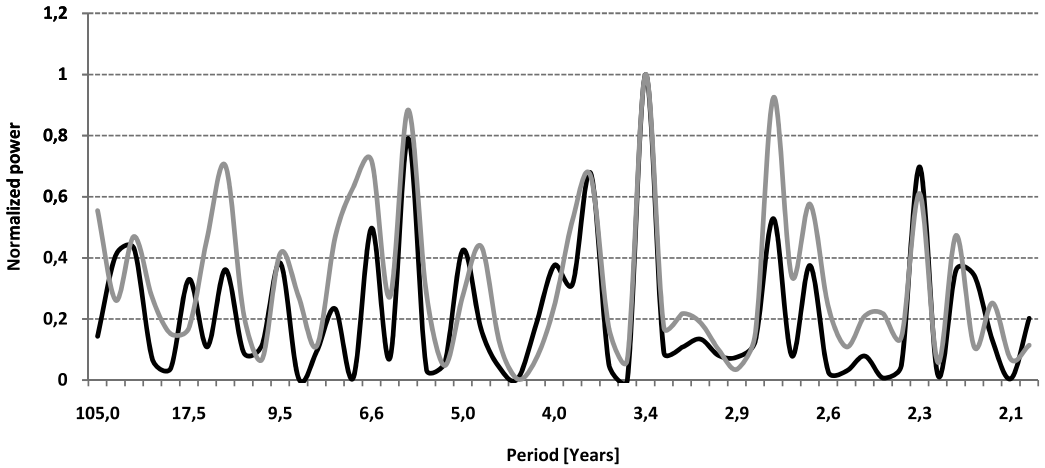

Figure 8. Normalized power spectra of observed (grey) and reconstructed (black) May to July mean temperatures from 1775–1879.

recognized 11 positive (later dates), but no negative (earlier) GHD anomalies exceeding the double standard deviation with respect to the 1645–1749 time span. Since the increase in the mean harvest date of about six days between the two subperiods is highly significant, it seems likely that at least some of the extreme anomalies are again caused by changing practices in viniculture. Nevertheless, a trend towards earlier harvest dates during the "modern" periods becomes clearly visible in Figure 4.

5.4. Temperature Reconstruction and Running Correlations

[42] The reconstruction criteria suggested by *Pfister* [1999] are met concerning the length of the overlapping period and the distance between the point of observation and the meteorological station. Also the preconditions for connecting two different (para-) phenological series, as demanded by *Pfister* [1985] are met, i.e. a comparable elevation of the sites observed and a useful correlation of the residuals: the vineyards are in similar altitudes and the significant correlation has a value of 0.52.

[43] May to July seasonal temperature was chosen for the reconstruction because it shows the highest overall correlation ($R = -0.79$) with GHD. The reason why the reconstruction of monthly mean temperatures must fail is best demonstrated by the running correlation between the mean monthly temperature of June and harvest dates (thin black curve in Figure 6). The course of the correlation curve is all the more remarkable because the correlation values scarcely reach the positive 90% significance level. Temperature data observed between 1775 and 1879 were used to fill the gaps within the GHD by linear regression. This improved the continuity of the running correlation curve. One might argue that correlating harvest dates to temperatures which had already been used for harvest date reconstruction, leads to creating artificially high correlations, but since only 6 out of 105 harvest dates are affected, this method seemed justifiable.

[44] A simple linear regression (as used by *Menzel* [2005] or *Meier et al.* [2007]) with GHD as the only predictor in part of the instrumental period (the calibration period), selected according to the results of the running correlations, is justified, since the correlation turns out to be really linear. No other type of regression yields a greater explained variance R^2 in the calibration period ($R^2 = 0.70$). Of course one might think of more sophisticated reconstruction methods, like the "inverse mechanistic growth model" used by *Chuine et al.* [2004].

[45] Since running correlation values drop remarkably during the verification period a *RE* value of 0.32 can be considered as lower limit of possible *RE* values. The fact that the absolute minimum can be found in the decade 1771–1780, as also in the work by *Etien et al.* [2008], which is known for being rather cold (Maunder Minimum), confirms a successful reconstruction.

[46] The constant increase in measured May to July mean temperature from the 1970s onwards is unique in the displayed time series.

5.5. Spectral Analysis

[47] As mentioned in the introduction and pictured in Figure 8 (para-) phenological data are particularly suitable for capturing interannual temperature variability. The result of the spectral analysis, namely a most prominent peak at a period of 3.4 years, is interesting when compared to the results obtained by *Shabalova and van Engelen* [2003], who reconstructed annual, summer (June-July-August) and winter (December-January-February) mean temperatures from A.D. 764 to 1705 for the Low Countries based upon documentary evidence. They found the most prominent peak in their fast Fourier transform (FFT) variance spectra in winter for a period of 3.5 years for reconstructed temperatures as well as for measured ones and in summer for a period of 2.5 years for reconstructed temperatures and 2.2 years for measured ones. Significant peaks can also be detected in their variance spectrum of reconstructed annual mean temperatures around 3.5 years and 5.2 years and in the variance spectrum of measured annual mean temperatures around 3.1 years and 5.2 years.

5.6. Comparison to Other Recent Reconstructions

[48] Figure 9 also demonstrates the limitations of temperature reconstructions. They may diverge considerably, and it is difficult to judge which one is the most "correct". In general, the quality of temperature reconstructions should increase with a growing number of predictors, like they were used by *Casty et al.* [2005a, 2005b], *Etien et al.* [2008] or *Dobrovolný et al.* [2009]. But it is obvious that *Casty et al.*'s [2005a, 2005b] reconstruction does not really match the corresponding temperatures at Hohe Warte, Vienna, until the decade 1851–1860, whereas *Dobrovolný et al.*'s [2009] reconstruction of mean May to July mean temperatures is more in line with the whole series of measured temperatures. Before the instrumental period, of course, it is hard to decide, which of the three reconstructions should be trusted most. The problem becomes more pronounced from 1660 backwards, because the two available reconstructions differ quite remarkably. The M shape around the decade 1771–1780 is only rudimentarily pronounced in *Dobrovolný et al.*'s [2009] and *Casty et al.*'s [2005a, 2005b] reconstructions. The excellent agreement ($R = 0.99$) between *Casty et al.*'s [2005a, 2005b] temperatures and the ones measured at Hohe Warte, Vienna, after 1900 is no surprise, since henceforward *Casty et al.*'s [2005a, 2005b] temperatures are identical with the CRU TS 2.0 data set. On the other hand, the consistency between our reconstructed temperatures and those observed at Hohe Warte, Vienna, in the decades 1781–1850 is to be expected as it concerns the calibration period. All in all, before 1900, all four different temperature curves (one measured and three reconstructed) match only during the three decades between 1851 and 1880.

6. Conclusions

[49] What is worth all the effort?

[50] Our work intended to construct a grape harvest series as continuous as possible. We extended the "historical" Klosterneuburg grape harvest series with the help of the "historical" Buergerspital data so that a nearly uninterrupted series ranging from 1523 to 1879 can be generated for the region of Vienna. Further, "modern" data for Klosterneuburg and Vienna are available between 1960 and 2007.

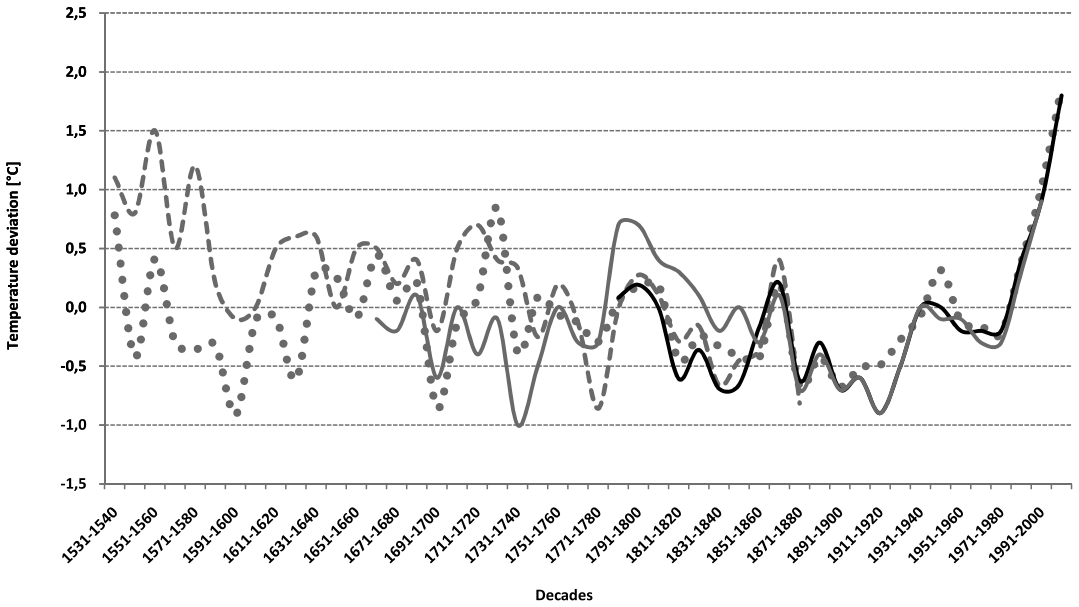

Figure 9. Deviations of reconstructed and observed temperatures at Hohe Warte, Vienna, of *Casty et al.*'s [2005a, 2005b] May to July mean temperatures at grid point 48.25°N and 16.25°E as well as of *Dobrovolný et al.*'s [2009] May to July Central European mean temperatures from the corresponding 1961–1990 mean; grey dashed line is deviation of reconstructed temperature from the 1961–1990 mean, grey solid line is deviation of *Casty et al.*'s [2005a, 2005b] temperature from the 1961–1990 mean, grey dotted line is deviation of *Dobrovolný et al.*'s [2009] temperature from the 1961–1990 mean, and black line is deviation of observed temperature from the 1961–1990 mean.

[51] Grape harvest dates before 1775 are valuable because of the lack of temperature information at Vienna and because GHD are strongly influenced by spring to (early) summer temperatures in the Austrian climatic region. Correlations between single to multiple monthly mean temperatures at Vienna, Hohe Warte, and GHD indicate that a combination of months should be preferred to single months when used as predictands for a temperature reconstruction. What kind of combination of months is most appropriate for a temperature reconstruction presumably differs temporally and locally and therefore has to be tested for each vine-growing site. For the region of Vienna we found the best correlation between GHD and the multi mean monthly temperatures from May to July ($R = -0.79$, $p = 0.01$). Running correlations were used in order to determine if there existed an optimal calibration period. In fact, between 1775 and 1850 the variance of the mean temperatures from May to July explains about 70% of the variance of GHD.

[52] We have demonstrated that meaningful decadal May to July mean temperatures starting in 1523 can be reconstructed with the help of a simple single proxy (GHD) linear regression. Looking at the reconstructed temperatures of this late spring/early summer season we found warm periods at the beginning of our reconstructed temperature series in the 16th century being almost as warm as those at the end of the 20th century. But then a more or less steady decline of late spring/early summer temperature followed with the coldest decade at the end of the 18th century. The temperature increase starting in the 1970s and continuing for more than 30 years seems to be unprecedented in the course of the 470 years under investigation.

[53] Anyhow, if comparing our results of mean May to July temperature to other recent ones [*Casty et al.*, 2005a, 2005b; *Dobrovolný et al.*, 2009], it is hard to decide, which temperature reconstruction is to be trusted most.

[54] In the course of this work the climatologic value of additional available parameters was assessed. Taking the quality index as an additional proxy, a biproxy temperature reconstruction back to 1523 seems possible. Other parameters such as quantity index or the price of wine must be regarded as less helpful, because they are influenced by local effects and economic trends, but they are interesting from the historical point of view. Flowering dates would be preferable to harvest dates for the reasons mentioned, but continuous data of this kind will be hard to find before 1730. GHD from 1775 to the present can be used for supplying information about changing viticultural practices and temperature-grapevine relationships respectively. An interesting aspect for a continuative work from a historical point of view would be to compare consecutive 30 year periods in order to detect the decade(s) when the viticultural changes took place.

[55] **Acknowledgments.** We are grateful to Reinhard Böhm, This Rutishauser, Isabelle Chuine, Johannes Friedberger, Karl Holubar, Petr Dubrovolný, and the reviewers for giving support and providing valuable suggestions. The BACCHUS project was funded by the Austrian Ministry of Science and Research and by ZAMG, the Austrian national meteorological service, to which we also want to express our thanks.

References

Auer, I., et al. (2007), HISTALP–Historical instrumental climatological surface time series of the greater Alpine region 1760–2003, *Int. J. Climatol.*, *27*, 17–46, doi:10.1002/joc.1377.

Bauer, K. (2008), *Weinbau*, Oesterreichischer Agrarverlag, Vienna.

Böhm, R., P. D. Jones, J. Hiebl, D. Frank, M. Brunetti, and M. Maugeri (2009), The early instrumental warm-bias: A solution for long central European temperature series 1760–2007, *Clim. Change*, doi:10.1007/s10584-009-9649-4, in press.

Brázdil, R., C. Pfister, H. Wanner, H. von Storch, and J. Luterbacher (2005), Historical climatology in Europe—The state of the art, *Clim. Change*, *70*, 363–430, doi:10.1007/s10584-005-5924-1.

Briffa, K. R., T. J. Osborn, F. H. Schweingruber, P. D. Jones, S. G. Shiyatov, and E. A. Vaganov (2002), Tree-ring width and density data around the Northern Hemisphere: Part 1. Local and regional climate signals, *Holocene*, *12*, 737–757, doi:10.1191/0959683602hl587rp.

Büntgen, U., D. C. Frank, D. Nievergelt, and J. Esper (2006), Summer temperature variations in the European Alps, A.D. 755–2004, *J. Clim.*, *19*, 5606–5623, doi:10.1175/JCLI3917.1.

Casty, C., H. Wanner, J. Luterbacher, J. Esper, and R. Boehm (2005a), Temperature and precipitation variability in the European Alps since 1500, *Int. J. Climatol.*, *25*(14), 1855–1880, doi:10.1002/joc.1216.

Casty, C., et al. (2005b), European Alps temperature and precipitation reconstructions, ftp://ftp.ncdc.noaa.gov/pub/data/paleo/historical/alps, World Data Cent. for Paleoclimatol., Boulder, Colo.

Chmielewski, F.-M., and T. Rötzer (2001), Response of tree phenology to climate change across Europe, *Agric. For. Meteorol.*, *108*, 101–112, doi:10.1016/S0168-1923(01)00233-7.

Chuine, I., et al. (2004), Historical phenology: Grape ripening as a climate indicator, *Nature*, *432*, 289–290, doi:10.1038/432289a.

Defila, C. (2003), Klimaerwaermung und Phaenologie der Weinrebe, *Schweiz. Z. Obst Weinbau*, *20*, 9–11.

Dobrovolný, P., et al. (2009), Monthly, seasonal and annual temperature reconstructions for central Europe derived from documentary evidence and instrumental records since AD 1500, *Clim. Change*, doi:10.1007/s10584-009-9724-x, in press.

Etien, N., V. Daux, V. Masson-Delmotte, M. Stievenard, V. Bernard, S. Durost, M. T. Guillemin, O. Mestre, and M. Pierre (2008), A bi-proxy reconstruction of Fontainebleau (France) growing season temperature from A. D. 1596 to 2000, *Clim. Past*, *4*, 1–16.

Guiot, J., A. Nicault, C. Rathgeber, J. L. Edouard, F. Guibal, G. Pichard, and C. Till (2005), Last-millennium summer-temperature variations in western Europe based on proxy data, *Holocene*, *15*, 489–500, doi:10.1191/0959683605hl819rp.

Harflinger, O., E. Koch, and H. Scheifinger (2002), *Klimahandbuch der oesterreichischen Bodenschaetzung. Klimatographie Teil 2. Strahlung. Weinbau. Phaenologie*, 259 pp., Universitaetsverlag Wagner, Innsbruck, Austria.

Intergovernmental Panel on Climate Change (IPCC) (2007), *IPPC: Climate Change 2007: The Physical Science Basis. Contribution of Working Group I to the Fourth Assessment Report of the Intergovernmental Panel on Climate Change*, edited by S. Solomon et al., 996 pp., Cambridge Univ. Press, Cambridge, U. K.

Landsteiner, E. (1999), The crisis of wine production in late sixteenth-century central Europe: Climatic causes and economic consequences, *Clim. Change*, *43*, 323–334, doi:10.1023/A:1005590115970.

Lauscher, F. (1983), Weinlese in Frankreich und Jahrestemperatur in Paris seit 1453, *Wetter Leben*, *35*, 39–42.

Luterbacher, J., D. Dietrich, E. Xoplaki, M. Grosjean, and H. Wanner (2004), European seasonal and annual temperature variability, trends and extremes since 1500, *Science*, *303*, 1499–1503, doi:10.1126/science.1093877.

Luterbacher, J., M. A. Liniger, A. Menzel, N. Estrella, P. M. Della-Marta, C. Pfister, T. Rutishauser, and E. Xoplaki (2007), The exceptional European warmth of autumn 2006 and winter 2007: Historical context, the underlying dynamics and its phenological impacts, *Geophys. Res. Lett.*, *34*, L12704, doi:10.1029/2007GL029951.

Meier, N. (2007), Grape harvest records as a proxy for Swiss April to August temperature reconstructions, Diplomarbeit an der Philosophisch-Naturwissenschaftlichen Fakultaet, 91 pp., Univ. Bern, Bern.

Meier, N., T. Rutishauser, C. Pfister, H. Wanner, and J. Luterbacher (2007), Grape harvest dates as a proxy for Swiss April to August temperature reconstruction back to A.D. 1480, *Geophys. Res. Lett.*, *34*, L20705, doi:10.1029/2007GL031381.

Menzel, A. (2005), A 500 year pheno-climatological view on the 2003 heatwave in Europe assessed by grape harvest dates, *Meteorol. Z.*, *14*(1), 75–77, doi:10.1127/0941-2948/2005/0014-0075.

Menzel, A., et al. (2006), European phenological response to climate change matches the warming pattern, *Global Change Biol.*, *12*, 1969–1976, doi:10.1111/j.1365-2486.2006.01193.x.

Moberg, A., D. M. Sonechkin, K. Holmgren, N. M. Datsenko, and W. Karlén (2005), Highly variable Northern Hemisphere temperatures reconstructed from low- and high-resolution proxy data, *Nature*, *433*, 613–617, doi:10.1038/nature03265.

Pfister, C. (1985), *Klimageschichte der Schweiz 1525–1860. Das Klima der Schweiz von 1525–1860 und seine Bedeutung in der Geschichte von Bevoelkerung und Landwirtschaft*, vol. 1, 184 pp., Acad. Helv., Bern.

Pfister, C. (1999), *Wetternachhersage. 500 Jahre Klimavariationen und Naturkatastrophen 1496–1995*, 304 pp., Verlag Paul Haupt, Bern.

Pfister, C., R. Brázdil, B. Obrebska-Starkel, L. Starkel, R. Heino, and H. von Storch (2001), Strides made in reconstructing past weather and climate, *Eos Trans. AGU*, *82*(22), 248, doi:10.1029/01EO00141.

Pribram, A. F., R. Geyer, and F. Koran (1938), *Materialien zur Geschichte der Preise und Loehne in Oesterreich*, vol. 1, Carl Ueberreuters Verlag, Vienna.

Robinson, J., A. Dinsmoor, and R. E. Smart (1999), *The Oxford Companion to Wine*, Oxford Univ. Press, Oxford, U. K.

Rutishauser, T., J. Luterbacher, F. Jeanneret, C. Pfister, and H. Wanner (2007), A phenology-based reconstruction of interannual changes in past spring seasons, *J. Geophys. Res.*, *112*, G04016, doi:10.1029/2006JG000382.

Shabalova, M. V., and A. F. V. van Engelen (2003), Evaluation of a reconstruction of winter and summer temperatures in the Low Countries, AD 764–1998, *Clim. Change*, *58*, 219–242, doi:10.1023/A:1023474032539.

Sommer, M. (2008), Zusammenfassung der Analysekenndaten von authentischen Weinen verschiedener Jahrgaenge und deren weinbaulich-klimatische Interpretation, Diplomarbeit aus den Fachgegenstaenden Chemie der Fruechte und Fruchtprodukte, Math. Lehr- und Forsch. für Wein- und Obstbau, Klosterneuburg, Austria.

Xoplaki, E., J. Luterbacher, H. Paeth, D. Dietrich, N. Steine, M. Grosjean, and H. Wanner (2005), European spring and autumn variability and change of extremes over the last half millennium, *Geophys. Res. Lett.*, *32*, L15713, doi:10.1029/2005GL023424.

Yilmaz, Ö., and S. M. Doherty (1994), *Seismic Data Processing*, *Invest. Geophys.*, vol. 2, 526 pp., Soc. of Explor. Geophys., Tulsa, Okla.

C. Hammerl, T. Hammerl, E. Koch, C. Maurer, and E. Pokorny, Zentralanstalt für Meteorologie und Geodynamik, Hohe Warte 38, A-1190 Wien, Austria. (christian.maurer@univie.ac.at)

Extreme grape harvest data of Austria, Switzerland and France from A.D. 1523 to 2007 compared to corresponding instrumental/reconstructed temperature data and various documentary sources

C. Maurer, C. Hammerl, E. Koch, T. Hammerl and E. Pokorny

Theor. Appl. Climatol., 2011, **106**, 55-68

Theor Appl Climatol (2011) 106:55–68
DOI 10.1007/s00704-011-0410-3

ORIGINAL PAPER

Extreme grape harvest data of Austria, Switzerland and France from A.D. 1523 to 2007 compared to corresponding instrumental/reconstructed temperature data and various documentary sources

C. Maurer · C. Hammerl · E. Koch · T. Hammerl · E. Pokorny

Received: 16 March 2010 / Accepted: 13 January 2011 / Published online: 22 February 2011

Abstract The detection and quantification of extreme weather conditions in the past are important for correctly assessing the significance of today's extremes especially in the context of climate change. We specified extreme years by a synopsis of phenological data, temperature reconstructions and measurements and descriptive documentary sources starting in the 16th century. The spatial scale investigated is regional to interregional, covering Austria, Switzerland and north-eastern France. Thus, we defined a list of 36 extreme years (1536–2007), where two or more of several parameters (grape harvest data and/or mean temperatures) available at that time exceeded the two-sigma threshold with regard to a reference period of 105 years. In Western Europe, there were extreme spring to early summer temperatures and/or exceptional phenological observations on all three locations in 1542, 1718, 1811, 1822, 2003, 2006 and 2007. As only grape harvest data are on hand, our phenological dates can only indicate anomalous temperature conditions during spring and early summer, i.e. mean temperatures which significantly correlate to these phenological records. In addition to these data, we used independent documentary sources from the municipal archives of Retz, a town in Lower Austria, for affirming or amending these results.

C. Maurer · C. Hammerl · E. Koch (✉) · T. Hammerl · E. Pokorny
Zentralanstalt für Meteorologie und Geodynamik,
Hohe Warte 38,
1190 Vienna, Austria
e-mail: elisabeth.koch@zamg.ac.at

C. Maurer
e-mail: christian.maurer@univie.ac.at

C. Hammerl
e-mail: christa.hammerl@zamg.ac.at

T. Hammerl
e-mail: a0800446@unet.univie.ac.at

E. Pokorny
e-mail: elfriede.pokorny@telekabel.at

1 Introduction

Periods with highly anomalous weather conditions–notably, temperature and/or precipitation extremes and their impacts on human health, ecosystems and economic systems–have attracted the attention of people at all times (e.g. Manley 1958; Pfister 1985, 1999; Landsteiner 1999; Pfister and Brázdil 2006; Luterbacher et al. 2004, 2007). But what are the objective criteria for calling a precipitation event or a temperature condition "extreme"? Human beings are prone to overestimate current or recent weather extremes and to relativize those which date further back in time. Besides, the lifespan of man is much too short to correctly assess the significance of all weather extremes experienced (Brázdil et al. 2010; Dobrovolný et al. 2010). Furthermore, perceptions alter in the course of time (e.g. increasing comfort, like housing or clothing). Therefore, purely descriptive, direct information about this topic must be evaluated with some caution and experience.

In order to solve this problem, (early) instrumental records of temperature and/or precipitation can be consulted. Regrettably, continuous instrumental measurements of temperature (e.g. Vienna-Hohe Warte from 1775 onwards) and precipitation (e.g. Vienna-Hohe Warte from 1841 onwards) do not go back beyond the 18th century. Besides, homogenizing early instrumental (temperature) measurements means facing extraordinary complexities (Manley 1974; Böhm et al. 2010), such as the effect of urban growth, changes in observation hours or in the

immediate vicinity of the instruments, undetected instrumental errors, varying instrumentation and the results of imperfect or over-protected exposures.

What may help to detect extreme years is to tap the rich pool of non-descriptive proxies, especially biological data (Margary 1926; Lauscher 1978; Strestik and Verö 2000; Rutishauser et al. 2007; Sparks 2007; Jones et al. 2009), such as tree-ring density or–as in this paper–grape harvest data (GHD, see also Menzel 2005 or Garnier et al. 2010). Indeed, Rutishauser et al. (2008) point out that the temperature sensitivity of plant phenology alters in the course of centuries due to other long-term influences, like precipitation and snow covering. In addition, harvest data are always influenced by man—but if proxy data or reconstructions match the historical descriptions, the probability of having correctly determined an extreme event is high.

Extreme periods have been a research topic for many years. Jones and Briffa (2006), for example, tried to place the unusually cold year 1740 within a wider context. Briffa et al. (1992a, b, 1994) used tree-ring density records to reconstruct annually resolved series of average summer half-year temperatures and thereby found abnormal decades/years for northern Fennoscandia and North American regions. Büntgen et al. (2006) reconstructed common June to September temperature anomalies for the European Alps with the same kind of proxy data. Battipaglia et al. (2010) identified 44 summer extremes between 1550 and 2003 for Central Europe. They verified extremes based on tree-ring density from the higher elevations in the European Alps using documentary evidence from Switzerland, the Czech Republic and Central Europe. Just as tree-ring records are highly valuable if they stem from the northern tree line or high elevations (Frank and Esper 2005; Büntgen et al. 2007), GHD become valuable if, like in the Vienna region, vines grow in a climatic borderline zone where temperatures just permit vine growing (Maurer et al. 2009).

While most works on this topic focus on temperature reconstruction, we emphasized specifying extreme years by a synopsis of phenological data, instrumental temperature records, temperature reconstructions and descriptive historical sources on larger regional (Lower Austria) and interregional (Western Europe, i.e. Austria, Switzerland and north-eastern France) scales.

Three sub-periods are distinguishable for the Vienna region GHD and are used throughout the paper: 1523–1774, the "historic" pre-instrumental period, when vintage data and reconstructed temperatures are available; 1775–1959, the "historic" instrumental period, when temperature measurements were made from 1775 onwards, and GHD are available up to 1879; and finally, 1960–2007, the "modern" instrumental period, when GHD (and, of course, measured temperatures) are on hand (see Table 1).

2 Data

Different sources were investigated to get information about wine and weather phenomena for Vienna, the neighbouring Klosterneuburg (Lower Austria) and Retz (Lower Austria). We worked exclusively with original primary or secondary sources in order to avoid mistakes, which may arise using secondary literature only. More detailed information about Vienna, Klosterneuburg and the corresponding sources is found in Maurer et al. (2009).

2.1 Data for Klosterneuburg

Relevant manuscript sources were studied at the archives of the Klosterneuburg monastery; the bulk of information used came from Manuscript StAK MS 121: Gedenkbuch und Weinchronik, a chronicle written by Josef Bittmann, Klosterneuburg, in 1880. It contains highly detailed information about vine growing and weather phenomena from 1540 to 1879; in our study, this period covers a major part of the so-called "historical" years (1523–1959).

Further, we read through Manuscript StAK MS 102 (a chronicle covering the time span 1577–1742, written in 1775, copying information from so-called "Schreibkalender"), Manuscript StAK MS 122/1 (contemporary chronicle, 1781–1813, reporting national and international events), Manuscript StAK MS 122/2 (continuation of 122/1, 1813–1833), Manuscript StAK D 73 (contemporary chronicle, 1796–1802 of the monastery of St. Dorothea in Vienna), StAK Box 221 (Wetter und Zufällechronik, compiled by Willibald Leyrer in 1789, with information for the time span 1322–1691).

Apart from general information about weather and climate, specific information was collected about vintage, wine quality and wine quantity.

GHD for the so-called "modern" period (1960–2007) are available only from 1970 to 2007. They were compiled at Lehr- und Forschungszentrum für Wein- und Obstbau Klosterneuburg (Sommer 2008) from the original material (Schmuckenschlager 2007).

2.2 Data for Vienna

For the Vienna series, a standard work (Pribram et al. 1938) was used for the period 1523–1785 (Vienna-Buergerspital), which is a comprehensive, reliable, secondary source. Pribram evaluated primary sources at the municipal and provincial archives of Vienna. No relevant information is available for the period from 1786 to 1959.

Data of the period 1960–1999 again are from the Lehr- und Forschungszentrum für Wein- und Obstbau Klosterneuburg (Sommer 2008) and were extracted from the original material (Klosterneuburg 2000).

Table 1 List of parameters together with periods of availability, periods in use, periods of reference, reference mean and two-sigma value

	Harv. Buerg./Vienna	Harv. Klosterneuburg	Harv. Swiss	Harv. Burg.	CEuT-AMJJ	T-AMJJ, Vie.	T-AMJJ, Basel&Geneva	T-AMJJ, Stras.
available	1523-1749 & 1960-1999	1730-1879 & 1970-2007	1480-2006	1370-2007	1500-2007	1775-2007	1760-2007	1801-2007
used	1523-1749 & 1960-1999	1730-1879 & 1970-2007	1523-2006	1523-2007	1523-1774	1775-2007	1760-2007	1801-2007
reference period	1545-1649	1775-1879	1775-1879	1775-1879	1775-1879	1775-1879	1775-1879	1801-1905
reference period mean [days of year, °C]	279.0	283.6	286.3	273.8	14.1	15.2	14.5	14.6
reference period two sigma value [days, °C]	17.0	17.5	18.5	18.3	1.9	2.2	1.7	1.8

Parameters from left to right are harvest data of Buergerspital/Vienna, Klosterneuburg, the Swiss Plateau Region and Burgundy; the mean seasonal AMJJ–CEuT-temperature reconstruction and the mean seasonal surface AMJJ temperature at Vienna-Ho he Warte, at Basel&Geneva and at Strasbourg

The publication Versuch (1803) is a compilation of various entries and is used only for the purpose of comparison. Though its reliability is questionable, it was consulted because it is often mentioned in the relevant literature. Additional information for Vienna is also found in the Chronicle d'Elvert (1861), which was written by the town chronicler of Iglau, and in Pilgram (1788), who compiled his work from a variety of contemporary sources, for the whole of Austria.

2.3 Data for Retz

Retz is located in the Weinviertel region in north-western Lower Austria. The town was granted the privilege of wine trading by Emperor Friedrich III in 1458. This privilege was the basis for the future wealth of Retz, where a huge and multi-storied underground system of wine cellars was built.

For Retz (Lower Austria) also, secondary sources, such as "Geschichtliche Aufzeichnungen der Stadt Retz" (Löschnig and Stefl 1935) and "Denkwürdigkeiten der Stadt Retz" (Puntschert 1894; first edition, 1870), were used, but compared to and verified with information from manuscript sources, such as the accounts of the Retz Buergerspital (see Fig. 1) and the "Gedenkbuch der Stadt Retz" (1896–1933) by Victor Apeldauer (1933).

The chronicle "Denkwürdigkeiten der Stadt Retz" (covering A.D. 1057 to 1866) was written by Josef Karl Puntschert, town clerk in Retz and its first archivist. He arranged the records of the Retz archives according to a new system and had therefore an excellent knowledge of the local historical sources when he compiled the volume "Denkwürdigkeiten der Stadt Retz" in 1870. He did not only describe weather phenomena but also stated prices (in fl.=gulden) and quantity of wine per year [from 1356–1761, 1 *emer* (bucket) in Lower Austria=58 l; from 1762–1875, 1 *emer*=56.59 l; Sandgruber (1995)].

The "Geschichtliche Aufzeichnungen der Stadt Retz" (covering A.D. 1551 to 1933) is often mentioned in publications, but this compilation also relies on German sources and is thus not always relevant for the history of the Retz wine. A comparison with other sources is therefore indicated. Original contemporary sources are the comprehensive accounts of the Buergerspital in Retz. They contain detailed information–unfortunately with gaps–about wine grown in the Retz area for the period 1527–1860; thus, they serve as an excellent tool for verifying the later chronicles.

2.4 Data for Burgundy and the Swiss Plateau Region

GHD of Burgundy (1370–2007) and the Swiss Plateau Region (1480–2006) are derived from Chuine et al. (2004) and from Meier et al. (2007). In Burgundy (eastern France), these data were collected in parish and municipal archives. The grape variety "Pinot Noir" has been cultivated there since the 14th century, if not earlier. With regard to the Swiss Plateau Region (north-western Switzerland), GHD from 15 locations were incorporated in the time series.

2.5 Temperature data

Instrumental temperature data used for the stations Vienna-Hohe Warte (starting in 1775), Basel-Binningen (starting in 1760), Geneva-Cointrin (starting in 1760) and Strasbourg-Entzheim (starting in 1801) are from the HISTALP data collection (Auer et al. 2007) in the bias-corrected version

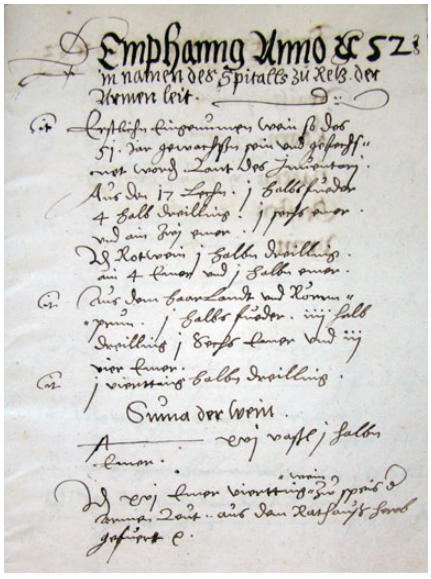

Fig. 1 Accounts of the Retz Buergerspital for the year 1552, original manuscript. Accounts of wine are described. Municipal archives, Retz (StARetz, Buergerspitalrechnungen 1552)

2008 (Böhm et al. 2010). The monthly Central European temperature (CEuT, 1500–2007) reconstruction, developed by Dobrovolný et al. (2010) from documentary index series from Germany, Switzerland and the Czech Republic (1500–1854) and 11 instrumental temperature records (1760–2007), was used for the pre-instrumental period.

3 Methods

3.1 The "historical" pre-instrumental period (1523–1774)

First of all, we searched for extreme values in the time series of grape harvest in the pre-instrumental period 1523–1774 with reference to the long-term mean 1775–1879 in the case of the "historical" Klosterneuburg, Burgundy and Swiss Plateau data (see Table 1). This procedure was repeated for the 1545–1649 mean in the case of the "historical" Vienna-Buergerspital GHD (see Table 1). These two special 105-year reference periods were chosen due to the overlapping of the phenological records of Klosterneuburg and the homogenized temperature series at Vienna-Hohe Warte and due to nearly continuous GHD (Maurer et al. 2009). Guided by the mean temperature–GHD correlation analysis performed for the "historical" instrumental period (see Section 3.2), we used Dobrovolný et al. (2010) CEuT reconstruction in the form of April to July multi-month (AMJJ)-mean temperatures for the search of temperature extremes (r=−0.61, p=0.01, between Vienna-Buergerspital GHD and AMJJ-mean temperature values for 1545–1649). The period 1775–1879 again constitutes the reference period for the CEuT series. An extreme value was defined as an event beyond the two-sigma threshold. In order to reduce the risk of mistakes resulting from possibly wrong entries in the chronicles or insufficiently reconstructed AMJJ temperatures, an extreme year in the pre-instrumental period was defined by phenological data and reconstructed temperatures as one where at least two out of four parameters (harvest data of Burgundy, the Swiss Plateau Region and the Vienna region, AMJJ temperature reconstruction) turned out to be extremely anomalous (see Table 2 and Figs. 2, 3 and 4, extreme years 1536–1719). For the overlapping period of the Vienna-Buergerspital and Klosterneuburg GHD 1730–1749, a given year was classified as extreme only if both harvest data in addition to a third parameter (harvest date of Burgundy or of the Swiss Plateau Region or AMJJ temperature reconstruction) showed exceptional values. The addition of the Burgundy GHD (Chuine et al. 2004, see Table 1), the Swiss Plateau GHD (Meier et al. 2007, see Table 1) and Dobrovolný et al. (2010) CEuT reconstruction (see Table 1, reference period 1775–1879 in all cases) implies that the extreme years were traced interregionally. On the basis of the long Burgundy GHD records (used for the purpose of this study from 1523–2007), we performed a Kolmogorov–Smirnov test to find a possible deviation from the assumed normal distribution. Since this test shows no statistically significant deviation, phenological data, like temperature data, are presumed to be normally distributed if the sample size is sufficiently large. As a consequence, applying a "2-σ-criterion" (as used by Chuine et al. 2004 and by Casty et al. 2005) for detecting extremes is justifiable.

3.2 The "historical" instrumental period (1775–1959)

For the "historical" instrumental period, we correlated different single- to multi-month temperature means of Vienna-Hohe Warte, Basel-Binningen, Geneva-Cointrin and Strasbourg-Entzheim to the GHD of Klosterneuburg, the Swiss Plateau Region and Burgundy. The mean temperatures of Basel-Binningen (located in the northeast of the Swiss Plateau Region) and Geneva-Cointrin (located in the southwest of the Swiss Plateau Region) were combined to arithmetic means before determining the correlations, in the following referred to as "Basel&Geneva". For calculating the correlation coefficients, we used the period 1775–1879 (see Maurer et al. 2009) in the case of Klosterneuburg. Its GHD were correlated to Vienna mean temperatures. The same reference period was applied in the case of the correlation between Swiss GHD and Basel&Geneva mean temperatures.

Table 2 List of years in the pre-instrumental period when two or more considered parameters showed extreme values

	Harv. Buerg.-Vie.	Harv. Swiss	Harv. Burg.	CEuT-AMJJ
1536			-2.3	2.7
1540	-2.4	-3.5		3.9
1542	2.2	2.8	2.2	
1559		-2.1	-2.8	
1571	-2.6	-2.2		
1590		-2.5	-2.2	
1599	-2.4	-2.4		
1603		-2.1		2.0
1611		-2.4		2.2
1616	-2.5	-3.2		2.7
1624		-2.2		2.0
1636		-2.1	-2.7	
1637		-2.4	-2.9	2.3
1638		-2.8	-2.3	2.7
1645			-2.1	2.3
1653	-2.1		-2.1	
1666	-2.1		-2.2	2.9
1675	2.9	2.7		
1684			-2.7	2.2
1718	-2.4	-3.4	-2.7	2.0
1719		-2.6	-2.6	

Figures depict sigma values with regard to the period 1545–1649 for the Vienna-Buergerspital GHD and with regard to the period 1775–1879 for the Swiss Plateau Region and Burgundy GHD as well as for the CEuT–AMJJ-temperature data. Grey shadings indicate positive harvest date extremes and negative temperature extremes

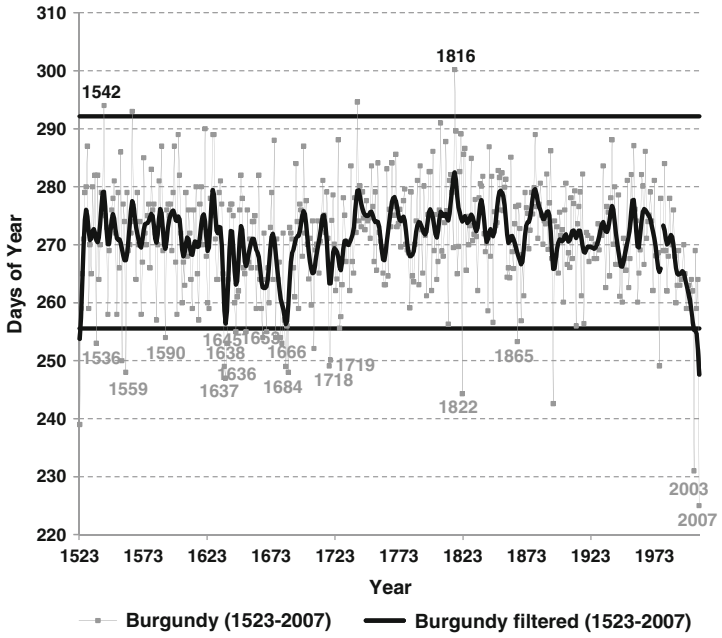

Fig. 2 Comparison of unfiltered and Gauss-filtered (30-year window) GHD (days of year) per year for Burgundy. *Horizontal lines* indicate corresponding two-sigma threshold with regard to the reference period 1775–1879. *Grey/black figures* mark years with extreme early/late grape harvest as listed for the corresponding site in Tables 2 and 3

The 1801–1905 period had to be taken in the case of the Burgundy GHD to Strasbourg mean temperature correlations. GHD were correlated to the annual mean temperature, the mean temperatures of April, May, June, July, April to July, May to June and May to July yielding statistically significant correlation coefficients between −0.25 and −0.83 (p=0.01 or 0.05, see also Maurer et al. 2009). Furthermore, we checked if the mean temperatures yielding the highest correlation coefficient for the Swiss Plateau Region (r=−0.83, p=0.01) and for Burgundy (r=−0.74, p=0.01) and the second highest correlation for the Vienna region (r=−0.76, p=0.01), i.e. April to July mean temperatures, also exhibited extremes from the given reference mean 1775–1879; 1801–1905 had to be taken for Strasbourg (see also Table 1).

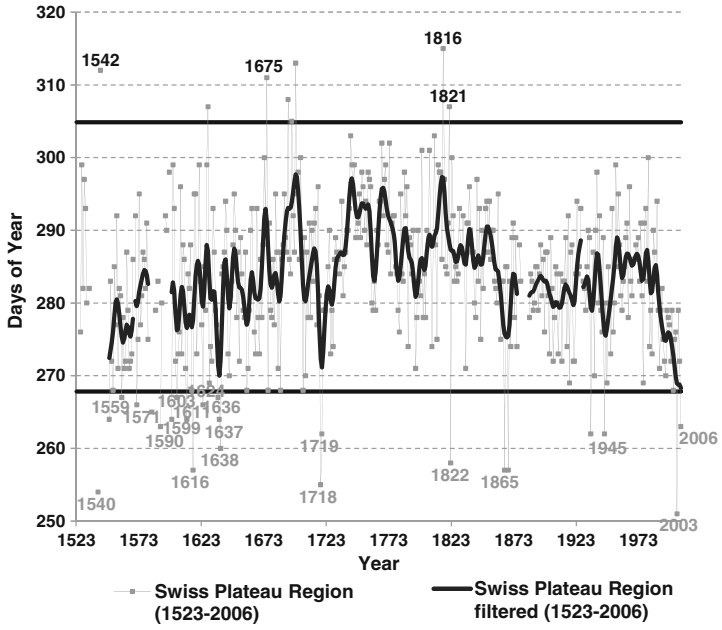

Fig. 3 Comparison of unfiltered and Gauss-filtered (30-year window) GHD (days of year) per year for the Swiss Plateau Region. *Horizontal lines* indicate corresponding two-sigma threshold with regard to the reference period 1775–1879. *Grey/black figures* mark years with extreme early/late grape harvest as listed for the corresponding site in Tables 2 and 3

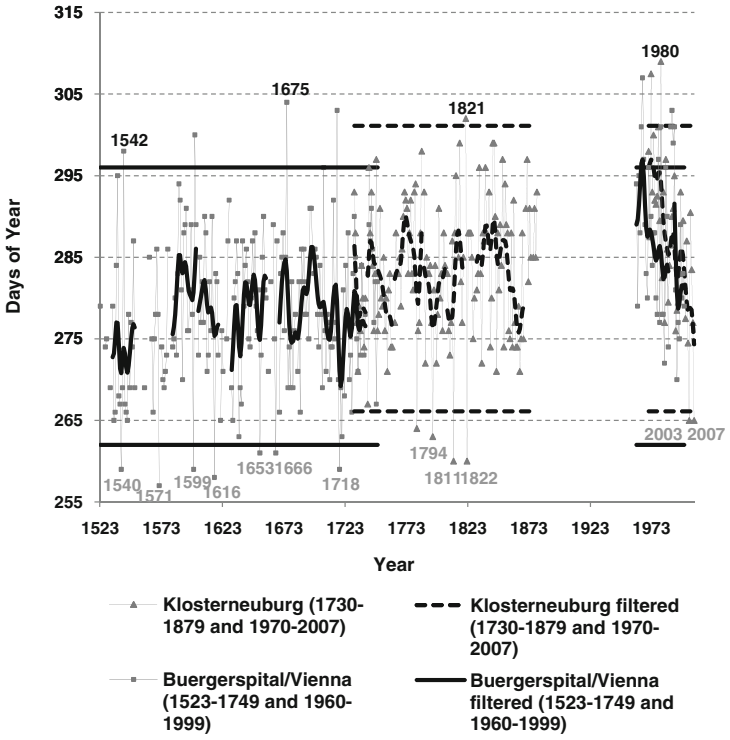

Fig. 4 Comparison of unfiltered and Gauss-filtered (30-year window) GHD (days of year) per year for Klosterneuburg and Buergerspital/Vienna. *Horizontal lines* indicate corresponding two-sigma threshold with regard to the reference periods 1775–1879, 1545–1649, respectively. *Grey/black figures* mark years with extreme early/late grape harvest as listed for the corresponding sites in Tables 2 and 3

The first part of Table 3 contains extreme years in the "historical" instrumental period (1794–1947; see also Figs. 2, 3 and 4), where at least two out of six (out of five before 1801) parameters (phenological records or the above-mentioned correlated mean temperatures) showed an extreme value.

3.3 The "modern" period (1960–2007)

The second part of Table 3 shows extreme years of the "modern" period (extreme years 1980–2007; see also Figs. 2, 3 and 4), where at least two out of six parameters (phenological records or the above-mentioned correlated

Table 3 List of years in the instrumental period when two or more considered parameters showed extreme values

	Harv. Vie.	Harv. Klo.	Harv. Swiss	Harv. Burg.	T-AMJJ, Vie.	T-AMJJ, Basel&Geneva	T-AMJJ, Stras.
1794	/	-2.4			2.8	2.7	/
1811	/	-2.7			3.0	2.1	2.6
1816	/		3.1	2.9		-2.2	-2.1
1821	/	2.1	2.2				
1822	/	-2.7	-3.1	-3.2		2.1	2.2
1837	/				-2.3		-2.2
1865	/		-3.2	-2.2		2.6	3.0
1945	/	/	-2.6			2.7	2.4
1947	/	/				2.9	2.9
1980	2.6	2.9				-2.1	
2000	/				2.1	2.0	
2003	/	-2.2	-3.8	-4.7	2.5	4.0	3.7
2005	/					2.2	2.4
2006	/		-2.5		2.1	2.8	3.1
2007	/	-2.2	/	-5.3	2.8	2.8	3.2

Figures depict sigma values with regard to the period 1545–1649 for the Vienna GHD and with regard to the period 1775–1879 for the Klosterneuburg, the Swiss Plateau Region and Burgundy GHD as well as for Vienna-Hohe Warte and Basel&Geneva temperature data. Strasbourg AMJJ-sigma values refer to the period 1801–1905. Grey shadings indicate positive harvest date extremes and negative temperature extremes. Slashes imply that no data are available

mean temperatures) turned out to be anomalous. The reference periods (1645–1649, 1775–1879, 1801–1905) are the same as for the "historical" period. For the overlapping period of Vienna and Klosterneuburg GHD 1970–1999 again both harvest data had to be extreme apart from a third parameter in order to classify the respective year as outstanding.

3.4 Comparison of extremes to other sources

Tables 2 and 3 list 36 years according to the criteria mentioned. We compared the extreme phenological and mean temperature values of these years to each other and to descriptive entries in historical chronicles and manuscripts (Tables 4 and 5) as well as to recent results found by Brázdil and Kotyza (2000), Casty et al. (2005), Brázdil et al. (2008) and Etien et al. (2008). The chronicles of Retz (Puntschert 1894; Löschnig and Stefl 1935) and the accounts of the Retz Buergerspital, considered in addition to the records of Klosterneuburg and Vienna-Buergerspital, constitute a more or less independent possibility of comparison.

In order to take full advantage of all the descriptive information given by several chronicles and manuscripts in the "historical" period (pre-instrumental as well as instrumental), numeric quality and numeric quantity indices of wine for every year were correlated to the GHD records of Klosterneuburg and Vienna-Buergerspital (see Maurer et al. 2009). Since the resulting coefficients are statistically significant (p=0.01 or 0.05) and negative throughout (−0.46 and −0.51 for quality and −0.23 and −0.30 for quantity), we concluded that very good/bad and very much/little wine sometimes follows very early/late GHD, which in turn indicate to some extent extreme warm/cold mean temperature conditions. However, caution is appropriate, since the findings of Brázdil et al. (2008) for the Czech Republic reveal that differences in mean temperatures are often insignificant for neighbouring categories of wine quality ("excellent", "good", "average", "bad" etc.) or even do not exist.

Brázdil and Kotyza (2000) studied climate fluctuations in the Louny Region (Czech Republic) in the 15th to 17th centuries, based on books of accounts of the town of Louny. Casty et al. (2005) list of years (1500–2004) with extreme warm mean summer (JJA) and annual mean temperatures exceeding the two-sigma threshold of the 20th century mean, is based on reconstructions (1500–1900, henceforward, CRU temperatures) for the European Alps, using a combination of long instrumental station data and documentary evidence. Etien et al. (2008) list of extremely warm reconstructed AMJJAS mean temperatures, exceeding the 1.5 standard deviation of the centennial average, was compiled using $\delta^{18}O$ records of Fontainebleau (France) latewood cellulose of both living trees and timber and the Burgundy grape harvest records in a bi-proxy reconstruction from A.D. 1596 to 2000. Brázdil et al. (2008) dealt with historical observations of the Czech lands before A.D. 1500 and in the 16th to 18th centuries.

4 Results

Tables 2 and 3 present extreme years selected according to the criteria mentioned in Chapter 3 for the pre-instrumental and instrumental periods. Tables 4 and 5 compare the information given in the literature used and the contemporary sources for the years listed in Tables 2 and 3.

As years with extremely advanced GHD, 1536, 1540, 1559, 1571, 1590, 1599, 1603, 1611, 1616, 1624, 1636, 1637, 1638, 1645, 1653, 1666, 1684, 1718, 1719, 1794, 1811, 1822, 1837, 1865, 1945, 1947, 2000, 2003, 2005, 2006 and 2007 were selected. Extremely delayed GHD were identified for 1542, 1675, 1816, 1821 and 1980. In the following, several special events are reported in greater detail:

The town chronicler of Jihlava (Czech Republic) said about the year 1540 in Vienna (d'Elvert 1861): "In Vienna and in other places many have poured out the wines because of a lack of barrels. Others have emptied the barrels with the old wine in the streets at night and filled them with the good, delicious new must. Some have not even been able to pick the grapes, because they could not buy any barrel."

For the year 1675, Leyrer (1789) noted: "Snow in May, ice, great damage in the vineyards—by bugs. This year the bugs have caused great damage in the vineyards almost everywhere, hence the government has ordered them to be collected, if possible. Sour and little wine." Puntschert (1894) recorded: "Snow at harvest time; the grapes had to be dug out of the snow."

For the year 1718, Puntschert (1894) reported: "Very good wine—within living memory no wine has grown as good, but medium vintage because of the great heat." The months of April and May in Lower Austria are described as warm and dry. The drought even resulted in a public order to pray for rain (Sammlung 1719). In the summer, an unbearable, long-lasting heat wave prevailed. With the exception of grapes, field crops turned out badly. People had to fight forest fires, and wells, rivers and lakes dried out (Versuch 1803).

For the year 1794, Manuscript MS 121 (1880) reads: "This year there is no winter, no snow and no coldness. On 15 May vines are flowering."

According to the entries in MS 121 and MS 122-2, 1821, very wet conditions dominated the vegetation period in nearly all European countries, leading to floods which destroyed large parts of the harvest. Cold winds, morning frost and snowfall are reported in some parts of Austria on

Table 4 Comparison of the extreme years of the "historical" pre-instrumental period as listed in Table 2 to diverse documentary sources as well as to extremes defined by Casty et al. (2005) and Etien et al. (2008)

	Vienna-Buergerspital Pribram et al. (1938) Fee for lease of vineyard per bucket must in kr.	Retz Buerger-spital	Puntschert (1894)	Pilgram (1788)	Leyrer (1789)	d'Elvert (1861)	Löschnig and Stefl (1935)	Casty et al. (2005)	Etien et al. (2008)
1536	kr. 90.–								
1540	kr. 52.50; good wine		very hot and dry summer; very early harvest; very good and strong wine	wine very good; hot and dry summer		big amount; ten buckets wine at Vienna for 2 fl.		X	
1542	kr. 90.–		very dry summer; bad wine year						
1559	kr. 120.–; big price rise	329 buckets	bad wine year, because of frost; big price rise	very small harvest because of frost			cold, wet year; little and sour wine		
1571	kr. 135.–	147 buckets					little and sour wine		
1590	kr. 135.–						very hot summer; little, but very good wine, exceptional during the past 100 years		
1599	kr. 120,–; good wine		good wine	very good wine			early, warm spring; very much and good wine		
1603	kr. 150.–						very dry, but fertile summer; very much and good wine		
1611	kr. 127.50						wet summer, cold autumn; pretty much wine, but bad quality		
1616	kr.165,–; damage by showers		damage by showers		extensive shower, ample rainfall		summer very hot; little, but very good wine		
1624							hot summer; little, but good wine		
1636	kr. 195.–						good and pretty much wine		X
1637	kr. 180,–; ruined by bugs			bugs in the vineyards			much and good wine; many vineyards not cultivated		X
1638	kr.105.–	33 buckets	droughty year				wet flowering period; little wine, but very good and very expensive; heavy wine		
1645	kr. 135,–; bad wine		bad wine	bad wine			good and fertile year; much and good wine		
1653	kr. 150,–	87 buckets					much and good wine		

1666	kr. 180,–	51 buckets		cold at the end of April; summer very dry	cold May with hoarfrost		pretty much and very good wine		
1675	kr. 225,–; little and bad wine	21 buckets	little and bad wine; 1 bucket = 1-3 fl.	little and bad wine	damage by bugs; little and sour wine		little and sour wine; very cold May with snow and frost	X	
1684	kr. 195,–; little and bad wine	60 buckets	bad wine year, little wine	little and bad wine	rot		heat and drought; early harvest; pretty much and very good wine		
1718	kr. 285,–; very good, medium harvest, because of great heat	80 buckets	early grape harvest; very good wine, medium harvest, because of great heat; 1 bucket = 3 fl.	big drought; very good wine			terrible heat, 9 months dry weather; early grape harvest; much and very good wine	X	X
1719	kr. 195,–; good and much wine, but extensive rot	217 buckets	good and much wine; large-scale rot; 1 bucket = 1.5 fl.	very good wine			very much and good wine		X

1 Gulden (fl.)=60 Kreuzer (kr.) according to the Coinage Code of the Austrian duchies of 1524

June 20. As a consequence, the refectory of the Klosterneuburg monastery had to be heated on June 24 and 25. MS 122-2 speaks of a "late grape harvest, the saddest in Austria within living memory" caused by the late coldness and the prolonged wetness.

5 Discussion and conclusion

5.1 Importance of the Vienna vintage data in the context of historical climatology

Our vintage data belong to the category of so-called "indirect" data (Brázdil et al. 2010) which refer to physically based events linked to weather and climate. These bio-physical data are in general more likely to cover the low-frequency component of climate than "direct" documentary evidence, e.g. descriptions of weather conditions, because no transformations have to be made from the raw data to index series. As a consequence, Brázdil et al. (2010) state that, e.g. phenophases may improve the reconstruction skill when used in combination with documentary index data. However, slow systematic changes in GHD (Garnier et al. 2010) due to technical improvements in viticulture, the evolution of the consumers' taste, changes in grape varieties or the development of road infrastructures are clearly visible in the last part of the Vienna region GHD time series at the end of the 20th century. This implies that trends on a century scale in temperature reconstructions based on GHD have to be interpreted with great caution (see also Section 5.5).

5.2 Extreme years on different scales

We found extreme years on a greater regional (Lower Austria) and on an interregional (Austria, Switzerland and north-eastern France) scale. In 1542, 1718, 1822 and 2003, extreme phenological events occurred at all three vine-growing sites, but outstanding temperature conditions for Central Europe or in all the corresponding towns (Vienna, Basel&Geneva and Strasbourg) can be confirmed only for 1718 and 2003. The harvest was remarkably advanced on all three locations (Vienna/Klosterneuburg, Burgundy and the Swiss Plateau Region), although there is quite a big geographical distance between the Swiss Plateau Region and Burgundy on the one hand and Vienna/Klosterneuburg on the other. The correlation coefficients between, e.g. Vienna-Buergerspital and Burgundy (r=0.46), Vienna-Buergerspital and the Swiss Plateau Region (r=0.65) and Burgundy and the Swiss Plateau Region (r=0.79, p=0.01 in all three cases), confirm that this analogy is not a coincidence. However, bearing the geographical locations in mind, one will understand that the data of Burgundy and the Swiss Plateau Region show the highest correlation, whereas the Vienna and Burgundy data reveal the lowest correlation. The highly significant correlation of GHD all over Central and Western Europe is referred to by Le Roy Ladurie (1977) and Rutishauser et al. (2007). Le Roy Ladurie (1977) attributes this to a large-scale effect of temperature regimes.

The years 1540, 1571, 1599, 1616, 1653, 1666, 1675, 1794, 1811, 1821, 1837, 1980, 2000, 2006 and 2007 show extremes in the Vienna region (GHD or AMJJ-mean temperature) and at

Table 5 Comparison of the extreme years of the "historical" instrumental period as listed in Table 3 to diverse documentary sources as well as to extremes defined by Casty et al. (2005) and Etien et al. (2008)

	Puntschert (1894)	MS 121 (1880)	Löschnig and Stefl (1935)	Casty et al. (2005)	Etien et al. (2008)
1794	very good wine; 1 bucket = 2 fl.	always warm; good harvest, good wine; 1 bucket = 4 fl.	at the end of March all plants and trees turned green; excellent wine		
1811	excellent wine; "extra-wine" 80-85 fl.; in August "extra-wine"185 fl.; red wine 190 fl.; vinegar 60 fl.	early spring proved to be rather cold; September big heat; excellent harvest and wine; 1 bucket = 20 fl.	"Famous, brilliant, first class wine year. Very much and excellent wine, as in 1783."	X	X
1816	wine of medium grade; 1 bucket = 60 fl.; „extra-wine" 70 fl.; 1812er wine 40 fl.	July and August warm; September and October rainy and cold; small harvest and sour wine; 1 bucket = 32 fl.	frosty April with snow at Easter; much rain in the following months; bad harvest; little and sour wine	X	
1821	bad wine; 1 bucket = 12 fl.	small harvest and sour wine; 1 grape pannier = 3 fl.	wine damage caused by worms; small harvest; little wine, bad quality		
1822	excellent but medium harvest; 1 bucket (wine) = 32 fl.; vinegar 23 fl.	small harvest and excellent wine; 1 bucket = 30, 35 and 40 fl.	hot summer; much and very good wine, as in 1811	X	X
1837	bad harvest; 1 bucket = 8 fl. 30 kr.	always rainy and cold until 5 August, after that sunny and warm; small harvest and sour wine; 1 bucket = 2 fl. ("Convention Currency")	little and bad wine; regional bad harvest		
1865	little harvest, good wine; very dry year; 1 bucket = 10-12 fl.	rainy and cold July; September sunny; small harvest; 1 bucket = 11 and 12 fl. ("Convention Currency")	pretty much wine of excellent quality, one of the most excellent wines of the century		

1 Gulden (fl.)=60 Kreuzer (kr.) according to the Coinage Code of the Austrian duchies of 1524. After the national bankruptcy in 1811, the "Vienna Currency" (W. W.) was introduced, followed by the "Convention Currency" in 1819

least in one of the other time series (Burgundy GHD, Swiss Plateau GHD, CEuT-AMJJ temperatures, Basel&Geneva temperatures, Strasbourg temperatures) where again 1540 (see Glaser et al. 1999 for a detailed description of that year), 1616, 1666, 1794, 1811, 1837, 1980, 2000, 2006 and 2007 are confirmed with regard to temperature in the CEuT series or at least in one of the corresponding towns. For 1811 and 2006, we even could find exceptional mean temperatures in all three towns. So, all the above years can also be considered extreme on an interregional scale. The years of 1794, 1811 and 1980 experienced exceptional phenological data only in the Vienna region, but in some French and/or Swiss vineyards, extreme grape harvest data could have been observed because of the detectable, remarkable temperature conditions. The years 1837 and 2000 are free from any outstanding phenological extremes; yet, these are imaginable for some places owing to the temperature information available.

In 1590, 1603, 1624, 1636, 1637, 1638, 1719 and 1865, the descriptive entries of the Retz chronicles fit phenological conditions in Burgundy and/or the Swiss Plateau Region. So, some of these years might also have been extreme on an interregional scale. But as stated in Sections 1 and 3.4, one has to be careful when judging on the basis of (purely descriptive) information about wine quality and quantity. For the year 1865, which is within the instrumental period, no extreme temperature is detectable at Vienna-Hohe Warte, despite the wine in Retz being praised as one of the most excellent of the century.

In 1611, a wet summer in Retz seems to be responsible for a grape harvest of minor quality. The years of 1559 and 1816 seem to be quite contradictory on an interregional scale.

The years of 1945, 1947 and 2005 seem to have been outstanding at least in north-eastern France and/or in north-western Switzerland.

Looking at extremes defined as values greater than the two-sigma threshold, one finds remarkable results at the turn of the 20th to the 21th centuries, the "modern" period. All temperature extremes are positive with regard to the period mean 1775–1879/1801–1905 and all extreme years–with the exception of one–selected according to the criteria mentioned in Chapter 3 occur after 1999. The year of 2003 features extreme values: never before had Burgundy (42.8 days advanced with regard to the 1775–1879 period) and the Swiss Plateau Region (35.3 days advanced with regard to the 1775–1879 period) experienced such an early harvest date. All three available phenological data and all three considered mean temperatures showed extreme values. The year 2007, the last year in Table 3, exhibits three positive temperature extremes and a remarkable negative grape harvest extreme in Burgundy of nearly 50 days (5.3σ).

Outstanding results are that three out of only 6 years with negative temperature extremes and/or positive grape harvest extremes cluster in the period 1816 to 1837. Besides, there was not a single extreme negative AMJJ temperature in the CEuT series from 1523 until 1774, and not a single negative or positive extreme AMJJ temperature at Vienna-Hohe Warte can be found between 1874 and 1983. Also, the phenological and temperature extremes themselves have the same sign (+/−) during one considered year and the opposite sign with respect to each other.

5.3 Comparison to documentary evidence of the Czech Republic

Concerning our list of extreme years, Brázdil and Kotyza (2000) note for 1540 that the beginning of the harvest, as well as the harvest of barley, oats and peas in particular, occurred earliest that year with regard to the whole period under study (1517–1622). In the year 1542, which appears as a cold extreme in our list, ice could be found on stagnant water even on June 7, following a very cold May. In 1571, in contrast to GHD considered in the present paper, hop picking took place latest in mid-October with regard to the whole period 1517–1622. The year 1599 is marked by a very early grape harvest in the Louny region in mid-September, and wages were paid for clearing bilge between the wheels at one Louny mill, which could have been the consequence of a dry period with a low water level. Several heavy downpours in July and August of 1603, which apparently affected the grain, cannot be found in the recordings for Retz.

In the year 1616, the beginning of the rye harvest was the earliest, as was the end of the harvest with regard to the period 1517–1622. The reason may have been an extraordinary drought starting already in April and lasting throughout the summer, which is also described as hot. As a consequence, rivers dried up, and a water-level mark was added on the so-called “hunger stone” on the left bank of the river Elbe at Decin. Winter grains yielded average harvests, but spring cereals and other field crops shrivelled. Grass withered, and the aftermath was not mown. The vintage at Louny was completed in mid-October, yielding good, but not much, wine. According to the information in Brázdil et al. (2008), in 1616, the harvest in the Bohemian town Louny took place on September 8, after a very warm and dry summer, thus being the earliest recorded one in this region in the 17th century. This recording fits very well our findings for the considered year (see also the results from Brázdil and Kotyza 2000 above).

In contrast, the 2 years with the latest harvest data of the century, namely 1608 and 1619, do not appear in our list of extremes. The entry in the Retz chronicle by Löschnig and Stefl (1935) for 1614 contradicts the description of abundant wine in Louny, which led to a halt in beer production in Litomerice, but both Retz chronicles confirm that 1627 was a disastrous year for winegrowers. However, as we do not have a single extreme anomaly for the 2 years 1614 and 1627 in our records, they do not appear in Table 2 or 4. Damage due to late frost in May 1666 in various villages in southern Moravia is reflected in Pilgram (1788, see Table 4) but cannot be proven for Retz.

For 1816, Brázdil et al. (2008) found the latest grape harvest date in the Znojmo GHD series which covers almost the whole 19th century. The year 1816 is also listed in Tables 3 and 5 because remarkable extremes occurred in Switzerland and north-eastern France, but not in the Vienna region.

As to the wine failure in the last two decades of the 16th century all over Central Europe, Landsteiner (1999) and Löschnig and Stefl (1935) confirm a very difficult period for winegrowers, and their notes correlate well with information from the towns Litomerice and Zidlochovice. In Puntschert (1894), no information about wine can be found between 1572 and 1599, which is to some extent an indication of an unfavourable time period. The only 2 years which bunch out positively in all records are 1590 and 1599, which–due to two phenological extremes every year–are also listed in Tables 2 and 4.

5.4 Restrictions and GHD as proxy for temperature extremes

Since GHD as well as the significantly correlated April to July mean temperatures are existent, the exclusiveness of the given years refers to spring to (early) summer temperature conditions. Another restriction comes from gaps in the Vienna and Klosterneuburg phenological data, which are missing completely from 1880 to 1959. The year 1740, for example, which is pictured by Löschnig and Stefl (1935) as well as by Puntschert (1894) as a year with a severe winter, cold summer and wine which could not even be converted to vinegar, is not included in our list of extreme years, since we were able to verify an extreme only for Burgundy. In the Vienna region (Vienna-Buergerspital and Klosterneuburg), GHD simply were not recorded, perhaps merely because the vintage was so bad. Furthermore, as the sensitivity of individual grape varieties to temperature means in the vegetation period differs, GHD not consistently derived from one variety every year may give a falsified picture of amplitudes in extreme years. However, for the Vienna region, there is no information about vine varieties except for the “modern” instrumental period in Klosterneuburg, and a change of varieties is bound to occur during a period of several centuries.

These limitations are strengthened by the fact that GHD are the result of somehow subjective decisions, a drawback of this kind of data noted by, e.g. Chuine et al.

(2004), Meier et al. (2007), Rutishauser et al. (2008) and Leijonhufvud et al. (2008, 2010). Rainy weather conditions, social traditions, commercial decisions or warfare give rise to uncertainties, which can hardly be assessed. Therefore, strictly natural information, like flowering data, have to be distinguished from culturally influenced information, like harvest date or wine quantity (Brázdil et al. 2008).

Looking at the pre-instrumental period, we evaluated 19% accordance with CEuT–AMJJ extremes for outstanding Buergerspital-Vienna GHD, 38% accordance for outstanding Swiss Plateau Region GHD and 33% accordance for outstanding Burgundy GHD. Turning to the extreme years in the instrumental period, we found that in 31% of the given years (with both kinds of data available), an extreme harvest date at Klosterneuburg occurred together with a corresponding AMJJ-temperature extreme recorded at Vienna-Hohe Warte. The analogous numbers for the Swiss Plateau Region GHD/Basel&Geneva-AMJJ temperatures and Burgundy GHD/Strasbourg-AMJJ temperatures add up to 43% and 33%. So, in general, the accordance is not overwhelming, but interestingly, the values for the Swiss Plateau Region are in both periods superior to the ones for Burgundy, which are again superior to the ones reached in the Vienna region.

Pertaining to the temperature reconstructions of Casty et al. (2005) and Etien et al. (2008), an agreement with our extreme year evaluation can be found in 27% and 31% of possible years, i.e. extreme years according to our criteria, where a respective temperature reconstruction is available and also yields an outstanding value.

One reason for the lack of accordance is that phenological data are not perfectly correlated to temperature. For example, the year 1837 exhibits several (only two of them are shown in Table 3) quite remarkable negative mean temperature extremes but no outstanding positive GHD. However, there are other reasons too for this lack of correlation. We have to bear in mind that simply the choice of the threshold 2σ and/or the observation made only in one or some selected vineyards gives rise to missing extremes. According to Battipaglia et al. (2010), a lack of a common climate signal has to be partly attributed to identifying extremes on the basis of thresholds, where in our case, a σ value of 1.9 makes a year ordinary with regard to climate and/or phenology. Besides, summer weather patterns show less coherence than the ones for winter, due to a major influence of local radiation.

5.5 Problems of inhomogeneity in the "modern" instrumental period

The delays in the grape harvest in the Vienna region in 1980 look record breaking, though a previous work (Maurer et al. 2009) indicated that a change in vinification took place, at least in the Vienna region. This means facing an extraordinary inhomogeneity regarding the "modern" instrumental period, which–given only one fragmentary time series for the Vienna region–is not quantifiable. Changes in viticultural practices and/or grape varieties have to be held responsible for a slowly developing inhomogeneity in GHD. When using the same reference periods (1545–1649 for Vienna and 1775–1879 for Klosterneuburg), a greater magnitude and a more frequent occurrence of positive GHD extremes are probable. Therefore, harvest extremes for Vienna and Klosterneuburg in 1980 (+22.0 and +25.0 days) are clearly an overestimation, and those for Klosterneuburg in 2003 (−19.0 days) and 2007 (−19.0 days), an underestimation, which becomes evident when comparing them to the harvest data of Burgundy and the Swiss Plateau region (see Table 3). On the other hand, the more extreme values of Burgundy and the Swiss Plateau Region in 2003 are comprehensible because the core of the estival high was located west of Austria.

For the year 1980, no outstanding negative mean temperature extremes can be found at Vienna-Hohe Warte. Nevertheless, the Rasser chronicle (2010) for Gumpoldskirchen reports that the viticultural cycle in this year was delayed by about 8 days in May and by about 10 days in August. June proved to be cool and sometimes rainy. Grapes ripened rather slowly, and their quantity was reduced by 20–30% compared to that of the previous year.

5.6 Contradictory information

For 1571, Löschnig and Stefl (1935, see Table 4) information about wine quality and quantity disagrees with the fact that the grape harvest at the Vienna-Buergerspital, as in the Swiss Plateau Region, was significantly advanced. So, the question arises if the information offered by the chronicle for that year is wrong or is valid for another location (see Section 2.3). The accounts of the Retz Buergerspital to a certain degree confirm the information given in Löschnig and Stefl (1935), insofar as the wine produced was less than in other years (e.g. 1569, 244 buckets; 1570, 147; 1571, 147; 1572, 200).

In 1666, the accounts of the Retz Buergerspital do not confirm the information given in Löschnig and Stefl (1935, see Table 4) of much and very good wine, insofar as the wine produced in 1666 (51 buckets=2,958 l) was less than, e.g. in the year 1664 (130 buckets=7,540 l). There is no information in Puntschert (1894).

The year of 1816 has a special character because there seems to be no correlation between extremes, as far as they are defined in the way described in Chapter 3, on a larger interregional scale. However, this special character must be seen in the context of the eruption of the Tombora in April 1815 together with a weak sun-spot maximum during 1816 (Milham 1924), which caused individual cold spells during summer (June to August). Burgundy and the Swiss Plateau Region experienced

the latest harvest ever since, and corresponding negative AMJJ-mean temperature extremes occurred at Basel&Geneva and at Strasbourg. Against all expectations, we have got no entries for the region of (mean temperature extremes) and around (phenological records) Vienna in Table 3. It should be noted that Pfister (1999) compares 1816 to 1675, where, according to Table 2, the harvest at the Vienna-Buergerspital was delayed, as in the Swiss Plateau Region.

Contradictory descriptive information on a small regional scale (e.g. 1645 and 1684, Puntschert 1894 versus Löschnig and Stefl 1935) is rare, but it occurs and may be expected, due to local influences and errors made in transcriptions. Besides, the latter compilation–as said before (see Section 2.3)–also relies on German sources and is thus not always relevant for the wine history of Retz. Clearly, compilations often contain misinterpretations or copying mistakes, but primary sources may also be biassed from different causes. Thus, Puntschert (1894) for the year 1684 spoke of a bad wine year and of little wine, in contrast to Löschnig and Stefl (1935) who recorded anomalous heat and drought and an early, rich harvest of very good wine. Therefore, original sources like the accounts of the Retz Buergerspital can be of great value in order to verify the information in the chronicles written later. For 1684, they report a rather meagre harvest of 60 buckets in Retz, which supports the description given by Puntschert (1894).

Acknowledgements We are grateful to Isabelle Chuine, Thomas Dammelhart (Stadtarchiv Retz), Johannes Friedberger (Höhere Bundeslehranstalt für Wein und Obstbau), Karl Holubar (Stiftsarchiv Klosterneuburg), Erich Landsteiner, Günter Müller, Petr Dobrovolný, Rudolf Brázdil and This Rutishauser for giving support and providing valuable suggestions. The BACCHUS II project was funded by the Austrian Federal Ministry of Science and Research and by ZAMG, the Austrian national meteorological service, to whom we also want to express our thanks.

References

Apeldauer V (1933) Memorial book of the town Retz [Gedenkbuch der Stadt Retz] Retz

Auer I et al (2007) HISTALP—historical instrumental climatological surface time series of the greater Alpine region 1760–2003. Int J Climatol 27:17–46. doi:10.1002/joc.1377

Battipaglia G, Frank D, Büntgen U, Dobrovolný P, Brázdil R, Pfister C, Esper J (2010) Five centuries of Central European temperature extremes reconstructed from tree-ring density and documentary evidence. Glob Planet Change 72:182–191. doi:10.1016/j.gloplacha.2010.02.004

Böhm R, Jones PD, Hiebl J, Frank D, Brunetti M, Maugeri M (2010) The early instrumental warm-bias: a solution for long central European temperature series 1760–2007. Clim Change 101:41–67. doi:10.1007/s10584-009-9649-4

Brázdil R, Kotyza O (2000) History of weather and climate in the Czech lands IV. Masaryk University, Brno, Utilisation of economic sources for the study of climate fluctuation in the Louny Region in the fifteenth-seventeenth centuries, 350 pp

Brázdil R, Zahradnícek P, Dobrovolný P, Kotyza O, Valásek H (2008) Historical and recent viticulture as a source of climatological knowledge in the Czech Republic. Geografie 113(4):351–371

Brázdil R, Dobrovolný P, Luterbacher J, Moberg A, Pfister C, Wheeler D, Zorita E (2010) European climate of the past 500 years: new challenges for historical climatology. Clim Change 101:7–40. doi:10.1007/s10584-009-9783-z

Briffa KR, Jones PD, Bartholin TS, Eckstein D, Schweingruber FH, Karlén W, Zetterberg P, Eronen M (1992a) Fennoscandian summers from AD 500: temperature changes on short and long timescales. Clim Dynam 7:111–119

Briffa KR, Jones PD, Schweingruber FH (1992b) Tree-ring density reconstructions of summer temperature patterns across Western North America since 1600. J Climate 5(7):735–754. doi:10.1175/1520-0442

Briffa KR, Jones PD, Schweingruber FH (1994) Summer temperatures across northern North America: regional reconstructions from 1760 using tree-ring densities. J Geophys Res 25:835–844

Büntgen U, Frank DC, Nievergelt D, Esper J (2006) Summer temperature variations in the European Alps, A.D. 755–2004. J Climate 19:5606–5623. doi:10.1175/JCLI3917.1

Büntgen U, Frank DC, Kaczka RJ, Verstege A, Zwijacz-Kozica T, Esper J (2007) Growth/climate response of a multi-species tree-ring network in the Western Carpathian Tatra Mountains, Poland and Slovakia. Tree Physiol 27:689–702

Casty C, Wanner H, Luterbacher J, Esper J, Böhm R (2005) Temperature and precipitation variability in the European Alps since 1500. Int J Climatol 25(14):1855–1880. doi:10.1002/joc.1216

Chuine I, Yiou P, Viovy N et al (2004) Historical phenology: grape ripening as a climate indicator. Nature 432:289–290. doi:10.1033/432289a

d'Elvert C (1861) Chronicle of the royal town Iglau (1402–1607) by Iglau's town clerk Martin Leupold von Löwenthal. [Chronik der königlichen Stadt Iglau (1402–1607) vom Iglauer Stadtschreiber Martin Leupold von Löwenthal]

Dobrovolný P et al (2010) Monthly, seasonal and annual temperature reconstructions for Central Europe derived from documentary evidence and instrumental records since AD 1500. Clim Change 101:69–107. doi:10.1007/s10584-009-9724-x

Etien N, Daux V, Masson-Delmotte V, Stievenard M, Bernard V, Durost S, Guillemin MT, Mestre O, Pierre M (2008) A bi-proxy reconstruction of Fontainebleau (France) growing season temperature from A.D. 1596 to 2000. Clim Past 4:1–16

Frank D, Esper J (2005) Characterization and climate response patterns of a high elevation, multi-species tree-ring network for the European Alps. Dendrochronologia 22(2):107–121. doi:10.1016/j.dendro.2005.02.004

Garnier E, Daux V, Yiou P, García de Cortázar-Atauri I (2010) Grapevine harvest data in Besancon (France) between 1525 and 1847: social outcomes or climate evidence? Clim Change. doi:10.1007/s10584-010-9810-0

Glaser R, Brázdil R, Pfister C, Dobrovolný P, Barriendos Vallvé M, Bokwa A, Camuffo D, Kotyza O, Limanówka D, Rácz L, Rodrigo FS (1999) Seasonal temperature and precipitation fluctuations in selected parts of Europe during the sixteenth century. Clim Change 43(1):169–200. doi:10.1023/A:1005542200040

Jones PD, Briffa KR (2006) Unusual climate in Northwest Europe during the period 1730 To 1745 based on instrumental and documentary data. Clim Change. doi:10.1007/s10584-006-9078-6

Jones PD et al (2009) High-resolution palaeoclimatology of the last millennium: a review of current status and future prospects. Holocene 19(1):3–49. doi:10.1177/0959683608098952

Landsteiner E (1999) The crisis of wine production in late sixteenth-century Central Europe: climatic causes and economic consequences. Clim Change 43:323–334. doi:10.1023/A:1005590115970

Lauscher F (1978) New analyses of oldest and more recent phenological time series. [Neue Analysen ältester und neuerer phänologischer Reihen]. Arch Met Geoph Biokl B 26:373–385

Le Roy Ladurie E (1977) The history of sunshine and rainy weather. [Die Geschichte von Sonnenschein und Regenwetter.] In: Honegger C, Bloch M (eds) Script and material of history—proposals for a systematic acquisition of historic processes. [Schrift und Materie der Geschichte—Vorschläge zur systematischen Aneignung historischer Prozesse.] Frankfurt a M, pp 220–240

Leijonhufvud L, Wilson R, Moberg A (2008) Documentary data provide evidence of Stockholm average winter to spring temperatures in the eighteenth and nineteenth centuries. Holocene 18 (2):333–343. doi:10.1177/0959683607086770

Leijonhufvud L, Wilson R, Moberg A, Söderberg J, Retsö D, Söderlind U (2010) Five centuries of Stockholm winter/spring temperatures reconstructed from documentary evidence and instrumental observations. Clim Change 101(1–2):109–141. doi:10.1007/s10584-009-9650-y

Löschnig J, Stefl L (1935) Historical records of the town of Retz. [Geschichtliche Aufzeichnungen der Stadt Retz.] Österreichischer Wein- und Obstbaukalender, pp 149–179

Luterbacher J, Dietrich D, Xoplaki E, Grosjean M, Wanner H (2004) European seasonal and annual temperature variability, trends and extremes since 1500. Science 303:1499–1503. doi:10.1126/science.1093877

Luterbacher J, Liniger MA, Menzel A, Estrella N, Della-Marta PM, Pfister C, Rutishauser T, Xoplaki E (2007) The exceptional European warmth of autumn 2006 and winter 2007: historical context, the underlying dynamics and its phenological impacts. Geophys Res Lett 34:L12704. doi:10.1029/2007GL029951

Manley G (1958) The great winter of 1740. Weather 13:11–17

Manley G (1974) Central England temperatures: monthly means 1659 to 1973. Q J Roy Meteorol Soc 100:389–405

Margary ID (1926) The Marsham phenological record in Norfolk 1736–1925, and some others. Q J Roy Meteorol Soc 52:27–54

Maurer C, Koch E, Hammerl C, Hammerl T, Pokorny E (2009) BACCHUS temperature reconstruction for the period 16th to 18th centuries from Viennese and Klosterneuburg grape harvest data. J Geophys Res 114:D22106. doi:10.1029/2009JD011730

Meier N, Rutishauser T, Pfister C, Wanner H, Luterbacher J (2007) Grape harvest data as a proxy for Swiss April to August temperature reconstruction back to A.D. 1480. Geophys Res Lett 34:L20705. doi:10.1029/2007GL031381

Menzel A (2005) A 500 year pheno-climatological view on the 2003 heat wave in Europe assessed by grape harvest data. Meteorol Z 14(1):75–77. doi:10.1127/0941-2948/2005/0014-0075

Milham WI (1924) The year 1816-the causes of abnormalities. Mon Weather Rev 52(12):563–570

Pfister C (1985) History of the climate of Switzerland 1525–1860. The climate of Switzerland from 1525 to 1860 and its relevance in the history of population and agriculture, Volume 1. [Klimageschichte der Schweiz 1525–1860. Das Klima der Schweiz von 1525–1860 und seine Bedeutung in der Geschichte von Bevölkerung und Landwirtschaft, Band I.] Academica Helvetica, Bern, 184 pp

Pfister C (1999) Weather hindcast. 500 years of climate variability and natural disasters 1496–1995. [Wetternachhersage. 500 Jahre Klimavariationen und Naturkatastrophen 1496–1995.] Verlag Paul Haupt, Bern, 304 pp

Pfister C, Brázdil R (2006) Social vulnerability to climate in the "Little Ice Age": an example from Central Europe in the early 1770 s. Clim Past 2:123–155

Pilgram A (1788) Investigations of what is probable in meteorology through perennial observations. [Untersuchungen über das Wahrscheinliche der Wetterkunde durch vieljährige Beobachtungen] Joseph Edlen von Kurzbeck, k.k. Hofbuchdrucker, Wien

Pribram AF, Geyer R, Koran F (1938) Materials regarding the history of prices and wages in Austria, Volume 1. [Materialien zur Geschichte der Preise und Löhne in Österreich, Vol. 1.] Carl Ueberreuters Verlag, Wien

Puntschert JK (1894) Memorabilities of the town of Retz. [Denkwürdigkeiten der Stadt Retz.] Selbstverlag der Stadt Retz, Wien

Rutishauser T, Luterbacher J, Jeanneret F, Pfister C, Wanner H (2007) A phenology-based reconstruction of interannual changes in past spring seasons. J Geophys Res 112:G04016. doi:10.1029/2006JG000382

Rutishauser T, Luterbacher J, Defila C, Frank D, Wanner H (2008) Swiss spring plant phenology 2007: extremes, a multi-century perspective, and changes in temperature sensitivity. Geophys Res Lett 35:L05703. doi:10.1029/2007GL032545

Sammlung (1719) Compilation of histories of nature and medicine—as well as histories pertinent hereto of art and literature. 4th attempt. [Sammlung von Natur und Medicin—Wie auch hierzu gehörigen Kunst- und Literaturgeschichten. 4. Versuch] Michael Hubert, Breslau

Sandgruber R (1995) Economy and politics. Economic history of Austria from the Middle Ages to the present. [Ökonomie und Politik. Österreichische Wirtschaftsgeschichte vom Mittelalter bis zur Gegenwart.] In: Wolfram H (ed.) History of Austria, Volume 10 [Österreichische Geschichte, Bd. 10], 669 pp

Sommer M (2008) Résumé of the characteristics of an analysis of authentic wines of different vintages and their viticultural-climatic interpretation. Diploma thesis in the disciplines chemistry of fruits and fruit products. [Zusammenfassung der Analysenkenndaten von authentischen Weinen verschiedener Jahrgänge und deren weinbaulich-klimatische Interpretation. Diplomarbeit aus den Fachgegenständen Chemie der Früchte und Fruchtprodukte.] Mathematik, Lehr- und Forschungszentrum für Wein- und Obstbau, Klosterneuburg, Austria

Sparks TH (2007) Lateral thinking on data to identify climate impacts. Trends Ecol Evol 22(4):169–171

Strestik J, Verö J (2000) Reconstruction of the spring temperatures in the 18th century based on the measured lengths of grapevine sprouts. Q J Hungarian Meteorol Serv Időjárás 104(2):123–136

Versuch (1803) Attempt of a centennial history of vinification in Austria; from 1700 to 1800 from primary sources. [Versuch einer hundertjährigen Weinfechsungsgeschichte Österreichs; von 1700 bis 1800 aus Urquellen] Schmidbauer, Wien

Archival sources

News from Klosterneuburg 2000. [Mitteilungen Klosterneuburg 2000]

Rasser chronicle (2010) Manuscript, recordings of Rudolf and Franz Rasser, Gumpoldskirchen, private property. [Rasser Chronik (2010), Manuskript, Aufzeichnungen von Rudolf und Franz Rasser, Gumpoldskirchen, Privatbesitz]

Schmuckenschlager B (2007) Grape harvest data Agneshof Klosterneuburg. [Lesedaten Agneshof Klosterneuburg.] (manuscript)

StAK(losterneuburg) MS 121: Bittmann J (1880) Memorial book and wine chronicle [Gedenkbuch und Weinchronik]

StAK MS 102

StAK MS 122/1

StAK MS 122/2

StAK D 73

StAK Box 221 (Chronicle of weather and contingencies [Wetter und Zufällechronik], compiled by Willibald Leyrer in 1789)

StARetz, Accounts of Buergerspital [Buergerspitalrechnungen] 1527–1860

The median winter snowline in the Alps

M. Hantel and **C. Maurer**

Meteorol. Z., 2011, **20**(3), 267-276

Meteorologische Zeitschrift, Vol. **20**, No. 3, 267-276 (June 2011)

Open Access Article

The median winter snowline in the Alps

MICHAEL HANTEL* and CHRISTIAN MAURER

Research Platform 'Sensitive Mountain Limits of Snow and Vegetation', University of Vienna, Austria

(Manuscript received May 21, 2010; in revised form November 10, 2010; accepted November 10, 2010)

Abstract

The relative duration of snow cover in a season is a number between zero and unity; here it represents the probability to encounter, at a given station, snow of at least 5 cm depth. We use routine station data of snow depth for the winters 1961–2000 to explore the pattern of relative snow duration in the Alps. A horizontal isoline is drawn across all stations that exhibit 50 % snow duration; we consider this isoline the *median snowline*. We further introduce the *mountain temperature* as linear expansion of the Central European temperature with respect to station coordinates; it separates the large-scale European temperature from the local-scale vertical lapse rate and serves as substitute for the station temperature. The mountain temperature allows to condense the snow data of all stations and years into one analytical curve, the *state function of snow duration*. This curve yields every desired snowline; the median snowline coincides with the altitude of maximum sensitivity of snow duration to European temperature. The median snowline in winter is located at an average altitude of 641 m and slightly slopes downward towards the eastern Alps. The average altitude varies considerably from winter to winter under the influence of European temperature fluctuations; it shifts upward by about 123 m per °C climate warming.

Zusammenfassung

Die relative Dauer der Schneebedeckung in einer Jahreszeit ist eine Zahl zwischen Null und Eins. Hier wird sie als Wahrscheinlichkeit verstanden, an der betreffenden Station Schnee mit einer Mindesthöhe von 5 cm anzutreffen. Wir verwenden Routinedaten der Schneehöhe für die Winter 1961–2000, um das Feld dieser Größe in den Alpen zu untersuchen. Wenn man alle Stationen mit 50 % Schneedauer horizontal verbindet, so entsteht eine Höhenlinie, die wir als *Median-Schneelinie* bezeichnen. Wir führen die *Gebirgstemperatur* ein als lineare Entwicklung der mitteleuropäischen Temperatur nach den Stationskoordinaten; sie separiert die großskalige europäische Temperatur vom lokalen vertikalen Temperaturgradienten und ersetzt so die Stationstemperatur. Mit der Gebirgstemperatur lassen sich die Schneedaten aller Stationen und Jahre in einer analytischen Kurve zusammenfassen, der *Zustandsfunktion der Schneedauer*. Aus der Zustandsfunktion kann man jede gewünschte Schneelinie gewinnen; die Median-Schneelinie fällt mit der Höhe der maximalen Empfindlichkeit der Schneedauer bezüglich der Europatemperatur zusammen. Diese Linie liegt im Winter bei einer mittleren Höhe von 641 m und fällt leicht nach Osten hin ab. Die mittlere Höhe der Median-Schneelinie variiert beträchtlich von Winter zu Winter aufgrund von Schwankungen der Europatemperatur; sie wandert um rund 123 m pro °C Klimaerwärmung aufwärts .

1 Introduction

The idea of the snowline is not new. HANN (1883) has defined the *snowline* (or *snow limit*) as the lowest altitude of the perennial snow cover, equivalent to the lower boundary of the snow-covered area at the end of summer; it yields a climatological annual average. This concept has been adopted by KÖRNER (2003) based on TROLL (1961) who understands the snowline as thermal boundary above which the ground remains snow covered all-the-year. However, seasonal fluctuations are of similar impact upon the snowline, also in accord with HANN (1883); for example, at Mt. Säntis (NE-Switzerland) he locates the snowline at 740 m in the second decade of December and at 1930 m in June. And for the Inn valley close to Innsbruck HANN (1908) finds, averaged over the north and south faces, a value of 667 m for the snowline in winter and 2575 m in summer. A modified approach is to consider the geographical distribution of snow cover. For example, the *Dictionary of Earth Science* (PARKER, 1997) defines the snowline as the boundary of an area with more than 50 % snow cover. As to recent applications, a study in the Indian Himalayas (KAUR et al., 2010) uses satellite measurements of monthly snow cover; the snowline is located at the elevation that separates the area with snow cover from the area free of snow.

These references are not exhaustive; yet they suffice to show that the snowline is not a generally accepted notion but remains somewhat vague. We have considered it worthwhile to rigorously define what we feel should be the natural meaning of the snowline and to demonstrate its climatological significance, here restricted to the winter season in the Alps.

Our 'natural' approach is to take the line that separates complete from zero snow cover. We place its average position where there is a 50 % probability to encounter snow at any time, identical to 50 % probability for no

*Corresponding author: Michael Hantel, Research Platform 'Sensitive Mountain Limits of Snow and Vegetation', University of Vienna, Theoretical Meteorology Research Forum, Berggasse 11/2/3, A-1090 Wien, e-mail: michael.hantel@univie.ac.at

DOI 10.1127/0941-2948/2011/0495

0941-2948/2011/0495 $ 4.50

snow. We will get this information from observed snow depths by connecting neighbored climate stations with the same *relative snow duration*; relative snow duration is the percentage of days in a given season with snow depth above a specified threshold. This understanding applies principally to every value of relative snow duration between zero and unity. Here we want to focus upon the 50 %-snowline, called the *median snowline*.

It is the first purpose of this study to find, from observed data, the altitude of the median winter snowline in the Alps, including its time fluctuations from year to year. The second purpose is to understand the mechanism that generates the field of snowlines. We shall show that the controlling agent is the mean winter temperature of continental Europe. We will particularly demonstrate that the median snowline is unique in that it represents the altitude of maximum sensitivity of snow cover duration with respect to European temperature.

The snowline concept is the novelty of this paper. Its main goal is to develop a theoretical understanding with which the qualitative description of a snowline can be formalized and quantitatively derived from snow depth measurements. It will be based upon the following earlier publications: HANTEL et al. (2000), referred to as 'Paper I'; WIELKE et al. (2004) together with WIELKE et al. (2005), 'Paper II'; and HANTEL and HIRTL-WIELKE (2007), 'Paper III'. In Paper I the dependence of relative snow duration upon European temperature has been investigated for Austrian climate stations; the same has been done for Swiss climate stations in Paper II. The theoretical model has been rigorously developed in Paper III.

The present study is organized as follows. We start with the data description and, in a preliminary step, study the mean altitude of 50 %-snow duration in the Alps from one individual winter to the next; only snow data are used in this step. Then we review our model (i.e., Papers I, II, III); it combines *local-scale snow* information with *continent-scale temperature* information and condenses both into one formula, called the 'state function of snow duration'; it represents the entire data volume of the entire observation period. From the state function all relevant parameters can be analytically derived. They yield the innovative quantity presented here: altitude and horizontal pattern of the median snowline, complete with its temperature sensitivity and time trend.

2 Basic data and quality checks

As *snow data base* for winter (DJF) we take the 'All Alps' snow depth data set 1961–2000 from the 268 climate stations used in Paper III. Measured quantity is the *snow depth*, observed daily at each station (Fig. 1). Following Paper I, a day with snow depth above or below threshold 5 cm is counted as $\nu = 1$ or $\nu = 0$. The DJF

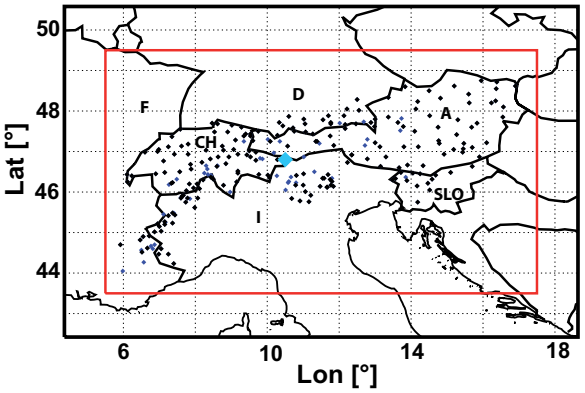

Figure 1: Location of Alpine climate stations providing the basic snow duration data set. Blue rhomboids: stations that do not pass the correlation criterion; black rhomboids: stations used for the final evaluation. Average of CRU temperature over red box in inset (5.5–17.5°E, 43.5°–49.5°N) is representative for European temperature. Thick light blue rhomboid: Position of $x = 0$, $y = 0$ in definition of mountain temperature.

average of ν yields the relative snow duration $\overline{\nu} = n$ of this station winter. n is close to 1 at high stations in cold winters ('always snow') and close to 0 at low stations in mild winters ('never snow'). The frequency distribution of n (not shown) is bimodal with a minimum of less than 40 station winters around $n = 0.5$ and maxima of more than 80 winters close to $n = 0$, $n = 1$.

If less than 15 observations at a station are reported in a given winter the respective station winter is *a priori* dropped. This excludes 11 stations. The year of a specific winter is referenced according to its January; for example, winter 2000 is December 1999, January 2000, February 2000. The first winter (1961) of the record comprises only January and February, the December of the year 2000 has not been used.

Further, station winters with exactly $n = 0$ and those with exactly $n = 1$, referred to as 'saturated', are also *a priori* dropped. The reason is that saturated snow data do not carry relevant information since they have observation variance zero; we do not accept them as measurements (for further discussion of this point see section 4). This excludes 7 stations which report only saturated data. Each of the remaining stations contains at least one unsaturated n-value (most of them much more).

Observing the two *a priori* requirements just described yields the basic station data set. It consists of 250 stations (black and blue rhomboids in Fig. 1) yielding 10000 principally usable station winters. Many of these stations still contain individual winters that are saturated and thus have also to be dropped. This procedure ends with 5705 unsaturated n-values, one for each station winter (corresponding to 22.8 winters per station).

As *temperature data base* we take the monthly gridded CRU temperatures (BROHAN et al., 2006) with a horizontal resolution of 0.5 degrees. These are averaged

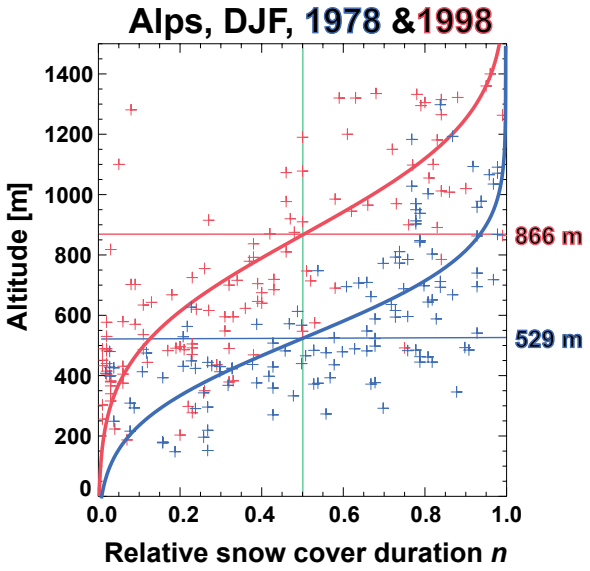

Figure 2: Relative duration n of snow cover at 'All Alps' climate stations in the winters of 1978 (blue) and 1998 (red), plotted versus station altitude z. Fit with logistic model $P(z)$ = $\Phi(\chi)$ with Φ = error function and χ=$\sqrt{2\pi}r_0(z - z_0)$. Parameters in 1978 (131 data points): r_0^{1978} =1.76(±0.46)×10^{-3}m^{-1}; z_0^{1978} =529(±30) m. Parameters in 1998 (132 data points): r_0^{1998} =1.33(±3.66)×10^{-3}m^{-1}; z_0^{1998} =866(±109) m. Note that 7 blue and 16 red crosses which were used for estimating the fit profiles could not be drawn because they are outside the plot.

horizontally over the Alpine-dominated part of Central Europe (5.5°-17.5°E and 43.5°-49.5°N, referred to as 'small area' in the following, identical to the red box in Fig. 1) and time-averaged over the winter. This procedure yields a time series of 40 values of *European temperature* T characterising each winter of the observation period.

In Papers I-III we had chosen the area 5-25°E and 42.5°-52.5°N ('large area' in the following, not drawn in Fig. 1) for averaging the CRU data. It may appear doubtful to place the temperature of the Alps in the context of a Europe-wide average. In order to clear this point we have compared the 'large area'-average $T_{CRUlarge}$ of Paper I with the 'small area'-average $T_{CRUsmall}$ of the present Fig. 1; note that the 'small area' comprises all useable climate stations. The correlation of the two 40-year time series $T_{CRUlarge}$ and $T_{CRUsmall}$ is 0.98. This suggests that the continental-scale average of the CRU data is a fairly robust quantity (see also Fig. 4 below). Here we will use T = $T_{CRUsmall}$ as reference European temperature. After all, the resolution of the data that define this T corresponds to the resolution of global climate observational fields [typically 125 km, see UPPALA et al. (2005)] and global climate models [for example, the atmosphere/ocean model HadCM2 has a horizontal resolution 2.50°× 3.75°, see BUONOMO et al. (2007)].

Station temperatures are also available at all stations of Fig. 1. However, we do not use them in this study with the two exceptions of Fig. 5 and Fig. 7. It is only in these two figures that we compare the results found with the CRU-data to those found with station temperatures.

As *quality check for the snow data* we adopted a criterion already used in Papers I-III: We require that the linear correlation coefficient between n and T during the observation period should be negative at each station. 43 stations (comprising 335 station winters or 5.9 % of the total n-values) that violated this condition (blue symbols in Fig. 1) were discarded, leaving 207 useable stations. The mean altitude of these is 728±412m[1] (63 stations are located below 500 m a.s.l., 108 are between 500 m and 1500 m a.s.l. and 36 are above 1500 m a.s.l.). The surviving 5370 n-values for 5370 station winters represent the snow data base of this study (black symbols in Fig. 1, corresponding to 25.9 winters per station).

3 Mean altitude of the median snowline

The snow duration comes as function of time θ and of the space coordinates x, y, z of the climate station:

$$n = n(\theta, x, y, z). \tag{3.1}$$

We plot n versus altitude z in a given year, irrespective of x, y. The fit curve $P(z)$ for n must not be linear since n is the mean of the binary stochastic variable ν. For variables of this type a *logistic curve* is the proper fitting function (HOSMER and LEMESHOW, 2000). Out of the class of logistic curves (MAZUMDAR, 1999) we take here the error function[2].

Such curve is fitted to the blue symbols in Fig. 2, valid for 1978. The fit curve cuts the median value n = 0.5 at an altitude H^{1978} = 529 m. We consider H as the averaged *altitude of the median snowline*; it is equal to the reference parameter z_0 of the interpolating error function (see caption of Fig. 2).

The winter of 1978 was relatively cold (European temperature T^{1978} = -0.08°C). The milder winter 1998 (T^{1998} = 2.52°C) generates lower relative snow durations (red symbols in Fig. 2) which yield the average median snowline altitude H^{1998} = 866 m (see caption of Fig. 2). BENISTON et al. (2003), using Swiss data from 18 observing sites, consider also snow cover duration versus altitude profiles but restricted to a linear fit; they find, opposite to our result of Fig. 2, a smaller vertical slope in cold than in mild winters.

The result H^{1998}>H^{1978} is as expected: The snowline tends to be higher when the temperature is higher.

[1] All standard deviation estimates in this study are given as one sigma.
[2] Choice of the error function has been convenient in our programming but is not mandatory here; one could take other logistic functions in Fig. 2 as well. On the other hand, in section 4.2 below, the error function follows from the laboratory model of HANTEL and HIRTL-WIELKE (2007) and in this sense is mandatory.

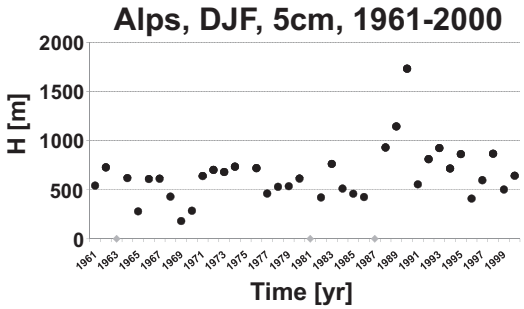

Figure 3: Median snowline altitude H (for each year determined according to Fig. 2) for Alpine climate stations plotted versus time. Light grey dots: Data points excluded because fit has yielded a negative H-value (see text).

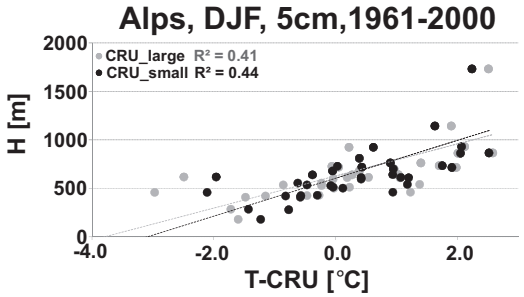

Figure 4: Altitude H of median snowline (determined according to Fig. 2) for Alpine climate stations plotted versus European temperatures $T_{CRUlarge}$ and $T_{CRUsmall}$.

The data of Fig. 2 for H and the data for T allow a first estimate of the sensitivity of the snowline altitude with respect to European temperature:

$$\frac{\Delta H}{\Delta T} = \frac{866\text{m} - 529\text{m}}{2.52°\text{C} + 0.08°\text{C}} = 130\,\frac{\text{m}}{°\text{C}} \qquad (3.2)$$

This result from just the two winters comes surprisingly close to the much better founded estimate to be calculated below that will be based upon all winters 1961–2000.

Fig. 3 shows the time series of H over the 40-year observation period. In some years the fit yields a negative H. This is formally possible since the logistic function is not restricted to altitudes $z>0$; we consider the 3 corresponding H-values (light grey rhomboids in Fig. 3) as outliers.

The upward increase of n in the individual profiles 1978 and 1998 in Fig. 2 is evidently due to the familiar upward decrease of temperature; this is a local effect. Conversely, the gross difference between the entire profiles 1978 and 1998 is a large-scale effect caused by the European temperature. This interpretation is supported by relating the time series of H in Fig. 3 to the time series of T for the same period. The corresponding scatter diagram is shown in Fig. 4 for the two European temperatures defined above. The difference between the impact of either $T_{CRUlarge}$ or $T_{CRUsmall}$ in Fig. 4 is marginal, the correlation is significant in both cases.

Fig. 4 suggests that the interannual altitude fluctuations of the median snowline (Fig. 3) are controlled by the European temperature. This European effect of Fig. 4 (from now on represented by $T = T_{CRUsmall}$) needs to be separated from the familiar vertical lapse rate effect of Fig. 2. It is for this purpose that we have developed the model that will be reviewed in the next section.

4 Review of the snow duration model

The snow duration model as we use it here has grown in steps from Paper I for Austrian climate stations [HANTEL et al. (2000)], over Paper II for Swiss stations [WIELKE et al. (2004) together with WIELKE et al. (2005)], to Paper III for All-Alps stations [HANTEL and HIRTL-WIELKE (2007)]. The concepts required will be reviewed in this section.

4.1 The probabilistic model – the local mode

Basic hypothesis of our probabilistic model is that the seasonal snow cover duration n is in approximate thermodynamic equilibrium with seasonal mean temperature t. We describe this mechanism through a normally distributed stochastic variable from an ensemble with mean t and standard deviation ϵ. The probability P that t is less than a reference t_0 is [see standard statistics texts, e.g. TAYLOR (1997)]:

$$P(t) = \Phi\left(\frac{t_0 - t}{\epsilon}\right). \qquad (4.1)$$

Φ is the *error function* (BRONSTEIN et al., 1999) defined as:

$$\Phi(\chi) = \frac{1}{\sqrt{2\pi}} \int_{\vartheta=-\infty}^{\chi} e^{-\vartheta^2/2} \mathrm{d}\vartheta. \qquad (4.2)$$

The more t is below t_0, the more positive is the argument of Φ in (4.1) and the closer to unity is P.

In the ideal case (an experiment with distilled water in the laboratory, see Fig. 3 of Paper III) we interpret t as temperature (t_0 = freezing temperature). When equilibrium has been reached P is identical to the probability to find water in the frozen phase. We eliminate ϵ in Eq. (4.1) in favor of the negative parameter s_0 by putting $-\epsilon^{-1} = \sqrt{2\pi} s_0$. The probability for ice is now:

$$P(t) = \Phi(\chi) \qquad \text{with} \qquad \chi = \sqrt{2\pi}\, s_0 (t - t_0). \quad (4.3)$$

A preliminary form of this model was first applied (in the so-called 'local mode') to snow duration data in winter and spring at individual Austrian climate stations (Paper I, Figs. 4, 6, 7) and at Swiss climate stations

(Paper II, Fig. 1); the parameters s_0, t_0 were determined through fitting the theoretical function to the data[3]. For t we first chose the European temperature T. The results were encouraging. Papers I, II showed that at individual climate stations the interannual T-variations cause a strong n-variation, quite well described by the model (4.3).

4.2 Revisiting the error model of Paper I

Before proceeding some remarks are necessary concerning the error model applied for estimating the parameters s_0 and t_0 in (4.3). The nonlinear fit used here as well as in Paper I follows standard statistical interpolation recipes [e.g., TAYLOR (1997)] and consists of minimizing the cost function:

$$J(s_0, t_0) = \sum_{i=1}^{I} \left[\frac{n_i - n^i}{\sigma(n_i)} \right]^2 \qquad (4.4)$$

The index i for the data points runs from 1 to I, with I the number of station winters. n_i is the measured snow duration and $n^i = P(t_i)$ is the nonlinear model value with t_i the measured temperature.

$\sigma(n_i)$ is the standard deviation of the measured n_i. We may recall that n is calculated from the daily ν (with $\nu = 0$ for snow depth below threshold, $\nu = 1$ for snow depth above threshold). Now it can be shown that the stochastic quantity ν is Bernoulli-distributed (DEGROOT, 1986). It has a parabolic variance distribution; the variance of n at the limits of the interval is exactly zero. For this reason saturated values $n_i = 0$, $n_i = 1$ cannot be accepted as observations; the corresponding weight $1/\sigma(n_i)^2$ would make the respective term infinite in the cost function. It follows that saturated n's do not belong to a snow duration data sample and have *a priori* to be dropped.

These specifications of the nonlinear fit yield the parameters s_0 and t_0 that make J a minimum. There is a further specification in the error model of Paper I that concerns the 'rectified' fit and the 'extended' fit. In Papers I-III the extended fit was used which tends to overestimate the parameter s_0. We shall not use these fits here but exclusively apply the nonlinear fit represented by $J(s_0, t_0)$, together with the parabolic profile for $\sigma(n_i)$.

4.3 The probabilistic model – many stations

When many climate stations are involved the role of the temperature requires further analysis. We shall from here on reserve the letter t for station temperature (seasonal average of local daily station observations) and T for European temperature (seasonal average of area average of monthly gridded CRU temperatures). Instead of plotting n in the local mode as function of T one could as well plot n, still in the local mode, as function of t (this was done in Fig. 1 of Paper III). The reason is that t and T are quite well correlated at individual stations (see, e.g., Fig. 6 of Paper III). The plot $n(t)$, now for the present All-Alps set, is shown in Fig. 5, together

[3]In Paper I we used the hyperbolic tangent function for interpolation, without a physical argument. In Paper III we introduced the physical mechanism described here; it leads to the Gaussian error function for interpolation. The differences between hyperbolic tangent and error function are numerically small.

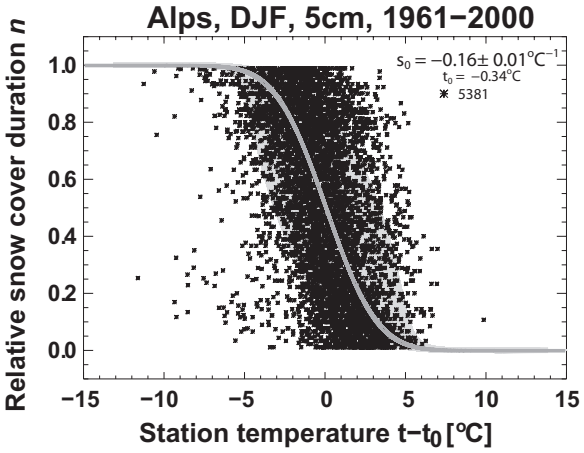

Figure 5: Winter snow duration n at 210 Alpine climate stations plotted versus station temperature. Thick grey curve $P(t)$ interpolates n-values. Each dot represents one out of 5381 station winters. Grey shading captures 68 % of data points (corresponding to one standard deviation in t-direction); shading does not show accuracy of fitted state curve. For discussion of parameters see text.

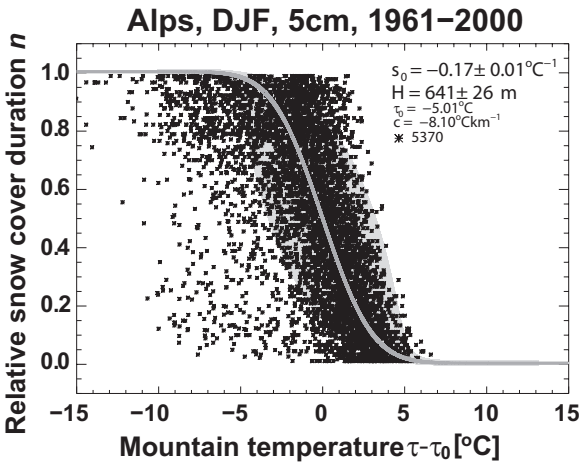

Figure 6: Winter snow duration n at 207 Alpine climate stations plotted versus mountain temperature. Thick grey curve $N(\tau)$ represents state function of n. Each dot represents one out of 5370 station winters. Grey shading captures 68 % of data points (corresponding to one standard deviation in τ-direction); shading does not show accuracy of fitted state curve. Selected parameters are shown in the inset; for discussion see text.

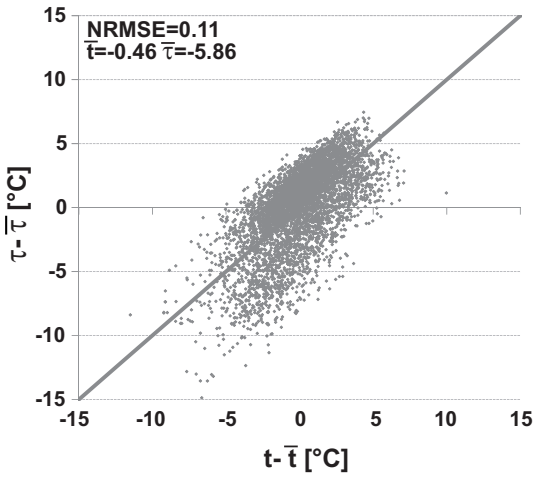

Figure 7: Scatter plot of mountain temperature τ (from the fit of the snow state function in Fig. 6) and station temperature t (from routine station data); $\overline{\tau}$, $\overline{t}$ are the corresponding mean values. NRMSE is the normalized root mean square error; normalization is made with the difference between largest and smallest observed t-anomalies.

with the interpolating function $P(t)$ defined in (4.3)[4].

Fig. 5 includes estimates for s_0, t_0. The parameter s_0 is the maximum temperature sensitivity of the snow duration.The value is to be interpreted as follows: When t decreases (increases) by 1 degree n increases (decreases) by 16 %. For example, a station with n = 0.5 (45 snow cover days per winter) would, under a hypothesized warming of 1°C, experience a decrease of the winter snow duration down to n = 0.34; this would correspond to a reduction by 14 snow days leaving meager 31 snow cover days per winter for this station.

4.4 The concept of mountain temperature

The plot $P(t)$ in Fig. 5 reveals the temperature dependence of n; however, the z-information of Fig. 2 is lost. It follows that snowlines cannot be gained from Fig. 5.

Now the station temperature t is influenced by two mechanisms: The large-scale climate process condensed in the European temperature T; and the local effects, notably the vertical lapse rate of temperature but also the horizontal temperature structure. Thus we have attempted to replace t through a combination of T and station coordinates x, y, z; they are condensed in the *mountain temperature* defined as[5]:

$$\tau = T + ax + by + cz \qquad (4.5)$$

[4]There are 5381 station winters in Fig. 5 instead of the 5370 available values. The reason is that the correlation criterion applied in Fig. 5 excludes not 43 but only 40 climate stations which adds 11 station winters to the number of data points.

[5]In Papers I-III the parameter τ was called 'Alpine temperature'; here we have switched to 'mountain temperature' for greater generality.

a, b, c are the constants of this linear expansion; (4.5) can equivalently be interpreted as multilinear regression analysis of t. We have plotted the station temperatures t and τ – the latter fitted from (4.5) with t as dependent variable – against each other with good results in a first step (70 % explained variance, details not shown).

4.5 The global mode and the state function of snow duration

We now change perspective. We will not get τ from the observed t-field, but from the n-field. We replace t through τ in (4.3) and understand $P(\tau)$ as probability of snowcover duration, with the same functional relationship as in (4.1); the parameters s_0, τ_0 (augmented by the coefficients a, b, c) are to be fitted to the observed snow data. In this way our equilibrium hypothesis above is implemented in the 'global mode' and yields what may be called the *state function of the snow duration*:

$$N(\tau) = \Phi(\chi) \qquad \text{with} \qquad \chi = \sqrt{2\pi}\, s_0(\tau - \tau_0). \qquad (4.6)$$

Φ is as defined in (4.2). $N(\tau)$ is specified by the *parameter vector* (s_0, τ_0, a, b, c). Time θ is implicit in the *data vector* (n, T, x, y, z) through the time dependence of the large-scale climate temperature $T(\theta)$. The parameter vector is estimated from the data vector through our fitting routine discussed above. Local temperature t is not involved.

4.6 Temperature sensitivity of the state function

Fig. 6 shows the state function for the Alpine data set. The profile $N(\tau)$ represents the observed n-data of all station winters over the entire period 1961-2000. The complete parameter vector is listed in Table 1 together with a couple of derived quantities. All error estimates have been obtained through a bootstrap routine (EFRON and TIBSHIRANI, 1998) with 2000 runs each. s_0 is the extreme slope of the curve $N(\tau)$ for $\tau = \tau_0$; the corresponding function value is $N(\tau_0) = 0.5$.

Fig. 6 yields practically the same interpolating curve as does Fig. 5 which suggests that t is reasonably represented by τ. This is independently shown in Fig. 7. The difference between the means $\overline{\tau}$, $\overline{t}$ in Fig. 7 corresponds to the difference between the fit constants τ_0, t_0 in Figs. 5, 6. The added value of the mountain temperature (4.5) is that large-scale and local-scale temperature effects become separated. The parameters a, b, c that define τ follow from the nonlinear fit of the observed n-data; no t-information is used for τ. Given this independence between the data sources of t and τ the NRMSE-value seen in Fig. 7 must be considered quite good (the most ideal value would be NRMSE = 0).

The fitted curve $N(\tau)$ from Fig. 6 is reproduced in Fig. 8 together with a statistical summary of the station winter data. Both Figs. 6, 8 suggest that the mountain

Table 1: Parameters of state function and derived quantities for winter snow duration. Snow data from Alpine climate stations 1961–2000. T = European temperature, θ = time. The term 'temperature gradient' refers to the gradient of the mountain temperature τ.

	State function parameters	
Quantity	Symbol	Numerical value
Parameters (fitted) of state function $N(\tau)$		
Maximum sensitivity of state curve	s_0	-0.17($\pm$0.01)$^{\mathrm{o}}\mathrm{C}^{-1}$
Reference parameter for τ	τ_0	-5.01($\pm$0.69)$^{\mathrm{o}}$C
West-to-east temperature gradient	a	-0.45($\pm$0.06)$^{\mathrm{o}}$C/$^{\mathrm{o}}$lon
South-to-north temperature gradient	b	0.42($\pm$0.24)$^{\mathrm{o}}$C/$^{\mathrm{o}}$lat
Altitudinal temperature gradient	c	-8.10($\pm$1.12)$^{\mathrm{o}}$C km^{-1}
Parameters (derived) of median snowline		
Altitude (valid for $\tau = \tau_0, x = 0, y = 0, T = 0.19^{\circ}$C)	$H = \frac{\tau_0 - T}{c}$	641 ($\pm$26) m
Temperature sensitivity	$\partial H/\partial T = -1/c$	123 ($\pm$17) m/$^{\mathrm{o}}$C
Altitude trend	$\Delta H/\Delta\theta = -c^{-1}\Delta T/\Delta\theta$	52 ($\pm$39) m/10 years

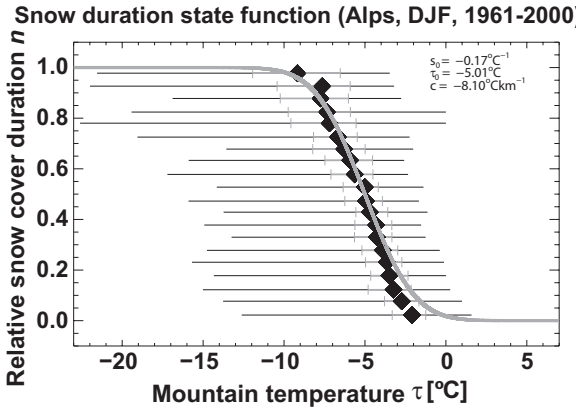

Figure 8: State function of snow duration at Alpine climate stations. Thick grey curve: Profile $N(\tau)$ reproduced from Fig. 6. Statistics of data points for 0.05-wide n-bins, drawn as median (black rhomboids), quartiles (grey bars) and minimum/maximum values (black whiskers).

temperature is not exactly normally distributed which is however of no consequence for the median snowline. The deviations of n from the interpolated curve have a distribution (not reproduced here) that is symmetric but sharper than normal because the fit is nonlinear; it is quite similar to Fig. 11-a in Paper III.

The sensitivity of the fitted snow duration with respect to mountain temperature is:

$$\frac{\mathrm{d}N}{\mathrm{d}\tau} = \frac{\mathrm{d}\Phi}{\mathrm{d}\chi}\cdot\frac{\mathrm{d}\chi}{\mathrm{d}\tau} = s_0\exp(-\chi^2/2); \qquad \text{specifically,} \quad \left[\frac{\mathrm{d}N}{\mathrm{d}\tau}\right]_{\tau=\tau_0} = s_0. \tag{4.7}$$

χ is specified through (4.6). As noted in Paper I, the sensitivity with respect to T is equal to the sensitivity with respect to τ:

$$\frac{\partial N}{\partial T} = \frac{\mathrm{d}N}{\mathrm{d}\tau}\underbrace{\frac{\partial\tau}{\partial T}}_{=1} = \frac{\mathrm{d}N}{\mathrm{d}\tau}. \tag{4.8}$$

The partial derivative is understood for fixed station vector (x, y, z). Note that (4.8) applies to all τ, not just to τ_0. Thus formula (4.8) represents the entire sensitivity profile of Alpine climatological snow cover. The sensitivity is maximum for $\tau = \tau_0$, adopted at the altitude of the median snowline; above and below the sensitivity decreases and becomes zero at very low and very high altitudes.

A point much discussed in Papers I and II is to what extent s_0 depends on the specifications of the error model. Our earlier evaluations yield, with the nonlinear fit, a value for s_0 between -0.13°C^{-1} [only Switzerland data; see Fig. 3 of WIELKE et al. (2005)] and -0.20°C^{-1} [only Austrian data; see Fig. 8 of HANTEL et al. (2000)]. With the present All-Alps data we find s_0 = -0.17°C^{-1} (Figs. 6, 8 and Table 1). We consider this an acceptable coincidence, given the different data bases and the shorter observation period in papers I, II (1961-1990) as compared to the present study. These considerations show further that the All-Alps sensitivity -0.33 per °C warming, obtained with the extended fit and published in Paper III, must now be considered an overestimate. The maximum sensitivity s_0 = -0.17°C^{-1} found here is more realistic.

5 Characteristics of the snowline

Complete snowline information can be drawn from $N(\tau)$ by straight analytical reasoning; the mountain temperature concept allows to derive the characteristics of the snowline from the state function. The altitude of the median snowline is:

$$H(0.5, T, x, y) = \frac{\tau_0 - T - ax - by}{c}. \tag{5.1}$$

It follows from solving Eq. (4.5) for $z = H$ with the condition $\tau = \tau_0$; this yields the value $n = N(\chi = 0) = 0.5$ of the state function which is the definition of the median snowline. It is at this altitude that the temperature sensitivity adopts the extreme value s_0. $H =$ 641 m in Tab. 1 has been entered for $x = 0$, $y = 0$ (located in Tyrol, $\lambda = 10.5^{\mathrm{o}}$E, $\phi = 46.8^{\mathrm{o}}$N, thick blue rhomboid in Fig. 1). Note that the standard deviation of H in Tab. 1 is gained from the bootstrap results for τ_0 and c and does not take into account the interannual fluctuations of T; the estimate $\pm$ 26 m is smaller than might be concluded from the fluctuations seen in Fig. 3.

The altitude of an arbitrary snowline specified by n is:

$$H(n,T,x,y) = \frac{\tau(n) - T - ax - by}{c}; \quad \frac{\partial H}{\partial T} = -\frac{1}{c}. \tag{5.2}$$

The specification of $\tau(n)$ can be implemented through the inverse N^{-1} of the state function as $\tau(n) = N^{-1}(n)$. For example, for $n = 0.5$ the fitted N from Figs. 6, 8 yields $\tau = \tau_0 =$ -5.01°C. The partial derivative in (5.2) is understood for fixed snowline n and fixed station coordinates x, y. Eq. (5.1) is a special case of the general formula (5.2). Both reflect the downward move of the median snowline in cold years and the upward move in warm years (note that $c<0$).

The *temperature sensitivity of the snowline altitude*, $\partial H/\partial T$ according to (5.2), is constant across the entire domain and thus the same on all snowlines. The corresponding numerical value (Tab. 1) suggests that a climate warming of 1°C shifts all snowlines in the Alps about 123 m upward. This relatively accurate estimate is a new result of this study; it is in accord with the preliminary value (3.2) found above from the two years of Fig. 2.

On the other hand, the *temperature sensitivity of the snow duration*, $\partial N/\partial T$ according to (4.8), remains to be different for different locations in the domain; specifically, $\partial N/\partial T$ is absolutely low both for low and for high altitudes but extreme at the median snowline. Formula (4.8) implies that the temperature sensitivity of the snow duration is a function of $\chi(\tau)$; thus it can be gained analytically for all snowlines specified by τ.

The time trend of the median snowline can, with Eq. (5.2), be written:

$$\frac{\mathrm{d}H}{\mathrm{d}\theta} = \frac{\partial H}{\partial T} \cdot \frac{\mathrm{d}T}{\mathrm{d}\theta} = -\frac{1}{c}\frac{\mathrm{d}T}{\mathrm{d}\theta} \tag{5.3}$$

Thus with the parameter c given it is the trend of T that controls the altitude trend of all snowlines. From the time series of T (data on the horizontal axis of Fig. 4, not explicitly elaborated here) we adopt $\Delta T/\Delta\theta =$ 0.44($\pm$0.32)°C/10 years. This (relatively insignificant) estimate is somewhat larger than the post-1975 trend 0.33°C/10 years for the northern hemisphere land areas [STRANGEWAYS (2010); see also the detailed trend discussion of SCHERRER et al. (2006)]. Formula (5.3) yields $\Delta H/\Delta\theta =$ 52 m/10 years (Tab. 1)[see also the discussion of snow cover trend published by DYE (2002)]. This trend estimate is however insignificant, due to the strong interannual fluctuations of T.

6 The 3D-pattern of the median snowline across the Alps

The median snowline in the Alps in winter is drawn in Fig. 9. The snowline is generated by cutting the horizontally inclined plane $H(n,T,x,y)$ with the earth's surface for fixed $\tau(n)$, here $\tau = \tau_0$, fixed European temperature (mean value 1961–2000), fixed parameters a, b, c and variable horizontal coordinates x, y. The parameters are taken from Table 1.

The inclination of the plane $H(n,T,x,y)$, i.e., the horizontal slope of the snowline altitude, is gained by differentiating formula (5.2) with respect to x in eastern and to y in northern direction, with n and T kept constant. This yields:

$$\begin{aligned} \frac{\partial H}{\partial x} &= -\frac{a}{c} = -56\frac{\mathrm{m}}{^{\circ}\mathrm{longitude}}; \\ \frac{\partial H}{\partial y} &= -\frac{b}{c} = 52\frac{\mathrm{m}}{^{\circ}\mathrm{latitude}} \end{aligned} \tag{6.1}$$

This estimate corresponds to a (significant) downward slope of about 560 m from the western to the easternmost Alps ($\Delta x \approx 10^{\circ}$longitude) and a (non significant) upward slope of about 150 m from the southern to the northern Alps ($\Delta y \approx 3^{\circ}$latitude). This is made visible in Fig. 9 by the perimeter of the plane $H(0.50,T,x,y)$ which is drawn in red color.

With regard to other possible snowlines a higher located one would generate a much smaller area than does the 50 % snowline in Fig. 9. Another important difference between the snowline patterns of Fig. 9 and any other snowline is the difference in temperature sensitivity. It is a maximum for the median snowline, which implies that for high and low located stations a change of European temperature is of comparatively little impact upon the snowline.

The horizontal slope of the plane $H(n,T,x,y)$ is the same for all snowlines. This may not do justice to the complicated orography of the Alps; the simplification of our present model does not allow for a horizontal change of the lapse rate parameter c. Now it would be easy to implement more sophisticated functions than the simple linear expansion represented by our τ; for example, higher than linear expansions or thin-plate spline functions could be chosen. We have not done this in the present study; however, generalizations of this type will be a challenge for further study.

7 Conclusions

The *practical innovation* of this study is the snowline concept; it represents the entire winter snow information of the Alps in form of one simple visualization.

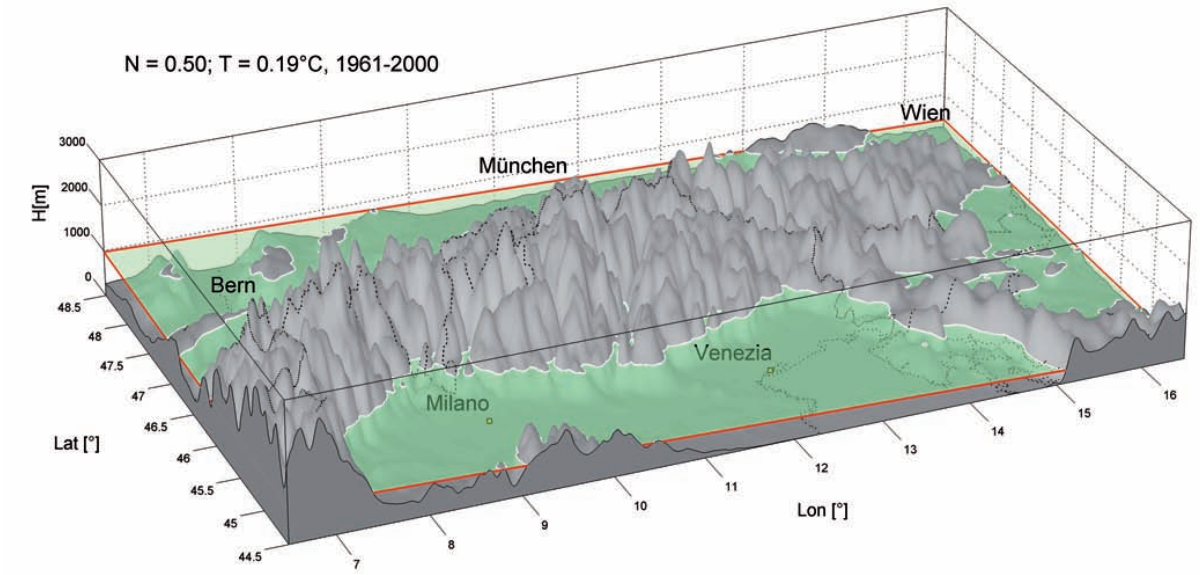

Figure 9: Surface $H(0.50, T, x, y)$ for winter snow duration probability 50 %. The median snowline (drawn white) is the intersection of this linear plane with orography for the special choice $\tau = \tau_0$ with τ_0 = -5.01°C.

Specifically the up-and-down motion of the winter snow cover from year to year becomes visible; for example, one could animate the snowline variations with time by running Fig. 9 through the entire climate period. We have shown that the most important snowline is the median snowline $n = 0.5$ because the sensitivity of the state function $N(\tau)$ at its altitude to changes in European temperature is a maximum.

The present evaluations have been limited to snow depth threshold 5 cm. We have made experiments with other thresholds (not reported here) but the results are much the same, except that the median snowline is located somewhat higher; an approximate estimate is an increase of H by about 30 m per cm threshold (not elaborated here in detail).

The *theoretical innovation* of the present model is that the entire snowline information can be drawn from the state function of the snow duration. The state function $N(\tau)$ is a monotonous function of the mountain temperature; both N and τ are gained from the entire set of available daily snow duration data of 207 stations covering the Alps over 4 decades, along with the annual mean winter temperature averaged over Europe. No information on station temperature t is required. Yet the field of τ is in the end well correlated with t. This suggests that the duration of winter snow cover is largely controlled by temperature; it justifies *a posteriori* our model application of the freezing/thawing process to the snow duration. Further, the separation between the small-scale local and the continental-scale European impact upon the station temperature is made visible through the mountain temperature. This makes the mountain temperature an analysis instrument for the snow duration because it reveals the dependence of the snowline upon the European temperature.

We hope that the present approach proves to be sufficiently robust so that it can be applied to, and will be fruitful for, other mountain regions of the world.

Acknowledgments

The CRU data were made accessible to us by Ian HARRIS (Climatic Research Unit, School of Environmental Sciences, University of East Anglia, UK). B. EGGEMANN, A. BIHLO, K. BRAZDA and M. SOMMER were helpful in designing Fig. 9; D. MAYER made the plot program for Fig. 9. L. HAIMBERGER, M. GOTTFRIED and V. GRUBISIC read a first draft of the manuscript and made valuable suggestions. The Austrian Academy of Sciences has supported this research over the years in the *Clean Air Commission* and in the *National Committee for the IGBP*. The University of Vienna has funded this research through its Research Platform Program.

References

BENISTON, M., F. KELLER, S. GOYETTE, 2003: Snow pack in the Swiss Alps under changing climatic conditions: an empirical approach for climate impacts studies. – Theor. Appl. Climatol. **74**, 19–31.

BROHAN, P., J.J. KENNEDY, I. HARRIS, S.F.B. TETT, P.D. JONES, 2006: Uncertainty estimates in regional and global observed temperature changes: a new dataset from 1850. – J. Geophys. Res. **111**, D12106.

BRONSTEIN, I.N., K.A. SEMENDJAJEW, G. MUSIOL, H. MÜHLIG, 1999: Taschenbuch der Mathematik – Verlag Harri Deutsch.

BUONOMO, E., R. JONES, C. HUNTINGFORD, J. HANNAFORD, 2007: On the robustness of changes in extreme precipitation over Europe from two high resolution climate change simulations. – Quart. J. Roy. Met. Soc. **133**, 65–81.

DEGROOT, M.H., 1986: Probability and Statistics, 2. Ed. – Addison-Wesley, 723 pp.

DYE, D.G., 2002: Variability and trends in the annual snow-cover cycle in Northern Hemisphere land areas, 1972–2000. – Hydrol. Process. **16**, 3065–3077.

EFRON, B., R.J. TIBSHIRANI, 1998: An Introduction to the Bootstrap – Chapman & Hall/CRC.

HANN, J., 1883: Handbuch der Klimatologie – Verlag von J. Engelhorn, Stuttgart, 764 pp.

HANN, J., 1908: Handbuch der Klimatologie. Band I Allgemeine Klimalehre – Bibliothek Geographischer Handbücher, N.F. Verlag von J. Engelhorn, Stuttgart, 394 pp.

HANTEL, M., L.-M. HIRTL-WIELKE, 2007: Sensitivity of Alpine snow cover to European temperature. – Int. J. Climatol. **27**, 1265–1275.

HANTEL, M., M. EHRENDORFER, A. HASLINGER, 2000: Climate sensitivity of snow cover duration in Austria. – Int. J. Climatol. **20**, 615–640.

HOSMER, D.W., S. LEMESHOW, 2000: Applied Logistic Regression – John Wiley and Sons, New York, 375 pp.

KAUR, R., A.V. KULKARNI, B.S. CHAUDHARY, 2010: Using RESOURCESAT-1 data for determination of snow cover and snowline altitude, Baspa Basin, India. – Ann. Glaciol. **51**, 9–13.

KÖRNER, C., 2003: Alpine Plant Life – Functional Plant Ecology of High Mountain Ecosystems – Springer, Berlin, 2nd edition, 344 pp.

MAZUMDAR, J., 1999: An Introduction to Mathematical Physiology and Biology – Cambridge University Press, Cambridge.

PARKER, S.P. (Ed.), 1997: Dictionary of Earth Science – McGraws-Hill, New York.

SCHERRER, S.C., C. APPENZELLER, M.A. LINIGER, 2006: Temperature trends in Switzerland and Europe: implications for climate normals. – Int. J. Climatol. **26**, 565–580.

STRANGEWAYS, I., 2010: Measuring Global Temperatures – Their Analysis and Interpretation – Cambridge University Press, Cambridge.

TAYLOR, J.R., 1997: An Introduction to Error Analysis – University Science Books, 327 pp.

TROLL, C., 1961: Klima und Pflanzenkleid der Erde in dreidimensionaler Sicht. – Naturwissenschaften **48**, 332–348.

UPPALA, S. M., P. W. KÅLLBERG, A. J. SIMMONS, U. ANDRAE, V.D.C. BECHTOLD, M. FIORINO, J. K. GIBSON, J. HASELER, A. HERNANDEZ, G.A. KELLY, X. LI, K. ONOGI, S. SAARINEN, N. SOKKA, R.P. ALLAN, E. ANDERSSON, K. ARPE, M.A. BALMASEDA, A.C.M. BELJAARS, L.V.D. BERG, J. BIDLOT, N. BORMANN, S. CAIRES, F. CHEVALLIER, A. DETHOF, M. DRAGOSAVAC, M. FISHER, M. FUENTES, S. HAGEMANN, E. HÓLM, B.J. HOSKINS, L. ISAKSEN, P.A. E.M. JANSSEN, R. JENNE, A.P. MCNALLY, J.-F. MAHFOUF, J.-J. MORCRETTE, N.A. RAYNER, RW. SAUNDERS, P. SIMON, A. STERL, K. TRENBERTH, A. UNTCH, D. VASILJEVIC, P. VITERBO, J. WOOLLEN, 2005: The ERA-40 Re-analysis. – Quart. J. Roy. Met. Soc. **131**, 2961–3012.

WIELKE, L.-M., L. HAIMBERGER, M. HANTEL, 2004: Snow cover duration in Switzerland compared to Austria. – Meteorol. Z. **13**, 13–17.

WIELKE, L.-M., L. HAIMBERGER, M. HANTEL, 2005: Corrigendum to 'Snow cover duration in Switzerland compared to Austria'. – Meteorol. Z. **14**, 857.

Coincidence of the alpine–nival ecotone with the summer snowline

M. Gottfried, M. Hantel, **C. Maurer**, R. Toechterle, H. Pauli and G. Grabherr

Environ. Res. Lett., 2011, **6**, 12pp

Coincidence of the alpine–nival ecotone with the summer snowline

2011 Environ. Res. Lett. 6 014013

(http://iopscience.iop.org/1748-9326/6/1/014013)

IOP Publishing Environmental Research Letters
Environ. Res. Lett. **6** (2011) 014013 (12pp) doi:10.1088/1748-9326/6/1/014013

Coincidence of the alpine–nival ecotone with the summer snowline

M Gottfried[1], M Hantel[2,4], C Maurer[2], R Toechterle[1], H Pauli[3] and G Grabherr[1]

[1] Research Platform Mountain Limits, University of Vienna, Faculty Center of Biodiversity, Rennweg 14, Wien 1030, Austria
[2] Research Platform Mountain Limits, University of Vienna, Theoretical Meteorology Research Forum, Berggasse 11, Wien 1090, Austria
[3] Institute of Mountain Research (IGF), Austrian Academy of Sciences, c/o Faculty Center of Biodiversity, University of Vienna, Rennweg 14, 1030 Wien, Austria

E-mail: michael.hantel@univie.ac.at

Received 19 November 2010
Accepted for publication 28 February 2011
Published 18 March 2011
Online at stacks.iop.org/ERL/6/014013

Abstract
The alpine–nival ecotone is the transition between the lower located alpine grassland/tundra zone and the upper located sparsely vegetated nival zone in the mountains. Its characteristics are qualitatively known. Here we study the dynamics of the ecotone through a quantitative approach based on plant data (from Mt Schrankogel, 3497 m, observations 1994 and 2004) and snow data (from 268 routine climate stations in the Alps, observations 1975–2004).

We introduce the nivality index as the area ratio of nival and alpine plants, and the snow duration as the length of the summer snow cover. We fit a nonlinear probabilistic model to our field data; it yields state functions of both quantities. The nivality index curve comprises the entire information of the plant data in one analytical function; the snow duration curve represents the equivalent for the full snow data set. Thus all relevant parameters of both quantities follow from the respective state function.

We find that the analytical profile of the alpine–nival ecotone at Mt Schrankogel (based on nivality index observations from the altitude interval 2910–3090 m) happens to sit right in the center of the independently determined summer snow profile across the entire Alps; specifically, the central altitude of the Schrankogel ecotone coincides almost perfectly with the central altitude of Alpine[5] snow duration. Both state functions show extreme temperature sensitivity at 2967 m (vegetation) and 2897 m (snow), and both altitudes exhibit a positive trend during the measurement period.

Keywords: alpine–nival ecotone, altitudinal species ranges, climate change, temperature sensitivity, high mountain vegetation, nivality index, snow duration, state function, probabilistic model

S Online supplementary data available from stacks.iop.org/ERL/6/014013/mmedia

1. Introduction

Mountain plant life is strongly determined by snow [1–7]. Both snow duration and temperature govern habitat suitability [3, 4, 8, 9] and generate the zonal arrangement of altitude-dependent vegetation, a common feature in all mountain systems of the world [10, 11]. Here we focus on the alpine–nival ecotone [3, 4, 12–14]. This is the relatively narrow transition that connects the alpine grassland/tundra zone with the upper sparsely vegetated nival zone. The qualitative concepts for identifying and understanding this phenomenon can broadly be classified as follows:

[4] Author to whom any correspondence should be addressed.
[5] We distinguish between the terms 'Alpine', which addresses the European Alps in a geographical/climatological context, and 'alpine', which describes a vegetation zone.

- The ecotone is defined through the position of the permanent snowline. This is a climatological concept based on connecting the remaining traces of the snow pack which survive the average summer [3, 15, 16].
- The ecotone is defined through the patchiness of vegetation cover which is not vertically constant but increases from lower to higher altitudes. Following this understanding, the alpine–nival ecotone is located in the zone in which the closed (predominantly alpine) vegetation is gradually replaced by an open (predominantly nival) vegetation [4, 17, 18].
- The ecotone is defined through the turnover from alpine to nival plant species. Alpine plants dominate extended regions of dwarf shrub heath or grasslands (alpine tundra) located at lower altitudes while the cryo-tolerant nival plants grow at higher altitudes, in scattered cushion fields, restricted to a few favorable habitats [2, 13, 19, 20].

It is the latter definition that we want to adopt in the present study as qualitative background of the phenomenon. We intend to proceed further by following a quantitative approach. A stringent formalization of the alpine–nival ecotone concept is still lacking in the literature; however, it is urgently needed in the context of current climate impact research concerning mountain systems.

It is our purpose to carry out this task, in a preliminary fashion, by quantifying and theoretically formalizing the state of the alpine–nival ecotone. We shall do this through independently constructing state functions for the mountain vegetation and the snow cover, both depending upon temperature. We shall use mountain vegetation data at one individual Alpine peak (Mt Schrankogel in Tyrol) and snow data for the entire Alps.

We introduce, in a first step, the nivality index and use it for an operational definition of the ecotone. The nivality index, defined as the area ratio of nival and alpine plant vegetation, is exclusively based on plant characteristics (see formula (1)).

In a second step, we compare the nivality index with the snow duration (see formula (2)) measured at routine climate stations. By using standard linear analysis techniques, we consider both independent quantities as functions of altitude and time.

The key step is the third: we relate both nivality index and snow duration profiles to the mountain temperature; the mountain temperature replaces the familiar station temperature. For this purpose we adopt a nonlinear probabilistic model originally designed for winter snow duration [21]. The emerging state functions, separately analyzed for vegetation and snow, will exhibit a pronounced coincidence of their characteristics.

The methodical independence of the vegetation from the snow analysis is an important aspect of this study. While ecological textbook wisdom maintains that nival plants and summer snow are intimately related [3, 4] our present evaluation strategy treats the nivality index as strictly independent upon local snow observation; similarly, the snow cover will be gained from observations that are strictly independent of vegetation observations. The coincidence between the nivality index and snow cover that we shall find at the end will therefore be a robust result.

2. Materials and methods

2.1. The nivality index

We have measured over the years, as part of the GLORIA program [13, 14, 22], the plant cover in the alpine–nival ecotone of Mt Schrankogel (figures 1(b)–(d)). Implemented on the south-west slope of this mountain are 162 permanent square measuring plots with an area of 1×1 m each, referred to as quadrats [22]. In two field campaigns (1994, 2004), we recorded the area cover of 50 vascular plant species (see supplementary data available at stacks.iop.org/ERL/6/014013/mmedia, section 1, for the full species list and groupings, including measurement details) and combined these into a nival and an alpine group [14, 20, 22–24]. The six nival species are (the nomenclature follows [25, 26]): *Androsace alpina, Cerastium uniflorum, Poa laxa, Ranunculus glacialis, Saxifraga bryoides*, and *Saxifraga oppositifolia*. The distribution of these species has its center above the closed alpine grassland. They occur commonly on summits above 3300 m and form the plant assemblages of the nival zone that are characteristic throughout the siliceous Alps. The 44 alpine species include: *Carex curvula, Oreochloa disticha, Silene acaulis, Minuartia sedoides, Festuca intercedens*, and *Agrostis rupestris*.

Within a quadrat the areas of all nival and alpine species (figure 1(d)) are added together into Σ_{niv} and Σ_{alp}, respectively. With these we define the mountain nivality index:

$$m = \frac{\Sigma_{\text{niv}}}{\Sigma_{\text{niv}} + \Sigma_{\text{alp}}}. \tag{1}$$

m is a number between 0 ('only alpine species in the quadrat') and 1 ('only nival species'). Averaged over all quadrats, the nival plants, in 1994, covered 13.8% and the alpine plants 14.3% of the area, which implies that the quadrats are only partially covered with vegetation (about a quarter). These coverages changed in 2004 to 10.1% nival and 15.0% alpine. The total number of independent usable m-values is 308 (153 m-values in 1994 and 155 in 2004)[6].

2.2. The snow duration

To relate the ecotone to snow [27], we take daily snow depth measurements from our Alpine data set 1975–2000 used earlier for winter and spring [21, 28–31], plus observations from Austria for 2001–2004, and use them for the summer seasons (JJA) 1975–2004. We count a day with snow cover below or above the threshold 2 cm [28] as $\nu = 0$ or 1. The average of this stochastic quantity (daily index $i = 1, \ldots, I$) yields the relative snow cover duration of this season:

$$n = \frac{1}{I} \sum_{i=1}^{I} \nu_i. \tag{2}$$

n is close to 0 at low stations for high temperatures ('never snow') and close to 1 at high stations for low temperatures

[6] There are 324 measured m-values but 16 had to be skipped because of saturation (see section 2.2).

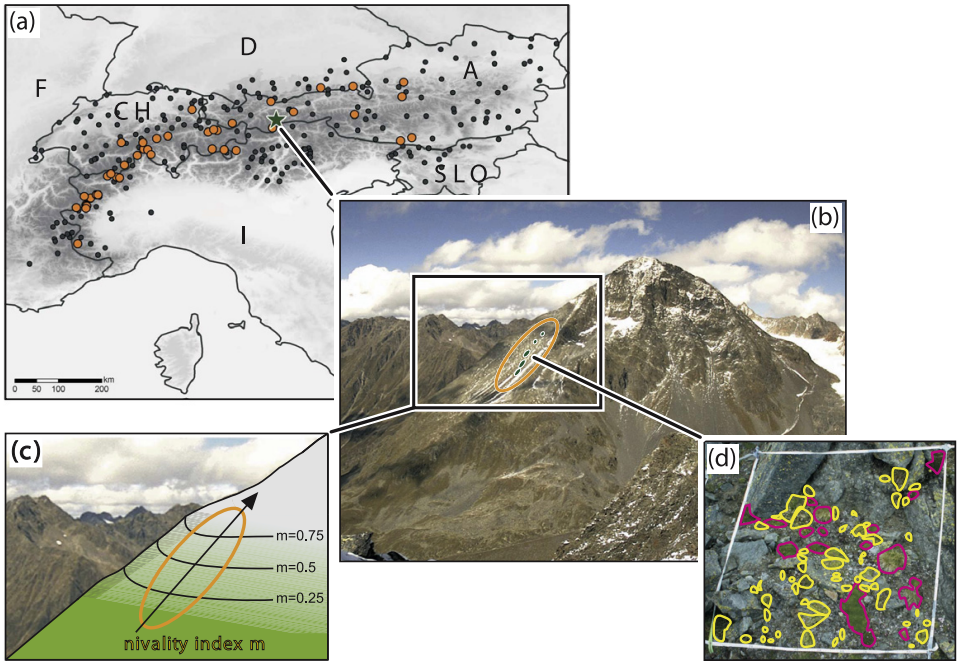

Figure 1. Schematic overview of data origins. (a) Routine climate stations in the Alps recording snow depth 1975–2004 (black dots); stations selected for present evaluation (orange dots); the location of Mt Schrankogel (47.04°N, 11.1°E, 3497 m) in Tyrol, Austria (green star). (b) Mt Schrankogel (5 September 2009, 13:15 UTC, from the south at a distance of about 2 km): the alpine zone is mostly snow-free, the nival zone is covered with snow, and the transition zone shows a typical patchwork pattern of snow-covered and snow-free areas. Field data collected in 1994 and 2004 on the south-west slope (orange ellipse) between 2900 and 3100 m. (c) Sketch of the theoretical concept of 'ecotone isolines'. (d) Typical field quadrat with alpine (red polygons) and nival plants (yellow polygons) taken at altitude 3010 m, 31 August 1994.

('always snow'). The extreme values 0 and 1 have estimated error zero (corresponding formally to infinite accuracy). These saturated observations must be excluded from further processing (this applies also for m) because they cannot be used in a fit that is based on accuracy estimates for the cost function (compare formula (S14) in the supplementary data available at stacks.iop.org/ERL/6/014013/mmedia; see also Hantel and Maurer [32]). Of the 268 European climate stations originally available (dots in figure 1(a)) only 40 were eventually used (orange points in figure 1(a)) mainly because of the saturation criterion for n (for details see [32] and supplementary data available at stacks.iop.org/ERL/6/014013/mmedia, section 2.2). Not all stations report unsaturated snow data in each year of the 30 year period; the total number of usable n-values was represented by 664 station summers. n, like m, comes as a function of θ (time) and z (altitude).

2.3. The central altitude

The ecotone comprises the entire transition zone and thus cannot be fully described by one single value of m. Yet we find it useful for a number of purposes to identify the ecotone by picking one specific isoline of m. Connecting in the horizontal direction different plots with m = const. at Schrankogel would generate ecotone isolines (schematically sketched in figure 1(c)). Out of the infinite number of such isolines we shall focus here on the median ecotone line $m = 0.5$ which seems to be the most natural choice. This virtual boundary is an idealized limit that separates the (lower located) area with mostly alpine plants from the (higher located) area with mostly nival plants; at $m = 0.5$ the cover of alpine and nival species is balanced. The geometrical position Z of this boundary in a given summer will be referred to as the central altitude of the ecotone.

Similarly, the specific value $n = 0.5$ of the snow duration defines the median snowline; it is located at the central altitude H. The concept of the median snowline has recently been elaborated on by Hantel and Maurer [32]. The idea is that the median snowline can be simply found from the observed snow duration. It is located where the probability of encountering snow in summer is 50%; this implies that at the same altitude the probability of encountering no snow would also be 50%.

We anticipate that the central altitudes Z and H will be dynamically related. One reason is that 7 weeks of summer snow cover (corresponding to $n = 0.53$ for JJA) is about the maximum that alpine species can stand [2].

The central altitude of the median ecotone line, averaged over the years 1994 and 2004, can be found by fitting a straight line through the measured $m(\theta, z)$ and determining the altitude Z at which $m = 0.5$. In a similar manner, the central altitude H of the median snowline, averaged from 1975 to 2004, is determined linearly from the measured $n(\theta, z)$.

2.4. Trend estimates of the nivality index and snow cover

At first glance, the trend of m cannot be determined because we have data for just two years (1994, 2004) which may indicate a time change at best but constitutes no trend. However, there are many plots in the vicinity of the central altitude that all show a relatively small but consistently negative time derivative:

$$\frac{\Delta m(z)}{10\ \text{years}} = \frac{m(2004, z) - m(1994, z)}{2004 - 1994} \tag{3}$$

for constant altitude z. The method of pairwise slopes [33] now offers a possibility of estimating the time trend of the nivality index in the form of the median of the ratio (3), averaged over a proper number of independently measured time derivatives $\Delta m(z)/(10\ \text{years})$ at different quadrats located at altitudes z. We shall provide not only the median but also the full pdf of the corresponding frequency distribution.

For the time change of n we will apply the same method. The median of the frequency distribution of

$$\frac{\Delta n(z)}{\Delta\theta} = \frac{n(\theta_2, z) - n(\theta_1, z)}{\theta_2 - \theta_1} \tag{4}$$

will be an estimate of the linear time trend of the snow duration. Formulas (3) and (4) are conceptually equal, but there is a conspicuous difference in data availability of m and n. The method of pairwise slopes uses all independently measured data in a time series for calculating 'time slopes' according to formula (4). If there are k time instants there are $k(k-1)/2$ different time slopes in (4). For $k = 2$ this yields just one, and this is the situation in formula (3). However, for the snow data n, as opposed to the vegetation data m, we have up to $k = 30$ different observation years at one climate station during the observation period 1975–2004 yielding up to 435 different time derivatives for this station located at altitude z.

A further task is to decide which altitude interval is to be allowed to contribute to the median. In the most ideal case the data should only be taken from plots located at the central altitude. However, this would severely limit the available data; thus we will be forced to take data from a considerably larger interval.

Taken together, these conventions yield a total of 140 nivality trend and 1810 snow trend data (see figure 3 below).

2.5. The mountain temperature

The dimensionless ratios m and n are formally similar; we attempt to analyze them using the same theoretical concept. For this we use a nonlinear probabilistic model [21, 28] developed recently for winter snow cover. The model interprets n as the probability Φ that water is frozen. Φ depends on the mean and variance of the station temperature t.

We shall nevertheless not use t in our probabilistic model because t is influenced by two independent mechanisms: the climate-scale surface temperature T and the contribution of local-scale temperature that depends linearly on the altitude z. Both mechanisms are mixed in t and cannot be distinguished. In order to explicitly separate the two effects we introduce (see supplementary data available at stacks.iop.org/ERL/6/014013/mmedia, figure S2) the mountain temperature as follows[7]

$$\tau = T + cz; \tag{5}$$

τ combines the large-scale European effect described by T with the small-scale vertical lapse rate effect due to z. The parameter c in the definition (5) is the vertical temperature gradient; it will not be specified externally but determined from the data fit. τ replaces t; it is the independent argument for the state function to be defined farther below. T is obtained from the monthly gridded CRU temperatures [34], with resolution half a degree in latitude and longitude, averaged horizontally over Europe [28] and time averaged over each of the summers 1975–2004. We use this European temperature T for the n-data (a total of 30 T-values, one for each summer of the record).

There is a secondary reason for introducing τ: station temperature is not available in our ecotone data set. Thus it is of practical importance that t can be replaced by the mountain temperature.

Other parameters like local aspect ratio or slope may also have an influence on τ. Yet we believe that their impact at Schrankogel is low because our plots are located in uniform terrain at the south-west face of the study mountain (see figure 1). As to the snow stations, the impact of local-scale aspect and slope is presumably stochastic. What is not stochastic is the dependence on latitude and longitude. We have studied this latter effect for the Alpine snow cover [32] and found that it is not very big. Here we prefer to skip it in order to have optimal consistency with the Schrankogel vegetation data.

2.6. The prior period concept

Despite their formal similarity, the ratios m, n cannot be naively compared since there is a basic difference between them due to lifetime: snow is generated from zero every year while vegetation has a lifetime of many years. This implies that the snow cover is in approximate balance with the seasonal environmental conditions of the actual year as expressed by T, whereas the nivality index has something like a 'memory' of the conditions of earlier years; it follows that m can normally not be in balance with T of the actual year.

As to the length of this memory we empirically decided, after some numerical experimentation, that 20 years is an acceptable first choice. We arbitrarily introduce the concept of a prior period as the preceding 20 year period that impacts the nivality index in 1994; thus, 1975–1994 will be referred to as

[7] In the original studies [21, 28] we had introduced Alpine temperature for τ; here we switch to mountain temperature for greater generality.

prior'94. The equivalent definition (period 1985–2004 referred to as prior'04) will be applied for m-values in 2004.

The estimate for the averaged European temperature T_{prior} will be gained through averaging T over the two prior periods ($T_{\text{prior'94}} = 17.68\,^{\circ}\text{C}$, $T_{\text{prior'04}} = 18.33\,^{\circ}\text{C}$). Both temperatures T_{prior} will be inserted into formula (5) for T to yield τ for the analysis of m; this gives a total of 308 τ-values (153 for $T_{\text{prior'94}}$ and 155 for $T_{\text{prior'04}}$). The prior period concept does not apply to τ in the analysis of n; here we have a total of 664 τ-values, one for each station summer.

2.7. The state function

With τ we introduce the state function N for the snow data:

$$N(\tau) = \Phi(\sqrt{2\pi}s_0[\tau - \tau_0]). \tag{6}$$

Φ was defined above as the probability that water is frozen. Mathematically, Φ is the Gaussian error integral. N interpolates measured values of n, T, z through the fitted parameters s_0 (extreme sensitivity of N), τ_0 (a reference constant), and c (an equivalent vertical lapse rate, implicitly required for τ as introduced above in formula (5)).

The model described by formula (6) implies that the snow duration n is in instantaneous equilibrium with the mountain temperature τ of the given season. This equilibrium assumption may be questionable for biotic systems [35]. Yet we suggest that the nivality index m follows a similar dependence upon τ, provided τ for this case is calculated for the corresponding prior period (replace T in (5) through T_{prior}); the two data years available at Mt Schrankogel may be the minimum for a first test if our model of n is applicable to m.

We implement this by replacing N through M in (6). The state curves $M(\tau)$, $N(\tau)$ interpolate measured values of m, n, respectively. We distinguish between M and N, if necessary, by adding subscripts m, n to the fitted parameters s_0, τ_0, c.

A caveat may be added here. Besides temperature there may be other influential processes like precipitation, wind, radiation and others that are not considered in our functional dependence of m. Yet our results are consistent with the assumption that, at the level of the present model, all these act together as stochastic noise while temperature is the leading ecological factor (e.g., [3, 4]).

The central altitudes are implicitly defined through the state function by setting $z = Z$ in (5) for the median ecotone line and $z = H$ for the median snowline; solving for Z and H, plus observing the condition $M(\tau_{0,m}) = \Phi(0) = 0.5$ for the ecotone and $N(\tau_{0,n}) = \Phi(0) = 0.5$ for the snowline, yields

$$Z = \frac{\tau_{0,m} - T_{\text{prior}}}{c_m}; \qquad H = \frac{\tau_{0,n} - T}{c_n}. \tag{7}$$

The parameters τ_0, c are of course different for ecotone and snow; they follow as fitted quantities of the respective state functions. Z can only be defined with T_{prior}. H, on the other hand, is for the actual year to be calculated with T for the same year; for the prior period it is to be calculated with $T = T_{\text{prior}}$ (necessary below in figure 4(c) for comparing the sensitivity profiles of vegetation and snow).

2.8. Sensitivity profiles of nivality and snow

The significance of the central altitudes Z and H can now be judged by considering the τ-slope of the state curves. We call the vertical profile $s(\tau)$ of the τ-slope the sensitivity profile[8]; it is the τ-derivative of the model function (6), applied to both M and N, and is negative throughout (supplementary data available at stacks.iop.org/ERL/6/014013/mmedia, formula [S5]).

The extremum s_0 of s is adopted at $\tau = \tau_0$; this argument of Φ yields $M = 0.5$, $N = 0.5$, which is the condition for the central altitudes. For all other values of τ, both above and below the central altitudes, the sensitivity $s(\tau)$ is absolutely smaller than $|s_0|$. It is this property of the central altitudes Z, H that *a posteriori* justifies our above choice of the median ecotone line located at $m = 0.5$ and median snowline located at $n = 0.5$.

The state function $M(\tau)$ and the sensitivity function $s_m(\tau)$ describe the observed nivality index data set equally well. However, $s_m(\tau)$ is more revealing and thus we consider $s_m(\tau)$ simply as the ecotone function. Similarly, we consider the snow function $s_n(\tau)$, the derivative of the state function $N(\tau)$, as the relevant description of the observed snow duration profile. Comparing the two sensitivity profiles $s_m(\tau)$, $s_n(\tau)$ with each other will yield the main result of this study.

2.9. The trend of the central altitudes

The central altitude Z of the ecotone is the average over the two observation years 1994, 2004; it is given, along with the central altitude H of the snow, by formula (7). In order to obtain an estimate for the trend of Z in this time interval (as well as for the trend of H in the interval 1975–2004) we proceed as follows.

The nivality index $m(\theta, z)$ is a function of time θ and, for given θ, a monotonic function of altitude z. Thus $z(\theta, m)$ is also a monotonic function of m. Now the time change of z for constant m can, by means of an elementary formula of analysis, be written as

$$\frac{\partial z(\theta, m)}{\partial \theta} = -\frac{\partial m(\theta, z)/\partial \theta}{\partial m(\theta, z)/\partial z}. \tag{8}$$

An appropriate estimate for the numerator of (8) is the median trend $\Delta m/\Delta\theta$. As regards the denominator, the vertical gradient of the state function $M\{\tau[T(\theta), z]\}$ in a given year θ would read (observing the chain rule of analysis at the central altitude Z)

$$\frac{\partial M}{\partial z} = \underbrace{\frac{\mathrm{d}M(\tau)}{\mathrm{d}\tau}}_{=s_{0,m}} \underbrace{\frac{\partial \tau[T(\theta), z]}{\partial z}}_{=c_m} = s_{0,m}c_m. \tag{9}$$

Thus by combining the observed trend of m with the analyzed parameters $s_{0,m}$ and c_m from the nonlinear fit, the trend of Z

[8] Following climatological parlance, we use the following nomenclature: the sensitivity of a climate function is its derivative with respect to large-scale temperature; the trend is its derivative with respect to time.

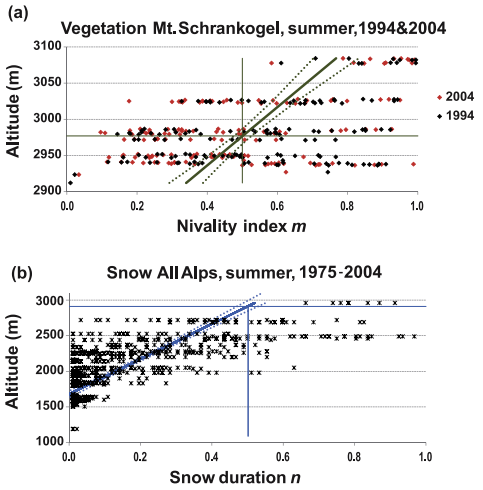

Figure 2. Vertical profiles of nivality and snow: ratios m, n plotted versus altitude z; only unsaturated data are included. Straight lines: linear regression. Dotted curves: 0.95 confidence. Note the scale difference of the two ordinates. (a) Nivality index m at Schrankogel for the two years 1994 (153 unsaturated observations used) and 2004 (155 observations); the regression line crosses $m = 0.5$ at $Z = (2977 \pm 5)$ m. (b) Snow duration n at climate stations in summer (Jun/Jul/Aug) for the period 1975–2004; the regression line crosses $n = 0.5$ at $H = (2911 \pm 40)$ m.

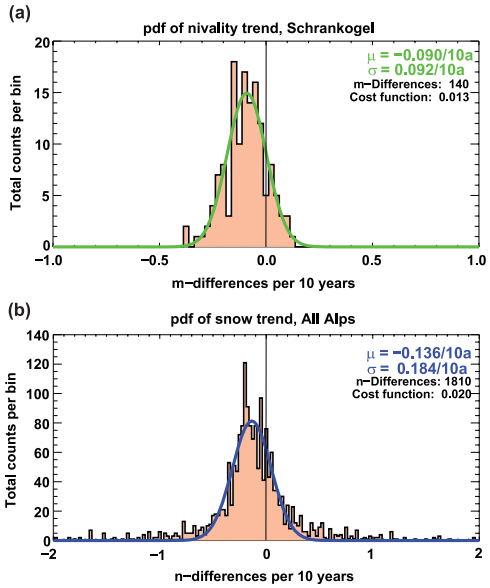

Figure 3. Probability density function of trend estimates for (a) the nivality index m at Schrankogel (1994, 2004) and (b) the snow duration n across the Alps (1975–2004). The data are assembled in bins of width 0.025/10 years. The cost function for the fit of the Gaussian curve is normalized. The total number of m-, n-differences is proportional to the area of the curve. The median μ and standard deviation σ of the Gaussian are given in the inset. The individual trend data are taken from altitude interval $Z \pm D_m/2$ for the nivality and $H \pm D_n/2$ for the snow.

can be gained from (8):

$$\frac{\mathrm{d}Z(\theta)}{\mathrm{d}\theta} = -\frac{1}{s_{0,m}c_m}\left[\frac{\partial m(\theta, z)}{\partial \theta}\right]_{z=Z}. \qquad (10)$$

An attractive aspect of this method is that no trend estimate of the observed climate temperature T is required. In fact, only the measured nivality index, including its time change, is taken as a basis for the trend estimate of the central altitude Z.

The equivalent approach can be applied for estimating the trend of the central altitude H of the snow duration $n(\theta, z)$ with the result

$$\frac{\mathrm{d}H(\theta)}{\mathrm{d}\theta} = -\frac{1}{s_{0,n}c_n}\left[\frac{\partial n(\theta, z)}{\partial \theta}\right]_{z=H}. \qquad (11)$$

We shall apply these formulas below.

3. Results

Of the three steps that have been sketched in section 1, the first has been achieved above by introducing the nivality index m, in parallel to the snow duration n. The second step will be to compare the observed m at Schrankogel with n measured at climate stations across the Alps. Since the data for both ratios come as functions of time θ and altitude z there are two substeps: compare the time-mean profiles $m(z), n(z)$ through linear regression analysis; and compare the time trends of $m(\theta), n(\theta)$ with each other through the method of pairwise slopes. Both substeps will be made with linear techniques; we consider this approach as preliminary. The third, and main, step will be the nonlinear analysis of the data $m(\theta, z)$ yielding the state function $M(\tau)$ and the ecotone function $s_m(\tau)$, and similarly the analysis of the data $n(\theta, z)$ yielding the state function $N(\tau)$ and the snow function $s_n(\tau)$.

3.1. Linear analysis with respect to altitude

Standard linear analysis of the Schrankogel data (figure 2(a)) and the Alpine snow data (figure 2(b)) describes the altitude dependence of m and n, irrespective of time; this yields the regression lines (R^2 = explained variance):

$$m(z) = 2.48(\pm 0.30)(z/\mathrm{km}) - 6.88(\pm 0.89); \qquad R^2 = 0.19 \qquad (12)$$

$$n(z) = 0.41(\pm 0.02)(z/\mathrm{km}) - 0.68(\pm 0.04); \qquad R^2 = 0.44 \qquad (13)$$

We use these formulas to determine the central altitudes at which the median values $m = 0.5$, $n = 0.5$ are adopted. This yields $Z = (2977 \pm 5)$ m for the vegetation and $H = (2911 \pm 40)$ m for the snow[9]. The numerical coincidence between Z and H is conspicuous and suggests that the nivality index and snow duration are closely related. This has additionally motivated our attempt to model both with the more involved

[9] Errors in this study are given as 1σ.

nonlinear probabilistic model below. For the various estimates of Z and H, see also table S6 in supplementary data (available at stacks.iop.org/ERL/6/014013/mmedia).

3.2. Linear analysis with respect to time

Figure 3(a) presents the frequency distribution of the observed 10 year trend estimates $\Delta m/\Delta\theta$ at 140 quadrats in the vicinity of Z, the altitude of the median ecotone line. Anticipating the halfwidth D_m of the ecotone function to be developed in the nonlinear analysis below, we have taken the data from the quadrats within the 214 m broad altitude band $Z \pm D_m/2$. This yields the median of the time change in the belt of the ecotone that is most sensitive with respect to temperature (sensitivity s_m between $s_{0,m}$ and $s_{0,m}/2$; see the green curves in figure 4(c) below). Equivalently, figure 3(b) presents the frequency distribution of the observed 10 year trend estimates $\Delta n/\Delta\theta$ for the snow duration in the vicinity of H, the altitude of the median snowline. The vertical width of this 992 m broad band has been chosen as $H \pm D_n/2$. This is a compromise between having enough data and staying sufficiently close to the central altitude. For this reason figure 3 will somewhat underestimate the median trends.

The curves of figure 3 yield the following trend estimates:

$$\frac{\Delta m}{\Delta\theta} = -(0.090 \pm 0.092)/10 \text{ years};$$
$$\frac{\Delta n}{\Delta\theta} = -(0.136 \pm 0.184)/10 \text{ years}. \qquad (14)$$

The uncertainties given represent one standard deviation so the estimates (14) are not at all significant. Yet they yield valuable information for the parallel reduction of the nivality index and the snow duration under climate change. The trend of the snow duration is somewhat stronger than that of the nivality index, which is to be expected.

3.3. Nonlinear probabilistic model analysis: the state functions

The state function $M(\tau)$ interpolates measured values of m (figure 4(a)). The curve parameters $s_{0,m}, \tau_{0,m}, c_m$ are listed in figure 5[10]. For the central altitude of the ecotone, $M(\tau)$ yields $Z = (2967 \pm 16)$ m (see also supplementary data available at stacks.iop.org/ERL/6/014013/mmedia, table S6), indistinguishable from Z found from linear regression.

The state function $N(\tau)$ for n is drawn in figure 4(b); curve parameters $s_{0,n}, \tau_{0,n}, c_n$ appear in figure 5. For the central altitude of the snowline we find $H = (2897 \pm 140)$ m (see also supplementary data available at stacks.iop.org/ERL/6/014013/mmedia, table S6), indistinguishable from H found from linear regression.

The physical significance of the fitted parameters (listed in figure 5) is as follows: s_0, a negative quantity, is the extreme value of the sensitivity profiles; this parameter

[10] Errors of the fitted parameters are given as 1σ, determined with the bootstrap method [36] using 2000 runs.

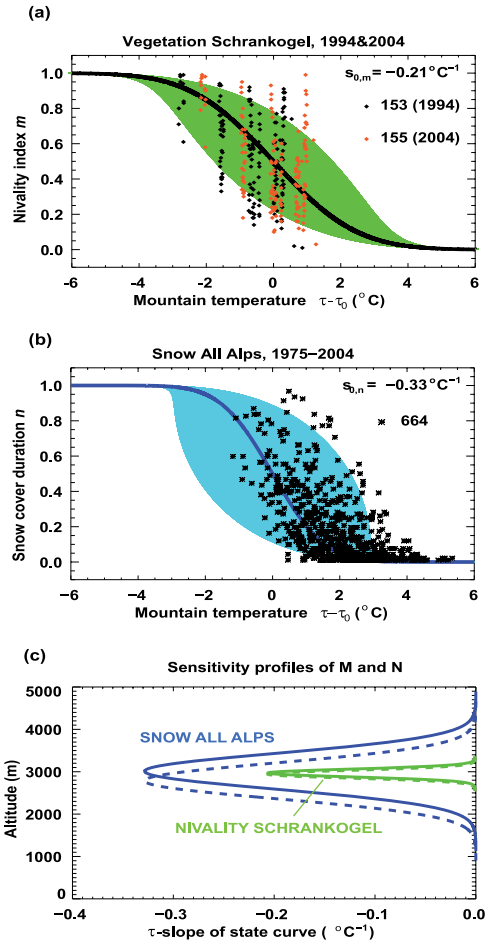

Figure 4. State curves for the nivality index and snow duration (Jun/Jul/Aug). (a) $M(\tau)$ for m at Mt Schrankogel (years 1994 and 2004). The shading captures 68% of the data points (corresponding to 1σ in the τ-direction); the shading does not show the accuracy of the fitted state curve. (b) As (a) but for state curve $N(\tau)$, applied to n at climate stations across the Alps (threshold 2 cm, all years 1975–2004). (c) Sensitivity profiles of state curves as a function of the altitude. Profiles of $M(\tau)$ are green, those of $N(\tau)$, blue. Profiles are projected to the temperature of prior'94 (dashed curves) and prior'04 (solid curves).

justifies choosing $m = 0.5$, $n = 0.5$ as the most important ecotone line and snowline, respectively. We may note here that the coincidence of Z and H is not best at $m, n = 0.50$ but at $m, n = 0.59$ (see supplementary data available at stacks.iop.org/ERL/6/014013/mmedia, table S7). The parameter c represents a temperature lapse rate. It is gained, without any station temperature information, from fitting vegetation and snow measurements. We find $c_m = -21.4\,^\circ\text{C km}^{-1}$, $c_n = -2.9\,^\circ\text{C km}^{-1}$. Clearly, these figures cannot be directly compared with usual lapse rates (typically $-6.5\,^\circ\text{C km}^{-1}$ in the free atmosphere). On the other hand, it seems remarkable that the c-values in our fits come out

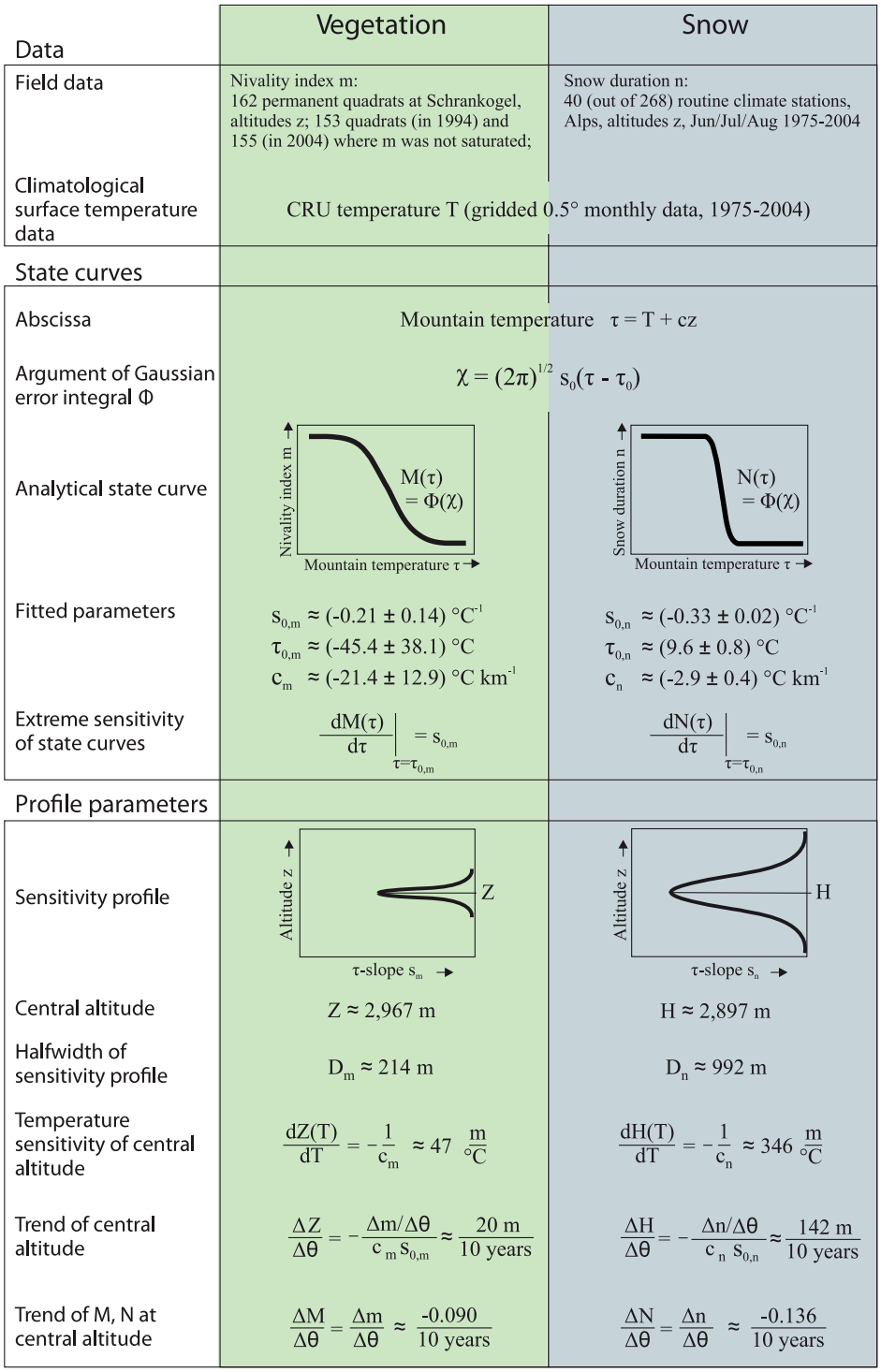

Figure 5. Summary of the concept and main findings of this study. Errors are only given for parameters of state curves; errors of derived quantities are cited in the text.

consistently negative (i.e., the corresponding temperature gradient is correctly directed downward). This proves that both vegetation data and snow data implicitly carry temperature information, consistent with our basic modeling hypothesis. τ_0 is a reference parameter in the fit with no obvious physical significance.

The sensitivity profiles $s_m(\tau)$ for $M(\tau)$ and $s_n(\tau)$ for $N(\tau)$ are drawn in figure 4(c) as a function of z. The snow function $s_n(\tau)$ represents the stochasticity which is realized as the fluctuation of snow cover from year to year, extreme at the altitude of the median snowline. Both the ecotone function $s_m(\tau)$ and the snow function $s_n(\tau)$ peak between about 2900 and 3000 m at their respective central altitudes Z, H and both move slowly upward from $T_{\text{prior'94}}$ to $T_{\text{prior'04}}$ (dashed and solid curves in figure 4(c); the trend is discussed in section 4). The coincidence between the parameters Z and H quantifies how well the ecotone function is embedded into the snow function. This coincidence is the main result of our study; it is a robust result because all vegetation plots of the measurement campaign at Schrankogel happened to sit right in the center of the snow profile of the Alps. This observation may be accidental; the ecotone function at a mountain different from Mt Schrankogel might be located off the center of the snow function valid for the Alps. However there are no data available at present so this problem must be left for later research.

The fitted parameters of the state functions and the quantities derived from them can be discussed from various perspectives. In the following we focus briefly upon their response with respect to temperature (sensitivities) and with respect to time (trends).

3.4. Sensitivity parameters

There are three sensitivity quantities listed in figure 5. First, there is the parameter s_0, referred to as the extreme sensitivity of state curves. Second, the entire sensitivity profiles: the ecotone function $s_m(\tau)$, and the snow function $s_n(\tau)$; the parameters $s_{0,m}$, $s_{0,n}$ are just the extreme values of the sensitivity profiles. Third, the temperature sensitivity of the central altitude; the latter quantity is the T-derivative of the central altitude of the respective median line as determined from equation (7):

$$\frac{\mathrm{d}Z}{\mathrm{d}T_{\text{prior}}} = -\frac{1}{c_m}; \qquad \frac{\mathrm{d}H}{\mathrm{d}T} = -\frac{1}{c_n}. \tag{15}$$

It yields the sensitivities of Z and H to European temperature T and is given by the inverse of the fitted temperature lapse rates. The result of equation (15) is valid for the entire observation period. Also listed in figure 5 are the halfwidths of the sensitivity profiles. $D_m = (214 \pm 129)$ m represents the halfwidth of the sharply defined ecotone while $D_n = (992 \pm 153)$ m stands for the much broader snow profile across the Alps.

3.5. Trend parameters

Time trend information of this study is condensed in figure 3. The pdfs of the trend estimates of the nivality index and of the snow duration have been gained with the method of pairwise slopes [33] as discussed above in section 2. The result, expressed in equation (14), can be interpreted as follows. For example, $\Delta m/\Delta\theta = -0.090/10$ years, when applied at the median ecotone line $z = Z = 2967$ m, would imply that the nivality index m at this altitude has been reduced from 0.50 in 1994 to 0.41 in 2004. This reduction would be much smaller at higher levels. As to snow, $\Delta n/\Delta\theta = -0.136/10$ years, when applied at the median snowline $z = H = 2897$ m, would imply that the snow duration n at this altitude has been reduced from 0.50 to 0.36 in ten years. This reduction would also be smaller at higher levels.

Further, inserting the estimates (14) into equations (10) and (11) we find

$$\frac{\Delta Z}{\Delta\theta} = -\frac{\Delta m/\Delta\theta}{s_{0,m}c_m} = (20.0 \pm 27)\frac{m}{10\text{ years}} \tag{16}$$

$$\frac{\Delta H}{\Delta\theta} = -\frac{\Delta n/\Delta\theta}{s_{0,n}c_n} = (142 \pm 193)\frac{m}{10\text{ years}}. \tag{17}$$

These trend estimates are not significant. Yet they can be interpreted in the sense that the ecotone line moves upward, presumably under the influence of the upward moving snow cover. The trend of the snow cover is considerably stronger; this reflects the fact that snow cover reacts instantaneously to climate change whereas the vegetation has a longer memory. The longevity of high mountain species causes strong inertia, influenced not only by the actual year but also by earlier years. This suggests that the nivality index which may have been in balance with the snow under stationary climate conditions runs out of balance when climate change sets in. However, these implications are largely speculative at present because the data accuracy is not yet sufficient.

4. Discussion

We have shown in this study that the altitude interval characteristic for the alpine–nival ecotone at Mt Schrankogel happens to sit right in the center of the snow profile across the entire Alps. The rigorously analyzed ecotone profile in figure 4(c) is located entirely within the snow profile.

Standard regression and frequency analysis of the original field data (figures 2 and 3) can only show that the nivality index $m(\theta, z)$ increases with altitude z and gently decreases with time θ; this traditional evaluation technique does not provide a dynamical explanation. The added value of our present nonlinear probabilistic model (schematically summarized in figure 5) is that the entire information of the observed $m(\theta, z)$ becomes condensed, with the mountain temperature τ, into state function $M(\tau)$ and ecotone function $s_m(\tau)$; the equivalent concentration is reached by $N(\tau)$ and $s_n(\tau)$ which fits the observed snow duration data $n(\theta, z)$. A prominent result is that the sensitivity profiles coincide at the central altitudes Z, H of the two curves (figure 4(c)). The state curves are time independent; yet the gentle upward shift of the sensitivity profiles from prior'94 to prior'04 seen in figure 4(c) follows from the parameters of M and N since the time dependence is implicit in τ through $T(\theta)$.

The central altitude of the snow profile varies somewhat with the specific choice of the season, in our case JJA. The choice of this temporal window for the evaluation of the snow data is justified as follows: Gottfried *et al* [2] have shown that snow melt takes place from early June until July around the alpine–nival ecotone at Mt Schrankogel. The earlier part of the growing season is the most decisive time for plant growth and reproduction while the time of winter onset (usually during September at Mt Schrankogel) is far less important [3]; therefore we excluded September from the snow analysis.

From the ecological perspective it remains to be asked how the approximate equilibrium process hypothesized here for the nivality index can be acceptable [35]. Stochasticity of the snow regime, understood as variance of the snow cover, and realized as unpredictability by the vegetation, peaks at the alpine–nival ecotone; this is consistent with the theoretical concept of ecotones as 'environmentally stochastic stress zones' [12].

Note that Van der Maarel [12] referred to ecotones in the sense of temporal fluctuation zones and termed boundaries that are structured by spatial gradients as ecoclines. The alpine–nival boundary shows both features: spatial gradients of (mean) temperatures, soil and substrate properties and vegetation patterns; and a temporal highly variable summer snow regime. Therefore we see justification for using the wider known term ecotone. The fluctuating snow regime triggers counteracting processes which hold the central altitude Z of the ecotone in balance.

Early snow melt in spring and late snow in autumn improve reproductive success [37, 38] but may also mean increased exposure to lethal frosts in the early and late seasons [5, 9, 39, 40]. Snow protection may thus be essential since even in mid-summer cold spells occur regularly, which affects plants with low frost tolerance [39, 41]. Snow, on the other hand, may interrupt seed production [38].

These elementary processes influence nival and alpine plants differently. Both groups can be distinguished not only by their altitudinal distribution centers [20, 23, 24] but also by their climatic niches. Nival plants are highly snow tolerant [2]. They maintain viable populations at snow rich sites; a typical example is that of *Ranunculus glacialis* which survives even one or two years of permanent snow pack [42]. Alpine plants, on the other hand, are known to prefer sites with less summer snow and warmer temperatures [2]. This favors, in the present climate warming stage, the more competitive alpine species over the nivals; typical examples are *Silene acaulis* and *Oreochloa disticha* which expanded at Mt Schrankogel mostly at the cost of *Androsace alpina*, 2nd *Saxifraga bryoides* and *Cerastium uniflorum* [22]. In the longer term the alpines tend to outcompete the nival plants during warm periods; the opposite happens during cold periods.

It appears that the alpine–nival ecotone is exactly at the place where these processes are in a state of dynamic equilibrium. This interpretation applies to the ecotone for both stationary and changing climate conditions. We conclude that the vegetation data m can indeed be evaluated with our probabilistic model and in this sense pass the test required above.

Figure 4(c) suggests that the ecotone profile moves upward under climate warming [43–45]. The trend reported elsewhere for the various vegetation zones worldwide is in the range 60–200 m per century [22, 46, 47]. Assuming this figure as the zeroth estimate for the globe with an estimated 0.74 °C centennial warming trend [48] we expect an order of magnitude temperature sensitivity of 81–270 m $°C^{-1}$. This figure can be contrasted with our sensitivity results $\Delta Z/\Delta T \approx (47 \pm 36)$ m $°C^{-1}$ for the ecotone at Mt Schrankogel and $\Delta H/\Delta T \approx (346 \pm 48)$ m $°C^{-1}$ for the summer snow profile at Alpine climate stations.

Our finding that the ecotone in figure 4(c) tends to follow the snow fluctuations is in accord with general ecological knowledge [3, 4]. Yet our estimates for the trends of the ecotone and the snow profile given in equations (16) and (17) are quite different; further, both have a large scatter. Thus they should be compared with caution. After all, our present analysis is the utmost one can press out of vegetation data from just one Alpine summit available, combined with a limited number of stations that report summer snow.

Despite being derived from a case study, the methodical framework presented here offers perspectives for application to other—bioclimatically similar—mountain systems. Another implication is biodiversity: as the extent of the nival zone is restricted by the upper elevation limit of mountain ranges, the ongoing shrinking of this belt may have considerable consequences for mountain biodiversity [49–52]. Thus the coincidence between vegetation and snow, as we have tried to quantify here, may shed new light on the mechanisms that govern vegetation and vegetation changes at the limits of plant life.

Acknowledgments

We thank Vanda Grubisic and Leopold Haimberger for valuable comments on a first version of the paper. This work has been supported by the University of Vienna, within its 'Research Platform' program, and by the GLORIA program (Austrian Academy of Sciences/IGF, University of Vienna, Austrian Federal Ministry of Science and Research, and MAVA Foundation for Nature Conservation).

References

[1] Billings W D and Bliss L C 1959 An alpine snowbank environment and its effects on vegetation, plant development, and productivity *Ecology* **40** 388–97
[2] Gottfried M, Pauli H, Reiter K and Grabherr G 2002 *Mountain Biodiversity—a Global Assessment* ed C Körner and E M Spehn (London: Parthenon) pp 213–23
[3] Körner C 2003 *Alpine Plant Life: Functional Plant Ecology of High Mountain Ecosystems* 2nd edn (Berlin: Springer) p 344
[4] Nagy L and Grabherr G 2009 *The Biology of Alpine Habitats* (Oxford: Oxford University Press) p 376
[5] Wipf S, Stoeckli V and Bebi P 2009 Winter climatic change in alpine tundra: plant responses to changes in snow depth and snow melt timing *Clim. Change* **94** 105–21
[6] Molau U, Nordenhall U and Eriksen B 2005 Onset of flowering and climate variability in an alpine landscape: a 10-year study from Swedish Lapland *Am. J. Botany* **92** 422–31

[7] Stanton M L, Rejmanek M and Galen C 1994 Changes in vegetation and soil fertility along a predictable snowmelt gradient in the Mosquito Range, Colorado, USA *Arct. Alp. Res.* **26** 364–74

[8] Harte J and Shaw R 1995 Shifting dominance within a monate vegetation community *Science* **67** 876–80

[9] Inouye D W 2008 Effects of climate change on phenology, frost damage, and floral abundance of montane wildflowers *Ecology* **89** 353–62

[10] Humboldt Av 1817 *De Distributione Geographica Plantarum Secundem Coeli Temperiem et Altitudinem Montium, Prolegomena* (Lutetiae Parisiorum: Libraria Greco-Latino-Germanica) p 249

[11] Wielgolaski F E 1997 *Ecosystems of the World; Polar and Alpine Tundra* (Amsterdam: Elsevier) p 930

[12] van der Maarel E 1990 Ecotones and ecoclines are different *J. Veg. Sci.* **1** 135–8

[13] Gottfried M, Pauli H and Grabherr G 1998 Prediction of vegetation patterns at the limits of plant life: a new view of the alpine–nival ecotone *Arct. Alp. Res.* **30** 207–21

[14] Pauli H, Gottfried M and Grabherr G 1999 Vascular plant distribution patterns at the low temperature limits of plant life—the alpine–nival ecotone of Mount Schrankogel (Tyrol, Austria) *Phytocoenologia* **29** 297–325

[15] Zingg T 1954 Determination of the climatic snowline on a climatological basis (Die Bestimmung der klimatischen Schneegrenze auf klimatologischer Grundlage) *Festschrift für Erwin Aichinger zum 60. Geburtstag* ed E Janchen (Vienna: Springer) pp 848–54

[16] Gross G, Kerschner H and Patzelt G 1977 Methodical investigations of the snowline in alpine glacier regions (Methodische Untersuchungen über die Schneegrenze in alpinen Gletschergebieten) *Z. Gletscherkunde Glazialgeol.* **12** 223–51

[17] Ellenberg H 2009 *Vegetation Ecology of Central Europe* (Cambridge: Cambridge University Press) p 756

[18] Dahl E 1986 *Ecosystem Theory Application* ed N Polunin (New York: Wiley) pp 35–62

[19] Heer O 1885 On the nival flora of Switzerland (Ueber die nivale Flora der Schweiz) *Neue Denksch. Allg. Schweiz. Ges. Gesammt. Nat.wiss.* **29** 1–114

[20] Braun J 1913 The vegetation of the nival zone in the Rhaetic–Lepontic Alps (Die Vegetationsverhältnisse der Schneestufe in den Rätisch–Lepontischen Alpen) *Neue Denksch. Schw. Naturforsch. Ges.* **48** 1–348

[21] Hantel M and Hirtl-Wielke L-M 2007 Sensitivity of Alpine snow cover to European temperature *Int. J. Climatol.* **27** 1265–75

[22] Pauli H, Gottfried M, Reiter K, Klettner C and Grabherr G 2007 Signals of range expansions and contractions of vascular plants in the high Alps: observations (1994–2004) at the GLORIA master site Schrankogel, Tyrol, Austria *Glob. Change Biol.* **13** 147–56

[23] Grabherr G, Gottfried M and Pauli H 2001 *Biomonitoring: General and Applied Aspects on Regional and Global Scales* ed C A Burga and A Kratochwil (Dordrecht: Kluwer) pp 153–78

[24] Reisigl H and Pitschmann H 1958 Upper limits of flora and vegetation in the nival belt of the central Ötztaler Alpen (Obere Grenzen von Flora und Vegetation in der Nivalstufe der zentralen Ötztaler Alpen (Tirol)) *Vegetatio* **8** 93–129

[25] Tutin T G, Heywood V H, Burges N A, Valentine D W, Walters S M and Webb D A 1964 *Flora Europaea* vol 1 (Cambridge: Cambridge University Press)

[26] Tutin T G, Heywood V H, Burges N A, Moore D M, Valentine D W, Walters S M and Webb D A 1968–80 *Flora Europaea* vol 2–5 (Cambridge: Cambridge University Press)

[27] Beniston M, Keller F and Goyette S 2003 Snow pack in the Swiss Alps under changing climatic conditions: an empirical approach for climate impacts studies *Theor. Appl. Climatol.* **74** 19–31

[28] Hantel M, Ehrendorfer M and Haslinger A 2000 Climate sensitivity of snow cover duration in Austria *Int. J. Climatol.* **20** 615–40

[29] Laternser M and Schneebeli M 2003 Long-term snow climate trends of the Swiss Alps (1931–99) *Int. J. Climatol.* **23** 733–50

[30] Wielke L-M, Haimberger L and Hantel M 2004 Snow cover duration in Switzerland compared to Austria *Meteorol. Z.* **13** 13–17

[31] Wielke L-M, Haimberger L and Hantel M 2005 Corrigendum to Snow cover duration in Switzerland compared to Austria *Meteorol. Z.* **14** 875

[32] Hantel M and Maurer C 2011 The median winter snowline in the Alps *Meteorol. Z.* (DOI:10.1127/0941-2948/2011/0495)

[33] Dery S J, Stieglitz M, McKenna E C and Wood E F 2005 Characteristics and trends of river discharge into Hudson, James, and Ungava Bays 1964–2000 *J. Clim.* **18** 2540–57

[34] Brohan P, Kennedy J J, Harris I, Tett S F B and Jones P D 2006 Uncertainty estimates in regional and global observed temperature changes: a new dataset from 1850 *J. Geophys. Res.* D **111** 12106

[35] Guisan A and Theurillat J-P 2000 Equilibrium modeling of alpine plant distribution: How far can we go? *Phytocoenologia* **30** 353–84

[36] Efron B and Tibshirani R B 1998 *An Introduction to the Bootstrap* (London: Chapman and Hall) p 436

[37] Ladinig U and Wagner J 2007 Timing of sexual reproduction and reproductive success in the high-mountain plant Saxifraga bryoides L *Plant Biol.* **9** 683–93

[38] Ladinig U and Wagner J 2009 Dynamics of flower development and vegetative shoot growth in the high mountain plant Saxifraga bryoides L *Flora* **204** 63–73

[39] Larcher W, Kainmüller C and Wagner J 2010 Survival types of high mountain plants under extreme temperatures *Flora* **205** 3–18

[40] Taschler D and Neuner G 2004 Summer frost resistance and freezing patterns measured *in situ* in leaves of major alpine plant growth forms in relation to their upper distribution boundary *Plant Cell Environ.* **27** 737–46

[41] Körner C and Alsos I G 2009 Freezing resistance in high arctic plant species of Svalbard in mid-summer *Bauhinia* **21** 25–32

[42] Moser W, Brzoska W, Zachhuber K and Larcher W 1977 Results of the IBP-Project 'Hoher Nebelkogel 3184 m' (Ergebnisse des IBP-Projekts 'Hoher Nebelkogel 3184 m') *Sitz.ber., Oesterr. Akad. Wiss.* **186** 387–419

[43] Grabherr G, Gottfried M and Pauli H 1994 Climate change effects on mountain plants *Nature* **369** 448

[44] Lenoir J, Gégout J C, Marquet P A, de Ruffray P and Brisse H 2008 A significant upward shift in plant species optimum elevation during the 20th century *Science* **320** 1768–71

[45] Parolo G and Rossi G 2008 Upward migration of vascular plants following a climate warming trend in the Alps *Basic Appl. Ecol.* **9** 100–7

[46] Walther G R *et al* 2002 Ecological responses to recent climate change *Nature* **416** 389–95

[47] Parmesan C and Yohe G 2003 A globally coherent fingerprint of climate change impacts across natural systems *Nature* **421** 37–42

[48] IPCC 2007 *Climate Change 2007: The Physical Science Basis. Contribution of Working Group I to the Fourth Assessment Report of the Intergovernmental Panel on Climate Change* ed S Solomon *et al* (Cambridge: Cambridge University Press) p 996

[49] Thuiller W, Lavorel S, Araujo M B, Sykes M T and Prentice I C 2005 Climate change threats to plant diversity in Europe *Proc. Natl Acad. Sci. USA* **102** 8245–50

[50] Gottfried M, Pauli H, Reiter K and Grabherr G 1999 A fine-scaled predictive model for changes in species distribution patterns of high mountain plants induced by climate warming *Divers. Distribut.* **5** 241–51

[51] Theurillat J-P and Guisan A 2001 Potential impact of climate change on vegetation in the European Alps: a review *Clim. Change* **50** 77–109

[52] Halloy S R P and Mark A F 2003 Climate-change effects on alpine plant biodiversity: a New Zealand perspective on quantifying the threat *Arct. Antarct. Alp. Res.* **35** 248–54

Supplementary Data for

Coincidence of the alpine-nival ecotone with the summer snowline

M. Gottfried, M. Hantel*, C. Maurer,

R. Toechterle, H. Pauli and G. Grabherr

Table of contents

*Corresponding author

This *Supplementary Data* provides measurement details of plant and snow cover, the plant list, data quality checks, lengthy theoretical derivations, discusses background parameter information and describes a few impact experiments of the original *Research Letter*.

1 Vegetation data

The vegetation data of this study have been gained at Mt. Schrankogel (47.04°N, 11.1°E, 3,497 m) in Tyrol, Austria.

1.1 Measurement details

Plant cover was recorded as area percentage of a *quadrat* (1 m × 1 m) according to the standard procedure in GLORIA (visual estimation supported by measuring tapes and plastic templates of various shapes and sizes); the typical recording error is $\leq 20\%$ (Sykes *et al.*, 1983; Kennedy & Addison, 1987; Nagy *et al.*, 2002; Pauli *et al.*, 2004).

The alpine-nival ecotone can be found everywhere at the Mt. Schrankogel slopes within the halfwidth D_m determined in the *Research Letter*; it is best developed at the SW-slope (Fig. 1b). Field campaigns in both 1994 and 2004 where conducted in late July and August. This is the typical peak period of alpine and nival plant cover development in the Central Alps.

For the snow data we have defined the period Jun/Jul/Aug as the summer season. This is the period where snow is pivotal for growth and survival of alpine and nival plants in the Alps. First winter snow may fall in September; however, climatic conditions in this period are not as decisive for these plants as the earlier part of the season (Körner, 2003).

1.2 Plant species list

The full list of vascular plants recorded in the study area of Mt. Schrankogel is given in Table S1. Nomenclature is after *Flora Europaea* (Tutin *et al.*, 1964, 1968-1980). For the classification into alpine and nival species see the *Research Letter*.

Table S1: List of nival and alpine plants

FULL NAME	ALPINE / NIVAL
Androsace alpina (L.) Lam.	nival
Cerastium uniflorum Clairv.	nival
Poa laxa Haenke	nival
Ranunculus glacialis L.	nival
Saxifraga bryoides L.	nival
Saxifraga oppositifolia L. subsp. *oppositifolia*	nival
Agrostis rupestris All.	alpine
Antennaria carpatica (Wahlenb.) Bluff & Fingerh.	alpine
Anthoxanthum odoratum L. subsp. *alpinum* (Á. & D.Löve) Jones & Melderis	alpine
Avenula versicolor (Vill.) M.Laínz subsp. *versicolor*	alpine
Botrychium lunaria (L.) Sw.	alpine
Cardamine resedifolia L.	alpine
Carex curvula All. subsp. *curvula*	alpine
Cerastium cerastoides (L.) Britton	alpine
Draba fladnizensis Wulfen	alpine
Erigeron uniflorus L.	alpine
Euphrasia minima Jacq. ex DC. subsp. *minima*	alpine
Festuca halleri All. subsp. *halleri*	alpine
Festuca intercedens (Hack.) Lüdi ex Bech.	alpine
Gentiana bavarica L.	alpine
Geum montanum L.	alpine

Geum reptans L.	alpine
Leontodon pyrenaicus Gouan subsp. *helveticus* (Mérat) Finch & P.D.Sell	alpine
Leucanthemopsis alpina (L.) Heywood subsp. *alpina*	alpine
Linaria alpina (L.) Mill.	alpine
Luzula spicata (L.) DC.	alpine
Minuartia sedoides (L.) Hiern	alpine
Minuartia verna (L.) Hiern subsp. *verna*	alpine
Omalotheca supina (L.) DC.	alpine
Oreochloa disticha (Wulfen) Link	alpine
Pedicularis aspleniifolia Flörke ex Willd.	alpine
Phyteuma hemisphaericum L.	alpine
Poa alpina L.	alpine
Polygonum viviparum L.	alpine
Potentilla frigida Vill.	alpine
Primula glutinosa Wulfen	alpine
Primula minima L.	alpine
Sagina saginoides (L.) H.Karst. subsp. *saginoides*	alpine
Salix herbacea L.	alpine
Saxifraga androsacea L.	alpine
Saxifraga exarata Vill. subsp. *exarata*	alpine
Saxifraga seguieri Spreng.	alpine
Sedum alpestre Vill.	alpine
Senecio incanus L. subsp. *carniolicus* (Willd.) Braun-Blanq.	alpine
Sibbaldia procumbens L.	alpine

Silene acaulis (L.) Jacq. subsp. *bryoides* (Jord.) Nyman (syn. *S. exscapa*)	alpine
Taraxacum officinale Weber agg.	alpine
Trisetum spicatum (L.) K.Richt. subsp. *spicatum*	alpine
Veronica alpina L.	alpine
Veronica bellidioides L.	alpine

2 Snow data

2.1 The snow cover duration data set

Basic snow data in this study is the number of snow days per season; the season is here the three months period June/July/August (92 days). The routine climate stations available (268 stations in total, black dots in Fig. 1a) provide records of observed snow depth in units cm for each day. During the summer months some stations without any snow cover report 'missing data'; this excluded an average of 78 stations per summer.

At the 190 stations remaining a given day was counted as one with snow cover ($\nu = 1$) when the snow depth was at least 2 cm; if snow cover was below this threshold we set $\nu = 0$. The stochastic ν-values were averaged over all days of the season; this yields the relative seasonal snow cover duration n, a number between 0 and 1. The impact of the threshold upon the results is minor (see Table S5 below).

2.2 Saturated data

The observation error of the snow duration is a maximum for $n = 0.5$ and zero for $n = 0$, $n = 1$; the reason is as follows Hantel *et al.* (2000). The observation $n = 0$ is typical for a climate station in the lowlands in summer; missing snow cover during summer ($\nu = 0$ on each day) cannot be in doubt for the observer, and thus is presumably free of error. Similarly, the observation $n = 1$, typical for a high-located station in winter, can also be considered free of error (ν always equal to 1). On the other hand, the snow duration $n = 0.5$ has presumably the largest fluctuation and thus the largest uncertainty. We have earlier tested this and found that the variance of $n = 0$, $n = 1$ is about zero while the variance of $n = 0.5$ is maximum. For these reasons the fit routine in the *extended error model* adopted form our earlier research (Hantel *et al.*, 2000) uses the

parabolic variance profile for n:

$$\sigma^2(n) = 4(1-n)n \tag{S1}$$

The consequence is that the observations $n = 0$, $n = 1$ have zero variance and thus, in the fit routine, infinite accuracy; these observations are referred to as *saturated*. Our convention now is that saturated observations have to be excluded from the fit. Saturation is by far the most important exclusion reason for snow duration data in summer, almost only because of $n = 0$. It reduces the 190 stations that remained above down to 79 useable stations representing 797 station summers.

What has just been said of the observation error of the snow duration applies in like manner to the nivality index, including the phenomenon of saturation. However, our data set for m had just 5% saturated data so that this criterion was, for the nivality index, of limited impact. No further exclusion conditions were applied to the nivality index data. Thus of the m-values from the 162 Schrankogel plots 153 were usable in 1994 and 155 in 2004.

2.3 Further data quality checks

A second exclusion reason only for the snow data, also introduced by Hantel *et al.* (2000) and implemented in our present data quality check, is the following. In order to distinguish the poorer from the more representative stations, the linear correlation coefficient r between n and T during the 30-year period was determined for each station. r should be negative, in accord with the basic notion of our model that an increase of T corresponds to a decrease of n. Data inconsistent with this hypothesis are *a priori* meaningless; the corresponding stations were discarded (39 stations in our present evaluation). However, most of the discarded stations

are ones with extremely few *n*-data (1-4 station summers); thus the data reduction due to the correlation criterion is limited to about 17% of unsaturated station summers.

40 Alpine climate stations eventually passed these quality checks (marked orange in Fig. 1a of the *Research Letter*), yielding a total of 664 station summers with useful snow data, plotted as individual dots in Fig. 4b as well as in Fig. 2b).

3 Nonlinear probabilistic model

Key hypothesis of the theoretical model applied in this study is that m and n are controlled by the mountain temperature τ. The corresponding plots have been reproduced in Fig. 4a, 4b of the *Research Letter*. The data eventually used in Fig. 4a, 4b are exactly the same as in Fig. 2a, 2b. The difference is that no model is involved in Fig. 2a, 2b (except for the assumptions implicit for linear regression) while in Fig. 4a, 4b also climate temperature information is used for the nonlinear fit.

Table S2: Table of symbols for nonlinear probabilistic model

Quantity	Nivality index m	Snow duration n
Independent space coordinates	z	x, y, z
Independent time coordinate	θ	θ
Measured field quantity	m	n
State curve (fitted from field data)	M	N
Extreme sensitivity of state curve (fitted)	$s_{o,m}$	$s_{o,n}$
Reference parameter for τ (fitted)	$\tau_{o,m}$	$\tau_{o,n}$
Altitudinal temperature gradient of τ (fitted)	c_m	c_n
Sensitivity profile (or τ-slope) of state curve	$s_m(\tau) = \mathrm{d}M/\mathrm{d}\tau$	$s_n(\tau) = \mathrm{d}N/\mathrm{d}\tau$
Central altitude = altitude of extreme sensitivity	Z	H
Halfwidth of sensitivity profile	D_m	D_n
10 year-trend of central altitude	ΔZ	ΔH
10 year-trend of nivality/snow at central altitude	ΔM (Δm)	ΔN (Δn)

For easy reference we present in this section an annotated summary of the main formulae used in our nonlinear probabilistic equilibrium model (Hantel *et al.*, 2000; Hantel & Hirtl-Wielke, 2007) for the snow duration n. The same model has been applied in this study to the nivality index m. The correspondence, including the convention for the letters used for the respective quantities, is as in Table S2. The first block in Table S2 comprises the external data, the second the fitted state curves, the third the quantities derived from the state curves.

3.1 The state function of the probabilistic model

In the following we describe the model exclusively for the snow duration n. Climate temperature T and station coordinates x, y, z are condensed in the *mountain temperature* defined as follows:

$$\tau = T + ax + by + cz \tag{S2}$$

The quantities a, b, c are the constants of a linear expansion (so-called *Taylor expansion*). τ is the argument of the state curve of the snow duration. The state curve N is defined as the probability P_G that a stochastic temperature variable, chosen out of an ensemble with mean τ, is less or equal to the reference τ_0:

$$N(\tau) = P_G(\tau, \tau_0) = \Phi(\chi) \quad \text{with} \quad \chi = \sqrt{2\pi}\, s_0 (\tau - \tau_0) \tag{S3}$$

This definition implies that P_G is also the probability to find water in the frozen phase, provided equilibrium has been reached; thus we refer to this approach as a *nonlinear probabilistic equilibrium model*. The subscript G indicates that the temperature variable with mean τ is Gaussian (i.e., normally distributed). Φ is the *Gaussian error integral* (Bronstein *et al.*, 1999) defined as:

$$\Phi(\chi) = \frac{1}{\sqrt{2\pi}} \int_{-\infty}^{\chi} e^{-t^2/2} \mathrm{d}t. \tag{S4}$$

The function N in Eq. (S3) is specified by the parameters s_0, τ_0, a, b, c, gained from the observed five-component data vectors (n, T, x, y, z) through a fitting routine. Time θ is implicit in the data vector through the time dependence of the European temperature $T(\theta)$.

When fitting the snow data with the 3D-Taylor expansion implemented in the mountain temperature (S2) we follow our earlier study (Hantel & Hirtl-Wielke, 2007); the reason is the horizontal climate shift across the Alps that is partly accounted for by a linear horizontal slope. Yet this recipe cannot be applied to the vegetation data since the observing plots of the Schrankogel quadrats have undistinguishable horizontal coordinates x, y; the useful data vector of the nivality index is (m, T, z). Consequently, and in order to have the same fitting routine for both data types, we arbitrarily set $a = b = 0$ also for the snow and use three-component data vectors (n, T, z).

Table S3: Fit parameters for different Taylor expansions in formula S4 for mountain temperature, evaluated for *n*-data.

Quantity	Taylor 1D	Taylor 3D
s_0 (1/°C)	-0.33±0.02	-0.31±0.02
τ_0 (°C)	9.60±0.82	9.03±0.67
a (°C/°lon)	0	0.32±0.14
b (°C/°lat)	0	-1.27±0.40
c (°C/km)	-2.89±0.40	-3.16±0.34
cost function per data point	0.29	0.22
$H_{1975-2004}$ (m)	2,897±140	2,827±126
D (m)	992± 153	968±119

With this convention the state function N in Fig. 4b of the *Research Letter* has been gained with the 1D-Taylor expansion; the curve N is specified by the three parameters $s_{0,n}, \tau_{0,n}, c_n$. When evaluated with the 3D-Taylor expansion the curve is the same within drawing accuracy. The parameters for both cases are listed in Table S3; the difference is for all parameters within error margins. Similarly, the state function M in Fig. 4a has also been gained with the 1D-Taylor expansion; the curve M is specified by the three parameters $s_{0,m}, \tau_{0,m}, c_m$. The parameters for the 1D-Taylor expansion of both m, n are also listed in Fig. 5 of the *Research Letter*.

3.2 The sensitivity profile

N represents the entire information contained in the data vectors (n, T, z). Formally it is time-independent; the climate trend $\mathrm{d}T/\mathrm{d}\theta$ can be implemented via τ and trend statements can be derived from the state function parameters s_0 and c. The τ-slope is the derivative of the state

144 function with respect to τ:

$$s(\tau) = \frac{\partial N(T,z)}{\partial T} = \frac{\mathrm{d}N(\tau)}{\mathrm{d}\tau} = s_0 \exp\{-\pi[s_0(\tau-\tau_0)]^2\} \tag{S5}$$

145

146 It is identical to the partial temperature derivative at constant altitude. The Gaussian function
147 $s(\tau)$ is referred to as *sensitivity profile*. In case of M we may consider the entire sensitivity
148 profile as representing the *ecotone*.

149 The sensitivity profile $s(\tau)$ reaches its extreme value s_0 at the argument $\tau = \tau_0$, corre-
150 sponding to $N = 0.5$; consequently, $s(\tau_0) = s_0$. We interpret this parameter as the extreme
151 sensitivity of N with respect to changes of the climate temperature T. These changes can be
152 the natural fluctuations from year to year; this is one interpretation for the snow duration data.
153 They can also be manifestations of a systematic shift of T due to a climate trend; this is another
154 interpretation for the snow duration data and, with all caution, our interpretation for the nivality
155 index data.

156 3.3 Further parameters derived from the state function

157 The fitted temperature sensitivity parameter s_0 can be transformed into a trend by means of the
158 trend $\Delta T/\Delta\theta$ from *prior'94* to *prior'04*. For example, $s_{0,m}$ yields a *fitted* time trend of M at
159 $z = Z$ of:

$$\frac{\Delta M}{\Delta\theta} = s_{0,m}\frac{\Delta T}{\Delta\theta} \tag{S6}$$

160

161 It can be compared with the *observed* time trend $\Delta m/\Delta\theta$ as implied in the frequency distribution
162 of Fig. 3a of the *Research Letter*.

163 This consideration can in opposite direction be used for an estimate of s_0, independent
164 upon the fit. This application reads:

$$s_{0,m} = \frac{\Delta m/\Delta\theta}{\Delta T/\Delta\theta} = \frac{\Delta m}{\Delta T}. \tag{S7}$$

165

166 From Fig. 3a we have $\Delta m/\Delta\theta = -0.090/10$ years, and from the trend of the prior temperature
167 $\Delta T/\Delta\theta = 0.65\,^\circ$C/10 years, yielding $s_{0,m} \approx -0.14/^\circ$C. This estimate can be compared with the
168 fitted $s_{0,m} = -0.21(\pm 0.14)/^\circ$C from Figs. 4, 5 of the *Research Letter*.

169 The sensitivity function $s(\tau)$ can, at fixed altitude z, be considered a function of T, or,
170 for fixed T, be considered a function of z; the latter mode has been used in Fig. 4c of the
171 *Research Letter*. Transformed from τ to the argument z, the extreme sensitivity s_0, defined for
172 $\tau = T + cH = \tau_0$, is adopted at the *central altitude* (the following example for the snow data):

$$H = \frac{\tau_0 - T}{c}; \quad \frac{\mathrm{d}H(T)}{\mathrm{d}T} = -\frac{1}{c} \tag{S8}$$

173

174 To apply the formula for H requires to fix a specific T. Since T changes from year to year this
175 implies that the sensitivity profile shifts up and down from year to year. The temperatures T
176 used in Fig. 4c are *prior'94* and *prior'04*.

177 Independent upon T is the temperature sensitivity $\mathrm{d}H/\mathrm{d}T$ of the central altitude. From
178 Eq. (S8), and equivalent to (S6), the parameter c can be used for an estimate of the trend of the
179 central altitude provided the trend of climate temperature is known:

$$\frac{\Delta H}{\Delta\theta} = -\frac{1}{c}\frac{\Delta T}{\Delta\theta} \tag{S9}$$

180

181 This implies that the parameter c controls the time trend of the central altitude of ecotone lines
182 and snowlines provided the trend of T is externally given. Another possibility to calculate the
183 time trend of the central altitude is to determine $\Delta T/\Delta\theta$ *a posteriori* from the trend in Fig. 3b
184 and from the fitted parameter s_0 according to:

$$\frac{\Delta H}{\Delta\theta} = -\frac{1}{cs_0}\frac{\Delta n}{\Delta\theta}; \quad \frac{\Delta T}{\Delta\theta} = \frac{1}{s_0}\frac{\Delta n}{\Delta\theta} \tag{S10}$$

185

186 which has the advantage to account at least partly for the unknown uncertainty in ΔT.

187 The halfwidth of the sensitivity profile, transformed from the argument τ to the altitude
188 argument z, is:

$$D = \underbrace{2\left(\frac{\log 2}{\pi}\right)^{0.5}}_{\approx .94}\frac{1}{s_0 c}. \tag{S11}$$

189

190 D does not depend on τ and thus is independent also upon T.

4 Adaptation of the extended error model

The fit routine used in our earlier work (Hantel *et al.*, 2000; Hantel & Hirtl-Wielke, 2007) needs to be somewhat modified for the purposes of the present study. In order to be self-contained we first summarize and generalize our extended error model [see section 4.3 *The extended fit* in the original publication (Hantel *et al.*, 2000)].

4.1 The 'extended fit' revisited

Input for the extended error model are pairs (n_i, T_i) of observed quantities seasonal snow duration n_i and European temperature T_i; the index i of the different observations runs from 1 to I. The model function is:

$$N(T) = \Phi\left(\sqrt{2\pi}s_0[T - T_0]\right) \tag{S12}$$

N interpolates the measured values of n_i and T_i through the fitted parameters s_0 (extreme sensitivity) and T_0 (a reference constant). The concept of mountain temperature is not needed at this stage. In the present application of the fit the observed quantity T in Eq. (S12) is replaced through $\tau = T + cz$ and the observational pairs (n_i, T_i) through triplets (n_i, T_i, z_i) with z_i the altitude of the observation station. This adds a further parameter c to be fitted without any further difference in the subsequent algorithm.

The modeled values follow from the observed values by means of the model function N and its inverse N^{-1} as:

$$n^i = N(T_i); \qquad T^i = N^{-1}(n_i) \tag{S13}$$

With the differences between measured and modeled values we define the cost function:

$$\sum_{i=1}^{I}(f_i^2+g_i^2) \equiv J_e(s_0,T_0) \quad \text{with} \quad f_i \equiv \frac{n_i-n^i}{\sigma_i}, g_i \equiv \frac{T_i-T^i}{\chi_i}. \tag{S14}$$

The fit consists in minimizing $J_e(s_0,T_0)$; the corresponding parameters s_0,T_0 are optimal. The variances are written as product of the *distribution error* (superscript a) and the *error scale* (superscript b) with calibration parameters σ_0,χ_0:

$$\sigma_i = \sigma_i^{\mathrm{a}}\sigma^{\mathrm{b}}, \quad \chi_i = \chi_i^{\mathrm{a}}\chi^{\mathrm{b}}; \quad \sigma_i^{\mathrm{a}} = \sigma_0\left[4(1-n_i)n_i\right]^{1/2}, \quad \chi_i^{\mathrm{a}} = \chi_0. \tag{S15}$$

σ_i is zero for $n_i = 0$ and $n_i = 1$ and maximum for $n_i = 0.5$ (as indicated by the shading in Fig. 4a, 4b); χ_i is a constant. The distribution errors $\sigma_i^{\mathrm{a}},\chi_i^{\mathrm{a}}$ are dimensionless. The error scales $\sigma^{\mathrm{b}},\chi^{\mathrm{b}}$ are the observed standard deviations; i.e., $\sigma^{\mathrm{b}} = v_m$, $\chi^{\mathrm{b}} = v_{t,m}$ in case of the nivality index and $\sigma^{\mathrm{b}} = v_n$, $\chi^{\mathrm{b}} = v_{t,n}$ in case of the snow duration (Table S4).

Table S4: Statistical parameters required for *extended fit*

Nivality		Snow	
Parameter	Value	Parameter	Value
$\bar{T}$ (°C)	18.01	$\bar{T}$ (°C)	18.01
ν_t (°C)	0.94	ν_t (°C)	0.94
$\bar{T}_m$ (°C)	18.01	$\bar{T}_n$ (°C)	17.77
$\nu_{t,m}$ (°C)	0.32	$\nu_{t,n}$ (°C)	0.78
$\bar{m}$	0.51	$\bar{n}$	0.19
ν_m	0.24	ν_n	0.21
α_m	1/308	α_n	29/692

The relative weights of the distribution errors are fixed as follows. We introduce a new parameter α and calibrate the constant parameters σ_0, χ_0 such that the mean weights for all n_i and T_i add to unity:

$$\sum_{i=1}^{I} \frac{1}{(\sigma_i^{\mathrm{a}})^2} = 1-\alpha \quad \Rightarrow \quad \sigma_0^2 = \frac{1}{1-\alpha} \sum_{i=1}^{I} \frac{1}{4(1-n_i)n_i}; \tag{S16}$$

$$\sum_{i=1}^{I} \frac{1}{(\chi_i^{\mathrm{a}})^2} = \alpha \quad \Rightarrow \quad \chi_0^2 = \frac{I}{\alpha}. \tag{S17}$$

In our earlier model we had made a sensitivity experiment [see Fig. 8 in Hantel *et al.* (2000); variation of α implemented by replacing σ^{b} through $\sigma^{\mathrm{b}} \times 10^{\nu}$ and varying ν]. The experiment had shown, in winter for the Austrian snow data, that the impact of α upon the fitted parameters s_0, T_0 was limited; after all, no independent estimates of these parameters were available. Thus we chose $\alpha = 0.5$ and kept the parameter constant throughout. In the present study we have

changed this (see next section).

4.2 Statistical parameters for the fit

The *extended error model* (Hantel *et al.*, 2000; Hantel & Hirtl-Wielke, 2007) was used in the fit runs to calculate the state curves M, N in Fig. 4 of the *Research Letter*. The fit algorithm finds s_0, τ_0, c by minimizing the cost function $C(s_0, \tau_0, c)$ which is a generalization of $J_e(s_0, T_0)$. The variance parameters σ_i, χ_i implicit in C are partly specified by $v_m, v_n, v_{t,m}, v_{t,n}$ as listed in Table S4 and partly specified by α; note that for any single σ_i the values m_i and n_i are also explicitly needed.

There are some additional parameters listed in Table S4. Of these, $\overline{T}$ is the mean of the CRU temperatures over the rectangle 5°-25°E, 42.5°-52.5°N, for the years 1975-2004; v_t is the standard deviation of individual T during this epoch. $\overline{T}_m$ applies also for the epoch 1975-2004; however, only the T's were used that actually enter the fit of Fig. 4a. Thus $\overline{T}_m$ is practically equal to the arithmetic mean of the T's during *prior'94* and *prior'04*. Correspondingly, the standard deviation $v_{t,m}$ is practically equal to half the difference between the mean T of *prior'94* and *prior'04*.

$\overline{T}_n$ is also valid for 1975-2004; however, only the T's were used that actually enter the fit of Fig. 4b. Thus $\overline{T}_n$ differs somewhat from $\overline{T}$. $v_{t,n}$ is the corresponding standard deviation. $\overline{m}$ is the mean of the m in Fig. 4a, v_m the corresponding standard deviation. The equivalent is valid for n.

As discussed in the previous section, the original choice of the relative weight of the contributions (in case of the nivality index) of the m- and the T-residuals in the cost function was $\alpha = 1/2$. Here we have adopted a more sophisticated choice. A number of μ independent observations, with one degree of freedom reserved for the mean, would yield $\mu - 1$ degrees of

freedom for the variance. After some experimentation and guided by the estimated trend of m from 1994 to 2004 discussed above, we chose:

$$\alpha_m = \frac{\mu_T - 1}{(\mu_T - 1) + (\mu_m - 1)}; \quad \alpha_n = \frac{\nu_T - 1}{(\nu_T - 1) + (\nu_n - 1)}. \tag{S18}$$

For the nivality index we have just $\mu_T = 2$ observations of T and $\mu_m = 153 + 155 = 308$ observations of m yielding $\alpha_m = 1/308$; for the snow duration we have $\nu_T = 30$ observations of T and $\nu_n = 664$ observations of n yielding $\alpha_n = 29/692$.

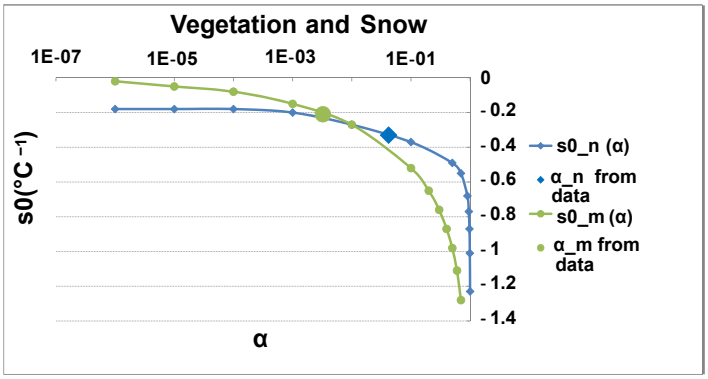

Figure S1: Impact of the relative weight α on the fitted s_0.

The impact of α upon s_0 in the vicinity of these values is demonstrated in Fig. S1. For example, with the parameter α_m=0.5 chosen in the original application Fig. S1 would yield $s_{0,m}$=−0.98/°C. This is far off the more conservative estimate $s_{0,m}$=−0.21/°C found with Eq. (S18) and eventually listed in Fig. 5 of the *Research Letter*. The impact of α_n=0.5 upon $s_{0,n}$ is numerically less dramatic but principally the same. Thus the independent estimate of s_0, discussed above in the context of Eq. (S7) for the case of $s_{0,m}$, is an *a posteriori*-proof that the choice of α according to (S18) is more appropriate than the original naive choice α=0.5.

5 Robustness of the results

In this section we discuss a couple of sensitivity experiments we have carried out for the purpose of checking to what extent our result are robust against our ignorance in certain parameters. The error of the fitted parameters (given in all cases as 1σ) was found with 2,000 bootstrap runs (Wielke *et al.*, 2004, 2005).

5.1 Results for the mountain temperature

The mountain temperature τ is a substitute for the station temperature. The latter has not been measured at Schrankogel plots. Thus τ is the only temperature available for the plant data in the evaluation of Fig. 4a.

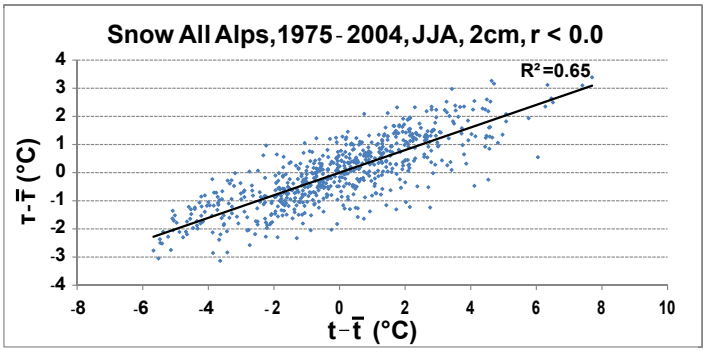

Figure S2: Correlation between mountain temperature and station temperature.

However, for the snow data the local temperature at the climate stations is available and has been compared in Fig. S2 with τ. The correlation is acceptable.

5.2 Impact of the snow threshold

The impact of the threshold for the snow duration upon the fitted parameters has been studied through choosing different thresholds. The result is as listed in Table S5; this demonstrates that

the impact is minor.

Table S5: Different thresholds of snow depth. Snow All Alps, JJA, 1D-Taylor expansion.

	1 cm	2 cm	3 cm	4 cm
s_0 (1/°C)	-0.32 ± 0.02	-0.33 ± 0.02	-0.34 ± 0.02	-0.34 ± 0.02
c (°C/km)	-2.93 ± 0.41	-2.89 ± 0.40	-2.95 ± 0.47	-2.96 ± 0.41
τ_0 (°C)	9.48 ± 0.80	9.60 ± 0.82	9.43 ± 0.97	9.38 ± 0.84
H (m)	2,891 ± 147	2,897 ± 140	2,899 ± 148	2,894 ± 137
D (m)	1,008 ± 160	992 ± 153	967 ± 160	938 ± 153
cost	0.27	0.29	0.32	0.33

5.3 Central altitudes of vegetation and snow sensitivity profiles

The central altitudes Z, H have been determined with two different algorithms: Linear regression (determined from Fig. 2a, 2b) and nonlinear probabilistic model (determined from Fig. 4a, 4b); this yields numerically different, but basically similar, results. These are listed in Table S6. Also listed is the difference, both for m and n, of the two results for the temperatures of *prior'94* and *prior'04*. The estimates 'nonl. prob.' are from the fitted state curves $M(\tau)$, $N(\tau)$ by applying the formula (S8) for H (which is equally valid for Z). T is the average of the CRU temperatures for the respective time period: $T(1994) = T(prior'94) = 17.68\,°\mathrm{C}$; $T(2004) = T(prior'04) = 18.33\,°\mathrm{C}$; $T(\mathrm{mean}) = T(1975-2004) = 18.01\,°\mathrm{C}$; parameters τ_0, c are from Fig. 5. The differences are in all cases minor. It may be noted, however, that the central altitude estimates for both m and n cluster around 2900 m which is equal within error limits; on the other hand, the trend estimate of H is considerably larger than that for Z. With regard to the 'nonl. prob.' fit two different trend estimates (line 3 and 5 in Table S6; formulae (S9)-first value, (S10)-second value) can be given.

As to demonstrate that the coincidence of H and Z (both adopted for n=m=0.5) is not accidental, we checked the coincidence for a range of n- and m-values; namely from 0.35 to 0.65. Table S7 suggests that the ecotone function is embedded into the snow function and therefore other choices for n and m would also be possible (as it is the case for n=m=0.6).

Table S6: Central altitudes Z, H and trends ΔZ, ΔH 1994-2004, unit m, of ecotone m and snow profile n.

	Fit specification	Altitude 1994	Altitude mean	Altitude 2004	10 years-trend
m	lin. regression: Z, ΔZ	2,962±7	2,977±5	2,990±7	+28±10
m	nonl. prob.: Z, ΔZ	2,952±16	2,967±16	2,982±16	+30±24*, +20±27^{+}
n	lin. regression: H, ΔH	2,837±50	2,911±40	3,042±50	+205±71
n	nonl. prob.: H, ΔH	2,782±140	2,897±140	3,007±140	+225±31*, +142±193^{+}

*calculated with formula (S9), smaller error due to missing error estimate in ΔT $^{+}$calculated with formula (S10)

Table S7: Z- and H- values for different m- and n- values

m	Z (m)	n	H (m)
0.35	2933	0.35	2735
0.4	2945	0.4	2791
0.45	2956	0.45	2844
0.5	2967	0.5	2897
0.55	2979	0.55	2950
0.6	2991	0.6	3004
0.65	3003	0.65	3060

5.4 Impact of the error of the climate temperature trend

The parameters derived from the nivality index state curve have an unknown systematic error due to our ignorance in choosing the proper climate temperature for the basis of the Taylor expansion. For this purpose we have tried to scan the domain of insufficient knowledge by a hypothetical sensitivity experiment. The key unknown quantity is the difference ΔT of the climate temperatures in the vegetation curve of Fig. 4a; this trend in the present evaluation is 0.65 °C. We have calculated the parameters of the nivality index state curve for ΔT from 0.2 to 1.4 °C. We find that the state curve parameters s_0, τ_0, c individually change considerably with ΔT as one would expect. However, within moderate distance ($\pm 20\%$) from the nominal $\Delta T =$ 0.65 °C, the parameters are not different within error margins. As to the derived parameters the ignorance in choosing ΔT is of no consequence for Z, D_m, ΔZ and ΔM.

References

Bronstein, I. N., Semendjajev, K. A., Musiol, G. & Mühlig, H. (1999) *Taschenbuch der Mathematik*. Verlag Harri Deutsch, Frankfurt am Main.

Hantel, M. & Hirtl-Wielke, L.-M. (2007) Sensitivity of Alpine snow cover to European temperature. *International Journal of Climatology*, **27**, 1265–1275.

Hantel, M., Ehrendorfer, M. & Haslinger, A. (2000) Climate sensitivity of snow cover duration in Austria. *International Journal of Climatology*, **20**, 615–640.

Kennedy, K. A. & Addison, P. A. (1987) Some considerations for the use of visual estimates of plant cover in biomonitoring. *Journal of Ecology*, **75**, 151–157.

319 Körner, C. (2003) *Alpine Plant Life—Functional Plant Ecology of High Mountain Ecosystems*.
320 2nd edition, Springer, Berlin.

321 Nagy, L. , Nagy, J. , Legg, C. J. , Sales, D. I. & Horsfield, D. (2002) Monitoring vegetation
322 change caused by trampling: a study from the Cairngorms, Scotland. *Botanical Journal of*
323 *Scotland*, **54**, 191–207.

324 Pauli, H. , Gottfried, M. , Hohenwallner, D. , Reiter, K. , Casale, R. & Grabherr, G. (2004) *The*
325 *GLORIA field manual - Multi-Summit approach* (European Commission DG Research, EUR
326 21213, Office for Official Publications of the European Communities, European Commission,
327 Luxembourg).

328 Sykes, J. M., Horrill, A. D. & Mountford, M. D. (1983) Use of visual cover assessments as
329 quantitative estimators of some British woodland taxa. *Journal of Ecology*, **71**, 437–450.

330 Tutin, T. G., Heywood, V. H., Burges, N. A., Valentine, D. W., Walters, S. M. & Webb, D.A.,
331 editors (1964) *Flora Europaea*. Volume 1. Cambridge University Press, Cambridge.

332 Tutin, T. G., Heywood, V. H., Burges, N. A., Moore, D. M., Valentine, D. W., Walters, S. M. &
333 Webb, D.A. editors (1968-1980) *Flora Europaea*. Volume 2–5. Cambridge University Press,
334 Cambridge.

335 Wielke, L.-M., Haimberger, L. & Hantel, M. (2004) Snow cover duration in Switzerland
336 compared to Austria. *Meteorologische Zeitschrift*, **13**, 13–17.

337 Wielke, L.-M., Haimberger, L. & Hantel, M. (2005) Corrigendum to Snow cover duration in
338 Switzerland compared to Austria. *Meteorologische Zeitschrift*, **14**, 875.

The snowline climate of the Alps 1961-2010

M. Hantel, **C. Maurer** and D. Mayer

Theor. Appl. Climatol., 2012, **DOI 10.1007/s00704-012-0688-9 (published online)**

Theor Appl Climatol
DOI 10.1007/s00704-012-0688-9

SPECIAL ISSUE

The snowline climate of the Alps 1961–2010

M. Hantel · C. Maurer · D. Mayer

Received: 14 October 2011 / Accepted: 30 April 2012

Abstract We study the probability for snow cover at a climate station. Connecting stations with the same probability yields the corresponding *snow line* (a figure between zero and unity). The climatological snow lines in the Alps are implicit in the *state function of snow duration*. This function, specified by just five parameters, depends upon the *mountain temperature*, a linear combination of the mean temperature over Europe and the 3D-coordinates of the stations. The influence of external parameters other than temperature (like snowfall, melting processes, station exposition) is treated as stochastic. The five state function parameters are gained for both winter (DJF) and summer (JJA) through a fitting algorithm from routine snow depth observations in 1961–2010 in Austria and Switzerland. Any desired snow line is defined by a linear surface with a characteristic value of the mountain temperature. The snow line appears when there is a cut between the surface and the orography. Temperature sensitivity of snow cover duration, analytically derived from the state function, is extreme at the *median snow line* (snow probability 0.50). Alpine-wide mean altitude of the median snow line is 793(±36)m in winter and 3.083(±1.121)m in summer. The snowline field slopes gently from west to east across the Alps (downward in winter, upward in summer) and oscillates up and down with the seasons. The sensitivity of the median snowline altitude to European temperature over the five decades of Alpine data is 166 (±5) m/°C in winter and 123 (±18) m/°C in summer. Global warming causes the snow lines to shift upward with time; in parallel, the area of the Alps that is at least 50 % snow covered in winter shrinks by −7.0 (±4.1) %/10 years.

M. Hantel ( ) · C. Maurer
Theoretical Meteorology Research Forum, Berggasse 11/2/3,
1090 Vienna, Austria
e-mail: michael.hantel@univie.ac.at

D. Mayer
Institute of Meteorology and Geophysics,
University of Vienna, Althanstrasse 14,
1090 Vienna, Austria

1 Introduction

The snow limit concept represents the intuitive notion that there is a well-defined transition between snow-covered ground and ground free of snow. The position where this transition happens is often clearly visible in the field, particularly in the mountains, sometimes locally with an accuracy of less than a meter. Connecting these positions yields the snow limit. This concept has been applied from the daily time scale over monthly to annual and decade-long periods. For example, it has been used by Hann (1883) and various subsequent authors. Further, in the geographical literature, Louis (1955) has analyzed the notion of the snow limit in detail; Louis considered, with focus upon the budgets of glaciers, the *climatological snow limit* as the position at which total snowfall and total ablation are in balance. A worldwide map of the snow limit (in relation to the tree line) has been provided by Hermes (1955).

We have recently (Hantel and Maurer (2011)) studied the snow limit concept in the more general context of the *snow line*. The basis of the snow line is the relative seasonal snow duration, obtained from daily routine measurements of the snow depth at a climate station. We interpret this as the probability to encounter snow cover. Connecting stations with the

Published online: 07 July 2012

same probability yields the corresponding snow line (a figure between zero and unity—see also the equivalent definition in the Dictionary of Earth Science, Parker (1997)). The snow limit is adopted for the specific value of 50 %; we refer to it as the *median snow line*. At the median snow line, the probability to *encounter snow* is equal to the probability to *encounter no snow*.

There is a physical reason for the significance of this boundary. The median snow line should be located where the sensitivity to temperature is extreme. In high and cold mountain regions with sizeable snow cover, the snow duration should be insensitive to an external large-scale warming or cooling; a similar reasoning applies to warm climate stations in the lowlands where there is no snow cover at all. Extreme temperature sensitivity should be found somewhere in between. This is in accord with general climatological experience (e.g., Laternser and Schneebeli (2003), Scherrer et al. (2004), and Durand et al. (2009)).

With this qualitative background, Hantel and Maurer (2011) have developed the quantitative *state function of snow duration* for the coherent mountain region of the Alps, for the climate period 1961–2000. The corresponding theory yields a formula for the state function which implies the definition of the snow lines and implies further that *the snowline field is controlled by the mountain temperature*, a linear combination of European temperature and 3D-station coordinates.

In this study, we want to corroborate these results, with the following innovative components. First, we will present evaluations for the 50-year climate epoch in 1961–2010, both for winter (DJF) and summer (JJA), for the Alpine region consisting of Austria (A) and Switzerland (CH); the results will be quite well in accord with our previous evaluations. Further, we will describe and implement a modified fitting algorithm to derive the parameter estimates for the state function; this theoretically improved method does not much change the results but in addition yields statistically sound estimates of the explained variance (Appendix 1). Finally, we will extend the mean snowline surfaces, valid for the entire Alpine region, into a couple of selected individual valleys; this may demonstrate the applicability, including its limits, of the present approach to the climate of a local station.

The paper is organized as follows: In the next section, we give a skeleton review of the model, stratified into its different levels of application. Data management is covered in Section 3. In accord with our basic hypothesis (i.e., the dependence of the snowline field solely upon the mountain temperature), we use as observed temperature data only the mean seasonal temperature, averaged over Europe, and as observed snow data only the daily snow depth at the climate stations (plus, of course, the 3D-station coordinates); other possible input parameters (e.g., local station temperature, snowfall, quantities describing the melting process, or the exposition of a climate station to radiation) are not used. In Section 4, we present standard ("naive") statistics without reference to the model. The model results come in Section 5 for the entire Alpine region and in Section 6 for the selected Alpine valleys. Trend estimates are discussed in Section 7. An outlook is given in Section 8.

2 Review of the model

The snowline model as we want to use it here (Hantel and Maurer (2011)) is based upon a snow cover model, originally designed for Austrian data by Hantel (1992), further developed in paper I (Hantel et al. (2000)), extended to Swiss data in paper II (Wielke et al. (2004) along with Wielke et al. (2005)) and applied to all-Alps data in paper III (Hantel and Hirtl-Wielke (2007)). The unifying concept is the hypothesis that the seasonal snow cover at a climate station is primarily controlled by the seasonal surface air temperature of the station. The station temperature, however, can eventually be replaced by the *montain temperature*, a linear combination of the area mean surface temperature T over Europe and the 3D-station coordinates. In this section, we review three different applications of the model, schematically sketched in Fig. 1.

2.1 Laboratory model (see Fig. 3 of Hantel and Hirtl-Wielke (2007))

In the physical laboratory (first column of Fig. 1) with actual temperature ϑ, we observe two phases ν of pure water: liquid water ($\nu = 0$) for ϑ above $t_0 = 0\,^\circ$C and ice ($\nu = 1$) for ϑ below t_0. The probability P to encounter ice is equal to the ensemble average $\langle\nu\rangle$. We further assume that there are stochastic temperature fluctuations, normally distributed, with ensemble mean $\langle\vartheta\rangle$ and standard deviation ϵ. For this setting, P is controlled by the temperature parameters as follows:

$$P(\langle\vartheta\rangle, \epsilon) = \Phi(\chi) \qquad \text{with} \qquad \chi = (t_0 - \langle\vartheta\rangle)/\epsilon. \tag{1}$$

Φ is the Gaussian *error function* defined as (Bronstein et al. (1999)):

$$\Phi(\chi) = \frac{1}{\sqrt{2\pi}} \int_{\vartheta=-\infty}^{\chi} e^{-\vartheta^2/2} \mathrm{d}\vartheta. \tag{2}$$

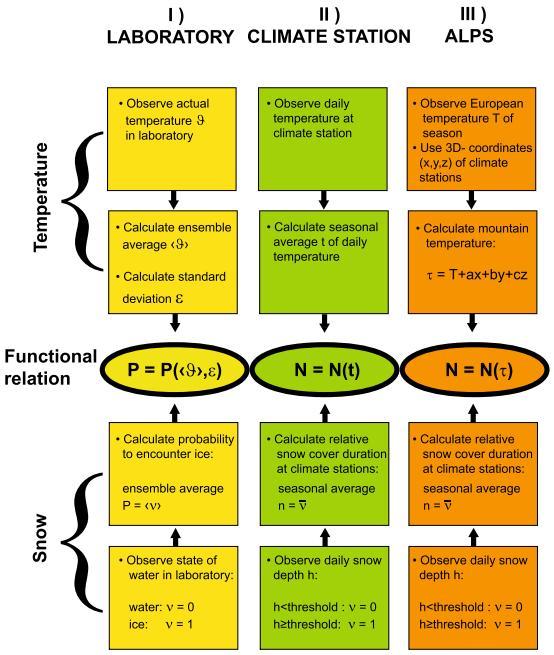

Fig. 1 Poster of different model versions. The unifying theoretical concept is a Gaussian error function $\Phi(\chi)$. It serves as an exact description of ice probability P with $\chi(\langle\vartheta\rangle, \varepsilon)$ in the laboratory (*first column*) and as logistic function N with $\chi(t)$ to describe snow probability as a function of local temperature t at individual climate stations (*second column*). With the mountain temperature τ and with $\chi(\tau)$, the error function serves as state function N to describe a relative seasonal snow duration, gained from snow data (plus European temperature and 3D-station coordinates), without using t (*third column*)

This model (Hantel and Hirtl-Wielke (2007)) yields the probability to observe ice in the laboratory.

2.2 Climate station model (see Fig. 4 of Hantel et al. (2000))

Application of the model Eq. 1 to station data is straightforward (second column of Fig. 1). We replace the standard deviation ϵ by the negative parameter $s_0 = -(\epsilon\sqrt{2\pi})^{-1}$ and put

$$N(t) = \Phi(\chi) \qquad \text{with} \qquad \chi = \sqrt{2\pi}\, s_0 (t - t_0). \tag{3}$$

N is the *snow duration function*. Its parameters s_0 and t_0 are fitted to seasonal snow cover n and mean temperature t, observed at a given climate station.

The parameters s_0 and t_0 should principally not differ from climate station to climate station. In other words, data from different stations at different elevations can be lumped together into N. This has, e.g., been done in Fig. 1 of Hantel and Hirtl-Wielke (2007) for Austrian stations and in Fig. 5 of Hantel and Maurer (2011) for all-Alps stations, both for the winters (DJF) of 1961–2000.

This type of plot reveals the dependence of the snow duration upon station temperature. However, the altitude dependence of temperature at the climate stations is mixed with the large-scale climate temperature of Europe. It follows that *snowline information cannot be gained from* $N(t)$.

2.3 Alpine-wide model (see, e.g., Fig. 6 of Hantel and Maurer (2011))

In order to identify snow lines, we note that the station temperature t is influenced by the large-scale climate process, represented by the *European temperature* T and by local effects, represented by the position (x, y, z) of the climate station. This suggests to introduce the *mountain temperature*:

$$\tau = T + ax + by + cz. \tag{4}$$

The model in Eq. 4 can be used for a multilinear regression analysis of t. The parameters a, b, and c would be the constants of this expansion. They would be gained through fitting the observed t against the predictor function τ.

In our application of the model (third column of Fig. 1), we go a step beyond: We will get the expansion parameters $a, b,$ and c not from the observed t but from the observed n, by replacing t through τ in Eq. 3; t_0 is replaced by the reference constant τ_0. This yields, with Φ as in Eq. 2, the state function of snow duration:

$$N(\tau) = \Phi(\chi) \qquad \text{with} \qquad \chi = \sqrt{2\pi}\, s_0 (\tau - \tau_0). \tag{5}$$

$N(\tau)$ is specified through the *parameter vector* (s_0, τ_0, a, b, c). Time θ is implicit in the *data vector* (n, T, x, y, z) through the time dependence of the large-scale European temperature $T(\theta)$. The parameter vector is estimated from the data vector trough a pertinent fitting routine (see Section 3.8).

With the strategy summarized in Fig. 1, we will fulfill the following goals:

- Split the station temperature t, through the concept Eq. 4 of mountain temperature τ, into a European scale and a local scale component;
- Show that τ (which now replaces t) can be gained from the snow duration data;

– Represent the snow cover of the entire Alps with one nonlinear profile, the *state function* $N(\tau)$ of snow duration;
– Show that N is controlled by European temperature T;
– Specify the median snow line by choosing $\tau = \tau_0$ in Eq. 4; the corresponding linear function of x, y, z for fixed T generates the median snow line (see Figs. 12 and 13 below).

The progress achieved is that all relevant properties of the snow cover, including the snowline field, across the 50-year observation period, can be analytically derived from the state function $N(\tau)$. We begin with the slope profile of the state curve:

$$\frac{\partial N}{\partial T} = \frac{\mathrm{d}N}{\mathrm{d}\tau} = \frac{\mathrm{d}\Phi}{\mathrm{d}\chi} \cdot \frac{\mathrm{d}\chi}{\mathrm{d}\tau} = s_0 \exp(-\chi^2/2);$$

$$\left[\frac{\mathrm{d}N}{\mathrm{d}\tau}\right]_{\tau=\tau_0} = s_0. \tag{6}$$

χ is specified through Eq. 5. As noted in Hantel et al. (2000), the partial derivative of N with respect to T (understood for fixed station vector x, y, z) is equal to the slope with respect to τ. We interpret these derivatives as sensitivities. Thus, the first equation of Eq. 6 represents the entire *sensitivity of Alpine climatological snow cover with respect to the European temperature*. The sensitivity is maximum for $\tau{=}\tau_0$, adopted at the altitude of the median snow line; above and below the sensitivity decreases and becomes zero at very low and very high altitudes. The half width of the sensitivity profile, transformed from the argument τ to the altitude argument z, is

$$D = \underbrace{2\left(\frac{\log 2}{\pi}\right)^{0.5}}_{\approx .94} \frac{1}{s_0 c}. \tag{7}$$

D does not depend on τ and thus is independent also upon T. By solving Eq. 4 for $z = H$, we find the altitude of an arbitrary snow line n:

$$H(n, T, x, y) = \frac{\tau(n) - T - ax - by}{c}. \tag{8}$$

$\tau(n)$ in this formula follows from Eq. 5 as the inverse $N^{-1}(n)$ of the state function. The function H, for fixed T, is a linear surface which, by cutting across the orography of the Alps, generates the pertinent snow line (Figs. 12 and 13). Temperature sensitivity of the snowline altitude, along with the slope components of the surface in eastward and northward direction, is given through

$$\frac{\partial H}{\partial T} = -\frac{1}{c}; \qquad \frac{\partial H}{\partial x} = -\frac{a}{c}; \qquad \frac{\partial H}{\partial y} = -\frac{b}{c}. \tag{9}$$

These formulae will be used below. Further derivatives with respect to altitude z (i.e., vertical gradient) and with respect to time θ (i.e., trend) can be found from the formulae in Eqs. 4, 5, and 6:

$$\frac{\partial N}{\partial z} = \frac{\mathrm{d}N}{\mathrm{d}\tau}\frac{\partial \tau}{\partial z} = \left(s_0 e^{-\chi^2/2}\right) \cdot c;$$

$$\frac{\partial N}{\partial \theta} = \frac{\mathrm{d}N}{\mathrm{d}\tau}\underbrace{\frac{\partial \tau}{\partial T}}_{=1}\frac{\mathrm{d}T}{\mathrm{d}\theta} = \left(s_0 e^{-\chi^2/2}\right) \cdot \frac{\mathrm{d}T}{\mathrm{d}\theta}. \tag{10}$$

This implies that both gradient and trend of N are extreme at the median snow line (i.e., at $\chi = 0$); above and below both decrease to zero with half-width D. Finally, the trend of the altitude of a given snow line follows from Eq. 8:

$$\frac{\partial H}{\partial \theta} = \frac{\partial H}{\partial T}\frac{\mathrm{d}T}{\mathrm{d}\theta} = -\frac{1}{c} \cdot \frac{\mathrm{d}T}{\mathrm{d}\theta}. \tag{11}$$

This implies that the altitudes of all snow lines have the same trend. In order to use Eqs. 10 and 11 for trend estimates, it is not sufficient to apply the present model. Also, required is an external estimate of the European temperature trend $\mathrm{d}T/\mathrm{d}\theta$ (e.g., from climatological data of the past or from a climatological model forecast).

3 Data management

The data vector (n, T, x, y, z) is organized around the independent arguments x,y, and z (which are the 3D-coordinates of the climate station) and time θ. Resolutions of θ used in this study are 1 day (θ^{**}), 1 month (θ^{*}), and one season (θ without superscript, winter = DJF and summer = JJA),[1] different for temperature and for snow.

[1]The first winter in 1961 comprises only snow and temperature data of the months January and February, while the last winter in 2010 comprises data of December 2009 and January and February 2010.

The snowline climate of the Alps 1961–2010

Table 1 Parameters of snow duration state function, period 1961–2000, DJF, 5 cm

	All Alps[a]	A + CH[b]	A + CH[c]	A + CH[d]
s_0 (°C^{-1})	−0.17 (±0.01)	−0.16 (±0.01)	−0.17 (±0.01)	−0.19 (±0.01)
τ_0 (°C)	−5.01 (±0.69)	−6.50 (±0.68)	−5.91 (±0.57)	−5.43 (±0.55)
a (°C/°lon)	−0.45 (±0.06)	−0.38 (±0.06)	−0.36 (±0.06)	−0.34 (±0.05)
b (°C/°lat)	0.42 (±0.24)	0.29 (±0.26)	0.33 (±0.25)	0.49 (±0.22)
c (°C/km)	−8.10 (±1.12)	−10.52 (±1.12)	−9.57 (±0.91)	−9.02 (±1.03)

Compare columns 1 and 3 for the impact of the different databases (all Alps versus A + CH). Compare columns 2, 3, and 4 for the impact of the different data quality criteria (i.e., "saturation" and "correlation"—these are discussed in Section 3.4 and 3.6). Evaluations in this table are made with the nonlinear fit (see Appendix 1).

[a]From Hantel and Maurer (2011), r <0.0 (see Fig. 6)

[b]This study, all unsaturated station seasons

[c]This study, r <0.0

[d]This study, $r < -0.3$

3.1 Representativeness of Austria + Switzerland for the Alps

In this study, we will use only snow cover data from Austrian and Swiss routine climate stations. This data basis corresponds to a combination of the data volume used in papers I and II. Main reason was the decision to cover the 50-year period 1961–2010. Extension of the database 1961–2000 for Austria (used in papers I and III) and Switzerland (used in papers II and III) by 10 years was easy to achieve. On the other hand, the extension of the database for Germany, France, Slovenia, and Italy would have been more involved and we skipped it for the present study.

This is justified since the results of the 40-year period considered in Hantel and Maurer (2011) do not significantly differ if we either use the all-Alps data or only data from A + CH. Both show essentially the same result within data accuracy as seen in columns 1 and 3 of Table 1. Thus, by restricting the present evaluation to the climate stations from Austria and Switzerland, we will yet be able to obtain results representative for the entire Alps.

3.2 European temperature

We adopt, in the same manner as in Hantel and Maurer (2011), the monthly gridded Climate Research Unit (CRU) temperatures (Brohan et al. (2006)) with a horizontal resolution of 0.5° as a *temperature database*. These we linearly average in horizontal direction over the Alpine-dominated part of central Europe (5.5°–17.5° E and 43.5°–49.5° N, identical to the rectangle sketched in Figs. 4 and 5) and with respect to time over winter (DJF) and summer (JJA). This procedure yields a time series (not reproduced here) of 50 values of European temperature $T(\theta)$ characterizing each winter and summer of the observation period 1961–2010 with one temperature per season and per year (time parameter θ).[2]

3.3 Snow duration and threshold

Original observation is snow depth h, measured daily (time parameter θ^{**}) at each climate station (coordinates of available stations x^{**}, y^{**}, z^{**}). From h, a daily value $\nu = 1$ or $\nu = 0$, depending upon threshold, is derived. The seasonal average of ν is the snow duration: $n = \overline{\nu}$. Thus, $n = n(\theta, x^{**}, y^{**}, z^{**})$ with yearly resolution (one value per season and station).

The impact of the threshold for discriminating h has been investigated by several authors. For example, Haiden and Hantel (1992) used a 1-cm data set, while Fliri (1992) recommends a minimum of 2 cm. Beniston (1997) has considered snow depth thresholds from 1 up to 150 cm.

Here, we choose 5 cm for winter, following paper I and Hantel and Maurer (2011), and 2 cm for summer, following Fliri (1992) and Gottfried et al. (2011); the latter authors have demonstrated (Table S5 in supplementary data of their paper) that in summer, the impact of the threshold upon the results is minor for thresholds from 1 to 4 cm.

3.4 Saturation of snow data

Snow duration data $n = 0$ and $n = 1$ are called saturated. They do not carry relevant information which

[2]The time series of the CRU temperature presently available ends in 2009. In order to prolong the series by 1 year, we use the fact that the mean temperature of the A + CH stations is highly correlated (98 %) with the CRU temperature. Thus we determined the 49-year average $\overline{t}_{\mathrm{A+CH}}$ and the 49-year average $\overline{T}_{\mathrm{CRU}}$. The missing CRU temperature for 2010 is generated as follows: $T_{\mathrm{CRU}}(2010) = t_{\mathrm{A+CH}}(2010) + (\overline{T}_{\mathrm{CRU}} - \overline{t}_{\mathrm{A+CH}})$. The correction is 1.8 °C.

Table 2 Overview of data selection

		Total	Unsaturated	Weak	Strong
DJF	Stations	145	142	128	91
	Seasons	7,250	4,509	4,379	3,463
JJA	Stations	145	58	27	15
	Seasons	7,250	768	646	447
DJF[a]	Stations	84	76	63	50

[a]From (Hantel et al. 2000)

makes them unacceptable as measurements. This point has been extensively discussed in paper I and again by Gottfried et al. (2011) and Hantel and Maurer (2011). The reason is that the daily snow "observation" parameter ν is Bernoulli distributed and as such has a parabolic variance distribution with variance zero for both $\overline{\nu} = 0$ and $\overline{\nu} = 1$. It follows that saturated observations have infinite accuracy which would make their contribution infinite in the cost function of the subsequent data fit.

Saturated data are dropped at the beginning of the evaluation procedure. The original data minus the saturated data will be referred to as the *processed data*. Saturation is by far the most important reason for excluding station seasons or even the complete data of one station (compare Table 2 and Appendix 2). Each of the remaining stations contains at least one unsaturated n value (most of them contain many more).

3.5 Altitude distribution of available n data

Figure 2 gives the number of processed snow duration observations (i.e., number of station seasons) available for Austria plus Switzerland as a function of altitude. The figure shows that in winter, the altitude of the median snow line is approximately located in the center of the station data whereas in summer it is located higher than most of the observed data. Thus, the winter state function will be superior in accuracy to the summer state function.

3.6 Correlation criteria for climate stations

In order to enhance data quality, we have calculated the linear correlation coefficient r between T and n and have investigated the impact of excluding stations with $r > 0$ ("weak correlation condition") and with $r > -0.3$ ("strong correlation condition"). We used the strong condition in paper I for the Austrian data set and in paper II for the Swiss data set. In our recent evaluations with the all-Alps data set, we used the weak condition, both for winter (Hantel and Maurer (2011)) and summer (Gottfried et al. (2011)).

In the present study, r was determined for both seasons and is reproduced for winter in Fig. 3 versus altitude. The stations that violate the two correlation conditions (red and blue rhomboids) tend to be concentrated at greater altitudes; these are mainly located in the inner Alpine valleys (see particularly Fig. 4). Further, the correlation of most of the red stations is based on only a few station seasons (see Appendix 2).

The impact of the two correlation criteria upon the number of stations used is summarized in Table 2. We introduced the criteria in paper I mainly for the purpose to improve the data quality. Starting from 76 unsaturated stations in Austria for winter, our weak

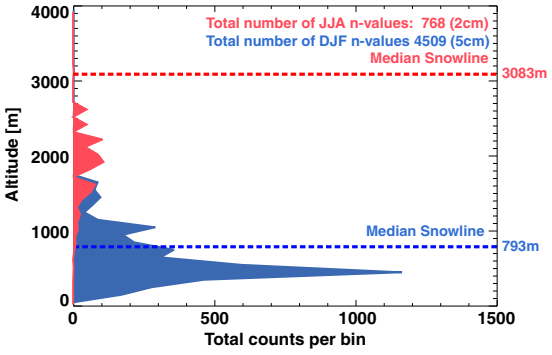

Fig. 2 Vertical frequency distribution of processed snow duration data from Austrian and Swiss climate stations (bin size = 100 m). For both seasons (winter in *blue*, threshold 5 cm; summer in *red*, threshold 2 cm), the altitude of median snow line is drawn as *dashed line*

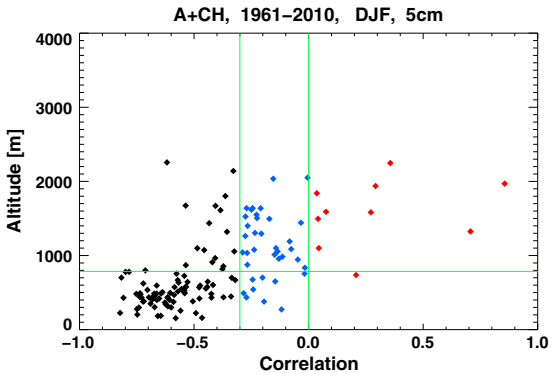

Fig. 3 Linear correlation coefficient $r(T, n)$ plotted versus altitude. Positive r in *red*, negative r larger than -0.3 in *blue*, r less than -0.3 in *black*

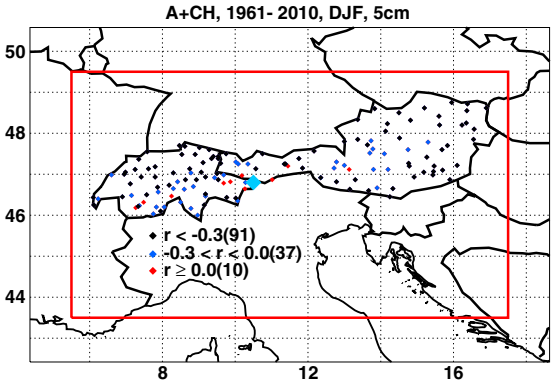

Fig. 4 Location of Austrian and Swiss climate stations, season winter (DJF). *Red* (*blue*) *rhomboids*: Stations that are excluded because they do not pass the weak (strong) correlation criterion (see also Fig. 3). *Black rhomboids*: Stations selected for the eventual data fit. *Thick blue rhomboid*: Reference zero for coordinate vector (x, y, z) in the definition of mountain temperature

criterion excluded 17 % of the stations; the strong criterion in paper I excluded another 17 %. Both measures together reduced the number of stations by 34 % down to 50 eventually used for the evaluation (last line of Table 2).

The present data reduction for winter (first line of Table 2) starts from 142 processed stations leading to 128 stations which obey the weak criterion and to 91 stations which obey the strong criterion; this corresponds to a net reduction by 36 % of the processed stations. For the purposes of the present study, we adopt the strong correlation criterion, essentially for the same reasons that have been considered relevant in paper I. Justification for our approach was that it excluded a priori erroneous and/or misleading data and enhanced the negative slope dependence of n upon T in the data set. A significant positive slope dependence (i.e., increase in n accompanied by *increase* in T) appeared only possible if the snow duration is governed by the *amount* of snowfall and not by the temperature after the snowfall, as assumed throughout our model (which includes the present model suite); this would imply that the snowfall amount is higher for high temperatures (e.g., due to the additional effect of moisture). It now appears that it is indeed the snowfall mechanism which causes some of the positive and most of the slightly negative correlation stations seen in Fig. 3.

In accord with papers I and II, stations that violate the strong correlation criterion (red and blue dots in Fig. 3) will be excluded in the present evaluation. As Table 2 shows, 3,463 station seasons (out of 4,509, corresponding to 77 %) survive our strong correlation criterion in winter (58 % in summer); thus, our remaining database is still more than sufficient. Geographic arrangement of the stations is shown in Figs. 4 and 5. These arguments in favor of our strict data quality requirements may not appear urgent because including the stations that violate the correlation conditions does not conspicuously change the eventual parameters of the fit that yields the snowline surface as given by Eq. 8. This is seen in Table 1 above (second to fourth columns): The parameters of the state function do not significantly differ if the weak or the strong correlation condition is enforced. In other words, the parameters of the state function do not yield a useful argument why the correlation criterion in one of its versions should be adopted or not. Instead, a useful argument will be the distribution function of residuals (Figs. 9 and 11).

The processed data minus the stations that violate the strong correlation criterion will be referred to as the *selected data* (identical to the last column of Table 2).

3.7 Eventual database of present snowline climatology

The specification of the data input and subsequent data flow for the present evaluation may now be summarized as follows:

- The fundamental data are station-observed snow depth $h(\theta^{**}, x^{**}, y^{**}, z^{**})$ and externally provided CRU temperature $T(\theta^{*}, x^{*}, y^{*}, z^{*})$.
- θ^{**} is the time with daily resolution, θ^{*} is the time with monthly resolution, and θ is the time with annual resolution.
- x^{**}, y^{**}, z^{**} are the space coordinates of the available climate stations; x^{*} and y^{*}, z^{*} are the space

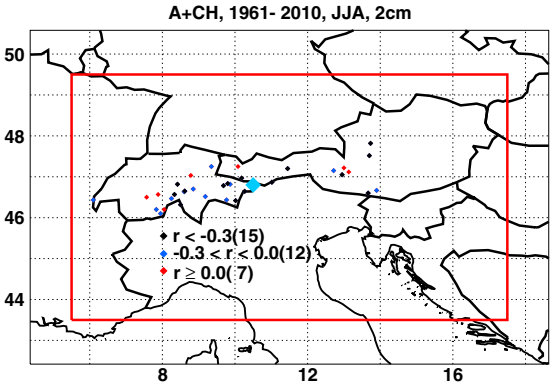

Fig. 5 Like Fig. 4, but for summer (JJA)

coordinates of the CRU grid points; and x, y, and z are the space coordinates of the selected climate stations.

– *Processed* data are unsaturated snow duration $n(\theta, x^{**}, y^{**}, z^{**})$, as well as European temperature $T(\theta)$ obtained by averaging $T(\theta^*, x^*, y^*, z^*)$ over the CRU grid points; they yield the processed data vector $\{n(\theta, x^{**}, y^{**}, z^{**}), T(\theta), x^{**}, y^{**}, z^{**}\}$.
– *Selected* data are snow duration $n(\theta, x, y, z)$ data that observe the strong correlation criterion, and European temperature $T(\theta)$; these together yield the selected data vector $\mathbf{D}=\{n(\theta, x, y, z), T(\theta), x, y, z\}$. **D** consists of five columns and 3,463 (447) rows for winter (summer).
– With **D**, we enter the model evaluation (see the next section and Appendix 1) which yields the parameter vector $\mathbf{Q}=(s_0, \tau_0, a, b, c)$; it consists of five columns and one row.

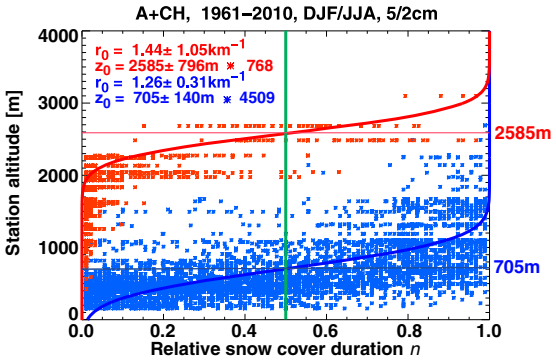

Fig. 6 Observed snow cover duration versus altitude. Data fitted with logistic model $P(z) = \Phi(\chi)$ with Φ = error function and $\chi = \sqrt{2\pi} r_0 (z - z_0)$. r_0 stands for the extreme slope of the fitted curve adopted at the abscissa value of $n = 0.5$ and the ordinate value of $z = z_0$. One *asterisk* represents one station season. Parameters shown in *inset*, *blue* for winter (mean temperature $T_{DJF} = 0.3$ °C), and *red* for summer ($T_{JJA} = 17.1$ °C)

3.8 Fitting algorithm

An innovative ingredient of this study is the numerical fitting procedure to obtain the parameter vector **Q** for the state function. In our recent work (papers I–III and also in Hantel and Maurer (2011)), we have followed the strategy to minimize the cost function defined as the mean quadratic difference between the observed snow duration and the model state function; the errors were estimated with the bootstrap method (Efron and Tibshirani (1998)). Limitation of this standard strategy is that the difference between the observed snow duration and the model state curve is not normally distributed.

When the observations become rectified with the inverse state function, however, these rectified observations can then be modeled with the rectified state function which boils down to a linear regression problem; the corresponding distribution of the eventual residuals of the response variable should be automatically normal (not demonstrated here but we have checked that). A comprehensive description of the so-called *generalized linear models* can be found in Fahrmeir and Tutz (2001). The formal details of our present approach are summarized in Appendix 1. The results are not significantly different compared with our earlier results. The main progress of the new linear fitting procedure (as we call it, compared to our previous nonlinear procedure) is that we now have normally distributed "observations." This implies that the bootstrap method will not be required anymore; instead, the error estimate is available from the regression formulae. Further, we get a theoretically sound estimate of the explained variance. These estimates (see below) are consistently 50 % and better which, in light of the amount of data (3,463 in winter and 447 in summer), make our subsequent results highly significant.

4 Naive statistics

We begin with some preliminary evaluations of the processed data; the correlation criterion is not yet applied and the model equations for τ and N are not used. Rather, we apply standard statistical measures in order to obtain background parameters as a basis for later verification. For this purpose, we run, with the processed data vector $\{n(\theta, x^{**}, y^{**}, z^{**}), T(\theta), x^{**}, y^{**}, z^{**}\}$ just introduced, a couple of preliminary ("naive") evaluations.

4.1 Snow duration versus altitude

Figure 6 shows the simplest approach to obtain the snow lines: Plot the observed snow cover duration n versus altitude z in all years for the entire period, irrespective of the horizontal coordinates x and y. Fit the data with a pertinent model and obtain every desired snow line. The fit curve $P(z)$ for n must not be linear since n is the mean of the binary stochastic variable ν. For variables of this type, a *logistic curve* is the proper fitting function (Hosmer and Lemeshow (2000)). Out of the class of logistic curves (Mazumdar (1999)), we take

here the error function.[3] This type of plot requires only snow and altitude data, no temperature. It is identical to the original snowline determination of Hantel and Maurer (2011) (Fig. 2).

Also drawn in Fig. 6 are the median snow lines for the extreme seasons. The altitude H is equal to the reference parameter z_0 of the interpolating error function (see legend of Fig. 6). z_0 represents the altitude of the extreme slope of the fitting curve. We find 705 m in winter and 2,585 m in summer. This allows to calculate the ratio

$$\frac{\Delta H}{\Delta T} = \frac{2,585\text{m} - 705\text{m}}{17.1°\text{C} - 0.3°\text{C}} = 112\,\frac{\text{m}}{°\text{C}}. \tag{12}$$

This is the simplest approach to obtain an estimate of the temperature sensitivity of the snow lines. It may be compared with the result 166(±5)m/°C which we will find below from the complete model evaluation.

4.2 Snow duration versus temperature

The next obvious naive diagram (not shown in this paper) is to plot n against temperature, either for *station* temperature t (Fig. 1 of paper III) or for *European* temperature T (Fig. 4 of paper I). Note, however, that n values from different climate stations can be lumped together into the same n, t plot but not into the same n, T plot because n, T plots are generally different for different climate stations.

On the other hand, t and T are linearly correlated for different climate stations with about the same slope (Fig. 6 of paper III). This is the reason why t can be replaced in our model through the mountain temperature.

4.3 Distribution of n-trend estimates

Figure 7 shows the simplest approach to obtain an estimate of the time trend of the snow duration. Following the method of pairwise slopes (Dery et al. (2005) as done in Gottfried et al. (2011)), we use all possible time trend estimates in the vicinity of the median snow line to get the pdf of the trend of the median snow duration. There is a faint indication of a negative trend (i.e., −3.3 %/10 years, equivalent to a reduction of 3 days of snow cover duration per 10 years, both for winter and summer), as expected from global warming. However, the trend in Fig. 7 over the 50 years 1961–2010 is largely insignificant, in both seasons. Note that all processed station seasons have been used for the pdf.

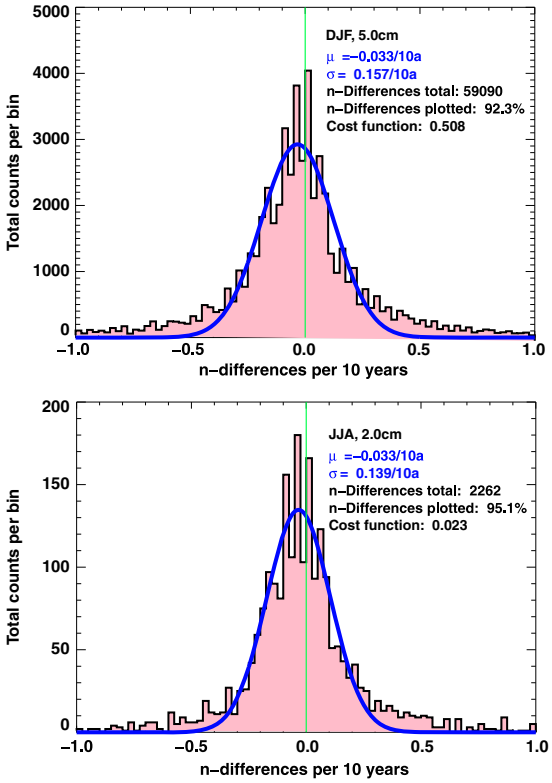

Fig. 7 Frequency distribution of trend estimates implicit in observed time series of snow duration. Data assembled in bins of width 0.025/10 years. Total number of n differences is proportional to area of the curve. Median μ and standard deviation σ of Gaussian given in *inset*. Individual trend data taken from altitude interval $H \pm D/2$. Data from processed Austrian and Swiss climate stations, winters and summers 1961–2010. *Abscissa* drawn is restricted to interval ±1/10 years; therefore, somewhat less than 100 % of n differences available are plotted

5 Snowline climate of the Alps 1961–2010

The snowline climate of the Alps is eventually condensed into the state function $N(\tau)$ of snow duration. The state function boils down the Alpine-wide 1961–2010 snow duration information from 3,463 station win-

[3] Choice of the error function has been convenient in our programming but is not mandatory here. Since we do not yet apply our model of Fig. 6, one could take other logistic functions for the interpolation as well; the altitudes of the snow lines would then become dependent upon the logistic function chosen.

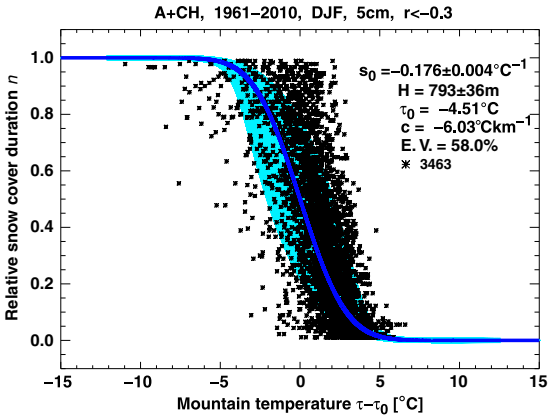

Fig. 8 Winter snow duration n at 91 Austrian and Swiss climate stations plotted versus mountain temperature. *Thick curve* $N(\tau)$ is the state function of n. Each *asterisk* represents one out of 3,463 station winters. *Colored shading* captures 68 % of data points (corresponding to one standard deviation in τ direction). Selected parameters are shown in the *inset* (*E.V.*, explained variance)

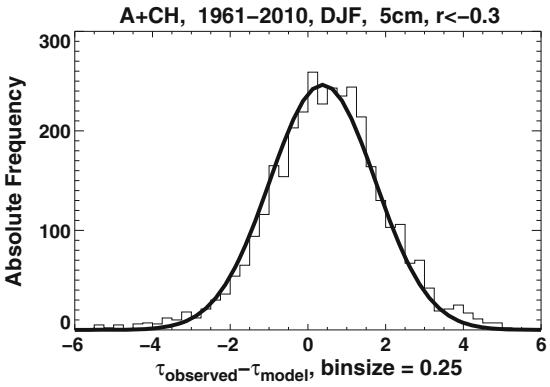

Fig. 9 Frequency distribution of deviations between observed mountain temperature and modeled mountain temperature τ in Fig. 8. Histogram fitted with normal distribution. Abscissa of maximum = 0.38

ters (447 station summers) into one parameter vector that consists of just five numbers for each season. This data reduction is the essential added value of the present snowline model.

5.1 State functions of snow duration for winters and summers in 1961–2010

Figure 8 shows $N(\tau)$ for winter; the corresponding parameters are listed in the second column of Table 3. They reproduce, by and large, the parameters[4] of the all-Alps state curve as obtained for the shorter period 1961–2000 (Figs. 6 and 8 of Hantel and Maurer (2011)). For example, we find for the snow duration sensitivity $s_0 = -0.18(\pm\ 0.004)\ ^\circ\mathrm{C}^{-1}$ while Hantel and Maurer (2011) reported $s_0 = -0.17(\pm 0.01)\ ^\circ\mathrm{C}^{-1}$. In light of the different data and the different evaluation procedure, this must be considered a robust result.

The scatter of the data in Fig. 8 should be Gaussian in τ direction since observed temperature fluctuations are about normally distributed. Figure 9 demonstrates that the pdf is indeed normal. Main reason for this desirable result is that we have excluded the snow duration data which violate the correlation criteria; including these would destroy the normality of the pdf in Fig. 9 (not demonstrated here). The observed and modeled mountain temperatures in Fig. 9 are defined as

$$\tau_{\mathrm{obs,i}} = T_i + a x_i + b\, y_i + c z_i; \qquad \tau_{\mathrm{mod,i}} = N^{-1}(n_i). \tag{13}$$

The input data $(n_i, T_i, x_i, y_i, z_i)$ are valid for one specific station season (index i); the components of the parameter vector $\mathbf{Q}$ implicit in τ_{obs} and in N^{-1} are from the fit for winter. Note that the normality of Fig. 9 is achieved without station temperature information; further, it is not enforced by the fitting routine.

The latter result may be summarized by saying that the snow duration preserves the information of local temperature. This is supported by the parameter c which represents the vertical lapse rate of temperature. The estimates for c in Table 3 come close to the observed mean value ($c = -6.5\ ^\circ$C/km in the standard atmosphere; see, e.g., Reuter et al. (2001), p. 166). The parameter $-1/c$ in Table 3 is given by the formula in Eq. (9) which shows the temperature sensitivity of the altitude of the snow lines (not just of the median snow line but of all snow lines). Its value in winter in Table 3, second column, is 166 m/°C. This result compares favorably with the estimate of 150 m/°C reported by Beniston (2010) and also compared with the preliminary estimate of 112 m/°C, which we have found in Fig. 6 according to Eq. (12).

The first three columns of Table 3 allow to compare the impact of the threshold in winter. Using the 3σ criterion for significance, the difference between the para-

[4] All error estimates in this paper are given as one standard deviation.

The snowline climate of the Alps 1961–2010

Table 3 Parameters of snow duration state function, period 1961–2010, A + CH, selected input data

	DJF 2 cm	DJF 5 cm	DJF 10 cm	JJA 2 cm
s_0 (°C^{-1})	−0.18 (± 0.004)	−0.18 (±0.004)	−0.14 (±0.005)	−0.08 (±0.01)
τ_0 (°C)	−3.72 (±0.12)	−4.51 (±0.14)	−6.96 (±0.27)	−7.96 (±2.65)
a (°C/°lon)	−0.22 (±0.01)	−0.21 (±0.01)	−0.28 (±0.02)	0.65 (±0.12)
b (°C/°lat)	−0.24 (±0.06)	0.01 (±0.07)	0.13 (±0.09)	−3.61 (±0.61)
c (°C/km)	−6.10 (±0.18)	−6.03 (±0.19)	−7.43 (±0.30)	−8.14 (±1.2)
D (m)	865 (±32)	887 (±36)	913 (±49)	1,472 (±299)
H (m)	654 (±28)	793 (±36)	974 (±55)	3,083 (±1121)
$-1/c$ (m/°C)	164 (±5)	166 (±5)	135 (±6)	123 (±18)
E.V. (%)	61	58	52	50

First three columns for winter (three different thresholds of snow depth), last column for summer. First five parameters: components of parameter vector **Q**, defined in the last point of Section 3.7. For definition of D and H, see Eqs. 7 and 8
E.V. explained variance of linear parameter fit

meters of the first two columns is not significant. Thus, our estimates of the temperature sensitivity (parameter s_0) and of the median snowline altitude (parameter H) appear to be robust; this has earlier been demonstrated for the threshold interval 1–4 cm of summer (see Table S5 of the supplementary data of Gottfried et al. (2011)).

Our quantities D and H for summer (fourth column of Table 3) can be compared with Gottfried et al. (2011) (Fig. 5, second column). The present estimates are not significantly different from their estimates (they find $D = 992$ m, $H = 2.897$ m).

This brings us to Fig. 10 which shows the state function of snow duration for summer.[5] Since the data situation for summer is considerably poorer than for winter (only about a tenth of station seasons were available, the position of observed data was below the median snow line), the parameters are considerably less accurate. This is also seen in Fig. 11. The deviation of the mountain temperature from the fitted curve has an approximate Gaussian profile indeed but gets shifted to the right of zero. This effect must be attributed to a systematic bias towards warm temperatures in Fig. 10 due to climate stations at low (and consequently relatively warm) altitudes with comparatively long snow duration caused by winter snow which still has not melted. This systematic effect is virtually absent in winter.

[5]The shading in Figs. 8, 10 is constructed as follows: For an arbitrary n the width of the shading in τ-direction is made proportional to $(1 - n)n$ which is the theoretical variance of a Bernoulli-distributed quantity like the snow cover duration. The factor of proportionality is chosen such that 68 % of all data points fall into the shaded area.

5.2 Snowline surfaces for winters and summers in 1961–2010

The altitude of a snow line n has been defined above in the formula in Eq. 8. The corresponding mountain temperature is specified through the inverse of the state function as $\tau(n) = N^{-1}(n)$. For example, for $n = 0.5$, the fitted N from Fig. 8 yields $\tau = \tau_0 = -4.51$ °C. The snow line altitude $H(x, y)$ according to Eq. 8 is *a planar surface that penetrates across the orography of the Alps*; the snow line is generated by the cut between the surface and the orography. Physically, the function $H(x, y)$ is an isothermal surface defined by constant τ.

Shown in Fig. 12 is the median snow line of winter. It is similar to the winter snowline pattern as published recently by Hantel and Maurer (2011). The difference

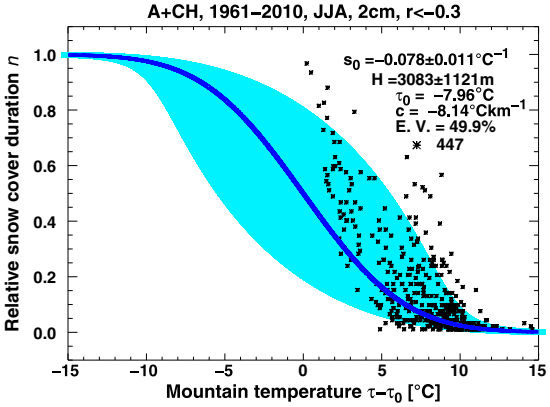

Fig. 10 As Fig. 8, but for summer (15 Austrian and Swiss climate stations, 447 station summers)

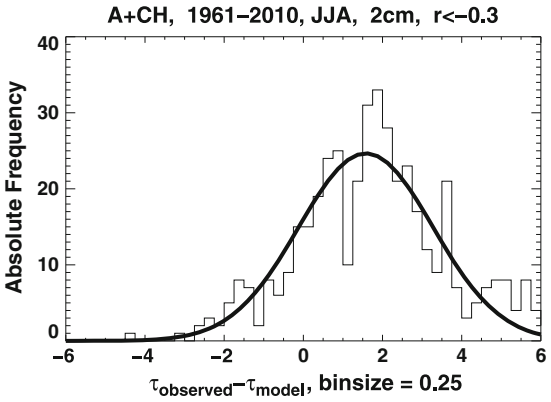

Fig. 11 Frequency distribution of deviations between observed mountain temperature and modeled mountain temperature τ in Fig. 10. Histogram fitted with normal distribution. Abscissa of maximum = 1.58

is the database (all Alps 1961–2000 originally, A + CH 1961–2010 here). The mean altitude (793 m) is larger than before (641 m); the west–east slope (−35 m/° longitude) is smaller than before (−56 m/° longitude). In light of the error of the parameters, the present and the earlier estimates are not significantly different.

The snow lines for higher snow probabilities are located above the median snow line. For example, the altitude of the snow line 90 % is about 500 m higher than the median snow line (plot not reproduced). This quantifies the altitude difference for different snow lines.

Figure 13 shows the median snow line for summer. Its mean altitude of 3,083 m indicates that snow cover probability in summer is restricted to the highest summits. This result, well in accord with general experience, may be useful for ecological purposes (Gottfried et al. (2011), their estimate of the median snow line altitude is 2,897 m). Since the database in summer is considerably smaller than in winter, the parameters of the snow line in summer have a limited significance.

While Fig. 12 represents the mean winter snowline conditions in the Alps for the period 1961–2010, we can also ask for the mean position in individual years, simply by picking the actual T in the mountain temperature for the specific year. In warm winters, the snowline surface rises; in cold winters, it sinks. The cutting of the snowline surface (i.e., the plane marked by the red boundary) across the topography of the Alps (i.e., the white circumference) generates a corresponding change of the snow-covered surface from year to year (i.e., the gray surface in Figs. 12 and 13). The time series of this area is drawn in Fig. 14 through implementing T of the actual year into Eq. 8. For example, the cold winter in 1963 showed about 2.4 times the mean area above the median snowline surface. Conversely, the warm winter in 2007 showed just 55 % of the mean area of 133,500 km^2.

6 Extension into individual valleys

With due caution, the snow lines can be used to illustrate the snow cover situation of individual Alpine

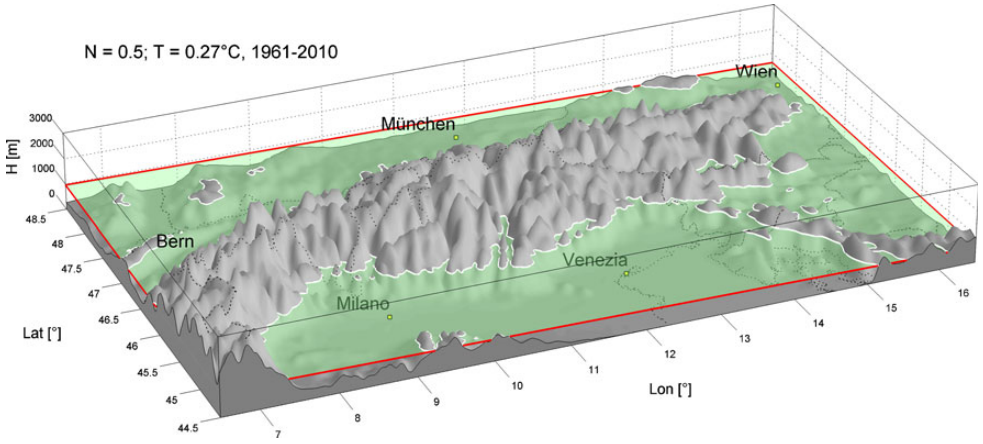

Fig. 12 Winter snow line 50 %, mean altitude 793 m. Drawn (*red circumference*) is planar surface $H(0.5, T, \lambda, \varphi)$ according to the formula in Eq. 8 for fixed $\tau = N^{-1}(0.5) = \tau_0 = -4.51$°C and fixed European temperature $T = 0.27$ °C. The median snow line (*white circumference*) is intersection with orography

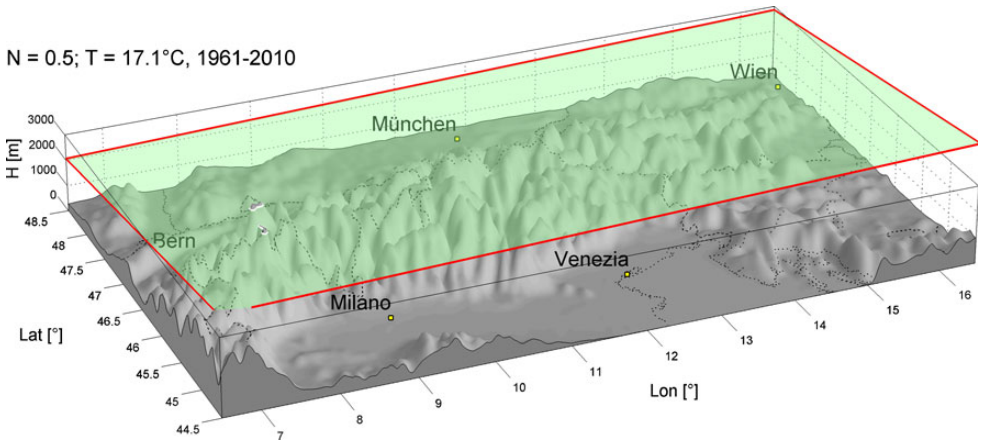

Fig. 13 Summer snow line 50 %, mean altitude 3,083 m. $\tau_0 = -7.96$ °C, $T = 17.1$ °C

valleys. Figure 15 demonstrates how the Alpine mean snow lines in 1961–2010 cut across the mountains around the climate station Innsbruck. The transition from snow probability 30 up to 95 % can be seen in the immediate vicinity of the climate station because the surrounding orography maps the snow lines over this large interval.

We would expect that the mean snowline surface, valid for the Alps, cannot possibly coincide with the actual snow situation in Innsbruck. In order to quantify the anticipated systematic and stochastic shift, we define the *equivalent altitude* H^* of Innsbruck. H^* is gained by projecting the relative snow duration n, measured in Innsbruck in each individual year, upon the state curve in Fig. 8; the emerging value of τ on the abscissa is then transformed into H^* through the formula in Eq. 8, plus using the coordinates x and y of Innsbruck and the European temperature T of the individual year. The values of H^* for individual years obtained in this manner are plotted in Fig. 16. The mean equivalent altitude is higher than the true altitude h of the station. This implies that the mean snow situation of Innsbruck is somewhat underestimated by our Alpine fit: The true snow cover at this station is such as if the station would be located 128 m higher. This is equivalently visible in the mean observed versus modeled snow cover duration in 1961–2010 in Innsbruck: $\overline{n} = 0.42$ versus $\overline{N} = 0.33$.

This difference is in accord with the accuracy of the parameters that specify the state function $N(\tau)$.

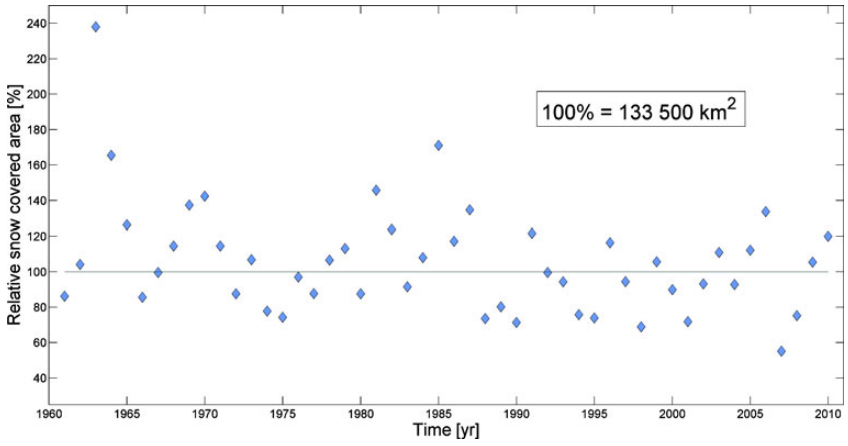

Fig. 14 Time series of area in the Alps that is at least 50 % snow covered (winters in 1961–2010). Area plotted as percentage of area that is located at or above the 50-year mean position of the median snow line (i.e., 133,500 km^2)

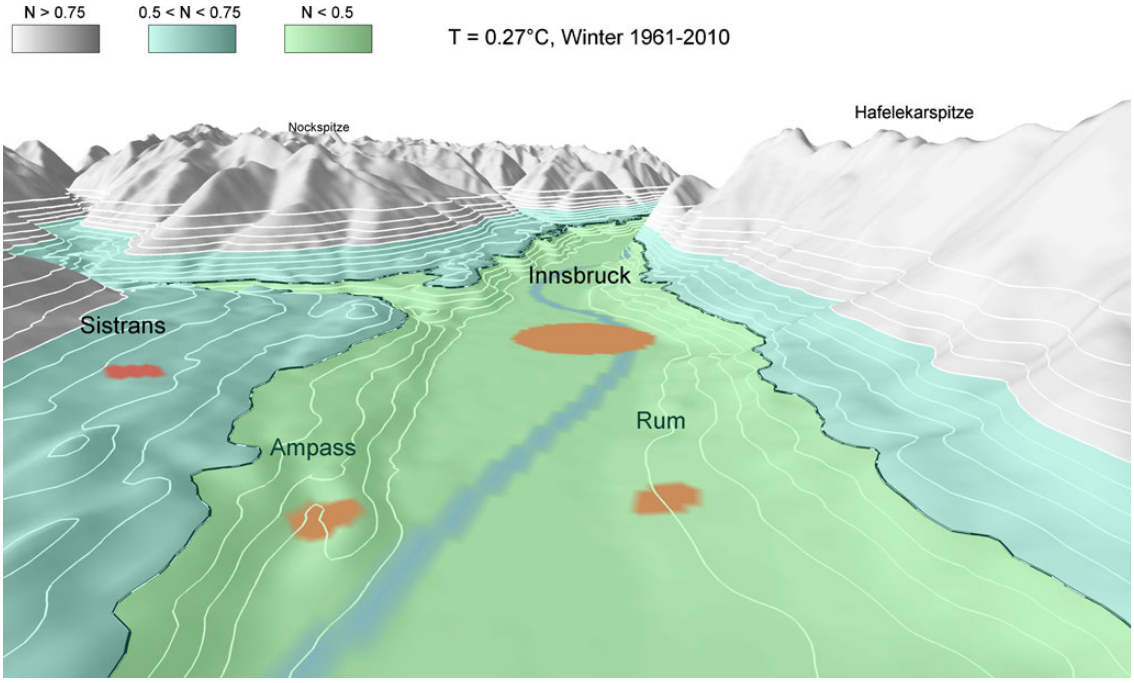

Fig. 15 View from the east towards climate station Innsbruck. Mean snow lines drawn from 30 % upward, increment 5 %, up to 95 %; median snow line (climate average in 1961–2010) in *black*

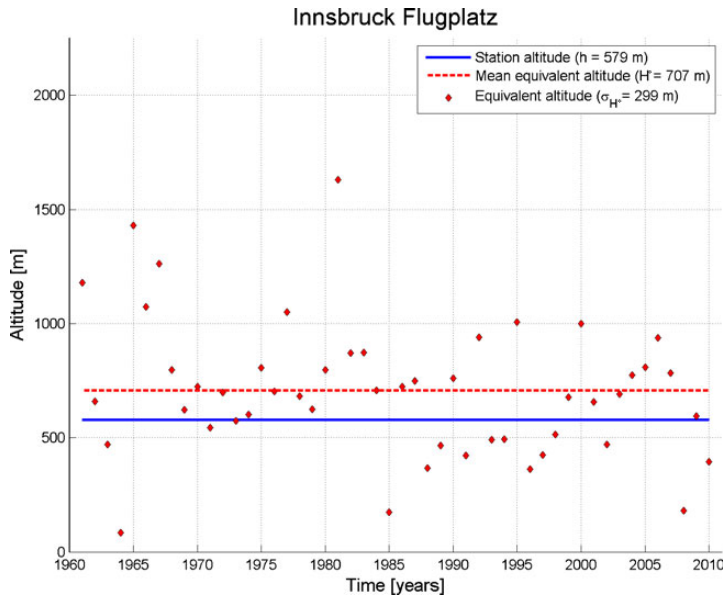

Fig. 16 Time series of equivalent altitude H^* for Innsbruck. For definition of H^*, see text

Other climate stations in our database have also been investigated. Ten of them have been selected. The small difference between H^* and h (last column in Table 4) indicates that the mean snow line altitude is quite well reproduced over the entire epoch in 1961–2010 for most of the selected stations. None of the differences is statistically significant; in other words, H^* and h are statistically equal. The sizeable scatter from year to year (as indicated by σ_{H^*}) demonstrates that only the climatological mean is acceptably reproduced by our evaluation whereas individual years may show appreciable deviation between implied and true station altitude.

7 Trend of snow lines

The climate epoch in 1961–2010 is characterized by climate warming which can also be found in the snow cover. The fact that the snowline climate of the Alps is externally controlled by the European temperature in our model allows to estimate trends of snow cover duration and of snowline altitude, provided that the time trend of the European temperature is specified externally.

We adopt here the trend $\mathrm{d}T/\mathrm{d}\theta = (0.30 \pm 0.17)°\mathrm{C/10a}$ of the CRU temperature for 1961–2010. The previous estimate for the winters of the 40-year period 1961–2000 used in Hantel and Maurer (2011) had been $\mathrm{d}T/\mathrm{d}\theta = (0.44 \pm 0.32)$ °C/10a; note the instability of these figures against changing the database. With the present trend estimate, using formulae Eqs. 10 and 11, we find for winter the following equations:

$$\frac{\partial N}{\partial \theta} = -0.054(\pm 0.031)/10\mathrm{a}; \qquad \frac{\partial H}{\partial \theta} = 50(\pm 28)\mathrm{m}/10\mathrm{a}. \tag{14}$$

The first figure is to be compared with the estimate $\Delta n/\Delta\theta = -(0.033 \pm 0.157)/10\mathrm{a}$ in Fig. 7; both are statistically equal. The estimate for the trend of N applies at the altitude of the median snow line, i.e., it is the extreme trend of N in the entire field; above and below the median snow line, it decreases gradually to zero, with half-width D. Conversely, the trend of H as represented by the second figure of Eq. 14 is valid for all snow lines from 0 to 1. It is directed upward but numerically weak. Equivalent calculations can be made with $\mathrm{d}T/\mathrm{d}\theta = (0.34 \pm 0.13)$ °C/10a for summer (adopt s_0 and c in Table 3) with about the same result.

Both estimates in Eq. 14 point into the expected direction: The *snowcover duration decreases* and the *snowline altitude increases* under the influence of global warming. However, the estimates are insignificant because the external temperature trend is insignificant.

A further trend, indirectly made visible by the snow lines, is the trend of the relative area above the median snow line adopted in individual years. It can be deduced from Fig. 14 and shows an insignificant decrease of $-7.0(\pm 4.1)$ %/10a.

Another application of our model would be to forecast the likely snow duration of the next season. Applications of that kind are principally possible with the output of present numerical weather prediction models but at present have a limited value due to the comparatively poor performance of seasonal temperature forecasts T for Europe. By specifying the desired snow line (e.g., the median snow line $n = 0.5$) and inserting it, together with the seasonal forecast of T, into formula Eq. 8, we would get the sloping surface $H(n, T, x, y)$ for the Alps in the season ahead.

8 Final remarks, conclusions, and outlook

The present study of the snowline climatology of the Alps has been based on the intuitive concept of the snow limit. This notion of snow research reaches

Table 4 Mean equivalent altitude H^* and corresponding standard deviation σ_{H^*} for selected stations

Station name	h (m)	λ (°)	φ (°)	r	H^* (m)	σ_{H^*} (m)	$H^* - h$ (m)
Wien-Hohe Warte	203	16.35	48.25	−0.75	295	253	92
Grono	382	9.15	46.25	−0.51	363	271	−19
Salzburg Airport	430	13.00	47.80	−0.80	493	202	63
Bregenz	436	9.75	47.50	−0.70	569	237	133
Neuchatel	487	6.95	47.00	−0.66	338	263	−149
Bad Ragaz	496	9.50	47.02	−0.60	650	249	154
Chur-Ems	555	9.53	46.87	−0.45	662	318	107
Innsbruck Airport	579	11.35	47.25	−0.54	707	299	128
Adelboden	1,320	7.57	46.50	−0.36	1510	432	190
La Dole	1,670	6.10	46.43	−0.41	1694	435	24
Villacher Alpe	2,140	13.67	46.60	−0.33	1666	296	−474

far into meteorology (Steinacker (1983)), hydrology (Bloeschl and Sivapalan (1995)), climatology in general (Hann (1883); Hann (1908)), mountain weather and climate (Barry (1992)), mountain biology and ecology (Körner (2003); Nagy and Grabherr (2009); Wipf et al. (2009)), and climate change (Karl and Trenberth (2003); Lemke et al. (2007); Clow (2010)), to name just a few fields.

Here, we have been interested in the length of time in a given season during which the snow on the ground exceeds a certain threshold. We have considered only the *state* component in the snow budget (i.e., the depth of the existing snow cover); this includes the tacit assumption that the measured snow cover is always in equilibrium with environmental temperature. Neither the *flux* component (i.e., the snow fall) nor the *source* component (the phase changes, i.e., the freezing/melting/evaporation processes at work in the snowpack) has been the subject of this study (for the terminology of state, flux, and source quantities in geophysical fluid budgets, see chapter 1 in the Landolt-Börnstein volume on the climate at the earth's surface (see Hantel (2005)). Thus, the present model is only applicable on time scales well above the daily scale.

We have introduced the notion of the *snow line* by connecting places at which the probability to encounter snow has a certain fixed value. The snow probability of a season can vary between 0 ("never snow") and 1 ("always snow"). This includes the snow limit as the special probability of 50 % for snow which constitutes the concept of the median snow line. Observational basis has been the daily snow depth data from the routine climate stations. Together with the mountain temperature, we have designed a model that compresses all quality-controlled seasonal snow probabilities (3,463 in winter, 447 in summer) into the state function $N(\tau)$ that is specified through just five Alpine-wide parameters. This is an enormous data reduction. Yet our model allows to derive from $N(\tau)$, through analytical means, various climatically relevant quantities. These include the temperature sensitivity of snow cover duration and snow line dynamics at all altitudes as well as the slope of the snow line surfaces in horizontal direction; further, they yield trend estimates.

Limitations of the present theory include the following:

- Snow amount is not necessarily correlated with snow cover duration. So one should be cautious in using the present results as implications that concern snow amount or snow height.
- The accumulation (snow fall) and ablation process (snow melt) is not explicitly included in the model. What we imply is that the corresponding growing and decaying phases cancel each other in a more or less stochastic way. This is a first approximation at best.
- The eventual Alpine-wide parameter vector $\mathbf{Q} = (\mathbf{s_0}, \tau_0, \mathbf{a}, \mathbf{b}, \mathbf{c})$ cannot possibly reproduce the snow duration characteristics at a local climate station. So one should be cautious in interpreting the present results locally.
- The key hypothesis of this study has been that the most influential quantity that controls the snow duration is the seasonal mean of temperature, averaged over Europe. While this applies quite well for the dynamics of the median snow line, the limits of this hypothesis should be kept in mind. One should be particularly cautious in interpreting our results in altitudes far off the altitude of the median snow line.

The notion of the snow probability is yet applicable on the local scale in the field as well as on the regional scale. It can be extended to land surface observations from satellite, as evidenced by satellite pictures which show the daily snow limit as a sharp line. For example, the MODIS satellite maps, on a worldwide scale, map the snow limit with a ground resolution of 4 km (which can be downscaled to below 1-km resolution; see also NOAA/NESDIS/OSDPD/SSD (2004)). A recent application is the study of Kaur et al. (2010) in the Indian Himalayas. These authors use satellite measurements of monthly snow cover; the snow limit is specified as the location that separates snow-covered from snow-free areas.

This concept is also used by Parajka et al. (2010) who successfully try to estimate snow cover from MODIS satellite data during cloud cover. They introduce a regional snowline method to distinguish between land pixels and snow pixels and find, for example, the altitude of the snow line on 23 January 2003 at about 900 m (subjectively estimated from Fig. 3); this is 100 m above our 50-year winter average of the median snow line.

Satellite time series of the snow limit and of snow probability at the ground, up to now, are still too short for climate studies of several decades. It is for this reason that we have restricted the present 50-year study to station data input. However, remote observations from satellite have the potential to yield a completely uniform and homogeneous observational background. Thus, in the long run, snow and snowline quantities will presumably be studied on basis of remote satellite observations.

Acknowledgements Discussions with many colleagues (notably Roger Barry, Michael Gottfried, Georg Grabherr, Vanda Grubisic, Leopold Haimberger, Michael Kuhn, Christian Schönwiese, Peter Speth, Reinhold Steinacker) helped to clear the snowline concept. The Austrian Academy of Sciences has supported

The snowline climate of the Alps 1961–2010

Table 5 Specifications of the nonlinear and the linear fit for the two different estimates $\mathbf{Q}'$ and $\mathbf{Q}$ of the parameter vector

	Nonlinear fit	Linear fit
Measured snow duration	n_i	$\eta_i = \Phi^{-1}(n_i)$
Variance	$\sigma_{n_i}^2 = M(1-n_i)n_i$	$\sigma_{\eta_i}^2 = 2\pi M(1-n_i)n_i \exp(\eta_i^2)$
Predictor	$\tau_i \to \chi_i \to \Phi(\chi_i) = \Phi_i$	$\tau_i \to \chi(\tau_i) = \chi_i$
Predictand	$n^i = \Phi_i$	$\eta^i = \chi_i$
Cost function $J(s_0,\tau_0,a,b,c)$	$\sum_{i=1}^{i=I} \left(\frac{n_i - n^i}{\sigma_{n_i}}\right)^2$	$\sum_{i=1}^{i=I} \left(\frac{\eta_i - \eta^i}{\sigma_{\eta_i}}\right)^2$
Resulting parameter vector	$\mathbf{Q}'=(s_0',\tau_0',a',b',c')$	$\mathbf{Q}=(s_0,\tau_0,a,b,c)$

this research over the years in the Clean Air Commission and in the National Committee for the IGBP. The University of Vienna has funded the investigations through its Research Platform Program. Further, the Austrian Science Fund (FWF) has financially supported the study (Project P21335).

Appendix 1—Generalized linear model

The estimate of the parameter vector $\mathbf{Q}=(s_0, \tau_0, a, b, c)$ for the state function N rests upon the selected data vector $\mathbf{D_i}=\{n_i, T_i, x_i, y_i, z_i\}$. The fitting algorithm of our model uses the function Φ as defined in Eq. 2. It constitutes a relationship between n and χ as defined in Eq. 5; χ is a linear transformation of the mountain temperature, Eq. 4. We repeat here the corresponding formulae for convenience:

$$\Phi(\chi) = \frac{1}{\sqrt{2\pi}} \int_{\vartheta=-\infty}^{\chi} e^{-\vartheta^2/2} \mathrm{d}\vartheta; \quad \chi = \sqrt{2\pi} s_0(\tau - \tau_0);$$

$$\tau = T + ax + by + cz. \tag{15}$$

Our theory consists in modeling the predictand n with the multivariate predictor τ which again is calculated from the measured (T, x, y, z). The measured n can be used in two different modes:

Observed snow duration: n_i;

transformed snow duration: $\eta_i = \Phi^{-1}(n_i)$. (16)

Both n_i and η_i represent the same observed snow duration, but both constitute different fitting modes: The *nonlinear mode* and the *linear mode*. Before discussing these, we consider the a priori error of n_i. Since the snow duration is Bernoulli distributed, the variance of n_i is

$$\sigma_{n_i}^2 = M(1-n_i)n_i, \tag{17}$$

as noted in paper I; M is a normalization constant. The variance of the transformed snow duration η_i is then

$$\sigma_{\eta_i}^2 = 2\pi M(1-n_i)n_i \exp(\eta_i^2). \tag{18}$$

This relation follows from the slope of Φ along with Eq. 17. The nonlinear fit (see Table 5) yields the parameter vector $\mathbf{Q}'$ through minimizing the cost function based on the observed n_i; the linear fit yields the parameter vector $\mathbf{Q}$ through minimizing the cost function based on the transformed η_i.

Both estimates $\mathbf{Q}'$ and $\mathbf{Q}$ are principally different. Which one is better? In our previous work, we have used the standard estimate $\mathbf{Q}'$. In the present study, we have switched to $\mathbf{Q}$. The linear fit has a considerably improved theoretical founding. Since the Gaussian error function Φ belongs to the family of responses with *exponential probability density functions*, the concept of generalized linear models is applicable as described by Fahrmeir and Tutz (2001). Fitting observations to functions of this type requires to rectify the originally measured data with the inverse of the pertinent model function (in our case, Φ^{-1}) and to fit the rectified data in the familiar framework of a linear (in our case multilinear) regression model. The ultimate reason for the superiority of the fit in the rectified mode is that the data distribution in this mode is normal while in the nonlinear mode it is not; thus, the maximum likelihood principle necessary for the eventual inference of the parameter vector applies only in the rectified mode.

The differences between $\mathbf{Q}'$ and $\mathbf{Q}$ are yet below the significance level (compare fourth column of Table 1 with second column of Table 3). All evaluations reported in the present study have been done with the linear fit.[6] $\mathbf{Q}$ is then used for the plots of the state function $N(\tau)$ for both seasons (Figs. 8 and 10).

[6] Except the evaluations in Table 1 and in Fig. 6—these have still been made with the nonlinear fit.

Appendix 2—List of stations

Table 6 Austrian and Swiss climate stations used in this study

Station name	Altitude (m)	Longitude (°)	Latitude (°)	r_{DJF}	N_{DJF}	r_{JJA}	N_{JJA}
Hohenau	155	16.90	48.62	**−0.58**	43	NA	0
Eisenstadt	159	16.55	47.85	**−0.47**	43	NA	0
Schwechat	184	16.57	48.10	**−0.66**	41	NA	0
Laa an der Thaya	187	16.38	48.72	**−0.65**	43	NA	0
Wien-Hohe Warte	203	16.35	48.25	**−0.75**	46	NA	0
Krems	223	15.60	48.42	**−0.49**	42	NA	0
Mariabrunn	226	16.23	48.20	**−0.82**	31	NA	0
Retz	256	15.95	48.75	**−0.56**	37	NA	0
Lugano	273	8.97	46.00	−0.12	31	NA	0
Sankt Pölten	277	15.62	48.20	**−0.75**	42	NA	0
Hörsching	298	14.18	48.23	**−0.74**	47	NA	0
Rheinfelden	300	7.80	47.18	**−0.60**	35	NA	0
Bad Gleichenberg	303	15.90	46.87	**−0.67**	36	NA	0
Basel-Binningen	316	7.58	47.55	**−0.61**	39	NA	0
Graz Flughafen	340	15.43	46.98	**−0.62**	46	NA	0
Reichersberg	350	13.37	48.33	**−0.69**	44	NA	0
Graz Universität	366	15.45	47.07	**−0.63**	45	NA	0
Gleisdorf	375	15.70	47.10	**−0.59**	48	NA	0
Grossraming	379	14.52	47.88	**−0.72**	41	NA	0
Locarno-Monti	379	8.78	46.17	−0.19	40	NA	0
Grono	382	9.15	46.25	**−0.51**	41	NA	0
Kremsmünster	383	14.13	48.05	**−0.72**	46	NA	0
Lobming	400	15.18	47.05	**−0.61**	47	NA	0
Wörtberg	400	16.10	47.22	**−0.66**	45	NA	0
Montreux-Clarens	405	6.90	46.45	**−0.68**	35	NA	0
Delmont	415	7.35	47.37	**−0.67**	42	NA	0
Oberleis	420	16.37	48.55	**−0.48**	35	NA	0
Geneve-Cointrin	420	6.12	46.25	**−0.65**	37	NA	0
Salzburg Flughafen	430	13.00	47.80	**−0.80**	47	NA	0
Zuerich Flughafen	431	8.53	47.48	**−0.62**	35	NA	0
Hallau	432	8.47	47.70	**−0.42**	37	NA	0
Biel	433	7.25	47.12	**−0.73**	44	NA	1
Changins sur Nyon	435	6.23	46.40	−0.27	14	NA	0
Bregenz	436	9.75	47.50	**−0.70**	48	NA	0
Schaffhausen-Ch-Fels	437	8.62	47.68	**−0.62**	32	NA	0
Guettingen	438	9.28	47.60	**−0.37**	23	NA	0
Feldkirch	440	9.60	47.27	**−0.74**	48	NA	0
Klagenfurt	447	14.33	46.65	**−0.34**	39	NA	0
Altdorf	451	8.63	46.87	**−0.68**	46	NA	0
Luzern	456	8.30	47.03	**−0.67**	45	NA	0
Bad Ischl	469	13.63	47.72	**−0.59**	39	NA	0
Altstaetten	473	9.53	47.38	**−0.74**	45	NA	0
Oeschberg	482	7.62	47.13	**−0.75**	40	NA	0
Sion-Aerodrom	483	7.33	46.22	**−0.42**	27	NA	0
Reichenau	486	15.83	47.70	**−0.67**	49	NA	0
Neuchatel	487	6.95	47.00	**−0.66**	41	NA	0
Bruck an der Mur	489	15.27	47.42	**−0.64**	49	NA	0
Mondsee	491	13.37	47.85	**−0.74**	49	NA	0
Kufstein	492	12.17	47.57	**−0.54**	38	NA	0
Hieflau	492	14.75	47.60	−0.28	38	NA	0
Bad Ragaz	496	9.50	47.02	**−0.60**	49	NA	0
Sankt Michael Bleiburg	500	12.35	46.92	**−0.54**	26	NA	0
Stift Zwettel	505	15.20	48.62	**−0.64**	46	NA	0

The snowline climate of the Alps 1961–2010

Table 6 (continued)

Station name	Altitude (m)	Longitude (°)	Latitude (°)	r_{DJF}	N_{DJF}	r_{JJA}	N_{JJA}
Glarus	515	9.07	47.05	**−0.57**	36	NA	0
Jenbach	530	11.75	47.38	**−0.54**	37	NA	0
Taenikon	536	8.90	47.48	**−0.70**	35	NA	0
Sion	542	7.37	46.23	−0.24	17	NA	0
Freistadt	548	14.50	48.50	**−0.55**	47	NA	0
Chur-Ems	555	9.53	46.87	**−0.45**	48	NA	0
Bern-Liebefeld	570	7.42	46.93	**−0.48**	44	NA	0
Interlaken	574	7.87	46.68	**−0.59**	35	NA	1
Comprovasco	575	8.93	46.87	**−0.44**	32	NA	0
Innsbruck Universität	577	11.38	47.25	**−0.53**	49	NA	0
Innsbruck Flugplatz	579	11.35	47.25	**−0.54**	49	NA	0
Pabneukirchen	595	14.82	48.32	**−0.66**	45	NA	0
Meiringen	595	8.18	46.73	**−0.47**	47	NA	1
Kolbnitz	603	13.30	46.87	**−0.42**	31	NA	0
Ebnat-Kappel	623	9.12	47.28	**−0.72**	42	NA	0
Fribourg	634	7.12	46.77	**−0.57**	41	NA	0
Mayrhofen	643	11.85	47.15	**−0.53**	41	NA	0
Reisach	646	13.15	46.63	**−0.44**	25	NA	0
Schiers	651	9.68	46.98	−0.15	19	NA	0
Lienz	668	12.78	46.82	**−0.57**	33	NA	0
Zeltweg	669	14.78	47.20	**−0.32**	41	NA	0
Bad Aussee	675	13.78	47.62	−0.24	35	NA	0
Mürzzuschlag	700	15.68	47.60	**−0.34**	43	NA	0
Irdning	702	14.10	47.50	−0.20	43	NA	0
Haidenhaus	702	9.02	47.65	**−0.82**	38	NA	0
Kollerschlag	725	13.83	48.60	**−0.54**	46	NA	1
Fey	737	7.27	46.18	**0.21**	17	NA	0
Zell am See	755	12.78	47.30	−0.02	39	NA	0
Langau im Emmental	755	7.80	46.93	**−0.58**	48	NA	1
St. Gallen	779	9.40	47.43	**−0.80**	50	NA	1
Stein Appenzell Ausserrhoden	780	9.35	47.38	**−0.78**	31	NA	0
Heiden	800	9.53	47.43	**−0.71**	36	NA	1
Landeck	818	10.57	47.13	**−0.38**	47	NA	0
Schoppernau	835	10.02	47.30	−0.02	22	NA	6
Seckau	855	14.77	47.27	**−0.37**	34	NA	1
Reutte	870	10.75	47.50	**−0.54**	34	NA	1
Mariazell/Sankt Sebastian	875	15.30	47.78	−0.27	41	NA	0
Einsiedeln	910	8.75	47.13	**−0.42**	42	NA	1
Rauris	945	13.00	47.22	−0.05	34	**0.54**	3
Vaettis	957	9.43	46.92	−0.13	25	NA	0
Elm	965	9.18	46.93	**−0.41**	32	NA	3
Chateau d'Oex	985	7.15	46.48	−0.11	42	NA	1
Tamsweg	1,012	13.80	47.12	−0.15	40	NA	1
Engelberg	1,035	8.42	46.82	−0.27	27	**−0.94**	3
La Brevine	1,042	6.60	46.98	−0.29	25	NA	1
Preitenegg	1,055	14.92	46.93	**−0.32**	37	NA	0
Guttanen	1,055	8.30	46.65	−0.14	33	NA	6
Chaumont	1,073	6.98	47.05	**−0.46**	40	NA	0
Robbia/Poschiavo	1,078	10.07	46.35	−0.24	45	NA	0
Oberiberg	1,087	8.78	47.03	−0.08	14	**0.83**	3
Loibl	1,098	14.25	46.45	**−0.49**	28	NA	3
Holzgau	1,100	10.35	47.25	−0.14	23	NA	4
Bad Gastein	1,100	13.13	47.12	**0.04**	28	**0.93**	4
Disentis	1,190	8.85	46.70	−0.08	35	−0.18	7
Schröcken	1,263	10.08	47.25	−0.28	13	**0.22**	20
Scuol (Schuls)	1,295	10.28	46.80	−0.21	25	NA	5

Table 6 (continued)

Station name	Altitude (m)	Longitude (°)	Latitude (°)	r_{DJF}	N_{DJF}	r_{JJA}	N_{JJA}
Stolzalpe	1,305	14.20	47.12	−0.23	32	NA	0
Adelboden	1,320	7.57	46.50	**−0.36**	30	**0.12**	9
Reckingen	1,325	8.25	46.47	**0.71**	6	−0.06	5
Sankt Jakob im Defreggental	1,400	12.35	46.92	−0.27	15	NA	6
Schöckl	1,436	15.47	47.20	**−0.43**	20	NA	2
Andermatt	1,442	8.60	46.63	−0.03	7	−0.15	16
Montana	1,495	7.48	46.32	**0.04**	27	NA	4
Simplon Dorf	1,495	8.05	46.20	−0.17	26	**0.68**	3
Bosco-Gurin	1,505	8.50	46.32	−0.23	11	**−0.91**	3
Kanzelhöhe	1,526	13.90	46.67	−0.28	20	−0.18	6
Graechen	1,550	7.83	46.20	−0.23	23	−0.06	4
Galtür	1,583	10.18	46.97	**0.27**	11	**−0.33**	23
Davos	1,590	9.87	46.82	**0.08**	9	−0.13	27
Hinterrhein	1,611	9.18	46.52	**−0.38**	8	−0.08	14
Feuerkogel	1,618	13.73	47.82	−0.25	13	**−0.32**	23
Zermatt	1,638	7.75	46.03	−0.21	15	NA	3
Muerren	1,639	7.88	46.57	−0.24	15	**0.11**	23
San Bernardino Dorf	1,639	9.18	46.47	−0.27	13	NA	2
La Dole	1,670	6.10	46.43	**−0.41**	12	−0.04	7
Saas Almagell	1,673	7.95	46.10	**−0.54**	9	−0.27	6
Sils Maria	1,802	9.77	46.43	**−0.36**	6	−0.23	17
Arosa	1,840	9.68	46.78	**0.04**	5	**−0.41**	42
Obergurgel	1,938	11.02	46.87	**0.29**	4	**−0.46**	40
Buffalora	1,970	10.27	46.40	**0.86**	3	**−0.35**	22
Grimsel Hospiz	1,980	8.33	46.57	NA	2	**−0.49**	46
Mooserboden	2,036	12.72	47.15	−0.15	3	−0.29	42
Krippenstein	2,050	13.70	47.52	−0.00	3	**−0.40**	46
Villacher Alpe	2,140	13.67	46.60	**−0.33**	12	**−0.60**	43
Patscherkofel	2,247	11.45	47.20	**0.36**	13	**−0.42**	45
Ospizio Bernina	2,256	10.02	46.42	**−0.62**	3	**−0.38**	27
Guetsch ob Andermatt	2,280	8.62	46.65	NA	1	**−0.57**	32
Grand St. Bernhard	2,479	7.17	45.87	NA	0	NA	0
Saentis	2,490	9.35	47.25	NA	2	−0.20	48
Weissfluhjoch	2,690	9.80	46.83	NA	2	**−0.73**	48
Sonnblick	3,105	12.95	47.05	NA	0	**−0.99**	4
Jungfraujoch	3,580	7.98	46.55	NA	0	NA	0

Stations are ordered according to altitude. Color key: red (blue), stations that are excluded because they do not pass the weak (strong) correlation criterion (see also Fig. 3); black, stations entering the eventual data fit

r correlation coefficient between snow duration and European temperature, *N* number of processed station seasons, *NA* no processed data with nonzero variance available for this station in this season

References

Barry RG (1992) Mountain weather and climate. Routledge, London

Beniston M (1997) Variations of snow depth and duration in the Swiss Alps over the last 50 years: links to changes in large-scale climatic forcings. Clim Change 36:281–300

Beniston M (2010) Impacts of climatic change on water and associated economic activities in the Swiss Alps. J Hydrol 412–413:291–296

Bloeschl G, Sivapalan M (1995) Scale issues in hydrological modelling: a review. Hydrol Process 9:251–290

Brohan P, Kennedy JJ, Harris I, Tett SFB, Jones PD (2006) Uncertainty estimates in regional and global observed temperature changes: a new dataset from 1850. J Geophys Res 111:D12106

Bronstein IN, Semendjajew KA, Musiol G, Mühlig H (1999) Taschenbuch der Mathematik. Verlag Harri Deutsch

Clow DW (2010) Changes in the timing of snowmelt and streamflow in Colorado: a response to recent warming. J Clim 23:2293–2306

Dery SJ, Stieglitz M, McKenna EC, Wood EF (2005) Characteristics and trends of river discharge into Hudson, James, and Ungava Bays 1964-2000. J Clim 18:2540–57

Durand Y, Giraud G, Laternser M, Etchevers P, Merindol L, Lesaffre B (2009) Reanalysis of 47 years of climate in the French Alps (1958–2005): climatology and trends for snow cover. J Appl Meteorol Climatol 48:2487–2512

Efron B, Tibshirani RJ (1998) An introduction to the bootstrap. Chapman & Hall/CRC

Fahrmeir L, Tutz G (2001) Multivariate statistical modelling based on generalized linear models. 2nd edn. Springer Verlag New York, Berlin, Heidelberg

Fliri F (1992) Der Schnee in Nord- und Osttirol 1895-1991–Ein Graphik-Atlas, Band 1+2. Universitätsverlag Wagner, Innsbruck

Gottfried M, Hantel M, Maurer C, Toechterle R, Pauli H, Grabherr G (2011) Coincidence of the alpine-nival ecotone with the summer snowline. Environ Res Lett 6:12 pp. link: http://iopscienceioporg/1748-9326/6/1/014013/

Haiden T, Hantel M (1992) Klimamodelle: Mögliche Aussagen für Österreich, Österreichische Akademie der Wissenschaften, Wien, pp 2.1–2.14

Hann J (1883) Handbuch der Klimatologie. Verlag von J. Engelhorn, Stuttgart

Hann J (1908) Handbuch der Klimatologie. Band I Allgemeine Klimalehre. Bibliothek Geographischer Handbücher, N.F. Verlag von J. Engelhorn, Stuttgart

Hantel M (1992) The climate of seasonal snow cover duration in the Alps. Austrian Contributions to the IGBP—National Committee for the IGBP—Austrian Academy of Sciences I:13–15

Hantel M (2005) Observed global climate. Landolt-Börnstein, New Series, Volume V/6, Springer, Berlin

Hantel M, Hirtl-Wielke LM (2007) Sensitivity of Alpine snow cover to European temperature (paper III). Int J Climatol 27:1265–1275

Hantel M, Maurer C (2011) The median winter snowline in the Alps. Meteorol Z 20(3):267–276

Hantel M, Ehrendorfer M, Haslinger A (2000) Climate sensitivity of snow cover duration in Austria (paper I). Int J Climatol 20:615–640

Hermes K (1955) Die Lage der oberen Waldgrenze in den Gebirgen der Erde und ihr Abstand zur Schneegrenze. Kölner geogr. Arb. 5, Geogr. Inst., Univ. Köln

Hosmer DW, Lemeshow S (2000) Applied logistic regression. Wiley, New York

Karl TR, Trenberth KE (2003) Modern Global climate change. Science 302:1719–1723

Kaur R, Kulkarni AV, Chaudhary BS (2010) Using RESOURCESAT-1 data for determination of snow cover and snowline altitude, Baspa Basin, India. Ann Glaciol 51: 9–13

Körner C (2003) Alpine plant life—functional plant ecology of high mountain ecosystems. 2nd edn. Springer, Berlin

Laternser M, Schneebeli M (2003) Long-term snow climate trends of the Swiss Alps (1931–99). Int J Climatol 23:733–750

Lemke P, Ren J, Alley RB, Allison I, Carrasco J, Flato G, Fujii Y, Kaser G, Mote P, Thomas RH, Zhang T (2007) Observations: changes in snow, ice and frozen ground. Cambridge University Press, Cambridge

Louis H (1955) Schneegrenze und Schneegrenzbestimmung. Geographisches Taschenbuch 1954/55. Wiesbaden

Mazumdar J (1999) An introduction to mathematical physiology and biology. Cambridge University Press, Cambridge

Nagy L, Grabherr G (2009) The Biology of Alpine habitats. Oxford University Press, Oxford

NOAA/NESDIS/OSDPD/SSD (2004) IMS daily Northern hemisphere snow and ice analysis at 4 km and 24 km resolution. National Snow and Ice Data Center, Digital media, Boulder, CO

Parajka J, Pepe M, Rampini A, Rossi S, Blöschl G (2010) A regional snow-line method for estimating snow cover from modis during cloud cover. J Hydrol 381:203–212

Parker SP (1997) Dictionary of earth science. McGraw-Hill, New York

Reuter H, Hantel M, Steinacker R (2001) Meteorologie. Walter de Gruyter, Berlin, pp 131–310

Scherrer SC, Appenzeller C, Laternser M (2004) Trends in Swiss alpine snow days: the role of local- and large-scale climate variability. Geophys Res Lett 31:L13215

Steinacker R (1983) Diagnose und Prognose der Schneefallgrenze. Wetter und Leben 35:81–90

Wielke LM, Haimberger L, Hantel M (2004) Snow cover duration in Switzerland compared to Austria (paper II). Meteorol Z 13:13–17

Wielke LM, Haimberger L, Hantel M (2005) Corrigendum to 'snow cover duration in Switzerland compared to Austria'(paper II). Meteorol Z 14:857

Wipf S, Stoeckli V, Bebi P (2009) Winter climate change in alpine tundra: plant responses to changes in snow depth and snowmelt timing. Clim Change 94:105–121

Kapitel 7

Appendix: Theoretische Innovationen und Details

7.1 "Nonlinear", "Rectified" und "Extended" Fit

In ihrer ersten Arbeit zur Klimasensitivität der Schneebedeckung (in Österreich) stellten die Autoren HANTEL et al. (2000) drei verschiedene Möglichkeiten vor, eine nichtlineare Funktion (Tangens-Hyperbolicus) an die relativen Schneebedeckungswerte von 85 österreichischen Stationen (Datengrundlage 1961-1990) als Funktion der Temperatur anzupassen: Erstens, den "Nonlinear" Fit, zweitens den "Rectified" Fit und drittens den "Extended" Fit. Durch einen Vergleich zwischen beobachtetem und modelliertem Trend innerhalb der Auswerteperiode im Zuge der eben präsentierten Publikation von GOTTFRIED et al. (2011) wurde auf empiristischem Weg klar, dass die Anpassung bzw. die Kostenfunktion abgeändert werden muss.

Daher sollen das Verhalten und die Eigenschaften des "Extended" Fits näher beleuchtet werden, da er von den oben genannten Autoren als optimal beschrieben wird, da ein mit Sicherheit vorhandener Fehler zu gleichen Teilen den Größen "Schneebedeckung" und "Temperatur" zugeschrieben wird.

7.1.1 "Extended" Fit versus "Nonlinear" Fit

Die Kostenfunktion im Falle des "Extended" Fits (vgl. dazu Formeln 15-23 in HANTEL et al. (2000)) lässt sich wie folgt anschreiben:

$$\sum_{i=1}^{I}(f_i^2 + g_i^2) \equiv J_e(s_0, T_0) \quad \text{mit} \quad f_i \equiv \frac{n_i - n^i}{\sigma_i},\ g_i \equiv \frac{T_i - T^i}{\chi_i}. \tag{7.1}$$

Die Abweichungsquadratsumme bei insgesamt I Datenpunkten bestehend aus den einzelnen Abweichungsquadraten zwischen beobachtetem n_i und modelliertem n^i auf der einen und beobachtetem T_i und modelliertem T^i auf der anderen Seite muss dabei derart minimiert werden, sodass die Parameter s_0 und T_0 im statistischen Sinne optimal sind. Die Standardabweichun-

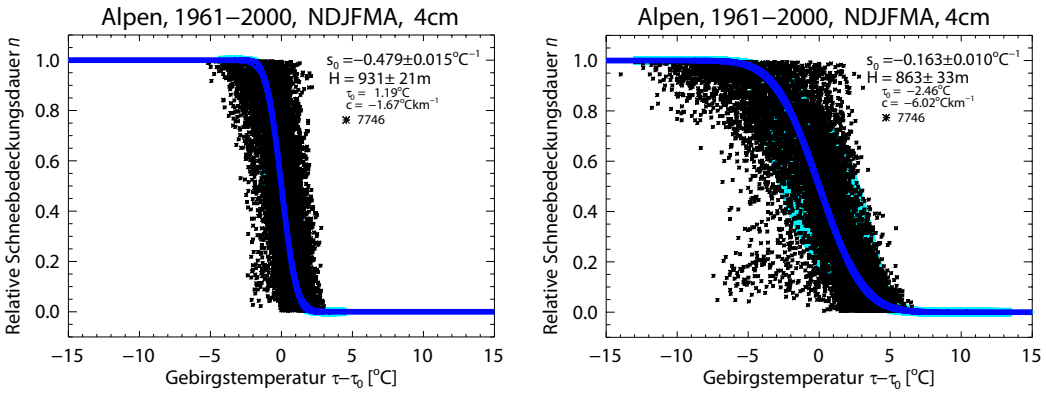

Abbildung 7.1: Extended (links) und Nonlinear (rechts) Fit im Vergleich. Datenbasis: Alpen, NDJFMA, 4cm, 1961-2000, kein Korrelationskriterium.

gen σ_i und χ_i ergeben sich gemäß HANTEL et al. (2000) aus dem Produkt zwischen einem Strukturterm (Index a) und einem Skalierungsterm (Index b):

$$\sigma_i = \sigma_i^{\mathrm{a}}\sigma^{\mathrm{b}}, \quad \chi_i = \chi_i^{\mathrm{a}}\chi^{\mathrm{b}}; \quad \sigma_i^{\mathrm{a}} = \sigma_0\left[4(1-n_i)n_i\right]^{1/2}, \quad \chi_i^{\mathrm{a}} = \chi_0. \tag{7.2}$$

Die Größen σ_0 und χ_0 ergeben sich im Fall des "Extended" Fits aus der Bedingung, dass die jeweilige Gewichtsumme gleich $\frac{1}{2}$ sein muss; das Profil von σ_i^{a} begründet sich aus der parabolischen Varianz einer Bernoulli- verteilten Größe (Details folgen später). Die Skalierungsterme sind nichts anderes als die entsprechenden Standardabweichungen der Stichproben.

Gemäß der Theorie von HANTEL and HIRTL-WIELKE (2007) darf die extreme Sensitivität s_0 nur von der mittleren Standardabweichung der Temperatur innerhalb der gerade betrachteten Saison (z.B. DJF) abhängen, nicht jedoch von jener innerhalb der Untersuchungsepoche (z.B. χ^b von 1961-2000). Damit steht die Kostenfunktion 7.1 *a priori* im Widerspruch zur Theorie, da nur bei unendlicher Standardabweichung innerhalb der Epoche der zweite Term der Kostenfunktion verschwindet und somit die Theorie erfüllt wird. Der Grenzfall des "Extended" Fits mit unendlicher Standardabweichung entspricht aber genau dem "Nonlinear" Fit, welcher nur einen Fehler in der Schneebedeckung berücksichtigt, die Temperatur hingegen als fehlerfrei annimmt. Dieses Konzept entspricht auch der natürlichen Empfindung, dass die Temperatur als unabhängige Variable die Schneebedeckung, also die abhängige Variable, steuert. Der "Extended" Fit in der vorliegenden Form wäre nur gerechtfertigt, wenn bei den zwei Variablen nicht klar ist, welche von beiden die unabhängige und welche die abhängige ist. Dass eine naive Betrachtung, die sich rein nach optischen Gesichtspunkten richtet, dem "Extended" Fit den Vorzug gibt, wird durch die Abbildung 7.1 illustriert.

Der "Extended" Fit zeichnet sich zwar durch eine deutlich geringere Streuung in der Datenpunktwolke aus (vgl. linkes und rechtes Bild in Abbildung 7.1), diese geringe Variabilität wird

aber durch die Minimierung der Temperaturabweichungsquadrate erzwungen. Die sich sofort aufwerfende Frage, wie sich die Datenpunktwolke in Richtung der Abszisse derart verändern kann, wird durch die Betrachtung einer zentralen Größe in der Auswertung, nämlich der *Mountain Temperature* bzw. *Gebirgstemperatur*, beantwortet, die gemäß HANTEL and HIRTL-WIELKE (2007); HANTEL and MAURER (2011); GOTTFRIED et al. (2011) und HANTEL et al. (2012) wie folgt definiert ist:

$$\tau = T + ax + by + cz \tag{7.3}$$

Das bedeutet aber, dass sich die τ- Werte bei festem T (Europatemperatur), x (Länge), y (Breite) und z (Höhe) je nach Anpassung und damit unterschiedlichen Werten für a, b und c verändern können.

Periode	$s_0[°C^{-1}]$	$c[°C/km]$	$a[°C/°lon]$	$b[°C/°lat]$	$\tau_0[°C]$	$\overline{n_H}$	$T_{CRU}[°C]$
1961-2000	-0.16	-6.02	-0.45	0.55	-2.46	0.556	2.74
1961-1990	-0.17	-6.08	-0.45	0.63	-2.45	0.565	2.54
1961-1980	-0.10	-10.93	-0.80	1.58	-5.74	0.605	2.52
1981-2000	-0.19	-4.82	-0.36	0.20	-1.63	0.505	2.93

Tabelle 7.1: Anpassungen für verschiedene Subperioden mit dem Nonlinear Fit. Datenbasis: NDJFMA, 4cm, kein Korrelationskriterium. $\overline{n_H}$: mittlere relative Schneebedeckungsdauer im Niveau $H_{1961-2000}$ der maximalen Empfindlichkeit (konkret $H\pm$ 50 m), T_{CRU}: Flächen- (5.5°-17.5°O / 43.5°-49.5°N) und Epochen- (1961-2000) Mittel der CRU-Temperatur.

Mit Hilfe von Tabelle 7.1 kommt man zu dem Resultat, dass der "Extended" Fit eine unrealistisch starke Steigung (s_0=-0.48 $°C^{-1}$) aufweist. Der "Nonlinear" Fit hat hingegen eine mit dem Trend über die Epoche 1961-2000 vereinbare Steigung (s_0=-0.16 $°C^{-1}$). Dies lässt sich gemäß der Formel 10 aus HANTEL et al. (2012) wie folgt zeigen:

$$\begin{aligned}\overline{n_{H,1961-1980}} = \overline{n_{H,1961-2000}} - s_{0,1961-2000}(T_{CRU,1961-2000} - T_{CRU,1961-1980}) = \\ = 0.556 - (-0.16°C^{-1})(2.74°C - 2.52°C) = 0.591\end{aligned} \tag{7.4}$$

$$\begin{aligned}\overline{n_{H,1981-2000}} = \overline{n_{H,1961-2000}} - s_{0,1961-2000}(T_{CRU,1961-2000} - T_{CRU,1981-2000}) = \\ 0.556 - (-0.16°C^{-1})(2.74°C - 2.93°C) = 0.523\end{aligned} \tag{7.5}$$

Man hat bei der Anwendung von Formel 10 prinzipiell zu beachten, dass diese eigentlich nur für infinit dezimale Änderungen $dT/d\theta$ gilt, da mit einer Temperaturzu(ab)nahme die Medianlinie

(und mit ihr das gaussische Sensitivitätsprofil) nach oben (unten) wandert, wodurch sich die Empfindlichkeit an der ursprünglichen Medianlinie laufend reduziert. s_0 hängt somit also von $\Delta T/\Delta\theta$ ab. Bei Temperaturänderungen von weniger als 1° (entspricht einer Höhenänderung der Medianlinie von rund 150m) ist der Fehler, den man durch das Ersetzen von $dT/d\theta$ durch $\Delta T/\Delta\theta$ macht, aber sehr gering. Die mittleren relativen Schneebedeckungsdauern im Niveau der maximalen Empfindlichkeit $\overline{n_H}$ der beiden Subperioden 1961-1980 (Gleichung 7.4) und 1981-2000 (Gleichung 7.5), 0.605 bzw. 0.505 aus Tabelle 7.1, lassen sich bei Kenntnis von $\overline{n_H}$ der Epoche 1961-2000 (=0.556) und s_0 eben dieser Auswerteperiode sowie der Differenz der CRU-Temperaturen der beiden Subperioden mit 0.591 und 0.523 annähern. Auch wenn diese Ergebnisse nicht perfekt sind, so ist doch deutlich, dass mit s_0 des "Extended" Fits wesentlich unrealistischere Trendabschätzungen erzielt würden. Ein noch ausgeklügelteres Verfahren zur Trendabschätzung, nämlich die Methode der "pairwise slopes", findet sich in den Arbeiten von GOTTFRIED et al. (2011) und HANTEL et al. (2012). Ein weiterer Aspekt von Tabelle 7.1 ist, dass für die Auswertung zumindest eine Klimanormalperiode (also 30 Jahre) verwendet werden sollte. Die Anpassung für die Epochen 1961-1990 und 1961-2000 sind im wesentlichen ident, wohingegen für die beiden Subperioden 1961-1980 und 1981-2000 deutlich andere Ergebnisse erzielt werden.

Eine wichtige Feststellung ist, dass die extreme Höhe, also dass Niveau größter Temperaturempfindlichkeit H (bei n=0.5), sich bei beiden Auswertungen kaum unterscheidet (931 m beim "Extended" Fit gegenüber 863 m beim "Nonlinear Fit" in Abbildung 7.1), also eine sehr robuste Größe ist. Wie man erwarten kann, liegt der Wert, bei vergleichbarem Threshold bezogen auf die DJF- Auswertung, im Winterhalbjahr (NDJFMA) etwas höher als im DJF (641 m, siehe HANTEL and MAURER (2011)).

Dass hier nun die Saison NDJFMA statt der für einen allfälligen Kunden wahrscheinlich relevanteren und in den vorherigen Publikationen analysierten Jahreszeit DJF betrachtet wird, hat den Grund, dass 1) bei dem niedrig gewählten Threshold (4cm) weniger Sättigungswerte n=1.0 als im DJF auftreten (mehr dazu später), 2) aufgrund der höheren Durchschnittstemperatur ein besserer Zusammenhang zwischen Temperatur und Schneebedeckung zu erwarten ist und 3) sich Niederschlagsanomalien, die die Beziehung zwischen Temperatur und Schneebedeckung stören könnten, über eine längere Periode eher ausgleichen. Somit sollte die Saison NDJFMA noch besser der Theorie entsprechen als die Saison DJF. Eine Analyse der Tabelle 7.2 bestätigt diese Annahme. Dazu wurde für die Prädiktoren x, y und z eine partielle Korrelationsrechnung im Hinblick auf ihre Wirkung auf den Prädiktanden n durchgeführt, die Korrelationen zwischen x und y (d.h. zwischen Länge und Breite), zwischen x und z (d.h. zwischen Länge und Höhe) und zwischen y und z (d.h. zwischen Breite und Höhe) berücksichtigt. Da die verwendete CRU-Temperatur T ein Mittel über eine nicht horizontale Fläche (Modelltopographie) ist, gibt es bei dieser Korrelation keine Abhängigkeiten mehr zwischen T einerseits und x, y und z andererseits. In der Saison NDJFMA erklärt die Höhe mit 52% den größten Anteil an der Varianz in der Schneebedeckungsdauer, was der natürlichen Empfindung entspricht. Die geographische Länge liegt mit 19% an zweiter Stelle, die geographische Breite und die großräumige Temperatur haben mit 5 bzw. 4% einen vergleichsweise geringen Einfluss. Im DJF reduziert sich die durch die Höhe erklärte Varianz in der Schneebedeckungsdauer um die Hälfte auf 27%, was

mit der natürlichen Wahrnehmung einhergeht, dass in der kältesten Zeit des Jahres weniger die vertikale Temperaturabnahme, sondern ebenso die Niederschlagsmenge eine bedeutendere Rolle spielt. Betrachtet man den Einfluss der großskaligen Temperatur in beiden soeben genannten Jahreszeiten (4 bzw. 7%), so erkennt man, dass deren Auswirkung auf die Schneedauer bei einer alpenweiten Auswertung nur gering ist, was auch die Ursache dafür sein dürfte, dass die Fitparameter relativ unabhängig von der Anwendung eines Korrelationskriteriums sind (siehe dazu auch den nächsten Absatz). Sowohl im NDJFMA als auch im DJF zeigt sich in etwa in gleicher Weise eine Zunahme der Schneebedeckungsdauer nach Osten (Kontinentalität des Klimas) und eine sehr schwache Abnahme nach Norden (Einwirkung des Südföhns als mögliche Erklärung). Im Sommer (JJA) gibt es hingegen eine deutliche Zunahme der Schneebedeckungsdauer nach Norden und eine schwache Abnahme nach Osten (auch hier ist die Kontinentalität die Ursache). Die Höhe spielt im JJA mit 50% erklärter Varianz wieder eine bedeutendere Rolle. Die Verhältnisse auf einem einzelnen Berggipfel, wie in der letzten Zeile von Tabelle 7.2 für den Schrankogel angeben, werden später noch diskutiert.

Saison	r^2_{n-T}	r^2_{n-z}	$r^2_{n-x/PC1}$	$r^2_{n-y/PC2}$	Datenp.
NDJFMA (1961-2000, ohne Korrelationskrit.,4cm)	0.04	0.52	0.19	0.05	7746
DJF (1961-2000, r <0.0, 5cm, HANTEL and MAURER (2011))	0.07	0.27	0.15	0.03	5370
JJA (1975-2004, r <0.0, 2cm, GOTTFRIED et al. (2011))	0.01	0.50	0.08	0.13	664
JJA-Schr.(1998-2006, ohne Korrelationskrit.)	0.27	0.07	0.25	0.05	279

Tabelle 7.2: Partielle erklärte Varianzen der relativen Schneebedeckungsdauer durch die CRU-Temperatur sowie die geographischen Prädiktoren, gemittelt über alle Stationen und die gesamte Untersuchungsepoche. Am Schrankogelgipfel (Schr.) sind die Längen-und Breitenangaben durch Principal Components (PCs) ersetzt. Alle Koeffizienten haben eine Signifikanz von größer als 99%.

Für die Ergebnisse von Abbildung 7.1 wurde kein Korrelationskriterium (zum Korrelationskriterium siehe HANTEL et al. (2000) und HANTEL et al. (2012)) verwendet, um mit den nachfolgenden Monte Carlo Experimenten absolut konsistent zu sein. Bezüglich der Sinnhaftigkeit eines Korrelationskriteriums (r <0.0 oder r <-0.3 zwischen CRU-Temperatur T und Schneebedeckungsdauer n an einer Station) lässt sich keine eindeutige Aussage treffen. Dieses Kriterium hat seine Wurzel in der schrittweisen Entwicklung der Theorie in der Arbeit von HANTEL et al. (2000). Zunächst wurde dort die Anpassung einer Tangens-Hyperbolicus Funktion an relative Schneebedeckungswerte nur an einzelnen Klimastationen vorgenommen, die Korrelation zwischen T und n an jeder dieser Stationen bestimmt und jene Stationen mit r <-0.3 in einer globalen Anpassung verwendet. Für das Korrelationskriterium könnte man argumentieren, dass man nur Daten in der Auswertung inkludieren möchte, die der Theorie nicht zuwider laufen, um über das gesamte Untersuchungsgebiet eine möglichst gute Anpassung zu erzielen. In Anbetracht der Tatsache (siehe HANTEL et al. (2012)), dass schwach negative oder sogar positive Korrelationen eher in größeren Höhen (wegen des stärken Niederschlagseinflusses) auf-

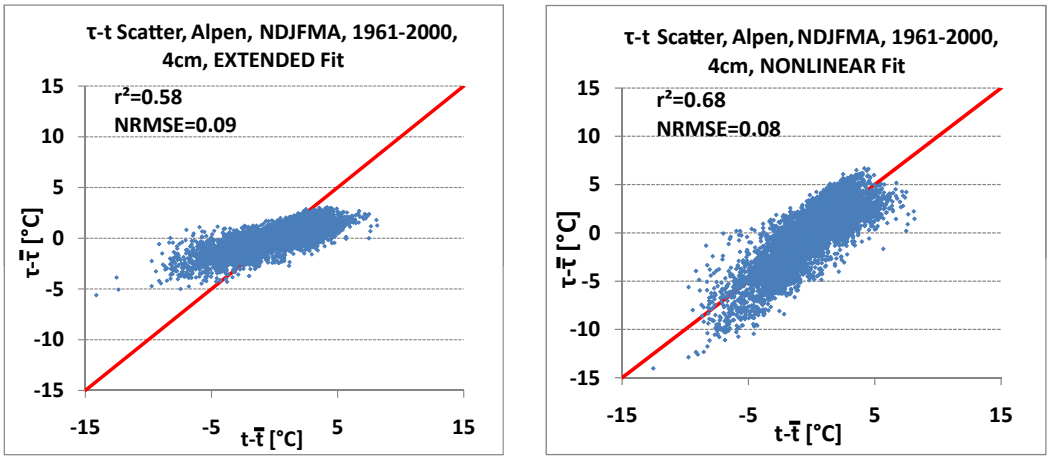

Abbildung 7.2: τ-t-Scatterplot für Extended und Nonlinear Fit im Vergleich. Datenbasis: Alpen, NDJFMA, 4cm, 1961-2000, kein Korrelationskriterium.

treten, die bei kleinen Thresholds deutlich jenseits der Höhe der maximalen Empfindlichkeit liegen, scheint dieser Zugang gerechtfertigt. Ein weiterer Anhaltspunkt ist die Verteilung der Residuen der Gebirgstemperatur, die nur bei Anwendung des starken Korrelationskriteriums wirklich gaussisch ist (siehe HANTEL et al. (2012)). Das heißt, dass nur bei Verwendung des Kriteriums r <-0.3 andere Einflüsse auf die relative Schneebedeckungsdauer als jener der Temperatur als Rauschen interpretiert werden können. Andererseits darf das Weglassen von Daten bei einer statistischen Auswertung natürlich kritisch hinterfragt werden. Die Diskussion relativiert sich allerdings, wenn man die Parameter miteinander vergleicht, die bei unterschiedlichen Qualitätsansprüchen an die Daten gewonnen wurden. Hier zeigt sich, dass bei gegebenem Threshold so gut wie kein Unterschied in den Ergebnissen auftritt (siehe HANTEL et al. (2012)). Die Ursache dafür wird begreifbar, wenn man sich den Anteil der Varianz an der Schneebedeckungsdauer, die die großräumige Temperatur bei einer alpenweiten Auswertung bestimmt, vergegenwärtigt.

Als nächster empiristischer Beleg für die klare Bevorzugung des "Nonlinear" Fits soll jenes Experiment dienen, das auch in HANTEL and MAURER (2011) zu finden ist. In einem Scatterplot (Abbildung 7.2) wird die Abweichung der Gebirgstemperatur τ bezogen auf den Mittelwert gegen die Abweichungen der Stationstemperatur t (in beiden Fällen handelt es sich natürlich um Saisonmitteltemperaturen) dargestellt. Hierbei erkennt man, dass die Abweichungen nur beim "Nonlinear" Fit eine vergleichbare Amplitude haben und somit entlang der roten 45°-Geraden liegen. Zudem ergeben sich bessere statistische Maßzahlen (erklärte Varianz r^2 und "Normalized Root Mean Square Error" $NRMSE$).

Als Bestätigung dafür, dass die Anpassung mit dem etwas unhandlichen Fehlerintegral als Modellfunktion einwandfrei gelungen ist, kann Abbildung 7.3 angesehen werden. Anstatt die eben genannte Funktion an die relativen Schneebedeckungswerte anzupassen, ist es alternativ möglich, ihre Ableitung, also die gaussische Wahrscheinlichkeitsdichtefunktion, mit den drei

Parametern s_0, c und τ_0 an die mit den entsprechenden CRU-Temperaturdifferenzen normierten Unterschiede in der Schneebedeckungsdauer zwischen zwei beliebigen Jahren einer Station anzupassen. Insgesamt gibt es dabei an jeder Station mit i Werten theoretisch $i(i-1)/2$ Differenzwerte. Es ist auch klar, dass sowohl negative als auch positive Differenzwerte auftreten, wobei die negativen in jeder Höhe überwiegen müssen, um ein Sensitivitätsprofil mit überall negativem Vorzeichen zu erhalten. Die Parameter a und b werden hier nicht berücksichtigt, da das Profil letztendlich mit dem aus der Anpassung des Fehlerintegrals gewonnenen analytischen Sensitivitätsprofil, das am Referenzpunkt $x = x_0$ und $y = y_0$ angenommen wird, verglichen werden soll. Dieser Vergleich zeigt, dass für NDJFMA und DJF (für letztere Jahreszeit vergleiche mit HANTEL and MAURER (2011)) die neu gewonnenen Parameter s_0 und H (und damit c und τ_0) sowie das Sensitivitätsprofil (grüne Rauten) in seiner Gesamtheit sehr gut zu den bereits ermittelten Werten bzw. dem analytischen Profil (blaue Kurve) passen.

7.1.2 "Rectified" Fit versus "Nonlinear" Fit

In der von HANTEL et al. (2000) dargestellten Form muss der "Rectified" Fit aufgrund der Überlegungen im vorigen Unterkapitel für den "Extended" Fit als noch unzweckmäßiger als Letzterer eingestuft werden. Eine Anpassung, die nur die Temperaturwerte berücksichtigt und bei der die Schneebedeckung als Prädiktor für die Temperatur dient, kann nur unrealistische Parameter liefern. Allerdings erweist sich der "Rectified" Fit als wertvolles Instrument im Sinne eines "Generalisierten Linearen Modells" (FAHRMEIR and TUTZ, 2001). Dabei werden die im Grunde Bernoulli-verteilten Schneebedeckungswerte mit der Umkehrfunktion der Modellfunktion annähernd auf Normalverteilung gebracht und die so transformierten Daten mit einer multiplen Regression (was dem "Rectified" Fit entspricht) angepasst. Eben diese Konzept wurde erstmals in der Arbeit von HANTEL et al. (2012) genutzt.

Bernoulli-verteilte Daten und deren Varianz

Gemäß der Gefriertheorie (HANTEL and HIRTL-WIELKE (2007), HANTEL and MAURER (2011)) wird ein gegebener Tag mit einer Schneehöhe gleich/über oder unter einem spezifizierten Threshold (=Schneehöhengrenzwert) mit ν=1 oder ν=0 diskretisiert. Die jahreszeitliche Mittelung von ν ergibt die relative Schneebedeckungsdauer n dieser Saison. Daraus folgt, dass die stochastische Größe ν eine Bernoulliverteilung (bzw. Binomialverteilung) mit Erwartungswert n aufweist. Wird nun eine der Verteilung entsprechende nichtlineare Funktion (z.B. Logit-, Tangens-Hyperbolicus Funktion oder Fehlerintegral) für eine Anpassung gewählt, erhält man nicht-normalverteilte Residuen (siehe HANTEL and HIRTL-WIELKE (2007)), was zur Folge hat, dass das Konzept der Kostenfunktion 7.1 nicht mehr exakt ist, da sich der Ausdruck der Kostenfunktion aus dem Exponenten der gaussischen Wahrscheinlichkeitsdichtefunktion (TAYLOR, 1997) unter der Bedingung eines Extremwertes (Maximierung der Wahrscheinlichkeit kleiner Residuen, 1. Ableitung gleich 0) ableitet.

Ein Merkmal von Bernoulli-verteilten Daten ist, dass sie ein parabolisches Varianzprofil aufweisen. Dazu betrachtet man eine Saison mit der Dauer von D Tagen. Es soll angenommen werden, dass an S Tagen ($0 \leq S \leq D$) Schnee über oder gleich einem spezifizierten Threshold

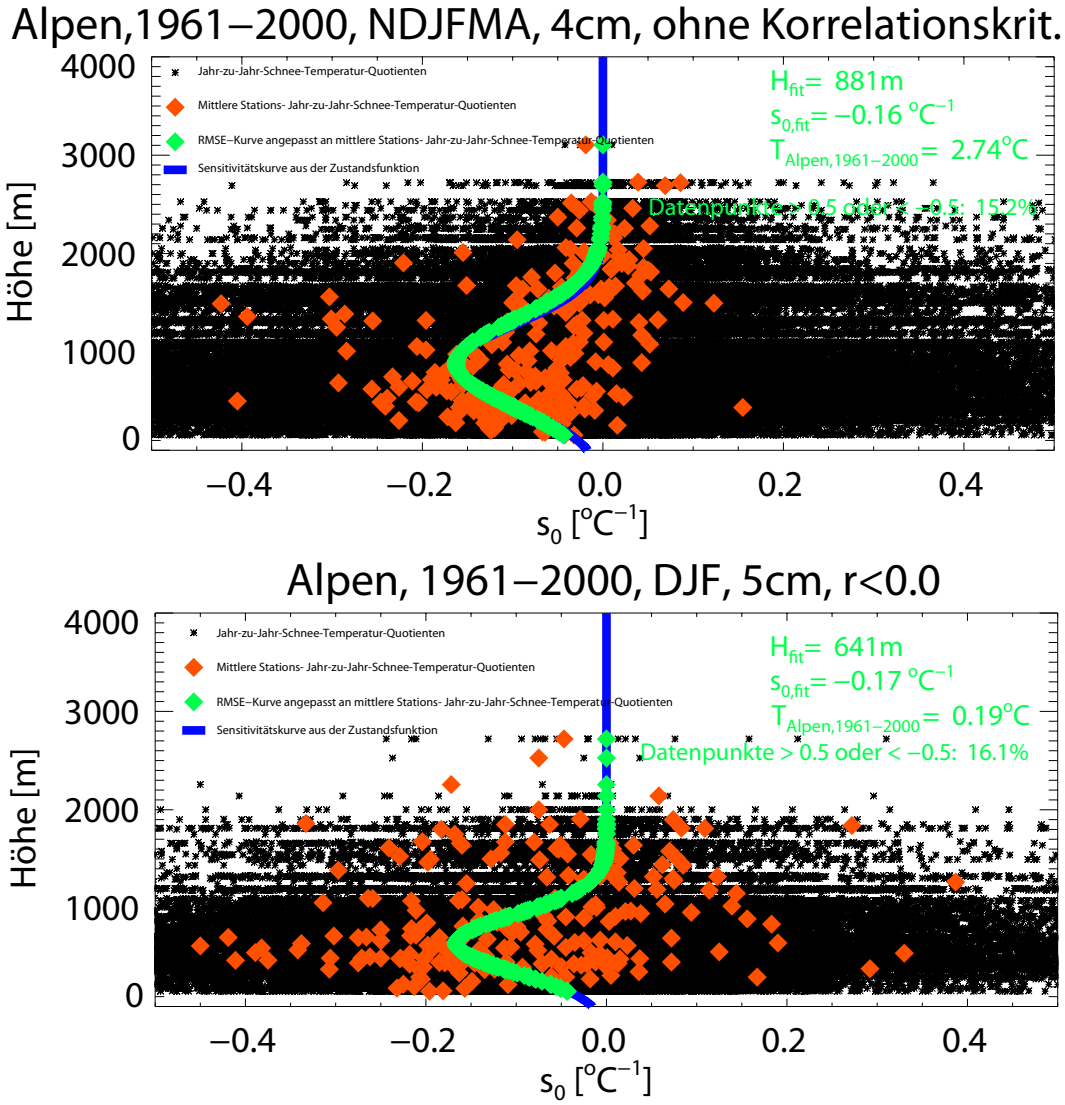

Abbildung 7.3: Analytisches, aus der Zustandsfunktion ermitteltes (blau) und an mittlere Stationsempfindlichkeiten (orange) angepasstes (grün) Sensitivitätsprofil

(ν=1) und dementsprechend an D-S Tagen Schnee unter dem Threshold (ν=0) beobachtet wird. Das ergibt das saisonale Mittel:

$$\overline{\nu} = \frac{S \cdot 1 + (D - S) \cdot 0}{D} = \frac{S}{D}. \tag{7.6}$$

Die Abweichung eines einzelnen Tages vom jahreszeitlichen Mittel berechnet sich dann zu:

$$\nu' = 1 - \frac{S}{D} \quad \text{an } S \text{ Tagen;} \qquad \nu' = 0 - \frac{S}{D} \quad \text{an } D\text{-}S \text{ Tagen.} \tag{7.7}$$

Das ergibt die Varianz von ν:

$$\overline{\nu'^2} = \frac{1}{D}\left\{\left(1 - \frac{S}{D}\right)^2 \cdot S + \left(-\frac{S}{D}\right)^2 \cdot (D - S)\right\}. \tag{7.8}$$

Durch Ausquadrieren erhält man schließlich:

$$\overline{\nu'^2} = \frac{S}{D}\frac{D - S}{D}. \tag{7.9}$$

Unter Berücksichtigung, dass n=$\overline{\nu}$ gilt und durch Eliminierung von S und D mit Formel (7.6) bekommt man:

$$\overline{\nu'^2} = n(1 - n). \tag{7.10}$$

Das ist genau jenes parabolische Varianzprofil, das von HANTEL et al. (2000) ohne die eben gemachte Ableitung verwendet wurde. Die Varianz verschwindet auf beiden Seiten des Intervalls (0 und 1). Das ist eine der entscheidenden Eigenschaften eines Bernoulli-verteilten Datensatzes (DeGROOT, 1986).

Dieses Ergebnis hat aber auch Implikationen für die Anpassung, da ja der Beobachtungsfehler von n mit der Formel (7.10) abgeschätzt wird zu:

$$\sigma_i^{\mathrm{a}}(n_i) \approx n_i(1 - n_i)^{1/2}. \tag{7.11}$$

Ein gesättigter Wert n_i, d.h., $n_i = 0$ oder $n_i = 1$, repräsentiert unendliche Genauigkeit. Eine derartige Beobachtung kann daher nicht in eine Anpassung mit einer Kostenfunktion der Art 7.1 eingehen. Das ist der ultimative Grund, weshalb gesättigte Schneedauerwerte n nicht berücksichtigt werden können.

Transformation der Bernoulli-verteilte Daten auf Normalverteilung, Generalisiertes Lineares Modell

Der Vorteil eines Generalisierten Linearen Modells ist, dass es wahrscheinlichkeitstheoretisch exakt ist. Die Begründung dafür (normalverteilte Residuen) wurde bereits erwähnt.

Folgende Schritte sind zu bewältigen, wenn das Konzept auf die Schneebedeckungswerte angewendet werden soll :

Als erster Schritt ist die Umkehrfunktion des Fehlerintegrals Φ^{-1} zu bilden und damit:

$$\eta_i = \Phi^{-1}(n_i), \tag{7.12}$$

wobei Φ gemäß (siehe auch HANTEL and HIRTL-WIELKE (2007) und HANTEL and MAURER (2011)):

$$\Phi(\chi) = \frac{1}{\sqrt{2\pi}} \int_{\vartheta=-\infty}^{\chi} e^{-\vartheta^2/2} \mathrm{d}\vartheta, \tag{7.13}$$

definiert ist. Nebenbei sei hier bemerkt, dass in der Praxis mit der numerisch approximierten *Errorfunktion* gearbeitet wird, die mit dem Fehlerintegral wie folgt zusammenhängt (BRONSTEIN et al., 1999):

$$\mathrm{erf}(x) = 2\Phi(\sqrt{2}x) - 1; \qquad \Phi(x) = \frac{1}{2}\left(\mathrm{erf}\left(\frac{x}{\sqrt{2}}\right) + 1\right) \tag{7.14}$$

Das führt dazu, dass sich im Argument χ der Faktor $\sqrt{2}$ heraus kürzt und die zwischen $x = -\infty$ und ∞ befindlichen Funktionswerte mit dem Faktor $\frac{1}{2}$ skaliert und um $\frac{1}{2}$ in positive Richtung verschoben werden. η_i ist der rektifizierte bzw. transformierte Schneebedeckungswert, welcher für beliebige n_i im beidseitig offenen Intervall]0,1[definiert ist. Damit sind im linearisierten Modell alle gesättigten Schneebedeckungswerte von vorn herein ausgeschlossen. η_i entspricht genau der Größe E_i in der Arbeit von HANTEL et al. (2000). Der entscheidende Unterschied ist aber, dass nicht die multiple lineare Regression:

$$T^i(n_i) = \frac{E(n_i)}{\sqrt{2\pi}s_0} - ax - by - cz + \tau_0 \tag{7.15}$$

wie in HANTEL et al. (2000) durchgeführt wird sondern:

$$\eta^i(\tau_i) = \sqrt{2\pi}s_0(\underbrace{T_i + ax + by + cz}_{=\tau_i} - \tau_0) \tag{7.16}$$

Der Ansatz in Gleichung 7.16 entspricht einer multiplen linearen Regression mit vier Prädiktoren, nämlich T, x, y und z sowie dem Prädiktanden η. Die rechte Seite der Gleichung 7.16 ist ebenso nichts anderes als das Argument χ des Fehlerintegrals Φ, das nach Anwenden der inversen Funktion übrig bleibt. Deshalb könnte man auch statt η^i ersatzweise χ^i schreiben. Im Idealfall wird η_i gleich η^i. Wird nun χ stark negativ, was stark positivem τ bei gleichzeitig negativem s_0 entspricht, so ist die Fehlerfunktion nur schwach größer als Null; wird χ aber stark positiv, was stark negativem τ bei gleichzeitig negativem s_0 entspricht, so ist die Fehlerfunktion nur schwach kleiner als Eins. Der Funktionswertebereich für η erstreckt sich im Bereich von $-\infty$ bis ∞, wobei konsistent zur obigen Überlegungen zum Argument χ negative η_i- Werte für $n_i < \frac{1}{2}$ und positive für $n_i > \frac{1}{2}$ mit $\eta_i = 0$ bei $n_i = \frac{1}{2}$ auftreten.

Um nun die klassische Darstellung einer multiplen linearen Regression zu erreichen, schreibt man:

$$\chi^i = S_0 T_i + \alpha x_i + \beta y_i + \gamma z_i + \chi_0. \tag{7.17}$$

wobei gilt:

$$s_0^* = \frac{S_0}{\sqrt{2\pi}}; \qquad a^* = \frac{\alpha}{S_0}; \qquad b^* = \frac{\beta}{S_0}; \qquad c^* = \frac{\gamma}{S_0}; \qquad \tau_0^* = -\frac{\chi_0}{S_0} \tag{7.18}$$

Die Bezeichnung "*" wurde gewählt, um den Unterschied zwischen dem Parametervektor $\mathbf{Q}=(s_0, \tau_0, a, b, c)$ und $\mathbf{Q}^*=(s_0^*, \tau_0^*, a^*, b^*, c^*)$ hervorzuheben. Den Parametervektor $\mathbf{P}=(S_0, \alpha, \beta, \gamma, \chi_0)$ bekommt man aus der Minimierung der Kostenfunktion:

$$J(S_0, \chi_0, \alpha, \beta, \gamma) = \frac{1}{2}\left[(\eta_i - \eta^i)^2\right]. \tag{7.19}$$

wobei [..] ein beliebiger, für den vorliegenden Fall noch genau zu definierender, Mittelungsoperator bzw. eine Gewichtsfunktion ist. Der Faktor $1/2$ hat keine tiefere Bedeutung und wird durch Bildung der Ableitungen eliminiert. Folgende Ableitungen in Bezug auf die Parameter sind zu bilden:

$$\frac{\partial J}{\partial S_0} = \left[(\eta_i - \eta^i)\underbrace{(-\frac{\partial \eta^i}{\partial S_0})}_{=-T_i}\right] = -[\eta_i T_i] + [\underbrace{(S_0 T_i + \alpha x_i + \beta y_i + \gamma z_i + \chi_0)}_{=\eta^i} T_i] = 0 \tag{7.20}$$

$$\frac{\partial J}{\partial \alpha} = \left[(\eta_i - \eta^i)\underbrace{(-\frac{\partial \eta^i}{\partial \alpha})}_{=-x_i}\right] = -[\eta_i x_i] + [\underbrace{(S_0 T_i + \alpha x_i + \beta y_i + \gamma z_i + \chi_0)}_{=\eta^i} x_i] = 0 \tag{7.21}$$

$$\frac{\partial J}{\partial \beta} = \left[(\eta_i - \eta^i) \underbrace{(-\frac{\partial \eta^i}{\partial \beta})}_{=-y_i} \right] = -[\eta_i y_i] + [\underbrace{(S_0 T_i + \alpha x_i + \beta y_i + \gamma z_i + \chi_0)}_{=\eta^i} y_i] = 0 \tag{7.22}$$

$$\frac{\partial J}{\partial \gamma} = \left[(\eta_i - \eta^i) \underbrace{(-\frac{\partial \eta^i}{\partial \gamma})}_{=-z_i} \right] = -[\eta_i z_i] + [\underbrace{(S_0 T_i + \alpha x_i + \beta y_i + \gamma z_i + \chi_0)}_{=\eta^i} z_i] = 0 \tag{7.23}$$

$$\frac{\partial J}{\partial \chi_0} = \left[(\eta_i - \eta^i) \underbrace{(-\frac{\partial \eta^i}{\partial \chi_0})}_{=-1} \right] = -[\eta_i] + [\underbrace{(S_0 T_i + \alpha x_i + \beta y_i + \gamma z_i + \chi_0)}_{=\eta^i}] = 0 \tag{7.24}$$

Durch Bilden der Korrelationsprodukte und Umordnen erhält man die Gauß' schen Normalgleichungen:

$$[T_i T_i] S_0 + [x_i T_i]\alpha + [y_i T_i]\beta + [z_i T_i]\gamma + [T_i]\chi_0 = [\eta_i T_i] \tag{7.25}$$

$$[T_i x_i] S_0 + [x_i x_i]\alpha + [y_i x_i]\beta + [z_i x_i]\gamma + [x_i]\chi_0 = [\eta_i x_i] \tag{7.26}$$

$$[T_i y_i] S_0 + [x_i y_i]\alpha + [y_i y_i]\beta + [z_i y_i]\gamma + [y_i]\chi_0 = [\eta_i y_i] \tag{7.27}$$

$$[T_i z_i] S_0 + [x_i z_i]\alpha + [y_i z_i]\beta + [z_i z_i]\gamma + [z_i]\chi_0 = [\eta_i z_i] \tag{7.28}$$

$$[T_i] S_0 + [x_i]\alpha + [y_i]\beta + [z_i]\gamma + \chi_0 = [\eta_i] \tag{7.29}$$

Dieses symmetrische Gleichungssystem für fünf Unbekannte kann im Gegensatz zum nichtlinearen Fall analytisch gelöst werden, sofern es nicht (fast) singulär (kleinster Singulärwert des Matrix-Vektor-Systems wäre im singulären Fall gleich Null) ist. Ebenso ist hier zur Bestimmung des Standardfehlers kein Bootstrapping (wie in HANTEL and HIRTL-WIELKE (2007) und Folgende) notwendig, sondern die Unsicherheiten in den Parametern können ebenfalls analytisch bestimmt werden.

Als letzten Schritt muss die parabolische Varianz $\sigma_i^{\mathrm{a}2} \approx (1 - n_i) n_i$ transformiert werden (σ^b erhält man aus der Standardabweichung der η_i, welche aber bei einer Kostenfunktion, die nur aus einem Summanden besteht, nicht relevant ist) da auch im linearen Modell die Randwerte (in der Praxis nahe -1 und 1, also weit weg von $-\infty$ und ∞) stärker als jene nahe 0 betont werden sollen. Das Verhältnis zwischen untransformierter $\sigma_{n,i}$ (entspricht σ_i^{a}) und transformierter Standardabweichung $\sigma_{\eta,i}$ ergibt sich aus der Ableitung des Fehlerintegrals Φ nach ihrem Argument χ:

$$\frac{\sigma_{n,i}}{\sigma_{\eta,i}} = \frac{\mathrm{d}\Phi(\chi)}{\mathrm{d}\chi} = \frac{1}{\sqrt{2\pi}} \exp\left(-\chi^2/2\right) \tag{7.30}$$

Einsetzten der "Messwerte" η_i für χ, quadrieren und auflösen nach $\sigma_{\eta,i}^2$ liefert schließlich:

$$\sigma_{\eta,i}^2 = 2\pi(1 - n_i) n_i \exp\left(\eta_i^2\right) \tag{7.31}$$

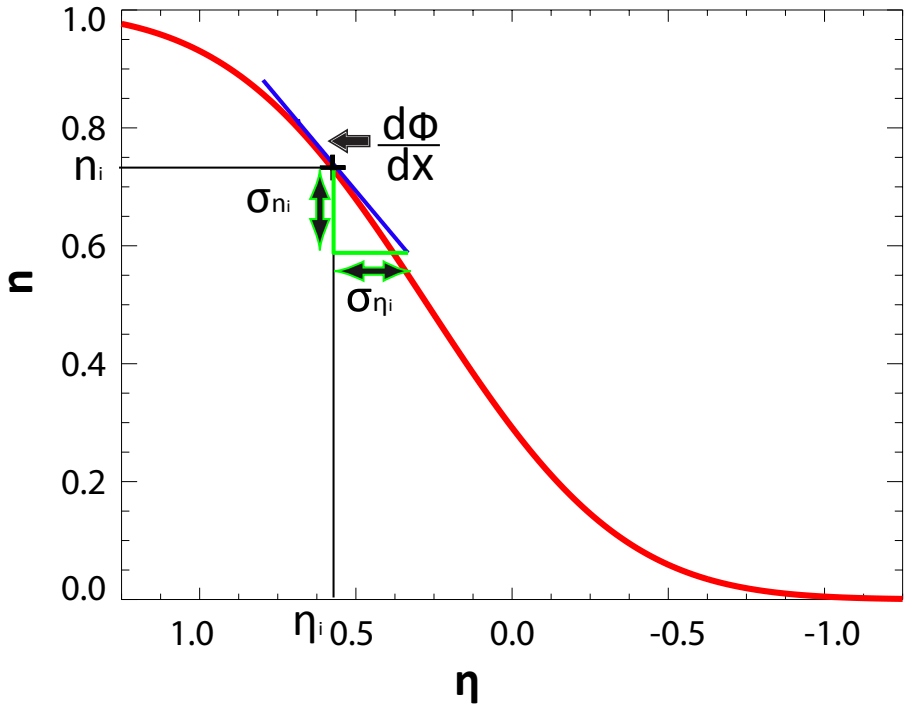

Abbildung 7.4: Skizze zur Ableitung der transformierten Gewichtsfunktion

und

$$[\,] \approx \frac{1}{\sigma^2_{\eta,i}} \tag{7.32}$$

Die Ableitung von Gleichung 7.31 soll durch Abbildung 7.4 veranschaulicht werden. Die zugehörige Gewichtsfunktion sowie all ihre Komponenten sind im ersten Teilbild von Abbildung 7.5 gezeigt. Die Ergebnisse in Abbildung 7.5 für NDJFMA (4cm, kein Korrelationskriterium) und DJF (5cm, r <0.0, siehe HANTEL and MAURER (2011)) stimmen zwar nicht genau mit den nichtlinearen Parameterresultaten überein, sind bei einem Intervall von $\pm 3\sigma$ aber auch nicht signifikant unterschiedlich. Die hier angegebene und im nächsten Unterabschnitt im Detail diskutierte "erklärte Varianz" macht deutlich, dass im NDJFMA bereits ohne jegliches Korrelationskriterium eine beachtliche erklärte Varianz, nämlich rund 72%, erzielt werden kann. Im DJF liegt der Wert zwar mit rund 51% auch noch ziemlich hoch, es bestätigt sich hier aber, dass die Saison NDJFMA besser die Theorie erfüllt als die Saison DJF. In den Abbildungen 7.6 und 7.7 erkennt man sehr schön, dass die Residuenverteilung von einer leicht nicht-normalen Form mit Exzess um 0 herum (siehe dazu HIRTL-WIELKE (2007)) in eine Normalverteilung übergeht. Genauso ändern sich die Verteilungen der beobachteten und modellierten Werte der abhängigen Größe (n oder η) auf eine- näherungsweise- Gaußverteilung.

Saison	$A[°C/°lon]$	$B[°C/°lat]$	$C[°C/km]$	DP
NDJFMA (1961-2000, ohne Korrelationskrit.)	-0.10(±0.01)	0.39(±0.03)	-2.65(±0.02)	9140
DJF (1961-2000, r <0.0, vgl. HANTEL and MAURER (2011))	-0.19(±0.01)	0.32(±0.03)	-2.39(±0.02)	9104
JJA (1975-2004, r <0.0, vgl. GOTTFRIED et al. (2011))	0.12(±0.01)	-0.02(±0.04)	-3.46(±0.03)	5798

Tabelle 7.3: Parameter der Anpassung t gegen T, x, y und z (DP: Anzahl der Datenpunkte).

Multilineare Regression mit t als Prädiktand und T, x, y und z als Prädiktoren

Eine weitere, interessante Anwendung der multilinearen Anpassung ist ein Fit der Form:

$$t = T + Ax + By + Cz \tag{7.33}$$

wobei t für die Stationsmitteltemperatur, T, x, y und z wiederum für das Flächen- bzw. das Epochenmittel der CRU-Temperatur und die geographische Position stehen. Die Anpassung hat keine Konstante; am Referenzpunkt ($x = x_0$ bzw. $x = 0$, $y = y_0$ bzw. y =0 und $z = z_0$ bzw. z =0) verschwindet die Anomalie $t - T$ im Idealfall. Tabelle 7.33 zeigt das Ergebnis für drei Saisonen. Zwar erhält man verständlicherweise nicht dieselben Werte wie für a, b und c, da die Anpassung unabhängig von jeglichen Schneebedeckungswerten erfolgt, aber auch hier zeigt sich konsistent zur vorhergehenden Auswertung eine Temperaturabnahme nach Osten und eine Zunahme nach Norden im Winter sowie eine Temperaturzunahme nach Osten im Sommer.

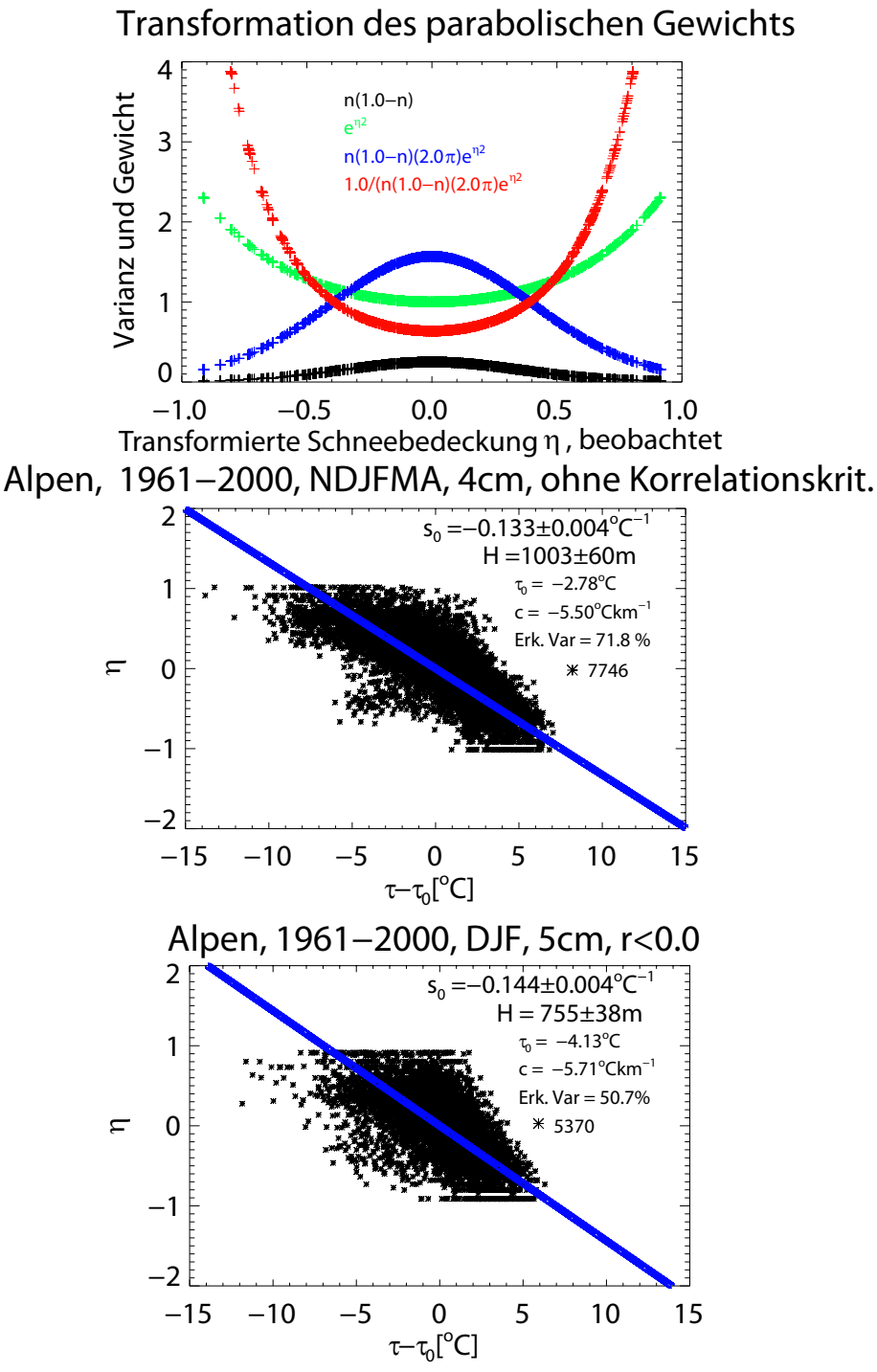

Abbildung 7.5: Lineare Modelle für NDJFMA und DJF sowie die dafür verwendete Gewichtung und deren Komponenten

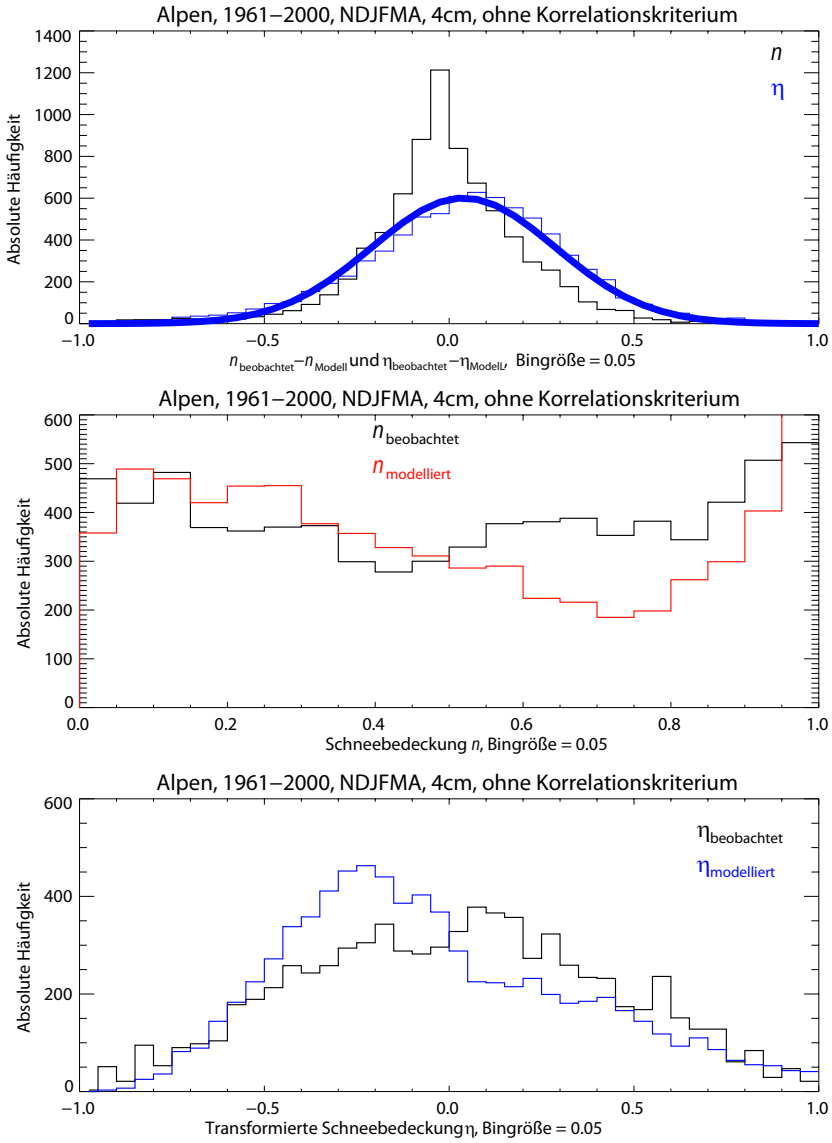

Abbildung 7.6: Residuen und Verteilungen (beobachtet und modelliert) der relativen Schneebedeckung n sowie der transformierten Größe η für NDJFMA

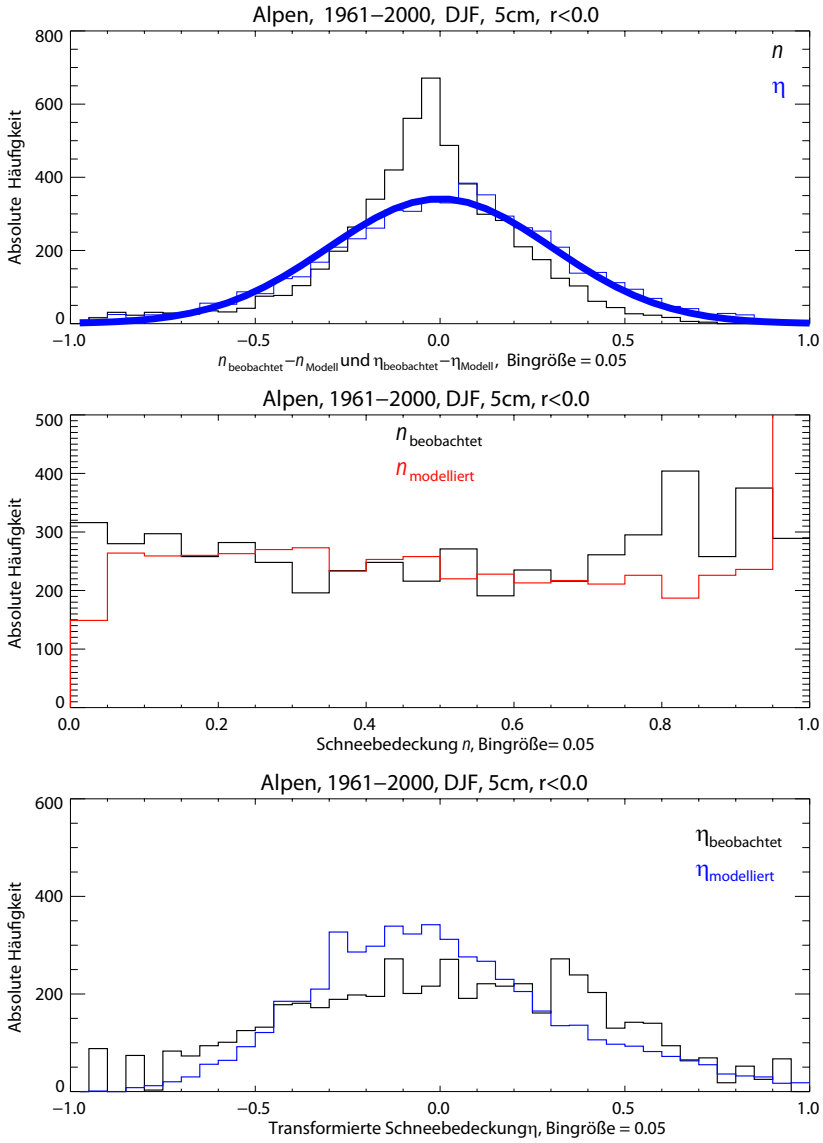

Abbildung 7.7: Residuen und Verteilungen (beobachtet und modelliert) der relativen Schneebedeckung n sowie der transformierten Größe η für DJF

7.1.3 Erklärte Varianz als Gütemaß

Auch wenn die einzelnen Parameter zumeist (die wichtigsten s_0 und c bei niedrigen Thresholds stets) einer Signifikanzprüfung in hohem Maß stand halten und sich der tatsächliche Trend in den Daten mit Hilfe der Parameter gut wiedergeben lässt, ist doch ein globales, allgemein verständliches Gütemaß für die Anpassung wünschenswert. Die erklärte Varianz ist im Prinzip leicht zu berechnen, doch hat man im konkret vorliegenden Fall folgende Dinge zu berücksichtigen: In Analogie zu einer Anpassung mit einer unterschiedlichen (vom jeweiligen Schneebedeckungswert abhängigen) parabolischen Gewichtung, sind sowohl Mess- als auch Modellvarianz bzw. die dazu gehörigen Mittelwerte mit diesen Gewichten zu berechnen. Im Falle der transformierten Schneebedeckungsdauer η ist die transformierte Gewichtsfunktion zu verwenden. Die normierten Gewichte sind bei transformiertem parabolischem Varianzprofil, wie in Formel 7.31 gegeben, definiert als:

$$w_i(n_i, \eta_i) = \frac{1}{2\pi(1-n_i)n_i \exp(\eta_i^2)} \Big/ \sum_I \frac{1}{2\pi(1-n_i)n_i \exp(\eta_i^2)}. \tag{7.34}$$

Die Gewichte ergeben sich also aus der inversen Varianz. Ihre Summe muss gleich Eins sein, weshalb eine Normierung in Gleichung 7.34 erforderlich ist. Hat man nun die Gewichtsfunktion $w_i(n_i, \eta_i)$ gemäß Formel 7.34 spezifiziert, kann man daran gehen, die verschiedenen Varianzen zu bestimmen. Dabei gilt allgemein bei Messwerten y_i und Modellwerten y^i:

$$\text{Totale Varianz bzw. Messvarianz} \quad = \quad \sum_I w_i (y_i - \sum_I w_i y_i)^2, \tag{7.35}$$

$$\text{Erklärte Varianz bzw. Modellvarianz} \quad = \quad \sum_I w_i (y^i - \sum_I w_i y_i)^2, \tag{7.36}$$

$$\text{Nicht erklärte Varianz} \quad = \quad \sum_I w_i (y_i - \sum_I w_i y_i)^2 - \sum_I w_i (y^i - \sum_I w_i y_i)^2 \tag{7.37}$$

mit w_i als normierter, von den Werten y_i abhängiger, Gewichtsfunktion.

Meist wird die erklärte Varianz in % als Quotient aus erklärter Varianz und totaler Varianz oder als Differenz zwischen Eins und dem Quotient aus nicht erklärter Varianz und totaler Varianz angegeben. Letzteres erfordert, dass sich für beliebige Gewichtsfunktionen w_i und ein beliebig dimensionales lineares Modell zeigen lässt, dass die nicht erklärte Varianz gleich der Abweichungsquadratsumme zwischen Beobachtungs- und Modellwert ist, sowie er in der Kostenfunktion auftritt. Dieser Sachverhalt soll im Folgenden für die in x nichtlineare, aber eindimensionale Regressionsgleichung $y^i = a + bx_i^2$ gezeigt werden.

Zunächst stellt man dazu die Kostenfunktion

$$\chi^2 = \sum_I w_i(y_i - a - bx_i^2)^2 \tag{7.38}$$

auf. Bilden der partiellen Ableitungen in Bezug auf a und b ergibt:

$$\frac{\partial \chi^2}{\partial a} = -2\sum_I w_i(y_i - a - bx_i^2) \tag{7.39}$$

und

$$\frac{\partial \chi^2}{\partial b} = -2\sum_I w_i(y_i - a - bx_i^2)x_i^2 \tag{7.40}$$

Null setzen von 7.39 und 7.40 führt auf die beiden Normalgleichungen:

$$a\sum_I w_i + b\sum_I w_i x_i^2 = \sum_I w_i y_i \tag{7.41}$$

und

$$a\sum_I w_i x_i^2 + b\sum_I w_i x_i^4 = \sum_I w_i x_i^2 y_i. \tag{7.42}$$

Multiplizieren von Gleichung 7.41 mit $\sum_I w_i x_i^2$ und von Gleichung 7.42 mit $\sum_I w_i$ und anschließendes Subtrahieren ergibt:

$$b(\sum_I w_i x_i^2 \sum_I w_i x_i^2 - \sum_I w_i \sum_I w_i x_i^4) = \sum_I w_i y_i \sum_I w_i x_i^2 - \sum_I w_i \sum_I w_i x_i^2 y_i. \tag{7.43}$$

Damit erhält man für den Koeffizienten b den Ausdruck:

$$b = \frac{\sum_I w_i \sum_I w_i x_i^2 y_i - \sum_I w_i x_i^2 \sum_I w_i y_i}{\sum_I w_i \sum_I w_i x_i^4 - \sum_I w_i x_i^2 \sum_I w_i x_i^2}. \tag{7.44}$$

Mit $\sum_I w_i$=1 und Reynold' scher Mittelung vereinfacht sich dies zu:

$$b = \frac{\sum_I w_i x_i'^2 y_i'}{\sum_I w_i (x_i'^2)^2}. \tag{7.45}$$

Aus 7.41 erhält man:

$$a = \sum_I w_i y_i - b \sum_I w_i x_i^2. \tag{7.46}$$

Für eine beliebige Abweichung zwischen Mess- und Mittelwert $y_i - \sum_I w_i y_i$ kann man nun schreiben:

$$(y_i - \sum_I w_i y_i) = (y_i - y^i) + (y^i - \sum_I w_i y_i). \tag{7.47}$$

Quadrieren beider Seiten und Anwenden der Gewichtsfunktion w_i ergibt:

$$\sum_I w_i (y_i - \sum_I w_i y_i)^2 = \sum_I w_i (y_i - y^i)^2 + \sum_I w_i (y^i - \sum_I w_i y_i)^2 + 2 \sum_I w_i (y^i - \sum_I w_i y_i)(y_i - y^i). \tag{7.48}$$

Einsetzen der Beziehung 7.46 für den Koeffizienten a sowie Ersetzen von y^i durch die Regressionsgleichung im dritten Term auf der rechten Seite von Gleichung 7.48 führt zu:

$$\begin{aligned}
2 \sum_I w_i (y^i - \sum_I w_i y_i)(y_i - y^i) &= 2 \sum_I w_i (\sum_I w_i y_i - b \sum_I w_i x_i^2 + b x_i^2 - \sum_I w_i y_i)(y_i - y^i) = \\
&= 2 \sum_I w_i (\sum_I w_i y_i + b(x_i^2 - \sum_I w_i x_i^2) - \sum_I w_i y_i)(y_i - y^i) = \\
&= 2 \sum_I w_i b (x_i^2 - \sum_I w_i x_i^2)(y_i - y^i) = \\
&= 2 \sum_I w_i b (x_i^2 - \sum_I w_i x_i^2)(y_i - (\sum_I w_i y_i + b(x_i^2 - \sum_I w_i x_i^2))) = \\
&= 2 \sum_I w_i (b(y_i - \sum_I w_i y_i)(x_i^2 - \sum_I w_i x_i^2) - b^2 (x_i^2 - \sum_I w_i x_i^2)^2).
\end{aligned} \tag{7.49}$$

Mit der Formel 7.45 für den Koeffizienten b zeigt man:

$$\begin{aligned}
2 \sum_I w_i (y^i - \sum_I w_i y_i)(y_i - y^i) &= 2b \sum_I w_i ((y_i - \sum_I w_i y_i)(x_i^2 - \sum_I w_i x_i^2) - b(x_i^2 - \sum_I w_i x_i^2)^2) = \\
&= 2b (\sum_I w_i (y_i - \sum_I w_i y_i)(x_i^2 - \sum_I w_i x_i^2) - \sum_I w_i (y_i - \sum_I w_i y_i)(x_i^2 - \sum_I w_i x_i^2)) = \\
&= 2b\, 0 = 0.
\end{aligned} \tag{7.50}$$

Damit hat man den Beweis erbracht, dass der dritte Term in Gleichung 7.48 verschwindet und die nicht erklärte Varianz und die Quadratsumme der Residuen äquivalent sind. Gemäß SCHÖNWIESE (1992) hängt der Zusammenhang zwischen Mess-, erklärter (Modell-) und nicht erklärter Varianz von der Linearität des Regressionsmodells (sollte gegeben sein) und der Datenverteilung (Stichproben sollten normalverteilt sein) ab. Die geforderte Linearität bezieht sich jedoch auf eine *Linearität der Regressionsgleichung in Bezug auf ihre Koeffizienten* (TAYLOR, 1997), nicht auf eine allfällige Linearität in Bezug auf den Prädiktor, wie sie bei der einfachen Regressionsgleichung $y_i = a + bx_i$, nicht aber im eben gezeigten Beispiel $y_i = a + bx_i^2$, auftritt. Hat man nun eine Regressionsgleichung, die in Bezug auf ihre Koeffizienten nicht linear ist (wie das bei dem Fehlerintegral als Modellfunktion der Fall ist) muss man diese durch eine geeignete Transformation linearisieren. Einfachstes Beispiel ist die Funktion:

$$y_i = a\, exp(bx_i). \tag{7.51}$$

Logarithmieren führt auf die Relation:

$$ln(y_i) = a + bx_i. \tag{7.52}$$

Für diese einfache Regressionsgleichung lassen sich wieder Normalgleichungen finden, welche für die beiden Koeffizienten

$$b = \frac{\sum_I w_i x_i' ln(y_i')}{\sum_I w_i x_i'^2}. \tag{7.53}$$

und

$$a = \sum_I w_i ln(y_i) - b \sum_I w_i x_i \tag{7.54}$$

liefern. Dieses Ergebnis kann unmittelbar mit jenem für $y_i = a + bx_i$ verglichen werden, das mit der Gewichtsfunktion $w_i = 1/N$ (N ist die Anzahl der Datenpunkte) beispielsweise in SCHÖNWIESE (1992) mit $b = x_i' y_i' / x_i'^2$ und $a = \bar{y_i} - b\bar{x_i}$ (mit "-" als dem arithmetischen Mittelwert) angegeben wird.

Passt man durch iterative Minimierung der Kostenfunktion (also durch Umgehung der Normalgleichungen) eine in den Koeffizienten nichtlineare Gleichung ohne erforderliche Transformation an, ist die relative erklärte Varianz nicht konsistent mit der von Eins subtrahierten relativen nicht erklärten Varianz. Zudem fällt bei der konkreten Datenauswertung auf, dass beide relativen Varianzwerte gegenüber den Ergebnissen des Generalisierten Linearen Modells (also jenes, das

durch eine Linearisierung des Regressionsproblems zustande kommt) zum Teil deutlich erhöht ist.

Aus diesen eben angeführten Gründen sollte in Zukunft das Generalisierte Lineare Modell mit transformierten Schneebedeckungswerten η gegenüber dem nichtlinearen Modell bevorzugt werden, will man eine wahrscheinlichkeitstheoretisch exakte Anpassung erreichen. Nichtsdestotrotz bestehen, wie später noch gezeigt wird, bei den in den drei Publikationen verwendeten Thresholds nur geringe Unterschiede zu den Parametern, die mittels der iterativen, nicht analytischen Anpassung gewonnen wurden.

7.2 Monte Carlo Experimente mit realistischen Daten

In der Arbeit von HANTEL and HIRTL-WIELKE (2007) wurde durch Monte Carlo Experimente eindrucksvoll gezeigt, wie die Standardabweichung σ der Temperatur innerhalb einer fiktiven Saison gemäß der Beziehung:

$$s_0 = -\frac{1}{\sqrt{2\pi}\sigma} \tag{7.55}$$

die extreme Steigung der Zustandsfunktion steuert. Die Art der damals gemachten Experimente impliziert, dass die relative Schneebedeckungsdauer n über die fiktive Saison exakt mit der Mitteltemperatur über diese Saison korreliert ist. Da das natürlich nicht realistisch ist und die Datenpunkte nur in seltenen Fällen genau auf der interpolierenden Kurve liegen, sollten nun in einem weiteren Schritt Monte Carlo Experimente mit realistischen (d.h. gestörten) Daten durchgeführt werden. Folgende zwei Punkte waren dabei von Wichtigkeit: Zu zeigen, dass 1) die Zustandsfunktion vom Klimamittel über die betrachtete Epoche (z.B. 1961-2000) unabhängig ist und 2) auch noch bei sehr verrauschten Daten eine brauchbare Steigung heraus destilliert werden kann.

Die Monte Carlo Experimente sind nun wie folgt angelegt, wobei die Anführungszeichen symbolisieren sollen, dass es sich um fiktive Zeit- bzw. Temperaturangaben handelt: 1) Zunächst legt man eine Klimamitteltemperatur (*Climate mean*) für eine "Epoche" (vergleichbar mit z.B. 1961-2000 im Falle realer Daten) fest. Mit Hilfe einer vorgegebenen Standardabweichung (σ_{jahr}) der Temperatur über die gesamte "Epoche" erzeugt man normalverteilte "Jahresmitteltemperaturen" (einige Tausend). 2) Zu diesen einzelnen Mitteltemperaturen können wiederum mit Hilfe einer Standardabweichung der einzelnen "Tage" (σ_{tag}) innerhalb einer fiktiven Saison "Tagesmitteltemperaturen" generiert werden. In den gegenwärtigen Experimenten wurden 100000 "Jahre" mit 100000 "Tage" langen Saisonen verwendet. 3) Weiters wendet man die "Gefriertheorie" (wie in HANTEL and HIRTL-WIELKE (2007)) bei vorgegebener Gefrierpunktstemperatur und Tagesmitteltemperaturen zur Erzeugung der fiktiven Messpunkte an. Wenn man nun eine nichtlineare Kurve (im vorliegenden Fall das Fehlerintegral) an die so generierten Datenpunkte anpasst, geht diese, unabhängig von der Art des Fits ("extended", "rectified" oder "nonlinear"; nach HANTEL et al. (2000)) genau durch alle Punkte. Bei n=0.5 erhält man auf der Abszisse gerade die vorher definierte Gefrierpunktstemperatur t_0. Die extreme Steigung s_0 lässt sich

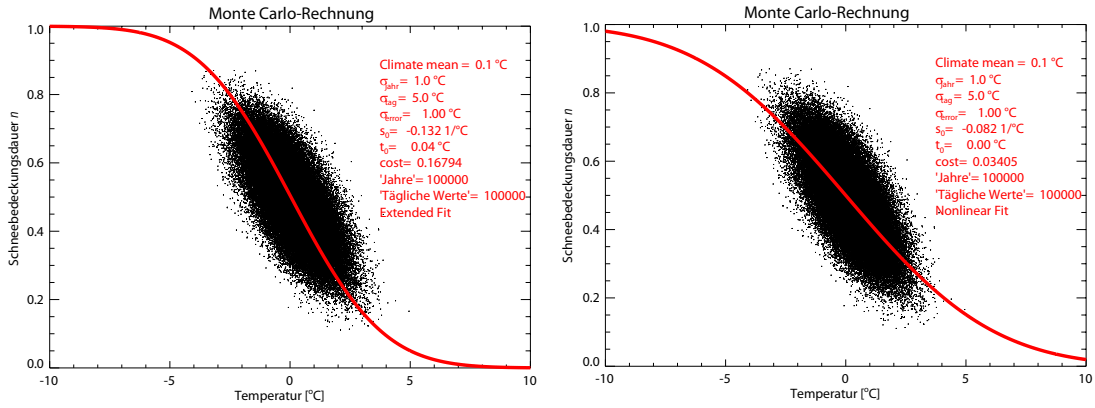

Abbildung 7.8: Monte Carlo Experiment für Extended und Nonlinear Fit im Vergleich. Parameter siehe Text, "cost": Wert der normalisierten Kostenfunktion.

exakt in die Standardabweichung der einzelnen "Tage" σ_{tag} umrechnen. Sie hängt ausschließlich von der mittleren Streuung *innerhalb* der "Saison" ab. 4) Nun sind, wie bereits festgestellt, die Verhältnisse in der Natur natürlich nicht so ideal. Man kann dann zwar wiederum eine nichtlineare Kurve anpassen, doch wird diese nur durch einen kleinen Bruchteil aller Punkte direkt hindurch gehen. Um eine solche Datenverteilung zu simulieren, berechnet man die relativen Schneebedeckungswerte für gestörte Mitteltemperaturen, wobei die Amplitude der Störung über σ_{error} gesteuert wird. Das ist die Standardabweichung einer Normalverteilung aus der zufällig Werte gezogen werden, welche als Grundlage für die Erzeugung von Schneebedeckungswerten dienen. Schließlich werden diese n-Werte den ungestörten Mitteltemperaturwerten zugewiesen. Das ist nun ein realistisches Monte Carlo Experiment, da in Wirklichkeit das Vorhandensein eines Schneetages nicht perfekt mit der täglichen Mitteltemperatur korreliert ist.

7.2.1 Auswirkungen einer zunehmenden Störung des Gleichgewichts zwischen Schneebedeckung und Temperatur

Zunächst wird eine Störamplitude σ_{error} von 1.0°C bei einem Klimamittel von 0.1°C angenommen. Für die Standardabweichung der "Epoche" σ_{jahr} wird 1.0°C, für jene der "Tage" der "Saison" σ_{tag} 5.0°C gewählt. Diese Parameterwahl ist- abgesehen von der Störamplitude- repräsentativ für die Situation im Kernwinter (DJF) der Alpen. Nun kann man wieder sowohl mit dem "Extended" als auch mit dem "Nonlinear" Fit Kurven anpassen. (Die letzte Optimierung der Anpassung, also der "Rectified" Fit nach HANTEL et al. (2012), kam hier noch nicht zur Anwendung.) Dabei zeigt sich (Abbildung 7.8), dass die extreme Steigung betragsmäßig gegenüber dem ungestörten Fall bereits bei beiden Fits vergrößert ist. Allerdings ist der Fehler beim "Extended" Fit (s_0=-0.132 $°C^{-1}$) 25 mal so groß wie beim "Nonlinear" Fit (s_0=-0.082 $°C^{-1}$). Der theoretische Wert für s_0 ergibt sich bei einem σ_{tag} von 5.0°C zu -0.080$°C^{-1}$. Das Ergebnis des Monte Carlo Experiments zeigt somit bei Kenntnis der theoretischen Wertes für s_0 am eindrucksvollsten auf, dass der "Extended" Fit nicht weiter berücksichtigt werden darf.

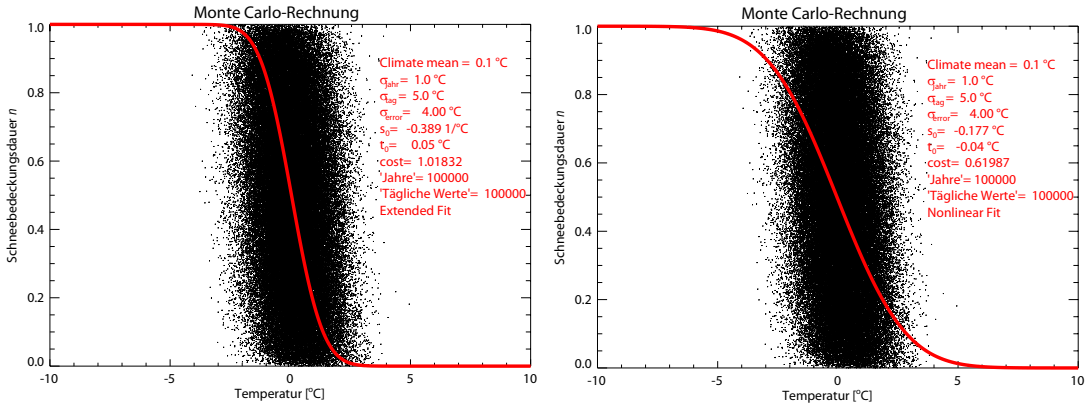

Abbildung 7.9: Monte Carlo Experiment für Extended und Nonlinear Fit im Vergleich. Siehe Abbildung 7.8 .

In einem nächsten Schritt gibt man der Störamplitude σ_{error} einen realistischeren Wert von 4.0°C. Nichtsdestotrotz bleibt die Schätzung der Störamplitude heuristisch, da man ihren wahren, zahlenmäßigen Wert natürlich nicht kennt. Führt man wieder beide Fit-Arten aus, steigt s_0 betragsmäßig dabei im Fall des "Extended" Fits auf -0.389 $°C^{-1}$ und im Fall des "Nonlinear" Fits auf -0.177 $°C^{-1}$ (siehe Abbildung 7.9). Das entspricht einer Verfünffachung von s_0 beim "Extended" Fit und einer Verdopplung von s_0 beim "Nonlinear" Fit gegenüber dem ungestörten Fall. Man beachte bei der Betrachtung der Resultate, dass das ermittelte s_0 im Fall des "Nonlinear" Fits bei einer Parameterwahl, die die Verhältnisse im Kernwinter der Alpen wiedergibt, mit dem Ergebnis der realen Daten, wie sie in HANTEL and MAURER (2011) und HANTEL et al. (2012) zu finden sind, sehr gut übereinstimmt.

Zusammenfassend kann man sagen, dass s_0 mit zunehmender Störamplitude σ_{error} betragsmäßig zunimmt; beim "Extended" Fit beträgt die Zunahme um ein Vielfaches mehr als beim "Nonlinear" Fit. Die Ursache liegt wohl darin begründet, dass mit wachsender Störung die Wahrscheinlichkeit steigt, eine relative Schneebedeckung von 0.0 bei tiefen Temperaturen oder eine von 1.0 bei hohen Temperaturen zu finden. Aber gerade diese Datenpunkte führen offenbar zu einer besonders starken Aufsteilung der Fitkurve beim "Extended" Fit (weil die Temperatur mit angepasst wird) und zu schwächeren Aufsteilung der Kurve beim "Nonlinear" Fit.

Der Verlauf von s_0 als Funktion von σ_{jahr} für sämtliche Störamplituden σ_{error} von 0 bis 8°C ist in Abbildungen 7.10 und 7.11 dargestellt. Beim "Nonlinear" Fit (Abbildung 7.10) ist nur eine Abhängigkeit von der Störamplitude σ_{error}, nicht aber eine von σ_{jahr} zu erkennen. Bis zu einem Wert von σ_{error}=2.0°C ist das Ergebnis verglichen mit dem theoretischen Erwartungswert nahezu ideal. Danach zeigen sich die eben vorhin festgestellte merkbare betragsmäßige Zunahme von s_0 sowie erratische Tendenzen. Damit erfüllt der "Nonlinear" Fit die Theorie dahingehend, dass s_0 nur von der (mittleren) Standardabweichung innerhalb einer "Saison", nicht aber von jener der "Untersuchungsepoche" abhängen darf. Der "Extended" Fit (Abbildung 7.11) erfüllt die Theorie- wie bereits gesagt- nicht. Bei einer extremen Störamplitude von σ_{error}=8.0°C und

einem sehr kleinen σ_{jahr} von 0.5°C gelangt man von der theoretisch erwartbaren Steigung von -0.080 $°C^{-1}$ zu knapp -0.700 $°C^{-1}$, was einer Verzehnfachung entspricht. Nur bei sehr kleinen Störamplituden und großen "Epochen"-Standardabweichungen ("Extended" Fit geht in "Nonlinear" Fit über) gelangt man wieder zum idealen Wert für s_0.

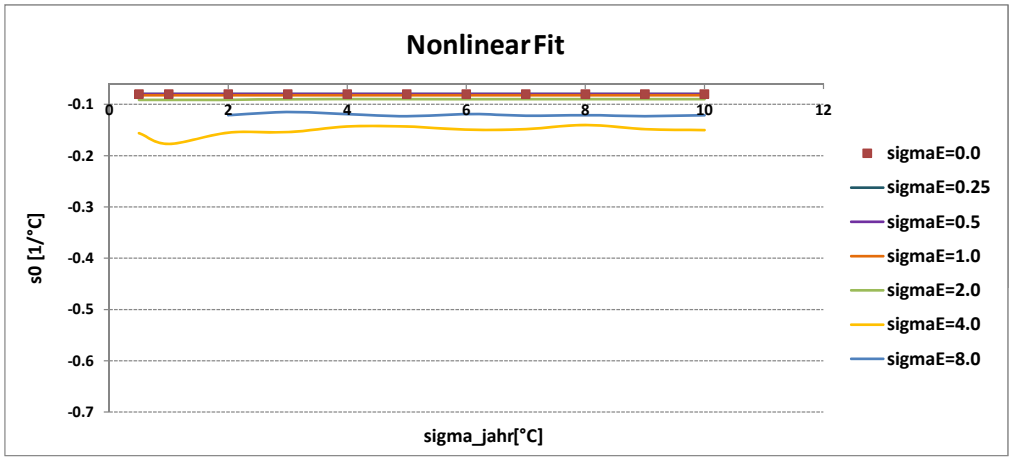

Abbildung 7.10: Monte Carlo Experiment für Nonlinear Fit als Funktion von σ_{jahr} für sämtliche Störamplituden σ_{error} (bzw. sigmaE).

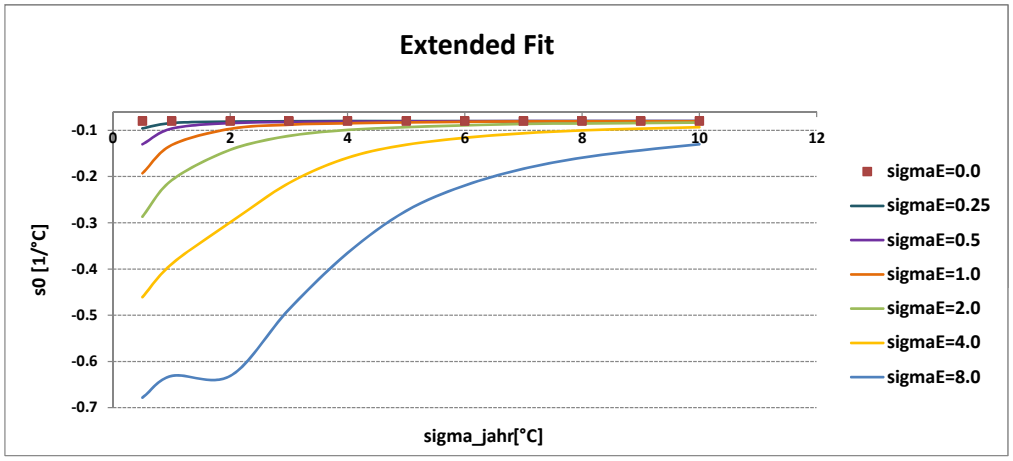

Abbildung 7.11: Monte Carlo Experiment für Extended Fit als Funktion von σ_{jahr} für sämtliche Störamplituden σ_{error}.

7.2.2 Auswirkungen verschiedener Klimamittelwerte auf die Klimasensitivität

Nun wird untersucht, inwieweit der Klimamittelwert (*Climate mean*) über die "Epoche" (z.B. 1961-2000 bei realen Daten) auf die eben gezeigten Ergebnisse einen Einfluss hat. Dazu setzt man das Klimamittel bei einer mäßigen Störamplitude von 1.0°C zunächst bei 2.0°C statt wie vorher bei 0.1°C fest. σ_{jahr} und σ_{tag} bleiben dabei unverändert. Ein weiteres Experiment wird mit einem Klimamittel von -4.0°C gemacht. In beiden Fällen (siehe Abbildung 7.12) ändert sich die extreme Steigung im Vergleich zum theoretisch erwartbaren Wert nicht.

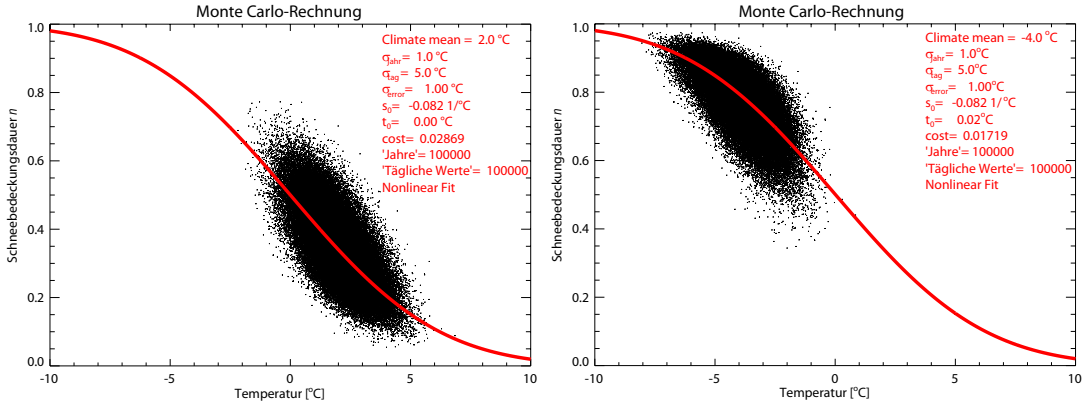

Abbildung 7.12: Monte Carlo Experiment bei Nonlinear Fit und unterschiedlichen Klimamittelwerten.

Die Punktwolke wandert lediglich entlang der Kurve hinunter oder hinauf. Das gilt auch bei höheren Störamplituden. Zudem ist das Verfahren nicht nur unempfindlich gegenüber unterschiedlichen Klimamittelwerten, sondern auch gegenüber Trends, da es egal ist, wie sich die Punktwolke im Lauf der "Epoche" geformt hat. Lediglich die mittlere Standardabweichung innerhalb der betrachteten "Saison" muss erhalten bleiben.

7.3 Datenverfügbarkeit und Threshold

Die Alpen zeichnen sich durch einen umfangreichen Datenvorrat (siehe Abbildung 7.13) aus. So gibt es bereits für den Beginn der Untersuchungsperiode 1961-2000 mehr als 160 Stationswinter pro Jahr, die Zahl steigt auf rund 240 Stationswinter ab den 80er Jahren. Ein Wert von ca. 150 Stationswinter pro Jahre wurde dagegen bei den SNOTEL-Beobachtungen in den Rocky Mountains erst Anfang der 80er Jahre erreicht, wobei zudem das Untersuchungsgebiet dort flächenmäßig wesentlich größer ist.

Der Terminus "Threshold" steht für die gewählte Grenzhöhe der Schneebedeckung (in cm), ab der ein Tag als Schneetag, also mit ν=1 klassifiziert wird. Die Frage nach dem besten Threshold zur Bestimmung der relativen Schneebedeckungsdauer lässt sich *a priori* nicht eindeutig beantworten. Bei einer Beantwortung der Frage sind jedenfalls folgende Gesichtspunkte zu

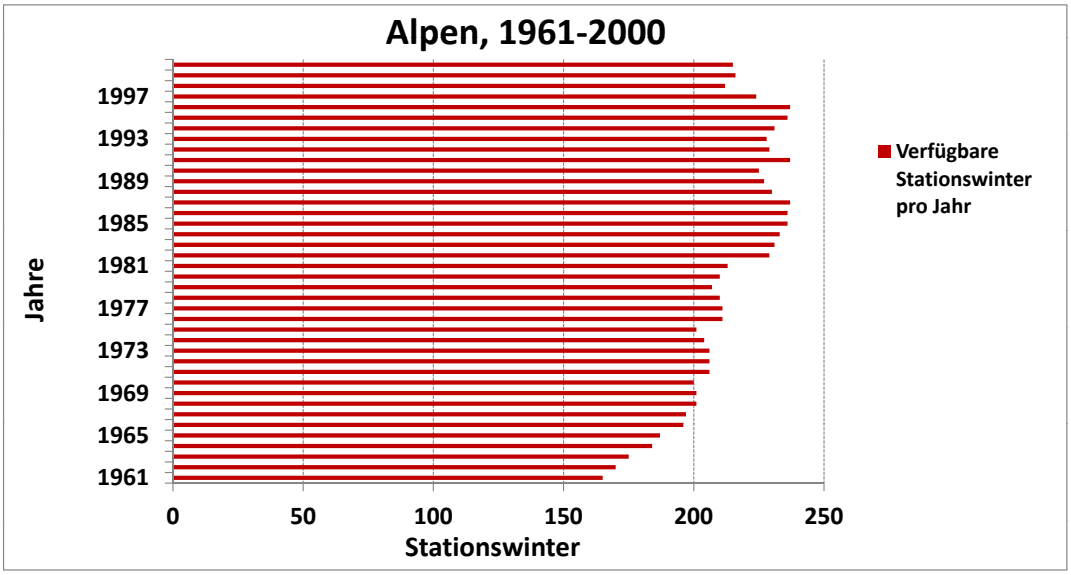

Abbildung 7.13: Verfügbare Stationswinter in den Alpen (A,CH, I, F, D, SLO) 1961-2000.

berücksichtigen: 1) Die Anpassung wird umso besser, je mehr ungesättigte (und dem jeweiligen Korrelationskriterium genügende) Schneebedeckungswerte vorliegen. Unter diesem Licht wird man jenen Threshold auswählen, bei dem die Anzahl der verwendbaren und einer Qualitätsprüfung stand haltenden Stationswinter, über die gesamte Epoche betrachtet, am größten ist. Gleichzeitig ist der anzahlmäßig optimale Wert auch jener Wert, bei dem die Datenpunkte gleichmäßig entlang der Fitkurve verteilt sind. Dies ist von Vorteil, wenn die Punkte nicht-wie im idealen, theoretischen Fall- auf der Kurve selbst liegen. Die Anzahl der vorhandenen Stationswinter im NDJFMA und DJF als Funktion des Thresholds und bei unterschiedlichen Qualitätsansprüchen an die Daten zeigt Abbildung 7.14. Die Zahl der theoretischen (Stationsanzahl mal Anzahl der Winter) und verfügbaren Stationswinter ist in beiden Saisonen und für alle Thresholds ident, erst bei der Anwendung der Qualitätskriterien (Sättigung und Korrelation) erkennt man deutliche Unterschiede. Diese sind durch die wesentlich größeren Schneehöhen im DJF bedingt und äußeren sich in dieser Jahreszeit in einer markanten Abnahme der Datenpunktzahl von den verfügbaren hin zu den ungesättigten Stationswintern, sodass der Vorrat an verwendbaren Stationswintern im NDJFMA beachtlich größer ist als im DJF (bei den kleinen Thresholds um ca. 2000). In beiden Saisonen bringt das starke Korrelationskriterium (r <-0.3) dann nochmals eine deutliche Reduktion der Stationswinter. Ebenso erkennt man in beiden Saisonen ein anzahlmäßiges Optimum an Stationswintern zwischen 2 und 8cm (der Bereich aller vorliegenden Auswertungen). Danach reduzieren sich die ungesättigten und die dem schwachen und dem starken Korrelationskriterium unterworfenen Stationswinter bis zu einem Threshold von 64cm um mehr als die Hälfte. 2) Unter dem Gesichtspunkt einer möglichst hohen Korrelation zwischen Schneebedeckung und Temperatur, sind kleiner Thresholds erstrebenswert. Kleinere Thresholds bedingen das Ausscheiden hoher, stark vom verfügbaren Niederschlag be-

einflusster, Stationen durch die sich in diesem Fall viel häufiger ergebende Sättigung, während Flachlandstationen begünstigt sind. 3) Die Interessen des Nutzers der Auswertung. So werden Tourismusverantwortliche bestimmt nach Wahrscheinlichkeiten für Schneebedeckungen von 30, 40cm oder mehr fragen. Bei einer klimatologischen Betrachtung von Schneegrenzen wie der Medianschneelinie sind hingegen Schneebedeckungen von 10cm oder weniger gefragt, da es darum geht, ein Aussage zu machen, ob eine Fläche schneebedeckt ist oder nicht.

Berücksichtigt man also diese drei Punkte, so erklärt sich die in sämtlichen Arbeiten zu dem Thema der Dissertation gewählte Schneehöhe von 5cm im Kernwinter (DJF) der Alpen. Bei der Sommerschneehöhe (JJA) ist der Spielraum andererseits sehr begrenzt, da die Alpen zu niedrig sind, um in der wärmsten Zeit des Jahres größere Schneebedeckungen aufzuweisen. Um genügend Werte ungleich 0 zu haben (vgl. Punkt 1), wird in dieser Jahreszeit stets ein Threshold von 2cm verwendet.

In den Abbildungen 7.15, 7.16, 7.17 und 7.18 sind die Werte für s_0, c, a, b, τ_0 und die erklärte Varianz als Funktion des Thresholds (logarithmische Thresholdinkremente) sowohl für das Winterhalbjahr NDJFMA als auch für den Kernwinter DJF dargestellt. Nachdem Ergebnisse ohne und mit schwachem (r <0.0) Korrelationskriterium bereits betrachtet wurden, liegt nun der Focus (s_0-Werte werden auch für das schwache Kriterium zum Vergleich gezeigt) auf Resultaten mit dem starken (r <-0.3) Korrelationskriterium. Dies soll deutlich machen, dass das Korrelationskriterium in den Ergebnissen offenbar nur eine untergeordnete Rolle spielt. Eine Analyse zeigt, dass im Bereich von 1 bis 8cm Threshold (also dem klimatologisch relevanten und stets betrachteten Schneehöhengrenzbereich) die Parameter bei kleinem Fehler (1σ) zumeist recht stabil sind. Bei s_0 und c existieren deutliche Unterschiede zwischen nichtlinearer und linearer Anpassung, bei a, b und τ_0 hingegen schwächere. Die Diskrepanzen sind generell im DJF größer als im NDJFMA. Das Muster im vom Threshold abhängigen Verlauf der Parameterwerte ist zumeist auch ziemlich verschieden zwischen den beiden Saisonen und kann nicht weiter interpretiert werden. Der mittels Bootstrapping (nichtlinear) und analytisch (linear) berechnete Standardfehler nimmt generell mit dem Threshold (abnehmende Anzahl an verwendbaren Stationswintern) zu und erreicht bei einem Threshold von 64cm markante Werte (NDJFMA), sofern die Anpassung nicht überhaupt fehlschlägt (DJF). Sehr wichtig ist der Verlauf der erklärten Varianz und hier vor allem jener für den wahrscheinlichkeitstheoretisch einwandfreien linearen Fall: Sowohl im NDJFMA (70%) als auch im DJF (60%) tritt ein Optimum bei einem Threshold von 4cm hervor, sodass sich der anfänglich intuitiv gewählte Threshold von 5cm im DJF (HANTEL et al. (2000), HANTEL and HIRTL-WIELKE (2007), HANTEL and MAURER (2011) und HANTEL et al. (2012)) *a posteriori* als jener herausstellt, der für das vorliegende Modell am besten geeignet ist. Dies ist ein eindeutiger Anhaltspunkt dafür, dass eine Beschränkung auf kleinere Thresholds zielführend und somit eine klimatologische Anwendung der vorliegenden Theorie gerechtfertigt ist. Jenseits eines Thresholds von 8cm beginnen die erklärten Varianzen (linear und nichtlinear) besonders im DJF stark abzusinken. Mögliche Gründe wurden bereits am Anfang des Unterkapitels im Zusammenhang mit der Wahl des Thresholds diskutiert.

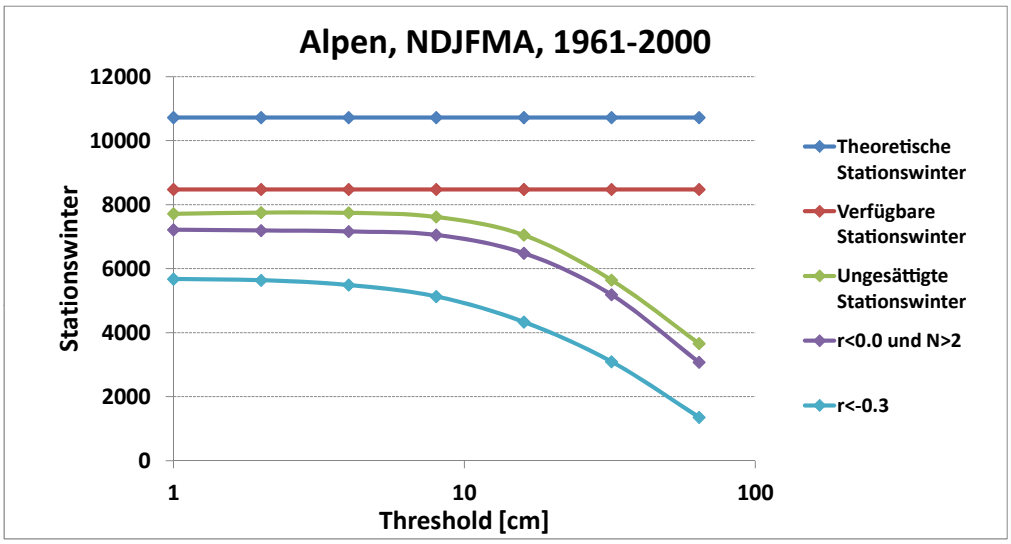

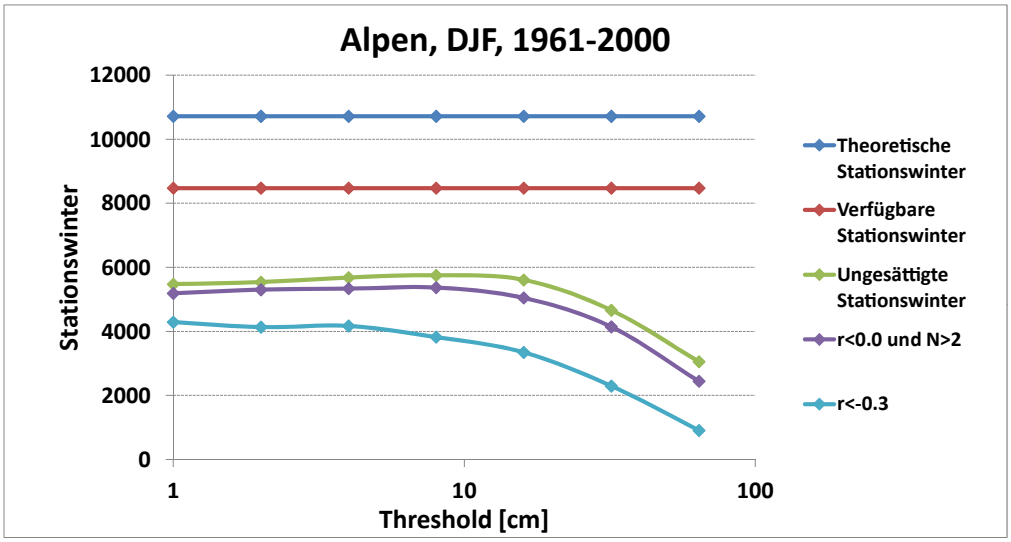

Abbildung 7.14: Verlauf der Stationswinter als Funktion des Thresholds bei unterschiedlichen Qualitätsansprüchen für NDJFMA und DJF.

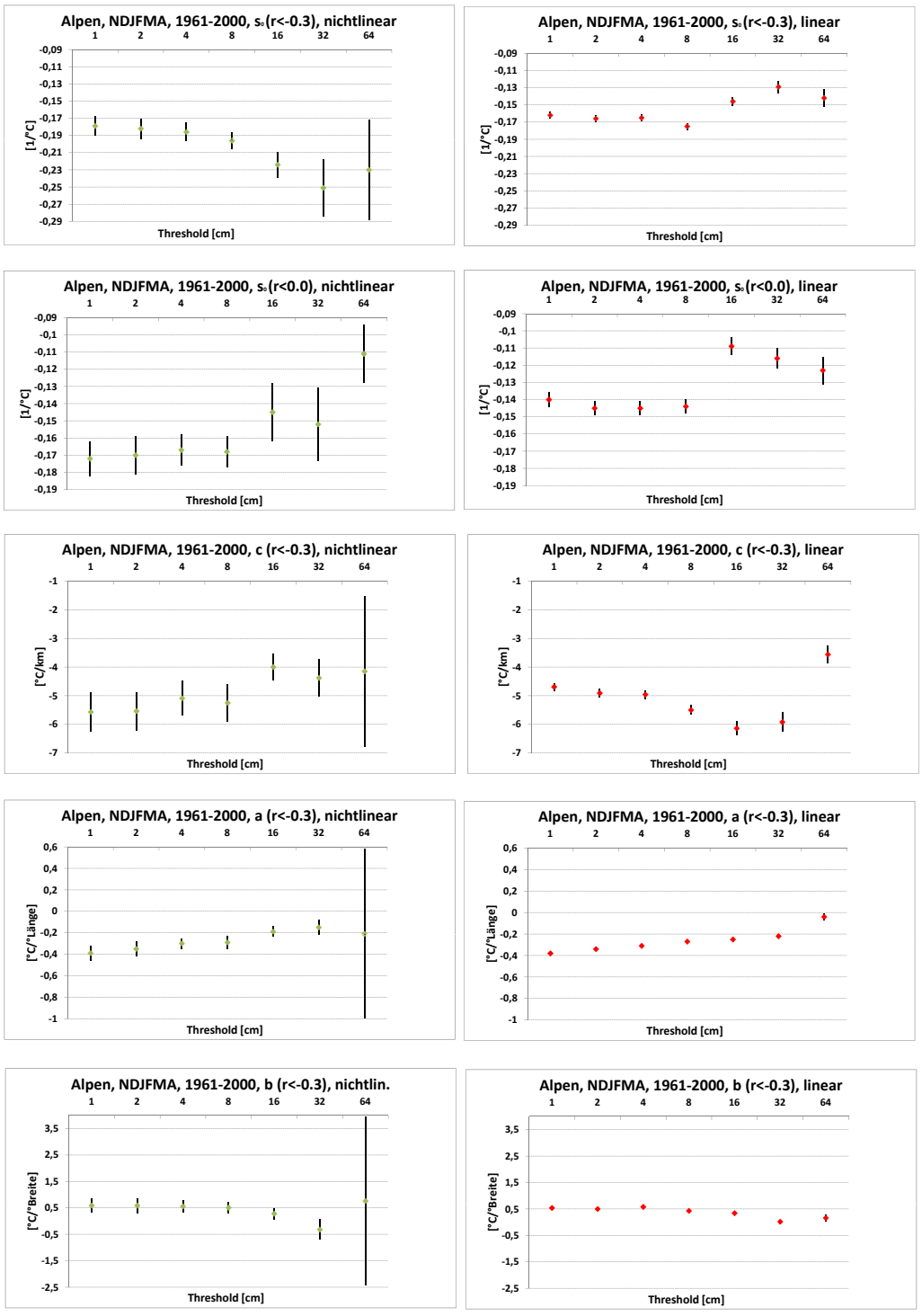

Abbildung 7.15: Verlauf von s_0, c, a, und b als Funktion des Thresholds mit Fehlerbalken für die nichtlineare (iterative) und die lineare (durch Normalgleichungen erzielte) Anpassung für NDJFMA.

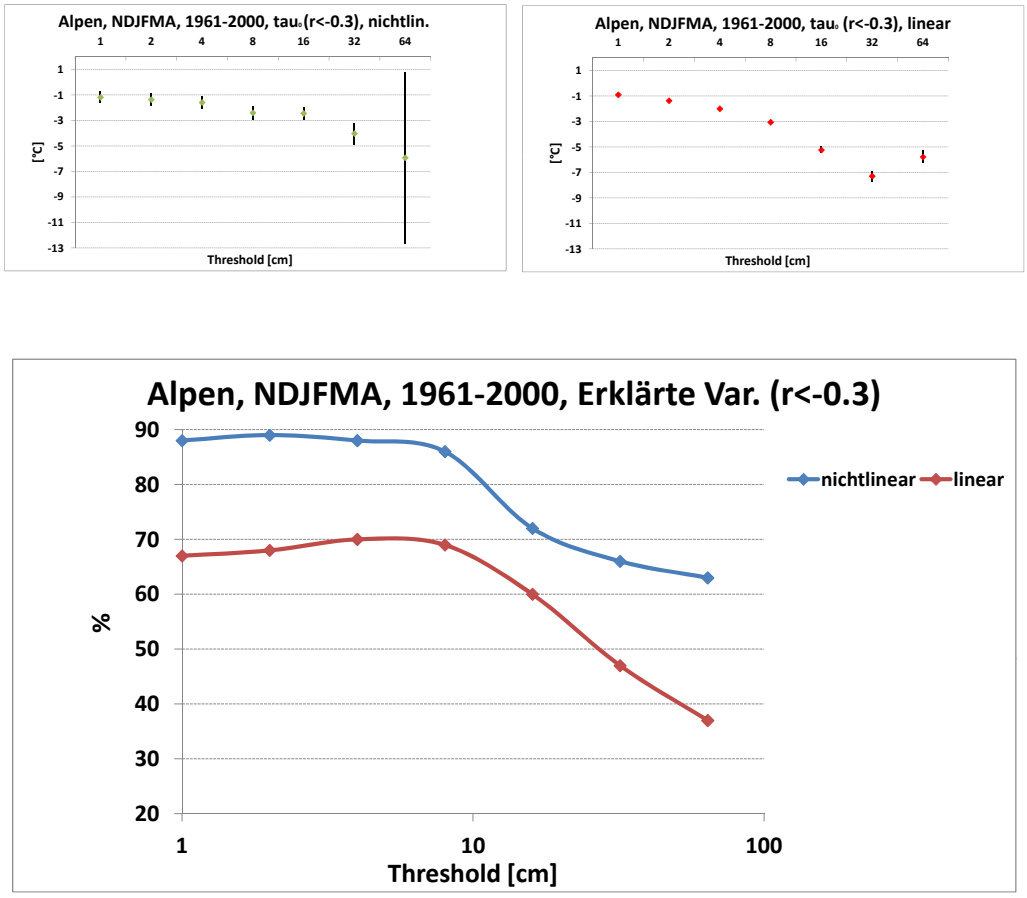

Abbildung 7.16: Verlauf von τ_0 und der erklärten Varianz als Funktion des Thresholds für die nichtlineare (iterative) und die lineare (durch Normalgleichungen erzielte) Anpassung für NDJFMA.

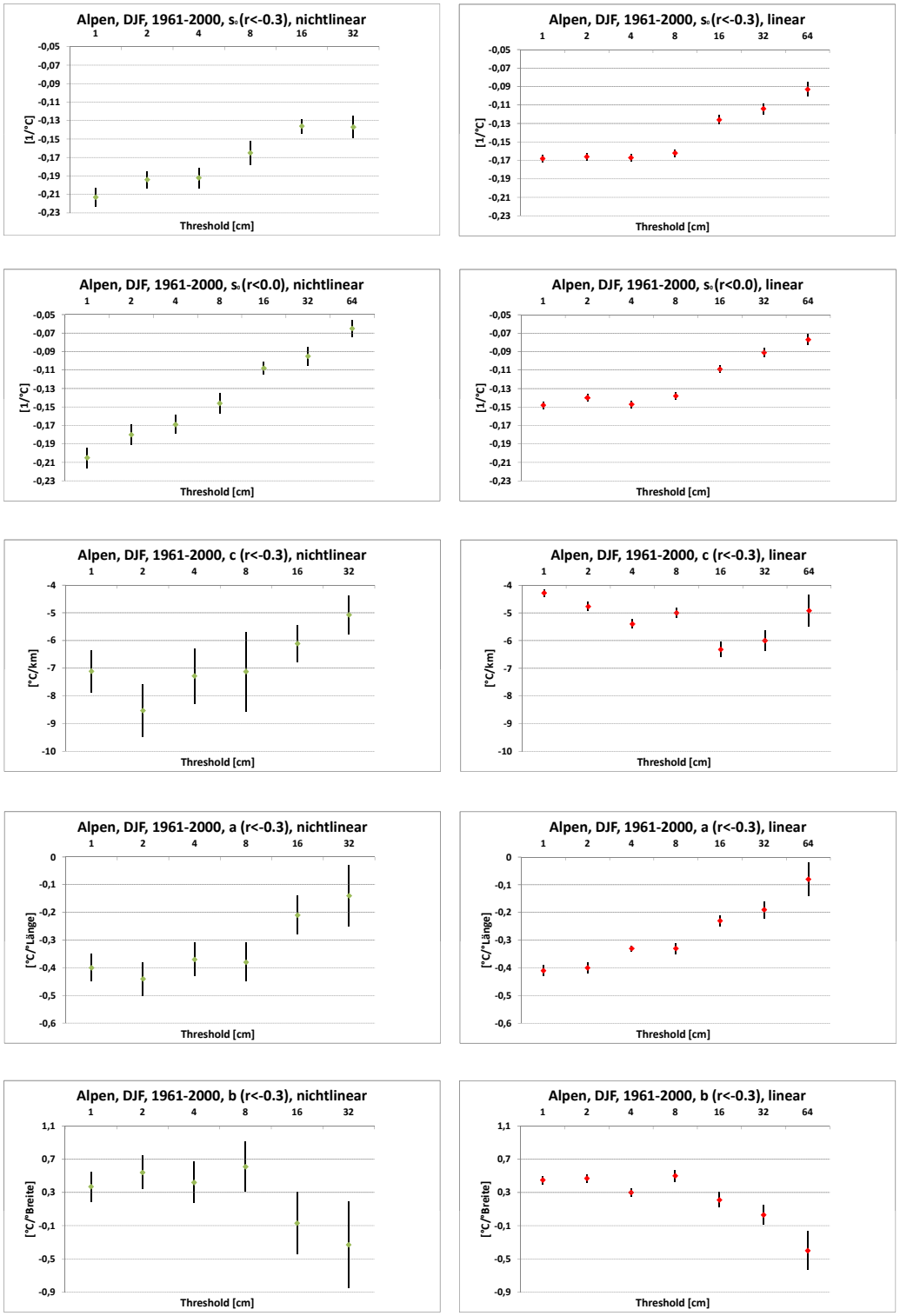

Abbildung 7.17: Verlauf von s_0, c, a, und b als Funktion des Thresholds mit Fehlerbalken für die nichtlineare (iterative) und die lineare (durch Normalgleichungen erzielte) Anpassung für DJF.

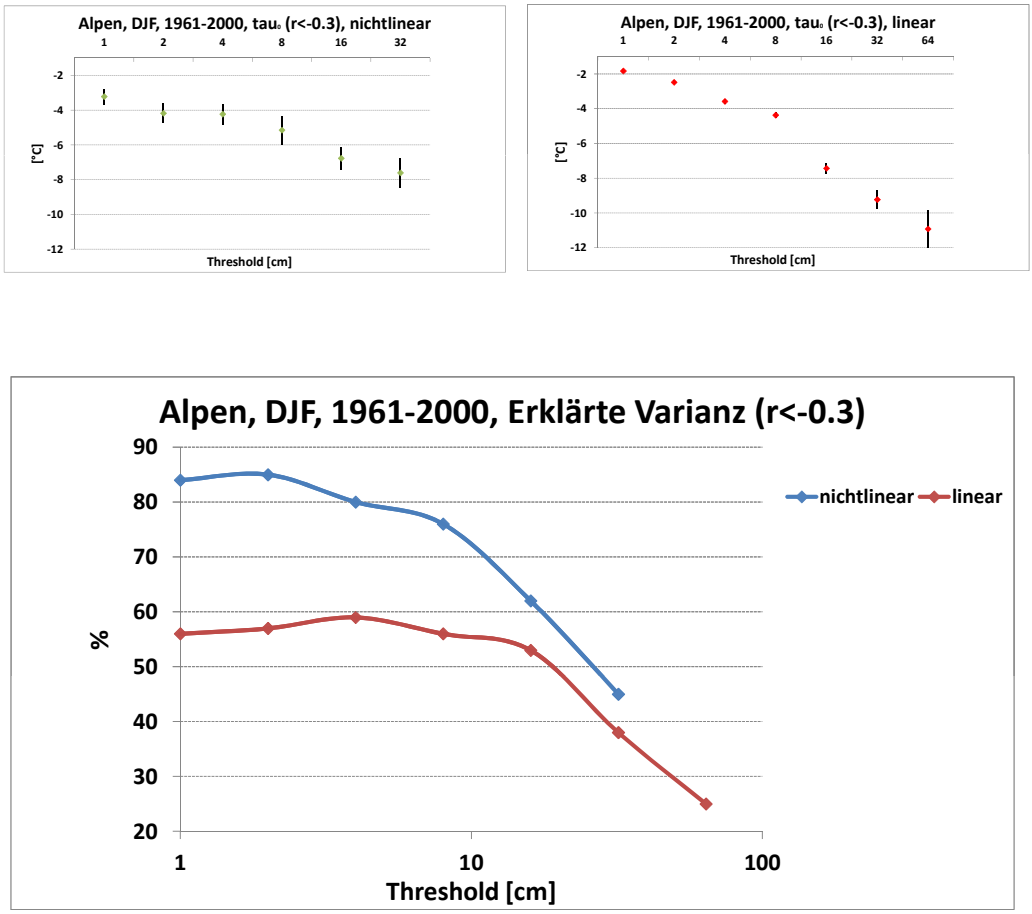

Abbildung 7.18: Verlauf von τ_0 und der erklärten Varianz als Funktion des Thresholds für die nichtlineare (iterative) und die lineare (durch Normalgleichungen erzielte) Anpassung für DJF.

7.4 Relative Schneebedeckungswerte aus Bodentemperaturmessungen

Wenn es darum geht, den kleinskaligen Einfluss der saisonalen Schneebedeckung auf z.B. die Hochgebirgsvegetation zu studieren, ist man auf alternative Methoden zur Schneehöhenbestimmung angewiesen. In einem ersten Versuch wurden dazu vom Department für Naturschutzbiologie, Vegetations- und Landschaftsökologie der Universität Wien Bodentemperaturlogger auf den Hängen des Schrankogels (3497m) in den Stubaier Alpen angebracht. Der Grundgedanke dabei ist, dass mit zunehmender Schneebedeckung der doch beträchtliche Tagesgang der Temperatur an einer steilen Gebirgsflanke markant reduziert werden sollte. Somit kann man auf Basis von mehrmals täglich gemessenen Bodentemperaturen die Diskretisierung ν=0 oder ν=1 durchführen. Die Detailarbeit zur Gewinnung von relativen Schneebedeckungswerten wurde dabei von TOECHTERLE et al. (2010) durchgeführt. Auf dieselbe Weise, wie beim Monte Carlo Experiment eine Gefrierpunktstemperatur vorgegeben und bei realen Stationsdaten ein vernünftiger Threshold ausgewählt wird, muss bei dieser Art der Schneedauerbestimmung ein Temperatur-Grenzwert als Threshold verwendet werden. Dabei gibt es im Prinzip zwei Möglichkeiten: 1) Man wählt eine mittlere Tagestemperatur als Threshold (z. B. 2°C wie in Abbildung 7.19, kodiert als "nsM2") oder man definiert den Threshold über eine Temperaturspanne, im konkreten Fall als Differenz zwischen Tagesmaximum und Tagesminimum. Ein Schneetag wird festgestellt, wenn die tatsächliche Tagesmitteltemperatur die vorgegebene Temperatur nicht überschreitet oder die tatsächliche Temperaturamplitude eine vorgegebene Temperaturspanne nicht überschreitet. Die erste Möglichkeit hat den Nachteil, dass bei sehr lockerem Schnee im Hochwinter Stellen, die durch Windeinfluss aper geworden sind, nicht als solche erkannt werden können. Dies ist bei der Betrachtung der Differenz der Extremwerte hingegen nicht der Fall, da sowohl im Winter als auch im Sommer das Vorhandensein/Nichtvorhandensein einer Schneedecke diesen Temperaturunterschied in etwa in der gleichen Weise mit sich bringt. Nichtsdestotrotz konnten im Kernsommer (JJA) die am besten mit den Parametern für die gesamten Alpen übereinstimmenden Ergebnisse mit ersterer Methode gefunden werden (siehe Abbildung 7.19). Hat man sich für eine der beiden Methoden entschieden, bleibt noch die Unsicherheit in der zahlenmäßigen Wahl des Thresholds, die wiederum Einfluss auf den Wert der relativen Schneedauer hat. Nach Überprüfen einer ganzen Reihe von möglichen Thresholds für die Tagesmitteltemperatur, erwies sich jener von 2°C als am besten geeignet.

Eine weitere Herausforderung bei der Anpassung einer Fitkurve bestand darin, brauchbare Prädiktoren zu finden. Geographische Länge und Breite scheiden in diesem Fall wegen der geringen Distanz zwischen den Messpunkten (alle auf einer Bergflanke gelegen) aus. Auch die Abhängigkeit von der Höhe ist nicht herausragend (7% erklärte Varianz, siehe Tabelle 7.2). Viel wichtiger ist die Lage der Punkte im Bezug auf die Mikrotopographie. Um in der Anpassung nicht zu viele Prädiktoren (wie Exposition oder Kurvatur ect.) zu haben, wurden Länge und Breite durch die ersten beiden Hauptkomponenten einer Hauptkomponentenanalyse der Mikrotopographie ersetzt (TOECHTERLE et al., 2010). Die erste Hauptkomponente (PC1) erklärt dabei 25% Varianz in der Schneebedeckungsdauer. Dieser Wert wird nur durch die durch die großräumige Temperatur erklärte Varianz von 27% übertroffen. Dieser im Vergleich zu den

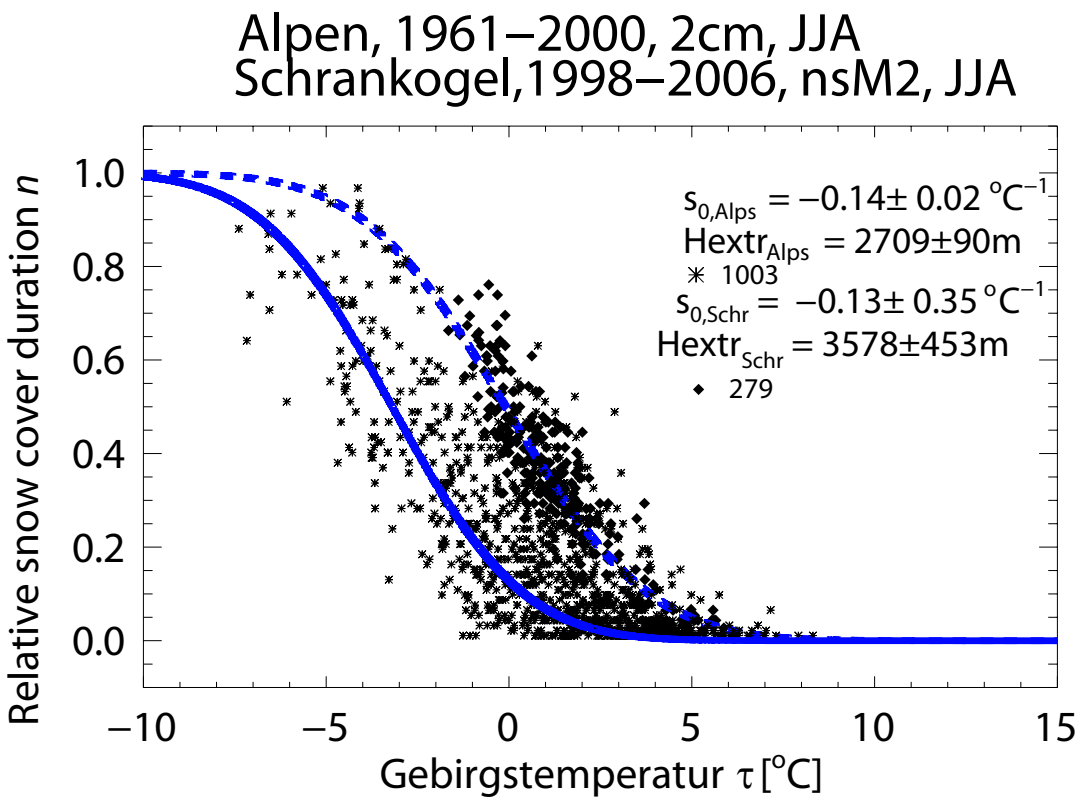

Abbildung 7.19: Zustandskurven für die gesamten Alpen (durchgezogen) und den Gipfel des Schrankogels (strichliert) .

alpenweiten Auswertungen sehr hohe Wert wird plausibel, wenn man bedenkt, dass sich das Messgebiet am Schrankogel nur über einen Bereich von wenigen hundert Metern erstreckt und somit nicht die vertikale Temperaturabnahme, sondern die Temperaturschwankungen von Jahr zu Jahr (und natürlich die Mikrotopographie) die Schneeverhältnisse im Messgebiet bestimmen.

Das Ergebnis der Anpassung für den Hochsommer (JJA), verglichen mit jener für die gesamten Alpen, sieht viel versprechend aus, wobei man auch betonen muss, dass am Schrankogel (1998-2006) nur etwa $\frac{1}{4}$ der Daten (279 Punkte) der gesamten Alpen (1961-2000) zur Verfügung stehen, was sich deutlich auf die Parameterunsicherheiten auswirkt. Die Steigung beider Zustandskurven ist mit -0.13°C^{-1} und -0.14°C^{-1} nahezu identisch, auch die Höhen maximaler Empfindlichkeit sind mit 2709m und 3578m nicht signifikant unterschiedlich. Die Verschiebung entlang der Abszisse (anderer τ_0-Wert) ist nicht relevant, da dieser Größe von vorn herein keine physikalische Bedeutung zukommt.

Literaturverzeichnis

APELDAUER, V. (1933). *Gedenkbuch der Stadt Retz*. Retz.

AUER, I. and et al. (2007). HISTALP– historical instrumental climatological surface time series of the greater Alpine region 1760 – 2003. *Int. J. Climatol.*, 27:17–46.

BOEHM, R., JONES, P. D., HIEBL, J., FRANK, D., BRUNETTI, M., and MAUGERI, M. (2010). The early instrumental warm-bias: A solution for long central European temperature series 1760– 2007. *Clim. Change*, 101:41–67.

BRONSTEIN, I. N., SEMENDJAJEW, K. A., MUSIOL, G., and MÜHLIG, H. (1999). *Taschenbuch der Mathematik*. Verlag Harri Deutsch.

BRÁZDIL, R. and KOTYZA, O. (2000). *History of weather and climate in the Czech lands IV: Utilisation of economic sources for the study of climate fluctuation in the Louny Region in the fifteenth-seventeenth centuries*. Masaryk University, Brno.

BRÁZDIL, R., ZAHRADNICEK, P., DOBROVOLNÝ, P., KOTYZA, O., and VALÁSEK, H. (2008). Historical and recent viticulture as a source of climatological knowledge in the Czech Republic. *Geografie*, 113(4):351–371.

CASTY, C., WANNER, H., LUTERBACHER, J., ESPER, J., and BOEHM, R. (2005). Temperature and precipitation variability in the European Alps since 1500. *Int. J. Climatol.*, 25(14):1855–1880.

CHUINE, I., YIOU, P., VIOVY, N., and et al. (2004). Historical phenology: grape ripening as a climate indicator. *Nature*, 432:289–290.

DeGROOT, M. H. (1986). *Probability and Statistics*. Addison-Wesley.

DOBROVOLNÝ, P. and et al. (2010). Monthly, seasonal and annual temperature reconstructions for central Europe derived from documentary evidence and instrumental records since AD 1500. *Clim. Change*, 101:69–107.

ETIEN, N., DAUX, V., MASSON-DELMOTTE, V., STIEVENARD, M., BERNARD, V., DUROST, S., GUILLEMIN, M., MESTRE, O., and PIERRE, M. (2008). A bi-proxy reconstruction of Fontainebleau (France) growing season temperature from A.D. 1596 to 2000. *Clim. Past*, 4:1–16.

FAHRMEIR, L. and TUTZ, G. (2001). *Multivariate statistical modelling based on generalized linear models*. Springer Verlag New York, Berlin, Heidelberg; 2nd ed.

GARNIER, E., DAUX, V., YIOU, P., and de COTRÁZAR-ATAURI, I. G. (2011). Grapevine harvest data in Besancon (France) between 1525 and 1847: social outcomes or climate evidence? *Clim. Change*, 104:703–727.

GOTTFRIED, M., HANTEL, M., MAURER, C., TOECHTERLE, R., PAULI, H., and GRABHERR, G. (2011). Coincidence of the alpine-nival ecotone with the summer snowline. *Environ. Res. Lett.*, 6:12 pp.

GOTTFRIED, M., PAULI, H., and GRABHERR, G. (1998). Prediction of vegetation patterns at the limits of plant life: a new view of the alpine-nival ecotone. *Arct. Alp. Res.*, 30:207–221.

GOTTFRIED, M., PAULI, H., REITER, K., and GRABHERR, G. (1999). A fine-scaled predictive model for changes in species distribution patterns of high mountain plants induced by climate warming. *Divers. Distribut.*, 5:241–251.

HANN, J. (1883). *Handbuch der Klimatologie*. Verlag von J. Engelhorn, Stuttgart.

HANN, J. (1908). *Handbuch der Klimatologie. Band I Allgemeine Klimalehre*. Bibliothek Geographischer Handbücher, N.F. Verlag von J. Engelhorn, Stuttgart.

HANTEL, M., EHRENDORFER, M., and HASLINGER, A. (2000). Climate sensitivity of snow cover duration in Austria. *Int. J. Climatol.*, 20:615–640.

HANTEL, M. and HIRTL-WIELKE, L.-M. (2007). Sensitivity of Alpine snow cover to European temperature. *Int. J. Climatol.*, 27:1265–1275.

HANTEL, M. and MAURER, C. (2011). The median winter snowline in the Alps. *Meteorol. Z.*, 20(3):267–276.

HANTEL, M., MAURER, C., and MAYER, D. (2012). The snowline climate of the Alps 1961-2000. *Theor. Appl. Climatol.*, DOI 10.1007/s00704-012-0688-9 (published online).

HIRTL-WIELKE, L.-M. (2007). *Die Beziehung zwischen der Schneebedeckung und Temperatur in den Alpen und den Rocky Mountains*. Dissertation an der Universität Wien.

JUNG, T., PALMER, T. N., RODWELL, M. J., and SERRAR, S. (2010). Understanding the Anomalously Cold European Winter of 2005/06 Using Relaxation Experiments. *Amer. Met. Soc.*, 138(8):3157–3174.

KÖRNER, C. (2003). *Alpine Plant Life: Functional Plant Ecology of High Mountain Ecosystems*. Springer, Berlin, ed. 2.

LANDSTEINER, E. (1999). The crisis of wine production in late sixteenth-century central Europe: Climatic causes and economic consequences. *Clim. Change*, 43:323–334.

LAUSCHER, F. (1978). Neue Analysen ältester und neuerer phänologischer Reihen. *Arch. Met. Geoph. Biokl. B*, 26:373–385.

LAUSCHER, F. (1983). Weinlese in Frankreich und Jahrestemperatur in Paris seit 1453. *Wetter und Leben*, 35:39–42.

LÖSCHNIG, J. and STEFL, L. (1935). *Geschichtliche Aufzeichnungen der Stadt Retz*. Österreichischer Wein- und Obstbaukalender.

MAURER, C., HAMMERL, C., KOCH, E., HAMMERL, T., and POKORNY, E. (2011). Extreme grape harvest data of Austria, Switzerland and France from A.D. 1523 to 2007 compared to corresponding instrumental/reconstructed temperature data and various documentary sources. *Theor. Appl. Climatol.*, 106:55–68.

MAURER, C., KOCH, E., HAMMERL, C., HAMMERL, T., and POKORNY, E. (2009). BACCHUS temperature reconstruction for the period 16th to 18th centuries from Viennese and Klosterneuburg grape harvest dates. *J. Geophys. Res.*, 114:D22106.

MEIER, N., RUTISHAUSER, T., PFISTER, C., WANNER, H., and LUTERBACHER, J. (2007). Grape harvest data as a proxy for Swiss April to August temperature reconstruction back to A.D. 1480. *Geophys. Res. Lett.*, 34:L20705.

PAULI, H., GOTTFRIED, M., and GRABHERR, G. (1999). Vascular plant distribution patterns at the low temperature limits of plant life - the alpine-nival ecotone of Mount Schrankogel (Tyrol, Austria). *Phytocoenologia*, 29:297–325.

PRIBRAM, A. F., GEYER, R., and KORAN, F. (1938). *Materialien zur Geschichte der Preise und Loehne in Oesterreich, vol. 1.* Carl Ueberreuters Verlag, Wien.

PUNTSCHERT, J. (1894). *Denkwürdigkeiten der Stadt Retz*. Selbstverlag der Stadt Retz, Wien.

SCHÄR, C. and JENDRITZKY, G. (2004). Hot news from summer 2003. *Nature*, 432:559–560.

SCHÖNWIESE, C. D. (1992). *Praktische Statistik für Meteorologen und Geowissenschafter*. Gebrüder Borntraeger Berlin, Stuttgart; 2nd ed.

SOLOMON, S., QIN, D., MANNING, M., CHEN, Z., MARQUIS, M., AVERYT, K. B., TIGNOR, M., and MILLER, H. L. (2007). *IPPC: Climate Change 2007: The Physical Science Basis. Contribution of Working Group I to the Fourth Assessment Report of the Intergovernmental Panel on Climate Change*. Cambridge Univ. Press, Cambridge, U. K.

TAYLOR, J. R. (1997). *An Introduction to Error Analysis: The study of uncertainties in physical measurements*. University Science Books, Sausalito, California, 2nd ed.

TOECHTERLE, R., GOTTFRIED, M., HANTEL, M., MAURER, C., PAULI, H., and GRABHERR, G. (2010). *Using topographic and temperature data to model snow distribution at the alpine-nival ecotone*. Presentation at the *Mountain Conference* (Sept. 2010, Perth, UK).

WIELKE, L.-M., HAIMBERGER, L., and HANTEL, M. (2004). Snow cover duration in Switzerland compared to Austria. *Meteorol. Z.*, 13:13–17.

YIOU, P., VAUTARD, R., NAVEAU, P., and CASSOU, C. (2007). Inconsistency between atmospheric dynamics and temperatures during the exceptional 2006/2007 fall/winter and recent warming in Europe. *Geophys. Res. Lett.*, 34:L21808.

Curriculum Vitae

Persönliche Daten:

Geburtsdatum:	20. Oktober 1980
Geburtsort:	Wien (Österreich)
Eltern:	Anna Maurer und Herbert Maurer
Familienstand:	ledig
E-Mail:	christian.maurer@univie.ac.at
Homepage:	http://www.univie.ac.at/theoreticalmeteorologyresearchforum/

Akademische Ausbildung:

1999–2007	Diplomstudien der Meteorologie und Geophysik an der Universität Wien
13. Dezember 2004	Diplom im Studienzweig Meteorologie (*Magister der Naturwissenschaften*)
26. März 2007	Diplom im Studienzweig Geophysik (*Magister der Naturwissenschaften*) mit ausgezeichnetem Erfolg abgeschlossen
Oktober 2007–	Doktoratsstudium im Studienzweig Meteorologie

Berufliche Erfahrung:

- Seit 12/05/01: Projektmitarbeiter (im GEO-Sekretariat) an der Zentralanstalt für Meteorologie und Geodynamik, Wien
- 12/01/01-12/04/30: Projektmitarbeiter an der Veterinärmedizinischen Universität, Wien, Institut für Öffentliches Veterinärwesen
- 11/04/01-11/12/31: Freier Projektmitarbeiter an der interfakultativen Forschungsplattform der Universität Wien "Sensitive Mountain Limits of Snow and Vegetation"; drei fertige Publikationen.
- 08/08/01-10/12/31: vertraglicher Projektmitarbeiter an der interfakultativen Forschungsplattform der Universität Wien "Sensitive Mountain Limits of Snow and Vegetation", Leitung emer. O. Univ.-Prof. Dr. Michael Hantel.
- 08/05/01-08/10/31: vertraglicher Projektmitarbeiter an der Zentralanstalt für Meteorologie und Geodynamik, Wien (Abteilung Klimatologie, Projekt BACCHUS "Klosterneuburg Wine and Climate Change in Lower Austria"); 08/11/01-11/03/31 weitere Projektmitarbeit auf Werkvertragsbasis; zwei fertige Publikationen (mit Erstautorenschaft).
- 07/04/23-08/04/22: einjähriger Vertrag als Universitätsassistent in Ausbildung am Institut für Meteorologie und Geophysik, Universität Wien, Abteilung Theoretische Meteorologie und Klimatologie, Leitung O. Univ.-Prof. Dr. Michael Hantel.
- 06/08: Processing seismischer Daten für Jaakko Pöyry Infra, Wien.

- 04/04: Analyse der Schnee- und Glatteistage in den Monaten Februar und März, Werkvertrag bei Meteo Media GmbH, Wien.
- 03/08: einwöchiges Praktikum beim ORF- Hörfunk, Wien.
- 02/08: Editieren eines aero- geoelektrischen Datensatzes, Werkvertrag bei der Geologischen Bundesanstalt, Wien.

Konferenzteilnahmen:

- European Geosciences Union (EGU)-Konferenz, Wien, Österreich, April 2009 (Vortrag)
- Österreichischer Meteorologentag 2009, Graz, Österreich, November 2009 (Poster)
- European Geosciences Union (EGU)-Konferenz, Wien, Österreich, Mai 2010
- Global Change and the World's Mountains, Perth, Vereinigtes Königreich, September 2010 (Poster)
- Treffen deutscher und österreichischer Meteorologen aus dem Fachbereich "Theoretische Meteorologie", Kloster Schöntal, Deutschland, Oktober 2010 (Vortrag)
- Climate Change in High Mountain Regions (on the occasion of the 125th Anniversary of Sonnblick Observatory), Salzburg, Österreich, August 2011
- Österreichischer Meteorologentag 2011, Klagenfurt, Österreich, November 2011(Vortrag)

Publikationen:

- BACCHUS temperature reconstruction for the period 16th to 18th centuries from Viennese and Klosterneuburg grape harvest dates; *Journal of Geophysical Research*, Vol. **114**, D22106, 13 pp., 2009, DOI: 10.1029/2009JD011730.
- The median winter snowline in the Alps; *Meteorologische Zeitschrift*, Vol. **20** (3), 10 pp., 2011, doi: 10.1127/0941-2948/2011/0495.
- Coincidence of the alpine - nival ecotone with the summer snowline; *Environmental Research Letters*, Vol. **6**, 12 pp., 2011, DOI: 10.1088/1748-9326/6/1/014013.
- Extreme grape harvest data of Austria, Switzerland and France from A.D. 1523 to 2007 compared to corresponding instrumental/reconstructed temperature data and various documentary sources; *Theoretical And Applied Climatology*, Vol. **106**, 14 pp., 2011, DOI: 10.1007/s00704-011-0410-3.
- The snowline climate of the Alps 1961-2010; *Theoretical And Applied Climatology*, 2012, DOI 10.1007/s00704-012-0688-9 (published online)